

## Phase I Update

# Near Infrared Camera and Multispectral Spectrometer

### In This Update...

Introduction / 1
NICMOS Focus Problem: The Issue and the Policy / 1
Selecting NICMOS Instrument Parameters in the Phase I Proposal Form / 3
Coronagraphy / 4
Error in the Handbook Sensitivity Curves for Extended Sources / 4
Limiting Sensitivity / 4
Revised Overhead Information / 5
Detector Decision Flow Chart / 6
NICMOS Instrument Handbook Errata / 7

---

## Introduction

This short document updates the information provided in the NICMOS Instrument Handbook for Cycle 7 phase 1 applications, correcting a number of mistakes, and identifies changes required due to our evolving knowledge of the instrument since the Handbooks completion. Since NICMOS has not yet been through its full ground test program, much of the information remains unaltered, and must still be treated as preliminary. However there are a number of important items which applicants must take into account.

---

## NICMOS Focus Problem: The Issue and the Policy

In most respects NICMOS is operating as planned, however, currently at its operating temperature Camera 3 cannot be simultaneously focused with Cameras 1 & 2. The cause of this differential focus shift is presently under investigation. It is possible that full confocality will be restored, however, this is not guaranteed. Meanwhile, good focus is still believed to be independently attainable on either Camera 3 or Cameras 1 & 2 jointly by moving the Pupil Adjust Mechanism.

Accordingly NASA, STScI and the IDT intend to implement commands to allow for independent focusing of each camera. This will be largely transparent to users. If a particular science program requires a switch between Camera 3 and either Camera 1 or 2 or vice versa during a SINGLE ORBIT, there will be an additional overhead due to this refocusing, which we estimate will be 5 min. Thus the total overhead involved will increase from 2 to 7 minutes. A revised version of Table 9.1, which gives the total overhead times is given below.

It is important to reiterate that the absence of a common focus does not affect the ability to work with a particular camera at the full sensitivity of NICMOS. Assessment of the focus situation as obtained on orbit will be carried out during SMOV and throughout Cycle 7 as necessary.

The biggest potential impact of these differing focii will be for "internal parallel" science (use of all three cameras simultaneously). If the present situation persists, the loss of sensitivity in Camera 3 incurred by focussing on Cameras 1 or 2 is around two magnitudes. Furthermore the images are sufficiently out of focus that they are doughnut shaped. Focussing on Camera 3 results in the complete loss of the ability to simultaneously obtain usable images from the other two cameras.

Pure parallels (NICMOS in parallel with another instrument) will still be possible, however observers may have to choose either Camera 3 or Cameras 1 & 2 for high quality focus. NICMOS parallel observers must clearly identify which of the two focus positions is required in their proposal.

Given the possibility that full confocality will be restored, and given the limited lifetime of the NICMOS mission, PROPOSALS WILL BE ACCEPTED FOR ALL PREVIOUSLY ADVERTISED OBSERVING MODES IN CYCLE 7.

If you wish to observe a single target with each camera in turn this focus shift will have no major impact apart from the increased overhead.

The impact on programs which need to use all three cameras to study extended sources is as follows:

1. Programs whose science ABSOLUTELY REQUIRES SIMULTANEOUS three camera confocality must make this clear in the abstract of their proposal. Such proposals will be accepted, but will, by default, be executed later in the Cycle, and must accept the risk that these proposals may prove to be infeasible if three camera confocality is not recovered, and will therefore not be executed at all.
2. Other programs must account for the extra time required to split the observation into exposures at the different focus positions. That is they must budget separately for Cameras 1 & 2 (together) and Camera 3, and request the implied additional orbits at Phase 1.
3. Users of Cameras 1 and 2 who believe that having camera 3 out of focus will not materially alter their science program must justify this in their proposal and take into account its commensurate reduction in sensitivity.

The TAC will be provided with up to date information and use their understanding of the situation to allocate orbits according to similar guidelines.

## Selecting NICMOS Instrument Parameters in the Phase I Proposal Form

Proposers are required to provide details on instrument configuration, mode, and spectral elements when completing the Phase I proposal form. The keywords are `\configuration`, `\mode`, and `\spectralelements` in Section 11, OBSERVATION SUMMARY, of the proposal form. It is stated in the Cycle 7 Call for Proposals that the relevant information is given in the instrument handbooks. For the convenience of the proposer, we are providing details of all supported NICMOS instrument configurations and operating modes, and a summary of the spectral elements (filters, grisms, and polarizers).

### Instrument configurations (`\configuration`)

The supported instrument configurations are NICMOS/NIC1, NICMOS/NIC2, and NICMOS/NIC3. These configurations are valid for all observations. The meaning of the three configurations is self-explanatory in calling out which of the three cameras is being specified.

### Operating modes (`\mode`)

The NICMOS operating modes relevant for Phase I are ACCUM, MULTACCUM, and BRIGHTOBJ. Also ACQ mode should be specified to signify if a coronagraphic target acquisition is needed. RAMP mode is available, but unsupported, see the Handbook for details.

### Spectral elements (`\spectralelements`)

NICMOS has a separate filter wheel with 19 filters (Spectral elements in Phase I terminology) each for each camera. Only one filter, grism, or polarizer per camera may be used at a given time, although on the observation summary form you should list each one to be used. A full listing of the spectral elements for NICMOS may be found on pages 36, 38 and 40 in Chapter 4 of the Instrument Handbook.

### Examples

Imaging observations with Camera 3:

```
\configuration {NICMOS/NIC3}
\mode          {MULTACCUM}
\spectralelements {F110W, F160W}
```

Spectroscopic observations with the grisms:

```
\configuration {NICMOS/NIC3}
\mode          {ACCUM}
\spectraelements {G141, F150W}
```

A coronagraphic observation:

```
\configuration {NICMOS/NIC2}
\mode          {ACQ, MULTACCUM}
\spectraelements {F187N, F187W}
```

---

## Coronagraphy

Information provided by the IDT indicates that due to diffraction effects associated with the coronagraphic mode of NICMOS, the usable area is for radii greater than 0.4 arcsec (compared to 0.3 arcsec given in the Handbook).

The expected performance of Camera 2 is that there should be a reduction in diffracted energy in the wings of a stellar PSF of approximately a factor 10 compared to the unmasked PSF.

---

## Error in the Handbook Sensitivity Curves for Extended Sources

The sensitivity curves presented in the Handbook for extended sources UNDERESTIMATE the signal-to-noise that will be achieved for a given source flux by a factor of two. That is you will obtain the predicted signal-to-noise for a source four times fainter than shown. Note that this does not affect the point source diagrams. Also, the tools provided on the World Wide Web correctly calculate the sensitivity for extended sources. We emphasize that using these tools is the favored way of carrying out sensitivity calculations as they are kept up-to-date with any new performance data which is obtained for NICMOS.

---

## Limiting Sensitivity

The definition of limiting sensitivity quoted in the Handbook in table 3.1 has caused some confusion. To clarify the meaning of this number the limiting fluxes



listed there are for a signal-to-noise of 5 for the BRIGHTEST pixel assuming that the source is centered in the pixel. The limiting flux for a point source obtained by integrating over the PSF will clearly therefore be fainter.

---

## Revised Overhead Information

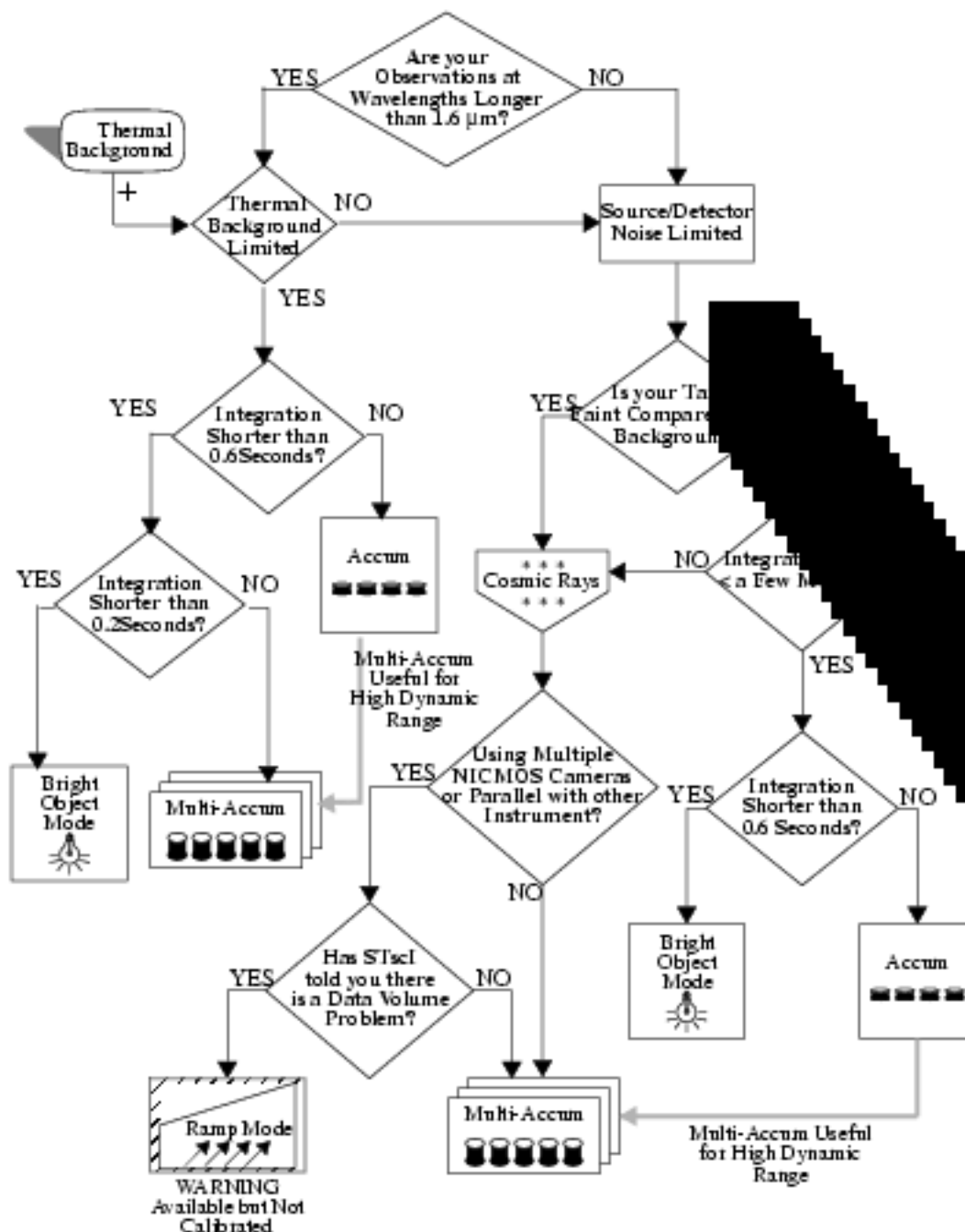
Below, we present a revised version of Table 9.1 giving detailed overhead information for NLCMOS. This corrects a typographical error and includes the expected additional overhead due to independent focussing of Cameras 1 and 2 compared to Camera 3.

**Table 9.1**

Action	Overhead
Target Acquisition (for coronagraphy)	65 seconds + the exposure time for 2 acquisition images
Change of Camera (from any to any WITHIN an orbit)	7 minutes
Change of Camera (from any to any BETWEEN orbits)	0 minutes (no overhead is charged)
Chopping of $X$ arcsec ( $> 2$ arcmin, with guide star re-acquisition)	$(X+31) + 6$ minutes for g.s. reacq

## Detector Decision Flow Chart

The flow chart presented in Figure 8.5 on page 119 of the Handbook has been revised to allow for the use of Multi-accumulate for bright targets. A target which requires an integration time less than 0.6 seconds but longer than 0.2 seconds can be observed in Multi-Accum mode instead of requiring the use of Bright Object Mode.



---

## NICMOS Instrument Handbook Errata

1. Chapter 6, page 76, "Optics"; Note that the NICMOS mirrors are silver coated and not gold coated as stated in the Handbook. The figure of 95% reflectivity is a wavelength weighted average of the measured performance of the NICMOS mirrors.
2. page 117 (Acquisition Mode) 1/4 of a Camera 2 pixel is 0.1875 arcseconds and not 0.13 arcseconds as stated.



---

Version 1.0  
June 1996

# Near Infrared Camera and Multi-Object Spectrometer Instrument Handbook



SPACE  
TELESCOPE  
SCIENCE  
INSTITUTE

STScI  
3700 San Martin Drive  
Baltimore, Maryland 21218

## User Support

For prompt answers to any question, please contact the Science Support Division Help Desk.

- **E-mail:** [help@stsci.edu](mailto:help@stsci.edu)
- **Phone:** (+10) 338-1082  
(800) 544-8125 (U.S., toll free)

## World Wide Web

Information and other resources are available on the NICMOS World Wide Web page:

- **URL:** [http://www.stsci.edu/ftp/instrument\\_news/NICMOS/topnicmos.html](http://www.stsci.edu/ftp/instrument_news/NICMOS/topnicmos.html)

## NICMOS Instrument Team

Name	Title	Phone	e-mail
David J. Axon	Instrument Scientist	(410) 338-4892	<a href="mailto:axon@stsci.edu">axon@stsci.edu</a>
Howard Bushouse	Scientific Programmer	(410) 338-4530	<a href="mailto:bushouse@stsci.edu">bushouse@stsci.edu</a>
Daniela Calzetti	Instrument Scientist	(410) 338-4518	<a href="mailto:calzetti@stsci.edu">calzetti@stsci.edu</a>
Doris Daon	Data Analyst	(410) 338-4485	<a href="mailto:daon@stsci.edu">daon@stsci.edu</a>
John W. MacKenty	Instrument Scientist	(410) 338-4599	<a href="mailto:mackenty@stsci.edu">mackenty@stsci.edu</a>
Christine Ritchie	Data Analyst	(410) 338-5042	<a href="mailto:ritchie@stsci.edu">ritchie@stsci.edu</a>
Chris Skinner	Instrument Scientist	(410) 338-5057	<a href="mailto:skinner@stsci.edu">skinner@stsci.edu</a>

## Revision History

Version	Date	Editors
1.0	June 1996	D.J. Axon, D. Calzetti, J.W. MacKenty, C. Skinner

## Acknowledgements

Acknowledgements: Significant contributions to the production of this Handbook have been made by Robin Auer, Wayne Baggett, Chris Blades, Howard Bushouse, Doris Daon, Ron Gilliland, Ray Kutina, Christine Ritchie, and Mark Stevens. We are grateful to Rodger Thompson, Glenn Schneider, the NICMOS Science Team, and Ball Aerospace for valuable inputs.

## Citation

In publications, refer to this document as:

Axon, D. et al., 1996, "NICMOS Instrument Handbook", Version 1.0 (Baltimore: STScI).

# Table of Contents

---

## Part I: Introduction ..... 1

### Chapter 1 Introduction ..... 3

*Purpose* ..... 3

Document Conventions ..... 4

*Layout* ..... 4

*NICMOS Proposal Preparation* ..... 7

*The Help Desk at STScI* ..... 8

*The NICMOS Instrument Team at STScI* ..... 8

*Supporting Information and the NICMOS Web Site* ..... 9

### Chapter 2 Special Considerations for Cycle 7 ..... 11

*NICMOS is a New Instrument* ..... 11

*Updates to Instrument Performance for Cycle 7* ..... 12

*Support of NICMOS Capabilities for Cycle 7* ..... 12

*NICMOS Functionality in Cycle 7* ..... 14

---

## Part II: User's Guide ..... 15

### Chapter 3 Overview of NICMOS ..... 17

*Instrument Capabilities* ..... 17

*Instrument Design* ..... 18

Physical Layout ..... 18

Imaging Layout ..... 20

Camera 1 .....	22
Camera 2 .....	22
Camera 3 .....	22
Placement and Orientation of Cameras .....	22
Comparison to WFPC2 and STIS .....	23
<i>Basic Operations</i> .....	25
Comparison to CCDs .....	25
Target Acquisition Modes .....	26
<i>Attached Parallels</i> .....	27
The Infrared Background .....	28
Conversion Between Fluxes and Magnitudes .....	32
<i>Designing NICMOS Observations</i> .....	32
 <b>Chapter 4 Imaging</b> .....	35
<i>Available Filters &amp; Optical Elements</i> .....	35
Nomenclature .....	36
<i>Filter Sensitivity Curves</i> .....	42
<i>Out-of-Band Leaks in NICMOS Filters</i> .....	44
<i>Point Spread Function</i> .....	45
Encircled Energy Predictions .....	45
Field Dependence .....	47
<i>NICMOS Aperture Definitions</i> .....	48
Aperture Definitions .....	48
<i>NICMOS Coordinate System Conventions</i> .....	49
<i>Orients</i> .....	49
 <b>Chapter 5 Coronagraphy, Polarimetry and Grism Spectroscopy</b> .....	51
<i>Coronagraphy</i> .....	51
Coronagraphic Acquisitions .....	52
Reuse Target Offset and Interactive Acquisitions .....	53
PSF Centering .....	54
Coronagraphic Decision Chart .....	54



<i>Polarimetry</i> .....	56
Instrumental Polarization .....	56
Theory.....	56
Polarimetry Decision Chart.....	58
<i>Polarimetric Sensitivity</i> .....	59
<i>Grism Spectroscopy</i> .....	64
Relationship Between Wavelength and Pixel .....	64
Multi-Object Spectroscopy.....	65
Grism Decision Chart.....	66
<i>Sensitivity</i> .....	68
Grism Sensitivity Curves.....	68

## **Chapter 6 Exposure Time Calculations**

<b>Calculations</b> .....	75
<i>Overview</i> .....	75
Instrumental Factors .....	76
<i>Calculating NICMOS Imaging Sensitivities</i> .....	78
Signal to noise Calculation .....	78
Exposure Time Calculation.....	80
Software Tools.....	82
Filter Sensitivity Curves .....	83
Signal to Noise for a Source.....	83
Saturation and Detector Limitations .....	83
<i>WWW Access to Imaging Tools</i> .....	83
<i>Examples</i> .....	84
Using Exposure Time and Signal to noise Calculators .....	84
Examples of Calculations by Hand.....	88
NICMOS Grism Sensitivity on the Web .....	90

## **Chapter 7 NICMOS Detectors**

<i>Physical Characteristics</i> .....	91
Detector Response Curves.....	91
Shading—a Detector Artifact.....	93
Read-Noise.....	95
Linearity and Saturation.....	95

Effect of Cosmic Rays .....	96
Intra-Pixel Sensitivity Variations .....	97
<i>Flat Field Response</i> .....	97
Characteristics of the Flat Fields .....	97
Wavelength Variations—Details .....	99
Special Situations .....	102
Extended Sources with Extreme Spatial Color Variations .....	104
Multi-Object Grism Spectroscopy .....	104

## **Chapter 8 Detector Readout Modes**..... 105

<i>Introduction</i> .....	105
Detector Resetting as a Shutter.....	107
Fast and Slow Readout Modes.....	107
<i>Accumulate Mode</i> .....	107
<i>Multiple-Accumulate Mode</i> .....	110
<i>Read Times and Dark Current Calibration in ACCUM and MULTIACCUM Modes</i> .....	112
<i>Bright Object Mode</i> .....	114
<i>Acquisition Mode</i> .....	116
<i>NICMOS Science Data</i> .....	117
<i>Summary and Quick Reference</i> .....	118

## **Chapter 9 Overheads and Orbit**

### **Time Determination** ..... 121

<i>Overview</i> .....	121
<i>NICMOS Exposure Overheads</i> .....	122
<i>Orbit Use Determination</i> .....	124
Example 1: A Two-Chop Pattern Using Multi-Accum and the Coronagraph.....	124
Example 2: Polarization Observations Using a Chop Pattern and MULTI-ACCUM .....	126
Example 3: Making a Map using Square-wave-dith .....	127
Example 4: Changing Cameras and Pattern .....	128
Example 5: Use of the Grism and ACCUM Mode.....	130

Example 6: Another Example of Mapping .....	131
Example 7: Observation of the Calibration Star	
P041-C.....	134

## Part III: Supporting Material ..... 137

### Chapter 10 Techniques for Background Measurement and Mosaicing ..... 139

<i>Introduction</i> .....	139
<i>Chopping and Dithering Strategies</i> .....	141
Compact Objects .....	142
Extended Objects .....	142
<i>Chopping and Dithering Patterns</i> .....	143
Dither Patterns .....	145
Chop Patterns .....	145
Combined Patterns .....	146
<i>Examples</i> .....	147
<i>Orienting Patterns</i> .....	152
<i>Phase II Proposal Instructions for Patterns</i> .....	152
Parameters .....	153
Types of Motions .....	153

### Chapter 11 Imaging Reference Material ..... 155

<i>Camera 1, Filter F090M</i> .....	156
<i>Camera 1, Filter F095N</i> .....	158
<i>Camera 1, Filter F097N</i> .....	160
<i>Camera 1, Filter F108N</i> .....	162
<i>Camera 1, Filter F110M</i> .....	164
<i>Camera 1, Filter F110W</i> .....	166
<i>Camera 1, Filter F113N</i> .....	168

<i>Camera 1, Filter F140W</i> .....	170
<i>Camera 1, Filter F145M</i> .....	172
<i>Camera 1, Filter F160W</i> .....	174
<i>Camera 1, Filter F164N</i> .....	176
<i>Camera 1, Filter F165M</i> .....	178
<i>Camera 1, Filter F166N</i> .....	180
<i>Camera 1, Filter F170M</i> .....	182
<i>Camera 1, Filter F187N</i> .....	184
<i>Camera 1, Filter F190N</i> .....	186
<i>Camera 2, Filter F110W</i> .....	188
<i>Camera 2, Filter F160W</i> .....	190
<i>Camera 2, Filter F165M</i> .....	192
<i>Camera 2, Filter F171M</i> .....	194
<i>Camera 2, Filter F180M</i> .....	196
<i>Camera 2, Filter F187N</i> .....	198
<i>Camera 2, Filter F187W</i> .....	200
<i>Camera 2, Filter F190N</i> .....	202
<i>Camera 2, Filter F204M</i> .....	204
<i>Camera 2, Filter F205W</i> .....	206
<i>Camera 2, Filter F207M</i> .....	208
<i>Camera 2, Filter F212N</i> .....	210
<i>Camera 2, Filter F215N</i> .....	212
<i>Camera 2, Filter F216N</i> .....	214
<i>Camera 2, Filter F222M</i> .....	216
<i>Camera 2, Filter F237M</i> .....	218
<i>Camera 3, Filter F108N</i> .....	220
<i>Camera 3, Filter F110W</i> .....	222
<i>Camera 3, Filter F113N</i> .....	224
<i>Camera 3, Filter F150W</i> .....	226
<i>Camera 3, Filter F160W</i> .....	228
<i>Camera 3, Filter F164N</i> .....	230
<i>Camera 3, Filter F166N</i> .....	232

<i>Camera 3, Filter F175W</i> .....	234
<i>Camera 3, Filter F187N</i> .....	236
<i>Camera 3, Filter F190N</i> .....	238
<i>Camera 3, Filter F196N</i> .....	240
<i>Camera 3, Filter F200N</i> .....	242
<i>Camera 3, Filter F212N</i> .....	244
<i>Camera 3, Filter F215N</i> .....	246
<i>Camera 3, Filter F222M</i> .....	248
<i>Camera 3, Filter F240M</i> .....	250

## **Chapter 12 Flux Units and Line Lists** .....

<i>Infrared Flux Units</i> .....	253
Background .....	254
Units for NICMOS .....	255
<i>Formulae</i> .....	255
Converting Between $F_n$ and $F_l$ .....	255
Conversion Between Fluxes and Magnitudes .....	256
Conversion Between Surface Brightness Units .....	257
<i>Look-up Tables and Software</i> .....	257
<i>Examples</i> .....	264
<i>Infrared Line Lists</i> .....	264

---

## **Part IV: Calibration** .....

### **Chapter 13 Calibration Pipeline** .....

<i>Overview and New Features</i> .....	275
Associations .....	276
Re-engineering .....	278
<i>NICMOS Pipeline</i> .....	278
Static Calibrations—calnica .....	278
Contemporaneous Observations—calnicb .....	281

<i>NICMOS Data Products</i> .....	282
Standard NICMOS Dataset Structure .....	282
IRAF Access .....	284
<b>Chapter 14 Expected Calibration</b>	
<b>Accuracies</b> .....	285
<i>Expected Accuracies</i> .....	285
Remarks .....	285
Areas of Significant Uncertainty .....	286
Provisional Cycle 7 Calibration Goals .....	287
<b>Chapter 15 Calibration Plans</b> .....	289
<i>Introduction</i> .....	289
<i>Thermal Vacuum Test</i> .....	290
<i>Servicing Mission Observatory Verification</i> .....	290
<i>Cycle 7 Calibration Program</i> .....	290
Photometry .....	292
Detector Performance.....	292
Flat Fields .....	292
Background Characterizations.....	292
Point Spread Function .....	292
Coronagraph.....	293
Grisms .....	293
Polarizers .....	293
Time Variability .....	293
<i>Photometric Calibration</i> .....	293
Flux Standards for NICMOS Absolute Calibration.....	293
Ground Based Calibrations.....	295
<i>References</i> .....	296
<b>Glossary</b> .....	297
<b>Appendix</b> .....	301
<i>Ramp Mode</i> .....	301
<b>Index</b> .....	309







# CHAPTER 1

# Introduction

## In This Chapter...

Purpose / 3

Layout / 4

NICMOS Proposal Preparation / 7

The Help Desk at STScI / 8

The NICMOS Instrument Team at STScI / 8

Supporting Information and the NICMOS Web Site / 9

The Near Infrared Camera and Multi-Object Spectrometer, NICMOS, is a second-generation instrument to be installed on the Hubble Space Telescope during the Second Servicing Mission in 1997. NICMOS will provide HST with infrared imaging and spectroscopic capabilities between 0.8 and 2.5 microns. From above the earth's atmosphere, NICMOS will have access to this complete spectral range without hindrance from atmospheric emission or absorption at a sensitivity and angular resolution not possible from the ground. This Handbook provides the instrument specific information you need to propose for HST observations (Phase I), design accepted proposals (Phase II), and understand NICMOS in detail. This chapter explains the layout of the Handbook and how to get additional help and information through the Help Desk and World Wide Web pages at STScI.

---

## Purpose

The *NICMOS Instrument Handbook* is the basic reference manual for the Near Infrared Camera and Multi-Object Spectrometer and describes the instrument's properties, expected performance, operations, and calibration. The Handbook is maintained by scientists at STScI. Dr. R.L. Thompson, the Principal Investigator for NICMOS, and scientific staff at Steward Observatory and Ball Aerospace kindly provided information and test data in support of this Handbook.

We have designed the document to serve three purposes:

- To provide instrument-specific information for preparing Cycle 7 observing proposals with NICMOS.
- To provide instrument-specific information to support the design of Phase II proposals for accepted NICMOS proposals in Cycle 7.
- To provide technical information about the operation and performance of the instrument which can help in the understanding of problems and in the interpretation of data acquired with NICMOS.

This Handbook is not meant to serve as a manual for the reduction and analysis of data taken with NICMOS. Near the start of the NICMOS observing era, we will publish an addition to the *HST Data Handbook* describing how to work with NICMOS data.

## Document Conventions

This document follows the usual STScI convention in which terms, words, and phrases which are to be entered by the user in a literal way on a form are shown in a typewriter font (e.g., `BRIGHT-RETURN`, `PP-SPLIT`). Names of software packages or commands (e.g., **synphot**) are given in bold type.

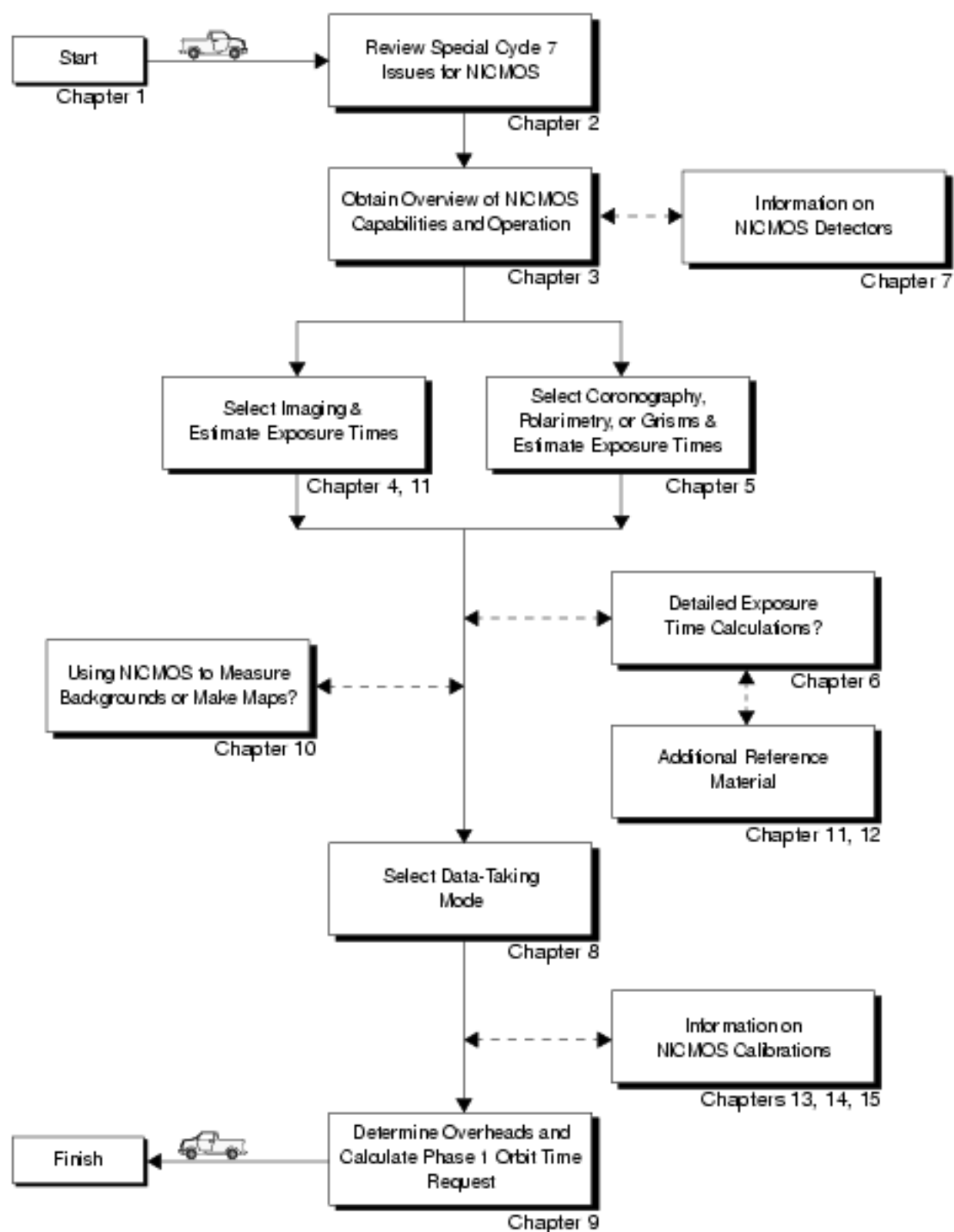
Wavelength units in this Handbook are in microns ( $\mu\text{m}$ ) and fluxes are mainly given in Janskys (Jy).

---

## Layout

NICMOS has a variety of imaging modes. The instrument provides direct imaging in broad, medium, and narrow-band filters at a range of spatial resolutions in the near infrared from 0.8 to 2.5 microns, together with broad-band imaging polarimetry, coronagraphic imaging and maskless grism spectroscopy. To guide you through NICMOS's capabilities and help optimize your scientific use of the instrument we have divided this Handbook into four parts: Part I - Introduction; Part II - Users's Guide; Part III - Supporting Material; and Part IV - Calibration. provides a roadmap to navigating the document; following the roadmap is a list of chapters and their contents.

Figure 1.1: Roadmap for Using the NICMOS Instrument Handbook



The chapters of this Handbook are as follows:

#### Part I - Introduction

- Chapter 1, *Introduction* on page 3.
- Chapter 2, *Special Considerations for Cycle 7* on page 11, describes special considerations for the use of NICMOS during Cycle 7.

#### Part II - Users Guide

- Chapter 3, *Overview of NICMOS* on page 17, provides an introduction to the full capabilities of NICMOS. A discussion is provided to help guide you through the technical details you will need to consider in choosing the optimum NICMOS configuration and in determining the number of orbits to request.
- Chapter 4, *Imaging* on page 35, provides a description of NICMOS's imaging capabilities including camera resolutions and throughputs. We have designed a set of curves for each NICMOS filter that can help estimate the exposure time needed for various signal to noise observations of both point and extended sources. Those are described in this chapter, and presented in Chapter 11.
- Chapter 5, *Coronagraphy, Polarimetry and Grism Spectroscopy* on page 51, provides detailed information on coronagraphic imaging, grism spectroscopy, and polarimetry.
- Chapter 6, *Exposure Time Calculations* on page 75, describes how to perform signal to noise calculations, either by using pencil and paper, or using software tools that are provided on the World Wide Web (WWW).
- Chapter 7, *NICMOS Detectors* on page 91, describes the basic properties of the detectors used in the three cameras including their physical characteristics, capabilities and limitations, including saturation and linearity.
- Chapter 8, *Detector Readout Modes* on page 105 explains the data taking modes which take advantage of the non-destructive readout capabilities of the NICMOS arrays. We give recommendations and guidelines the observer should adopt in choosing the most appropriate mode.
- Chapter 9, *Overheads and Orbit Time Determination* on page 121, provides information to convert from a series of planned science exposures to an estimate of the number of orbits, including spacecraft and NICMOS overheads. This chapter applies principally to the planning of Phase 1 proposals.

#### Part III - Supporting Material

- Chapter 10, *Techniques for Background Measurement and Mosaicing* on page 139, gives a guide to measuring the sky background when observing with NICMOS. This chapter describes the implementation of a pre-defined set of patterns which accomplish dithering and chopping from the field of interest, and allow easy generation of large mosaic images.

- Chapter 11, *Imaging Reference Material* on page 155, provides sensitivity information for each imaging filter, ordered by camera and increasing wavelength.
- Chapter 12, *Flux Units and Line Lists* on page 253, provides formulae and tables for the conversion of flux units, and a list of common infrared spectral lines.

#### Part IV - Calibration

- Chapter 13, *Calibration Pipeline* on page 275, briefly describes the processing of NICMOS data by the STScI pipeline and the data that will be sent to observers.
- Chapter 14, *Expected Calibration Accuracies* on page 285 summarizes the accuracies expected for NICMOS data calibrated by the STScI pipeline in Cycle 7.
- Chapter 15, *Calibration Plans* on page 289, provides an overview of the planned thermal vacuum (ground), SMOV (commissioning phase) and Cycle 7 calibration and verification plans.

---

## NICMOS Proposal Preparation

Use the *NICMOS Instrument Handbook* and the *Cycle 7 Call for Proposals & Phase I Proposal Instructions* (CP) when assembling your NICMOS Phase I Proposal. The CP provides policy and instructions for proposing; the *NICMOS Instrument Handbook* contains technical information about NICMOS, describing its expected performance, and presenting suggestions for use. The next chapter in the Handbook describes special considerations for Cycle 7.

If your Phase I proposal is accepted, you will be asked to submit a Phase II proposal in which you specify the exact configurations, exposure times and sequences of observations that NICMOS and the telescope should perform. To assemble your Phase II proposal, you should use the *NICMOS Instrument Handbook* in conjunction with the *Phase II Proposal Instructions*. These instructions describe the rules and syntax that apply to the planning and scheduling of NICMOS observations and provide relevant observatory information.

Our current understanding of NICMOS as an instrument is in its formative stages as the flight detectors have yet to be fully calibrated and we are currently in the middle of the development of the ground system to support NICMOS operations.



At this time, predictions of the performance of NICMOS should be treated as provisional, and users should adopt conservative expectations for the performance of the instrument in Cycle 7.

---

## The Help Desk at STScI

STScI maintains a Help Desk. The Help Desk staff at STScI quickly provide answers to any HST-related topic, including questions regarding NICMOS and the Cycle 7 Proposal Process. The Help Desk staff has access to all of the resources available at the Institute, and they maintain a database of answers so that frequently asked questions can be immediately answered. The Help Desk staff also provide STScI documentation, in either hardcopy or electronic form, including instrument science reports, instrument handbooks, and the like. Questions sent to the Help Desk during normal business hours are answered within one hour. Questions received outside normal business hours will be answered the next business day. Usually, the Help Desk staff will reply with the answer to a question, but occasionally they will need more time to investigate the answer. In these cases, they will reply with an estimate of the time needed to supply a full answer.

We ask that you please send all initial inquiries to the Help Desk. If your question requires a NICMOS Instrument Scientist to answer it, the Help Desk staff will put a NICMOS Instrument Scientist in contact with you. By sending your request to the Help Desk, you are guaranteed that someone will provide you with a timely response.

To contact the Help Desk at STScI:

- **Send e-mail:** [help@stsci.edu](mailto:help@stsci.edu)
- **Phone:** 1-410-338-1082

The Space Telescope European Coordinating Facility (ST-ECF) also maintains a help desk. European users should generally contact the ST-ECF for help; all other users should contact STScI. To contact the ST-ECF Help Desk:

- **Send e-mail:** [stdesk@eso.org](mailto:stdesk@eso.org)

---

## The NICMOS Instrument Team at STScI

STScI maintains a team of Instrument Scientists, Scientific Programmers and Data Analysts who support the development, operation and calibration of NICMOS. The team is also responsible for supporting NICMOS users. The table inside the front cover of this Handbook lists the current members of the NICMOS Instrument Team at STScI.

---

## Supporting Information and the NICMOS Web Site

The NICMOS Instrument Team at STScI maintains a World Wide Web page, as part of the STScI home page. The URL for the STScI NICMOS page is:

[http://www.stsci.edu/ftp/instrument\\_news/NICMOS/topics/nmos.html](http://www.stsci.edu/ftp/instrument_news/NICMOS/topics/nmos.html)

The STScI NICMOS web page includes:

- **Advisories:** This is where we will post updates to instrument performance as these are produced through ground testing and on-orbit investigations.
- **Documentation:** An electronic version of this Handbook will be maintained on the WWW site. In addition, more detailed technical information (not needed to propose for Cycle 7) concerning the development, performance, ground testing, operation and calibration of NICMOS itself are found in a series of NICMOS instrument science and calibration reports maintained on the web, while others can be obtained upon request from the Help Desk.
- **User Support:** Will contain general information on data reductions and support for HST users.
- **Software:** Some software can be retrieved or run directly over the web, including an exposure time calculator, and a flux units conversion program.
- **Frequently Asked Questions:** A list of frequently asked questions about NICMOS, and their answers, ranging from proposal preparation to data analysis.





## CHAPTER 2

# Special Considerations for Cycle 7

### In This Chapter...

NICMOS is a New Instrument / 11  
Updates to Instrument Performance for Cycle 7 / 12  
Support of NICMOS Capabilities for Cycle 7 / 12  
NICMOS Functionality in Cycle 7 / 14

HST's second servicing mission will put in place two second-generation instruments, NICMOS and STIS (the Space Telescope Imaging Spectrograph) while removing the Faint Object Spectrograph (FOS) and Goddard High Resolution Spectrograph (GHRS). In addition, a Fine Guidance Sensor (FGS) will be replaced and a solid state data recorder will be installed. The increased data capacity of the new recorder, exploited through a series of changes to the ground system, considerably increases the capacity of HST to take simultaneous data from multiple instruments running in parallel. Cycle 7 should indeed mark an exciting new phase in HST science. On the other hand, observers must appreciate that it will take time for us to understand, calibrate and optimize the use of these new instruments.

---

## NICMOS is a New Instrument

While planning your Cycle 7 observations, keep in mind that NICMOS will indeed be a *new* capability, as well as a new instrument. The sensitivities, brightness limits, and optical performance that are contained in this Handbook represent our best estimates at this time; in many cases they are based on component testing of either flight or flight-candidate optics and detectors. Integrated testing of NICMOS in a thermal vacuum chamber is currently scheduled for June 1996, and integrated operations with the ground system are scheduled for September 1996. On-orbit verification of NICMOS (SMOV) is

scheduled for March through June 1997. Since there has not been any infrared capability aboard HST before, the uncertainties associated with the introduction of any new instrument are, in this case, compounded by uncertainties regarding HST's performance as an infrared telescope.

---

## Updates to Instrument Performance for Cycle 7

We will publish updates to the sensitivities, performance, and capabilities of NICMOS presented in this handbook by mid-August. That update will reflect any new information about instrument performance obtained during ground testing which may affect your Phase I Proposal. This update will be mailed to all individuals who have requested the *NICMOS Instrument Handbook*; it will also be available upon request from the Help Desk, or can be downloaded from the STScI NICMOS WWW site (see "Supporting Information and the NICMOS Web Site" on page 9). Additional updates, applicable only to *accepted* Cycle 7 proposals, will be provided prior to Phase II Submission (in early 1997) as required.



Your NICMOS HST proposal for Cycle 7 must be based on the final sensitivities, performance, and capabilities published at that time.

---



---

## Support of NICMOS Capabilities for Cycle 7

We have established a set of core scientific capabilities of NICMOS which will be supported for Cycle 7 science and which are described in this handbook. These capabilities cover an enormous range of science applications and bring dramatic new capabilities to HST. In practice, the supported capabilities will be phased in during Cycle 7, as our understanding of the instrument and on-orbit performance grows. This phasing will optimize the likelihood that observations are successfully executed and assure that the requisite calibration observations are obtained.

NICMOS has additional capabilities that are not supported for Cycle 7. These capabilities are "available" in the form of *Engineering-only* modes, upon consultation with a NICMOS Instrument Scientist. If you find that your science *cannot* be performed with the capabilities described in this handbook, you may wish to consider use of an unsupported capability. The use of these capabilities requires approval from STScI and support for calibration may be limited or non-existent.

Unsupported capabilities include:

- The Field Offset Mirror (FOM). This mechanism permits offsetting of the NICMOS field of view (for all three cameras simultaneously) by up to 26 arcseconds in radius from the nominal position without motion of the HST itself. This results in some degradation of the image quality (both PSF and background masking). The primary usefulness of this capability is chopping or dithering to measure the sky background when NICMOS is operated in parallel with another science instrument—when NICMOS is unable to control the pointing of HST. As we explain later, only at the longest wavelengths do we expect that it will be necessary to measure the sky background, and for NICMOS prime pointings this will be accomplished by moving HST, not the FOM. Only in some parallel observing cases do we expect to operate the FOM.
- The RAMP readout mode. This detector readout mode is similar to a limited version of the MULTIACCUM mode with the processing carried out within the NICMOS instrument computer and only the final processed image downlinked. As more flexible processing can be carried out on the ground, the primary usefulness of this mode is that it demands a much smaller data volume than MULTIACCUM. With the anticipated installation of the Solid State Recorder (SSR), on-board data management and transmission are not presently viewed as limiting factors for NICMOS science operations. For NICMOS prime observations we do not expect to use RAMP readout mode. Whether it is needed for parallel observing when another instrument is prime will depend on data volume, and we will advise users at the appropriate time (Phase II).

Use of unsupported modes comes at a price, and these modes should be used only if the need and scientific justification are particularly compelling. Proposers should be aware of the following caveats in the use of unsupported modes:

- Calibrations for unsupported capabilities will not be provided by STScI. Observers must either determine that they can create calibration files from data in the HST Archive or they must obtain calibrations as part of their observations. The STScI pipeline will not calibrate data taken in unsupported modes but will deliver uncalibrated FITS files (or in some cases partially calibrated FITS files) to the observer and the HST Archive.
- STScI adopts a policy of *shared risk* with the observer for the use of unsupported capabilities. Requests to repeat failed observations taken using unsupported capabilities will not be honored if the failure is related to the use of the unsupported capability.
- User support from STScI for the reduction and analysis of data taken using unsupported capabilities will be limited and provided at a low priority. Users taking data with unsupported capabilities should be prepared to shoulder the increased burden of calibration, reduction, and analysis of these data.

Cycle 7 proposals which include use of unsupported NICMOS capabilities must include a justification of why the science cannot be done with a supported configuration, must include a request for any observing time needed to perform

calibrations, must justify the added risk of using an unsupported mode in terms of the science payback, and must include a demonstration that the observers are able to shoulder the increased burden of calibration, reduction, and analysis of their data.

---

## NICMOS Functionality in Cycle 7

There are aspects of the performance of NICMOS which require measurements on-orbit following the second servicing mission and which therefore will not be known until well after the Cycle 7 Phase II submission deadline. The most important of these is the level and stability of the HST-generated thermal background. Knowledge of this background, as discussed in Chapter 3, is necessary to determine the conditions under which offset measurements (chopping) of the sky are required and the frequency of such measurements. This potentially has a very large impact on the overheads associated with observations longward of about 1.6 microns.



---

Proposals with observations that may be limited by thermal background may have a delayed Cycle 7 Phase II submission deadline, and thus not be executed until the second part of the Cycle (probably July or August 1997). This will allow optimal use of the orbits granted by the TAC, but the number of available orbits will *not* be changed.

---

Proposals for observations which are limited by thermal background radiation and which may therefore require chopping will be evaluated with all other proposals by the Cycle 7 TAC using the assumptions outlined in this Handbook and any subsequent updates.

## CHAPTER 3

# Overview of NICMOS

### In This Chapter...

Instrument Capabilities /	17
Instrument Design /	18
Basic Operations /	25
Attached Parallels /	27
Designing NICMOS Observations /	32

In this Chapter we provide an overview of the basic properties and capabilities of NICMOS. We describe the optical and mechanical layout and the basic operation of the instrument. For those not familiar with IR array technology we compare the characteristics of these detectors with CCDs. In the final section in this chapter, we present a flowchart and a discussion to help you design a technically-feasible and scientifically-optimized NICMOS observing proposal.

---

## Instrument Capabilities

NICMOS, the Near Infrared Camera and Multi-Object Spectrometer, is an HST axial replacement instrument, containing three cameras designed for simultaneous operation. The NICMOS optics present the detectors with three adjacent but not spatially contiguous fields-of-view of different image scales. The instrument covers the wavelength range from 0.8 to 2.5 microns, and contains a variety of filters, grisms, and polarizers. Each camera carries a complement of 19 optical elements, selected through independent filter wheel mechanisms, one per camera.

The basic capabilities of the instrument, and the chapters which discuss them are:

- *IR imaging*: NICMOS provides high sensitivity from 1.1 to 1.6 microns, which is superior to that achievable on an 8m class telescope, and better sensitivity than the WFPC2 for all observations for wavelengths longward of 0.9 microns. Chapter 4 discusses the overall throughput of NICMOS and

the optical elements available in each camera. The low background will allow deep photometry. Our estimates of limiting sensitivities per pixel to give a  $5\sigma$  detection in a 60 minute integration are given in Table 3.1.

**Table 3.1:** Limiting Sensitivities per Pixel in Janskys for  $5\sigma$  Detection in 60 Minutes

Camera	Filter			
	F110W	F140W	F160W	F240M
bandwidth (microns)	0.8 to 1.35	0.8 to 1.8	1.4 to 1.8	2.3 to 2.5
NIC1	$1.5 \times 10^{-7}$ (J~25)	$1.7 \times 10^{-7}$ (J~24)	$4 \times 10^{-7}$ (H~23.5)	—
NIC2	$7 \times 10^{-8}$ (J~25.7)	—	$1.8 \times 10^{-7}$ (H~24.3)	$1.2 \times 10^{-5}$ (K~19.2)
NIC3	$6 \times 10^{-8}$ (J~25.8)	—	$1.1 \times 10^{-7}$ (H~24.7)	$7 \times 10^{-6}$ (K~19.9)

- *Grism Spectroscopy:* Camera 3, NIC3, has three gratings which provide a multi-object spectroscopic capability with a resolving power of  $R \sim 200$  over the full field of view of the camera. Their wavelength ranges are 0.8 to 1.2 microns, 1.1 to 1.9 microns, and 1.4 to 2.5 microns. Because the gratings are slitless, the spectra of spatially resolved objects are confused and multiple objects can overlap.
- *Imaging Polarimetry:* Three polarizing filters with pass directions of 0, 120, and 240 degrees are provided for the wavebands 0.8–1.3 microns in Camera 1, NIC1, and 1.9–2.2 microns in Camera 2, NIC2.
- *Coronagraphy:* A 0.3 arcsec radius occulting spot and cold mask, in the intermediate resolution Camera 2, NIC2, provides a coronagraphic imaging capability.

Chapter 5 discusses these special capabilities.

## Instrument Design

### Physical Layout

NICMOS is an axial bay instrument designed to replace the FOS in the HST aft shroud. Its enclosure contains four major elements: a graphite epoxy bench, the dewar, the fore-optics bench, and the electronics boxes. The large bench serves to establish the alignment and dimensional stability between the HST optics (via the latches or fittings), the room temperature fore optics bench, and the cryogenic optics and detectors mounted inside the dewar. The NICMOS dewar uses solid nitrogen as a cryogen for a projected on-orbit lifetime of approximately  $\pm 5 \pm 0.5$

years. Cold gas vented from the dewar is used to cool the vapor cooled shield (VCS) which provides a cold environment for both the dewar and the transmissive optical elements (i.e., the filters, polarizers, and grisms). The VCS is itself enclosed within two layers of thermal electrically cooled shells (TECs).

Figure 3.1 is an overview of the NLCMOS instrument; Figure 3.2 shows details of the dewar.

Figure 3.1: Instrument Overview

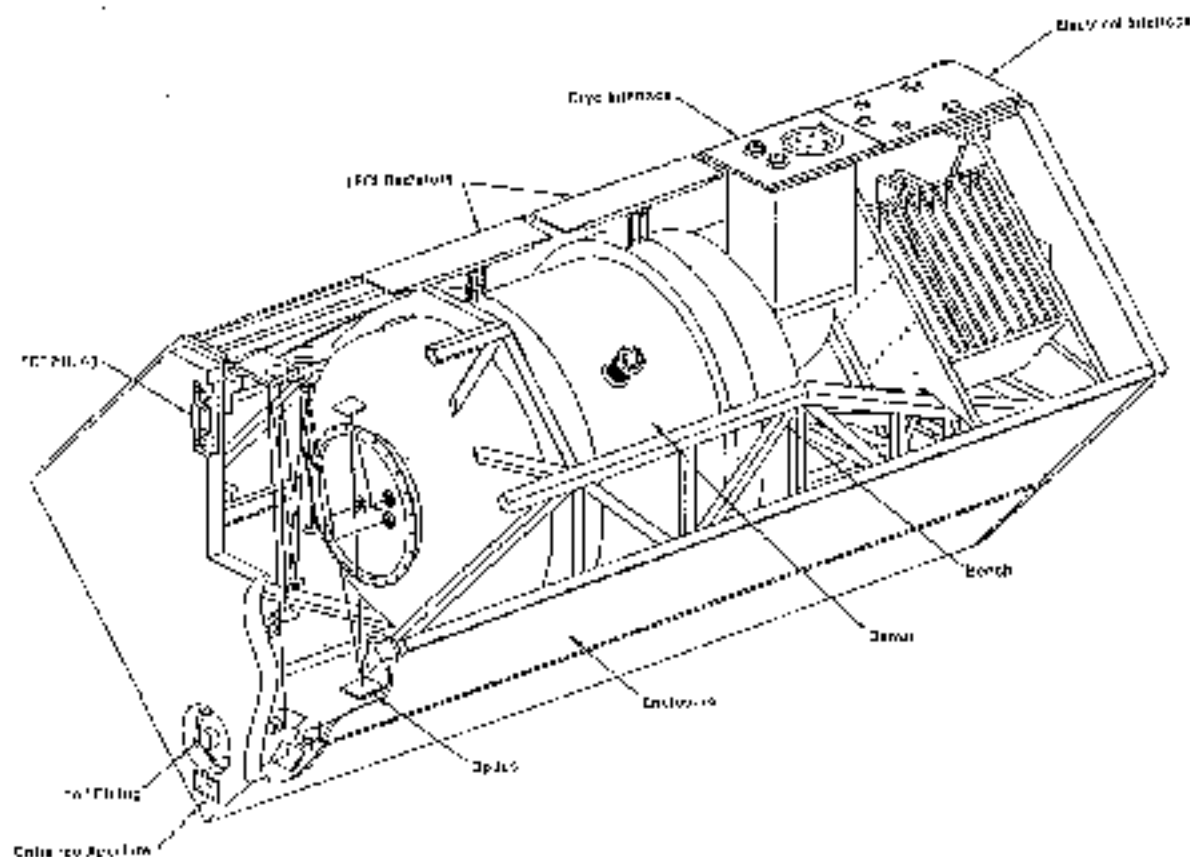
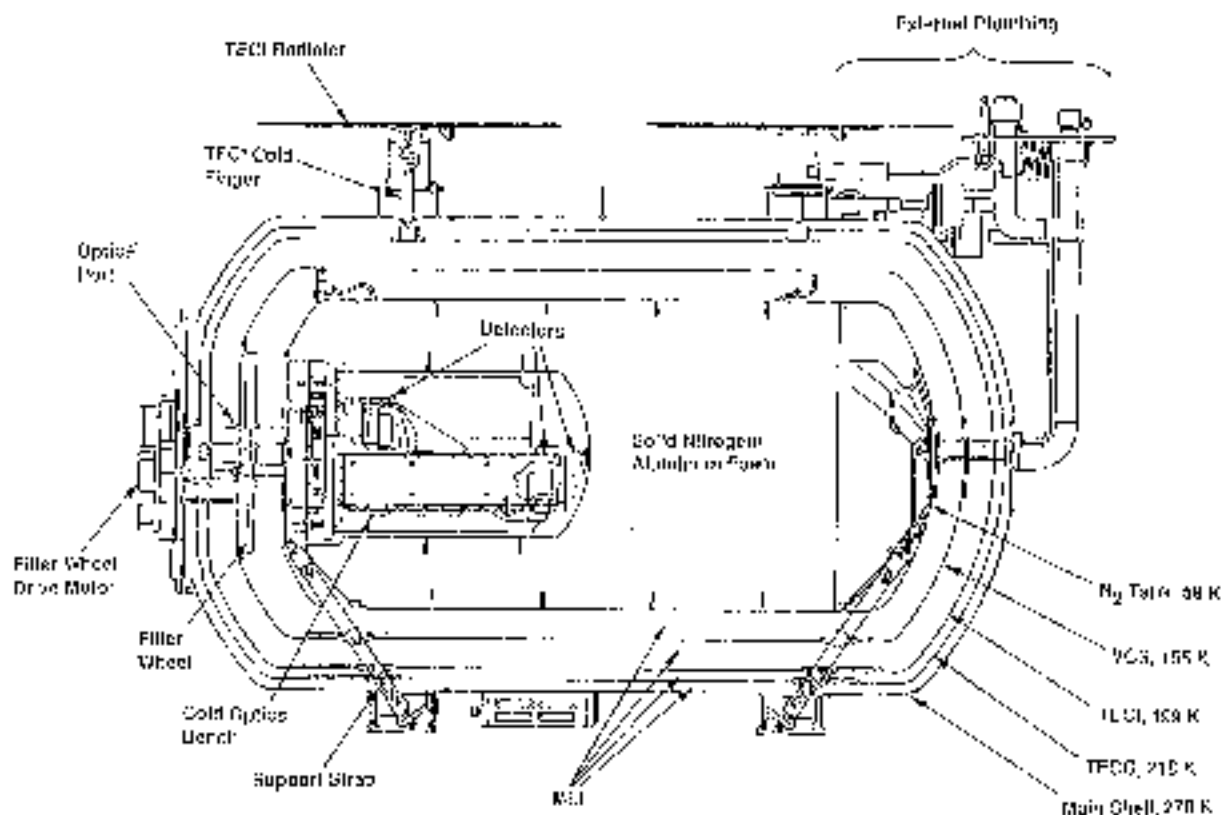


Figure 3.2: Solid Nitrogen Dewar

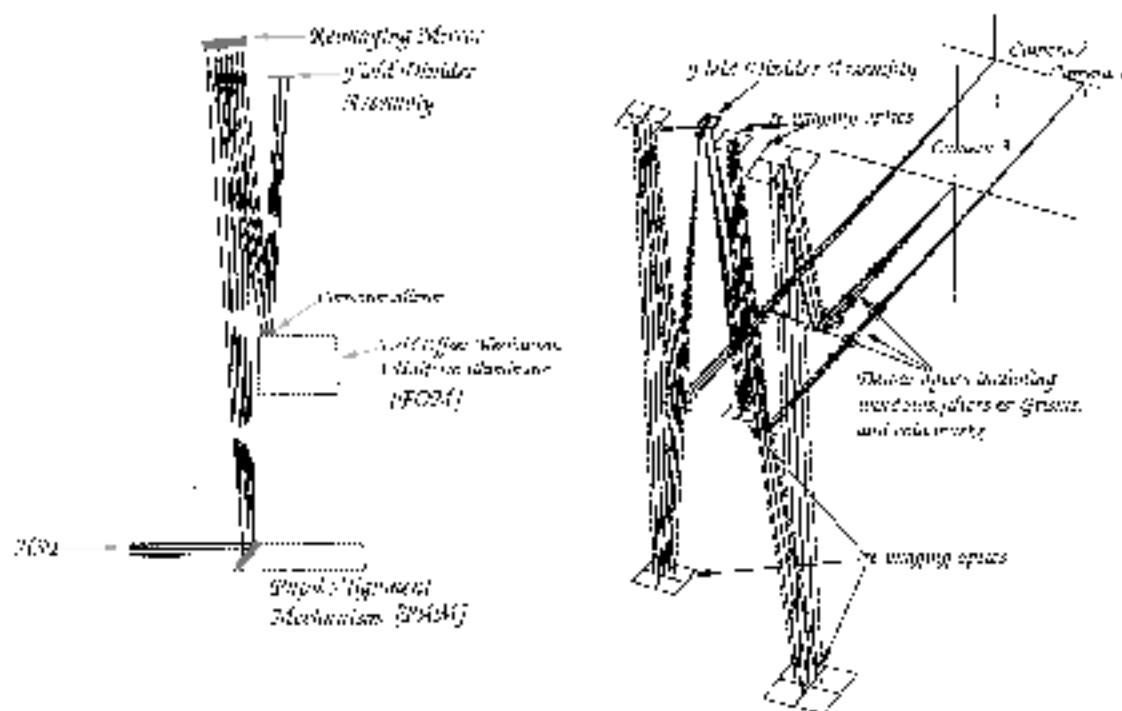


## Imaging Layout

The NICMOS fore-optics assembly is designed to correct the spherically aberrated HST input beam. As shown in the left hand panel of Figure 3.3 it comprises a number of distinct elements. The Pupil Alignment Mechanism/mirror (PAM) directs light from the telescope onto a re-imaging mirror which focuses an image of the OTA pupil onto an internal Field-Offset Mechanism (FOM) comprising a pupil mirror that provides a small offset capability (26 arcsec). An internal flat field source is also provided. The FOM provides correction for conic error in the OTA pupil.



Figure 3.3: Ray Diagrams of the NICMOS Optical Train. The left-hand panel shows the fore-optics. The right hand panel shows the field divider and re-imaging optics for the three cameras.



After the FOM, the Field Divider Assembly provides three separate but adjacent imaging fields, one for each camera (right hand panel of Figure 3.3). The dewar itself contains a series of cold masks to eliminate stray IR emission from peripheral warm surfaces.

A series of relay mirrors generate different focal lengths and magnifications for the three cameras, each of which contains a dedicated 256 x 256 pixel HgCdTe detector array that is based on the NICMOS 3 design. NICMOS will achieve diffraction limited performance in the high resolution Camera 1, NIC1, longward of 1.0 microns, and in Camera 2, NIC2, longward of 1.75 microns.

The operation of each camera is separate from the others which means that filters, integration times, readout times and readout modes can be different in each. The basic imaging properties of each of the cameras is summarized in Table 3.2.

**Table 3.2: Basic Imaging Parameters**

Parameter	Camera 1	Camera 2	Camera 3
Pixel Size (arcsec)	0.043	0.075	0.2
Field of View (arcsec x arcsec)	11 x 11	19.2 x 19.2	51.2 x 51.2
Diffraction Limited Wavelength ( $\mu\text{m}$ )	1.0	1.75	...

### Camera 1

Camera 1 (NIC1) provides the highest available spatial resolution with an 11 x 11 arcsec field of view and 43 milliarcsec sized pixels (equivalent to the WFPC2 PC pixel scale). The filter complement includes broad and medium band filters covering the spectral range from 0.8 to 1.8 microns and narrow band filters for Paschen  $\alpha$ , He I, [Fe II]  $\lambda$  1.6 $\mu\text{m}$ , and [S III]  $\lambda$  0.953  $\mu\text{m}$ , both on and off band. It is equipped with the short wavelength polarizers (0.8 to 1.3 microns).

### Camera 2

Camera 2 (NIC2) provides an intermediate spatial resolution with a 19.2 x 19.2 arcsec field of view and 75 mas pixels. The filters include broad and medium band filters covering the spectral range from 0.8 to 2.45 microns. The filter set also includes filters for CO, Brackett  $\gamma$ , H<sub>2</sub>, S2 (1-0)  $\lambda$  2.122  $\mu\text{m}$ , Paschen  $\alpha$ , HCO<sub>2</sub> + C<sub>2</sub>, and the long wavelength polarizers (1.9–2.1 microns). Camera 2 also provides a coronagraphic mask with a 300 milliarcsec radius.

### Camera 3

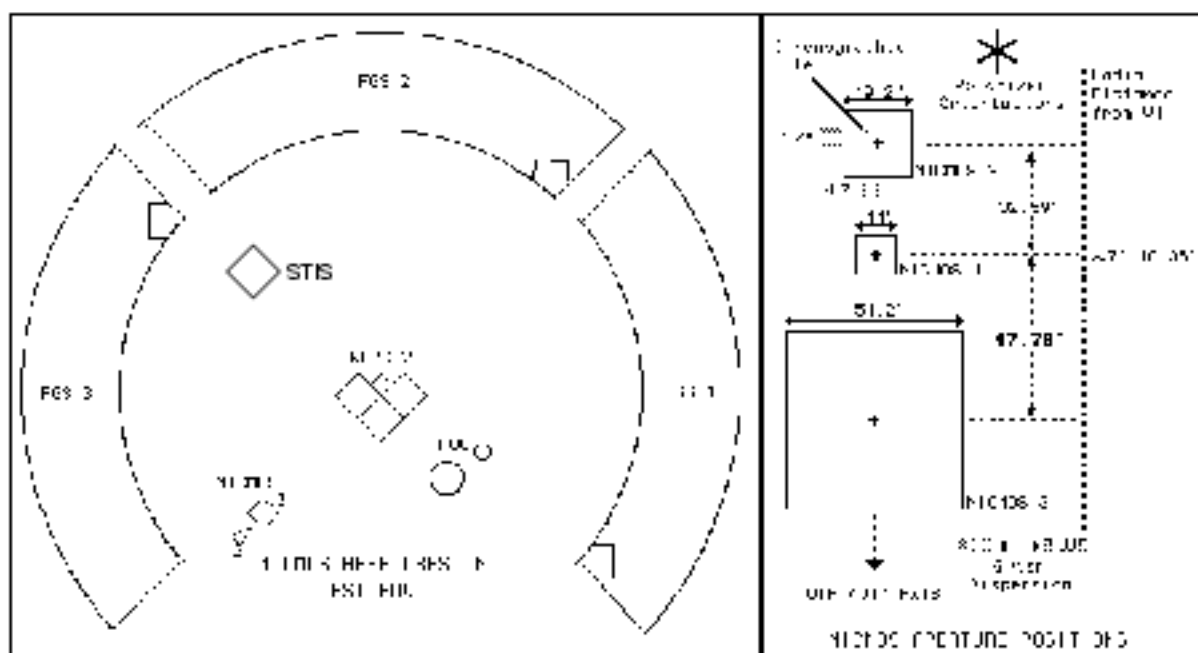
Camera 3 (NIC3) provides the lowest spatial resolution with a large 51.2 x 51.2 arcsec field of view and 200 milliarcsec pixels. It includes broad filters covering the spectral range 0.8 to 2.3 microns, medium band filters for the CO band (and an adjacent shorter wavelength continuum region), and narrow band filters for H<sub>2</sub>, S2 (1-0), [Si VI]  $\lambda$  1.962  $\mu\text{m}$ , Paschen- $\alpha$ , [Fe II]  $\lambda$  1.64  $\mu\text{m}$ , and He I  $\lambda$  1.083  $\mu\text{m}$ . Camera 3 also contains the multi-object spectroscopic capability of NICMOS with grisms covering the wavelength ranges 0.8–1.2 microns, 1.1–1.9 microns, and 1.4–2.5 microns.

## Placement and Orientation of Cameras

The placement and orientation of the NICMOS cameras in the HST focal plane is shown in Figure 3.4. Notice that the cameras are in a straight line pointing radially outward from the center of the telescope focal plane. From the observer's point of view the most important aspect of the layout of NICMOS comes when trying to plan an observation of an extended source with all three cameras simultaneously, when the user must bear in mind the relative positions and

orientations of the three cameras. Note that the gaps between the cameras are large, and therefore that getting good positioning for all cameras may be rather difficult.

Figure 3.4: NICMOS Field Arrangement



## Comparison to WFPC2 and STIS

In addition to NICMOS, between 0.8 and 1.0 microns HST offers the WFPC2 camera for wide field imaging. These two cameras complement each other. The Wide Field CCDs of WFPC2 have an imaging plate scale of  $\sim 0.1$  arcsec per pixel over each of the three chips, while the PC offers a plate scale of  $\sim 0.045$  arcsec per pixel on one CCD. The WFPC2 CCDs cover a much larger area of the sky (nearly  $160 \times 160$  arcsec) compared with NICMOS. On the other hand, NICMOS has increasingly higher sensitivity as we move towards 1.0 microns.

A unique feature of the WFPC2 is the presence of ramp filters which permit observations in any narrow bandpass up to  $9800\text{\AA}$ . These filters are limited to a  $\sim 10 \times 10$  arcsec field of view. The WFPC2 has a narrow band methane filter at  $8920\text{\AA}$ . Both WFPC2 and NICMOS have [S III] filters. NICMOS offers an adjacent off-band (or slightly redshifted) complementary filter.

In Table 3.3, we summarize the sensitivities of WFPC2 and NICMOS in their region of overlap. In this wavelength region WFPC2's sensitivity is dropping rapidly with increasing wavelength, while NICMOS's is rising. The signal to noise achievable in one hour on a  $V=20$  A0 star is seen to be comparable in the overlap region, and so the choice of which instrument to use is likely to be driven by the field of view desired (WFPC2's is much larger) and whether any further

observations are required at either shorter (WFPC2) or longer (NICMOS) wavelengths.

**Table 3.3: Comparison of WFPC2 and NICMOS Sensitivities for V=20 A0 Star**

Instrument	Filter	Mean Wavelength ( $\mu\text{m}$ )	Effective Width ( $\mu\text{m}$ )	Count Rate ( $\text{e}^-/\text{sec}$ )	S/N in one hour
WFPC2	F785LP	0.9366	0.2095	14	215 <sup>a</sup>
	F791W	0.8006	0.1304	30	314 <sup>a</sup>
	F814W	0.8269	0.1758	33	333 <sup>a</sup>
	F850LP	0.9703	0.1670	7.1	150 <sup>a</sup>
	FQCH4N (QnadD)	0.8929	0.0064	0.47	34,29 <sup>ab</sup>
	F953N	0.9546	0.0052	0.21	19,15 <sup>ab</sup>
	F1042M	1.0443	0.0611	0.20	18,15 <sup>ab</sup>
	LRF <sup>c</sup>	0.8000	0.0105	1.5	66
		0.9000	0.0113	0.64	40
		0.9762	0.0126	0.23	20
NICMOS	F090M <sup>d</sup>	0.8970	0.1885	2.0 <sup>e</sup>	90
	F095N <sup>d</sup>	0.9536	0.0088	0.14	12
	F097N <sup>d</sup>	0.9715	0.0094	0.18	16
	F108N (Camera 1)	1.0816	0.0094	0.17	15
	F110W (Camera 1)	1.1022	0.5920	6.6	160
	F110W (Camera 2)	1.1035	0.5915	14	260
	F110W (Camera 3)	1.1035	0.5915	26	350

a. Assumes two 1800 second exposures for cosmic ray removal.

b. Values given for WFC and PC.

c. LRF filter is continuously tunable from 0.371 $\mu\text{m}$  to 0.9762 $\mu\text{m}$ . LRF field of view is 10"×10".

d. These NICMOS filters are available only on Camera 1 which has field of view of 11"×11".

e. Count rates are for the central pixel on NICMOS.

The Space Telescope Imaging Spectrograph (STIS) also offers CCD based imaging to 1.1  $\mu\text{m}$  with 0.05" pixels and higher quantum efficiency than WFPC2 (although without a useful filter set). Additionally, STIS offers a large complement of slit and slitless spectroscopic capabilities that could complement near-infrared NICMOS science.

## Basic Operations

NICMOS employs three low-noise, high QE, 256x256 HgCdTe arrays in a passive dewar using solid N<sub>2</sub> as a coolant. The detector design is based on the NICMOS 3 design that many IR observers may have used; however, there are differences between the two (see Chapter 7). Here we summarize the basic properties of the NICMOS detectors most relevant to the planning of your observations.

The NICMOS detectors have dark current of less than 0.2 electrons per second and effective readout noise for a single exposure of approximately 30 electrons.

The NICMOS detectors are capable of very high dynamic range observations and have no count-rate limitations. The dynamic range, for a single exposure, is limited by the depth of the full well, or more correctly the onset of non-linearity, which limits the total number of electrons which can usefully be accumulated in any individual pixel during an exposure to ~180,000 electrons.

NICMOS has three detector read-out modes that may be used to take data (see Chapter 8). The simplest mode is *ACCUM* which provides a single integration on a source, albeit allowing a number of non-destructive read-out samples. A second mode, called *MULTIACCUM*, provides intermediate read-outs during an integration that subsequently can be analyzed on the ground. A third mode, *BRIGHTOBJ*, has been designed to observe very bright targets that would otherwise saturate the detector. *BRIGHTOBJ* mode reads-out a single pixel at a time. Due to the many resets and reads required to map the array there are substantial time penalties involved. *BRIGHTOBJ* mode may *not* be used in parallel with the other NICMOS detectors.

Users who require time-resolved images will have to use either *ACCUM* where the minimum exposure time is expected to be 0.6 seconds, and the minimum time between successive exposures is 20 seconds, or *MULTIACCUM* where the shortest spacing between exposures can be reduced to 0.3 seconds.

It is expected that *MULTIACCUM* mode will be used for most observations. It provides the best dynamic range and correction for cosmic rays, since post-observation processing of the data can make full use of the multiple readouts of the accumulating image on the detector. However, a sequence of *ACCUM* mode observations potentially offers a significant advantage for read noise limited observations using the *NREADS* option to decrease the effective read noise by up to a factor of ~3 (see Chapter 8). The actual read noise gain will be quantified during the ground testing of NICMOS early this summer and the results will be provided by mid-August 1996.

### Comparison to CCDs

These arrays, while they share some of the same properties as CCDs, are not CCDs and offer their own set of advantages and difficulties. Users unfamiliar with

IR arrays should therefore not fall into the trap of treating them like CCDs. For convenience we summarize the main points of comparison:

- As with CCDs, there is noise (read-noise) and time (read-time) associated with the reading out. In addition, there is an effect called *shading* which is an extraneous bias generated by the amplifiers immediately after reset of the arrays and which is a rapidly decaying function of time. Furthermore, the dark current associated with NICMOS arrays, while low for IR arrays, is quite substantial compared to that produced by the current generation of CCDs. The dark current may also be time-dependent.
- Unlike a CCD, the individual pixels of the NICMOS arrays are strictly independent and can be read-out non-destructively. Read-out modes have been designed which take advantage of the non-destructive read capabilities of the detectors to yield the optimum signal to noise for your science observations (see Chapters 7 and 8). Because the array elements are independently addressed, the NICMOS arrays do not suffer from some of the artifacts which afflict CCDs, such as charge transfer smearing and *bleeding* due to filling the wells. If, however, they are illuminated to saturation for sustained periods they retain a *memory* of the object in the saturated pixels. This is only really a worry for the photometric integrity of back to back exposures of very bright targets, as several detector flushes, which occur automatically when the detector is idle, rapidly clear the ghost images.

## Target Acquisition Modes

Most target acquisitions can be accomplished by direct pointing of the telescope. The user should use target coordinates which have been measured with the Guide Star Astrometric Support Package (GASP) to ensure the best accuracy with respect to the HST Guide Star Catalog. Particular care must be exercised with targets in Camera 1 due to its small field of view.

However, direct pointing will not be sufficient for coronagraphic observations since the achieved precision ( $\sim 1$  arcsec rms) is much larger than the 0.3 arcsec radius coronagraphic spot. *Note that this is a function of the total HST pointing error and not only the result of uncertainties in the target's coordinates.*

There are three target acquisition options for coronagraphic observations:

- An on-board acquisition (ACQ mode) can be obtained. This causes NICMOS to obtain an image of the target and rapidly position the brightest source in a restricted field of view behind the coronagraphic spot (see Chapter 5).
- The RE-USE TARGET OFFSET special requirement can be used to accomplish a positioning relative to an early acquisition image.
- A real time acquisition (INT-ACQ) can be obtained although this is costly in spacecraft time and is a limited resource.

While ACQ mode is restricted to coronagraphic observations in Camera 2, the last two target acquisition modes may be useful for positioning targets where

higher than normal (1–2 arcsec) accuracy is required (e.g., crowded field grism exposures).

## Attached Parallels

While many observers will be prepared to make good use of the capability of simultaneously using all three NICMOS cameras, some programs by their nature do not require more than one camera (e.g., studies of isolated compact objects). To make the most of the limited lifetime of NICMOS, observers are required to add exposures to their proposals to obtain the maximum amount of NICMOS data consistent with efficiently accomplishing their primary science program. Detailed instructions for this process will be included in the Phase II proposal instructions. Internal NICMOS parallel observations obtained under this policy will be known as *attached parallels* and will be delivered to the prime program's observer and will have the usual proprietary period.



This section applies only to Phase II proposals—you need not worry about this for your Phase I proposal.

The recommendations attached below are intended for General Observers (GOs) who do not establish a scientific rationale for observations with the two non-prime NICMOS cameras in their Phase I submission to the TAC. They are still subject to revision.

Table 3.4: Attached Parallel Recommendations

Pointing	Camera 1	Camera 2	Camera 3
Extragalactic	F160W	F110W, F160W	F110W, F160W -or- F160W, G141
Galactic Clouds	F164N, F166N	F110W, F160W, F205W	F110W, F160W, F222M
(if $\leq 4$ orbits)	F164N, F166N	F212N, F215N	F164N, F166N
Galactic Plane	F160W	F110W, F160W	F110W, F160W
(add if $> 1$ orbit)	F110W	F205W	F222M

Pointings are defined as:

- Extragalactic:  $> 5$  degrees above the galactic plane. An RA-Dec diagram will be provided in the Phase II proposal instructions to avoid requiring observers to convert target coordinates to galactic coordinates.

- Galactic Clouds: Dark/molecular cloud regions (e.g., OMC, rho Oph, etc.)
- Galactic Plane: all pointings not Extragalactic or Galactic Clouds.

The selection of a broad band imaging versus grism survey project should be made on the basis of the TAC selection of NICMOS pure parallel programs. As both programs are valuable, we feel that attached parallels should complement the observing programs. That is, if the observers are doing mainly broad band imaging with long integration times (~10 minutes), the attached program should do a grism survey, otherwise it should do imaging.

The motivations behind these surveys are briefly:

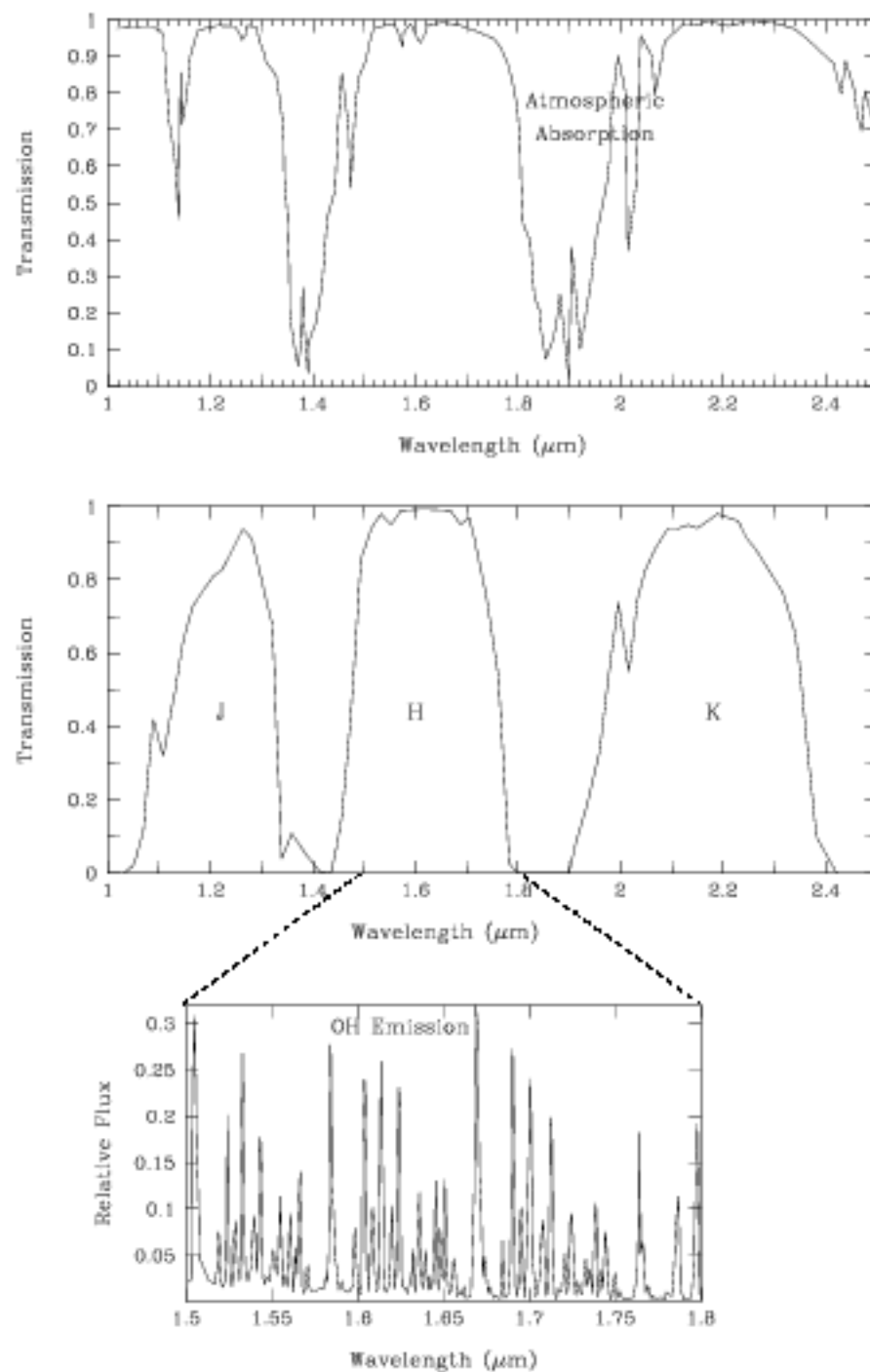
- Extragalactic: This survey is designed to acquire statistics on the numbers and colors of faint galaxies. Morphological classification will certainly be possible with Cameras 1 and 2 and often possible with Camera 3. The grism program will identify high redshift objects from their emission lines. The inclusion of Camera 1 will permit higher resolution observations of a small number of galaxies but is the lowest priority component of this survey.
- Galactic Clouds: This survey is predicated on the assumption that a significant fraction of the in-plane targets will be in highly obscured regions where the identification of and morphological information on strong FeII and H<sub>2</sub> sources will be possible. When sufficiently long pointings are available, three color imaging to detect very red sources would be carried out.
- Galactic Plane: This survey will acquire statistics on the faint low mass stellar populations in our galaxy. Generally three colors are desirable so the Camera 1 observations may be of limited value.

## The Infrared Background

From the ground, the infrared background is affected by telluric absorption and emission which limits the depth of astronomical imaging. As is well known, between 1 and 2.5 microns there are a number of deep molecular absorption bands in the atmosphere (top panel of Figure 3.5), and the bandpasses of the conventional near-IR bands of JHK were designed to sit in the gaps between these opaque regions (middle panel of Figure 3.5). Unfortunately, outside the absorption features there is also considerable background emission in both lines and continuum. Most of the background between 1 and 2 microns comes from OH and O<sub>2</sub> emission produced in a layer of the atmosphere at an altitude ~ 87 km (bottom panel of Figure 3.5).



**Figure 3.5: Atmospheric Absorption and Emission Line Spectrum in NICMOS Operational Range**



The location of HST above the atmosphere removes these terrestrial effects from the background. Now, the dominant sources of background radiation will be

the zodiacal light at short wavelengths and the thermal background emission from the telescope at long wavelengths. The sum of these two components will be a minimum at 1.6 microns (roughly the H band). All three NICMOS cameras carry broad-band filters which are centered on this spectral range.

At the shorter wavelengths, sensitivities will be affected by the zodiacal background which is, of course, strongly spatially dependent (see Table 3.5). Observations by the COBE satellite have implied that at positions 45 degrees out of the ecliptic the zodiacal background can be approximated as:

$$1.01 \times 10^9 / \lambda^{1.09} + 6 \times 10^{-8} B_{\lambda}(\lambda, T) \text{ photons cm}^{-2} \mu\text{m}^{-1} \text{ steradian}^{-1}$$

Where  $\lambda$  is the wavelength in  $\mu\text{m}$  and  $B_{\lambda}$  is the blackbody function for the zodiacal dust temperature  $T$  (roughly 265 K).

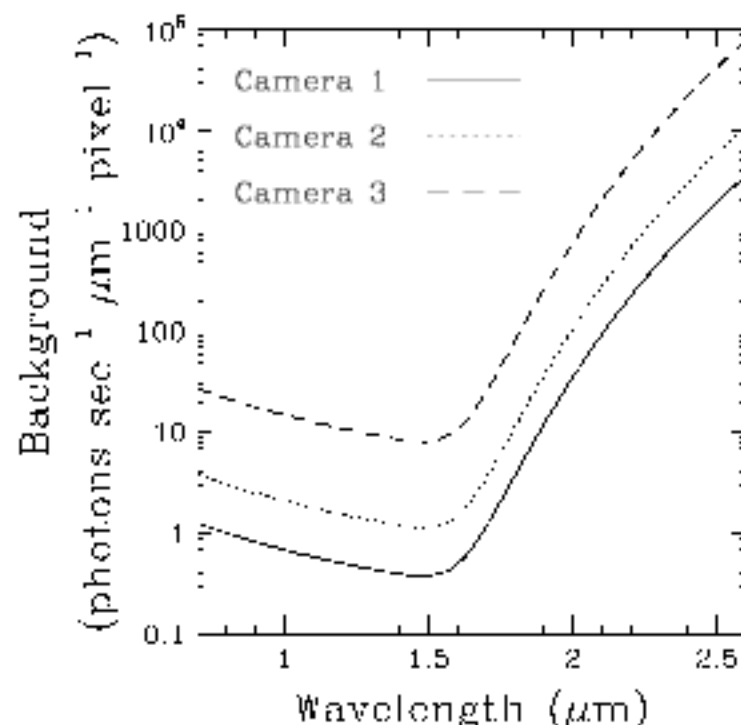
**Table 3.5:** Sky Brightness ( $V \text{ mag arcsec}^{-2}$ ) as a Function of Heliocentric Ecliptic Latitude and Longitude. "SA" denotes that the target is unobservable due to solar avoidance.

Heliocentric Ecliptic Longitude	Ecliptic Latitude						
	0°	15°	30°	45°	60°	75°	90°
180°	22.1	22.4	22.7	23.0	23.2	23.4	23.3
165°	22.3	22.5	22.8	23.0	23.2	23.4	23.3
150°	22.4	22.6	22.9	23.1	23.3	23.4	23.3
135°	22.4	22.6	22.9	23.2	23.3	23.4	23.3
120°	22.4	22.6	22.9	23.2	23.3	23.3	23.3
105°	22.2	22.5	22.9	23.1	23.3	23.3	23.3
90°	22.0	22.3	22.7	23.0	23.2	23.3	23.3
75°	21.7	22.2	22.6	22.9	23.1	23.2	23.3
60°	21.3	21.9	22.4	22.7	23.0	23.2	23.3
45°	SA	SA	22.1	22.5	22.9	23.1	23.3
30°	SA	SA	SA	22.3	22.7	23.1	23.3
15°	SA	SA	SA	SA	22.6	23.0	23.3
0°	SA	SA	SA	SA	22.6	23.0	23.3

At wavelengths longer than 1.6 microns the thermal background of the telescope rises and may have to be removed by obtaining off-source images. By using filtering techniques such as median filtering any contaminating sources in these offset fields can be removed in a composite background frame which can then be subtracted from the data.

Figure 3.6 shows the HST background for each of the three cameras (the solid line represents Camera 1, the dotted line represents Camera 2, the dashed line represents Camera 3) as a function of wavelength. This background has been calculated assuming a zodiacal light contribution consistent with the mean observed by COBE for an ecliptic latitude of 45°, and also includes thermal emission by the HST primary and secondary mirrors, with an assumed 20% emissivity (the actual emissivities of the HST mirrors are not yet known, but are likely to be lower than this), and the transmission of all the NICMOS fore-optics. It does not include the transmission of any filter, nor the response of the detectors.

Figure 3.6: HST Background for Each Camera



We will make direct observations to measure and establish the stability of the thermal contribution to the background during SMOV and early in Cycle 7. We expect to hold off from our planning and scheduling of Cycle 7 proposals that use the long wavelength region of NLCMOS until after we have measured the background and know how to correct for it.

For pointings very close to the Earth, the zodiacal background may be exceeded by the earthshine. The brightness of the earthshine falls very rapidly with increasing angle from the Earth's limb, and for most observations only a few minutes at the beginning and end of the target visibility period will be significantly affected. The major exception to this behavior is a target in the continuous viewing zone (CVZ). Such a target will always be rather close to the Earth's limb, and so will always see an elevated background (at the shorter wavelengths where zodiacal emission would ordinarily dominate). For targets faint enough that the background level is expected to be much brighter than the target, the observer is recommended to specify the *LOW-SKY* option. This will increase the minimum allowed Earth avoidance angle, requiring scheduling during a time for which the zodiacal background is no greater than 30%, above the minimum achievable level at the cost of a slight decrease of the available observing (visibility) time during each orbit. Note that this restriction is only helpful when observations are background limited.

## Conversion Between Fluxes and Magnitudes

Throughout the NICMOS documentation we will frequently use flux units of Janskys (Jy). A detailed discussion of the conversion between various units and Janskys is given in Chapter 12. Here we summarize the central wavelengths and zero-point fluxes for the more commonly encountered photometric bands in Table 3.6.

**Table 3.6:** Effective Wavelengths and Zero-points for Photometric Bands

Band	$\lambda$ [ $\mu$ m]	$F_0$ [Jy](CIT)	$F_0$ [Jy](UKIRT)
V	0.56	3540	3540
R	0.70	2870	-
I	0.90	2250	-
J	1.25	1670	1600
H	1.65	980	1020
K	2.2	620	657
L	3.4	280	290
L'	3.74	-	252
M	4.8	150	163
N	10.1	37	39.8
Q	20.0	10	10.4

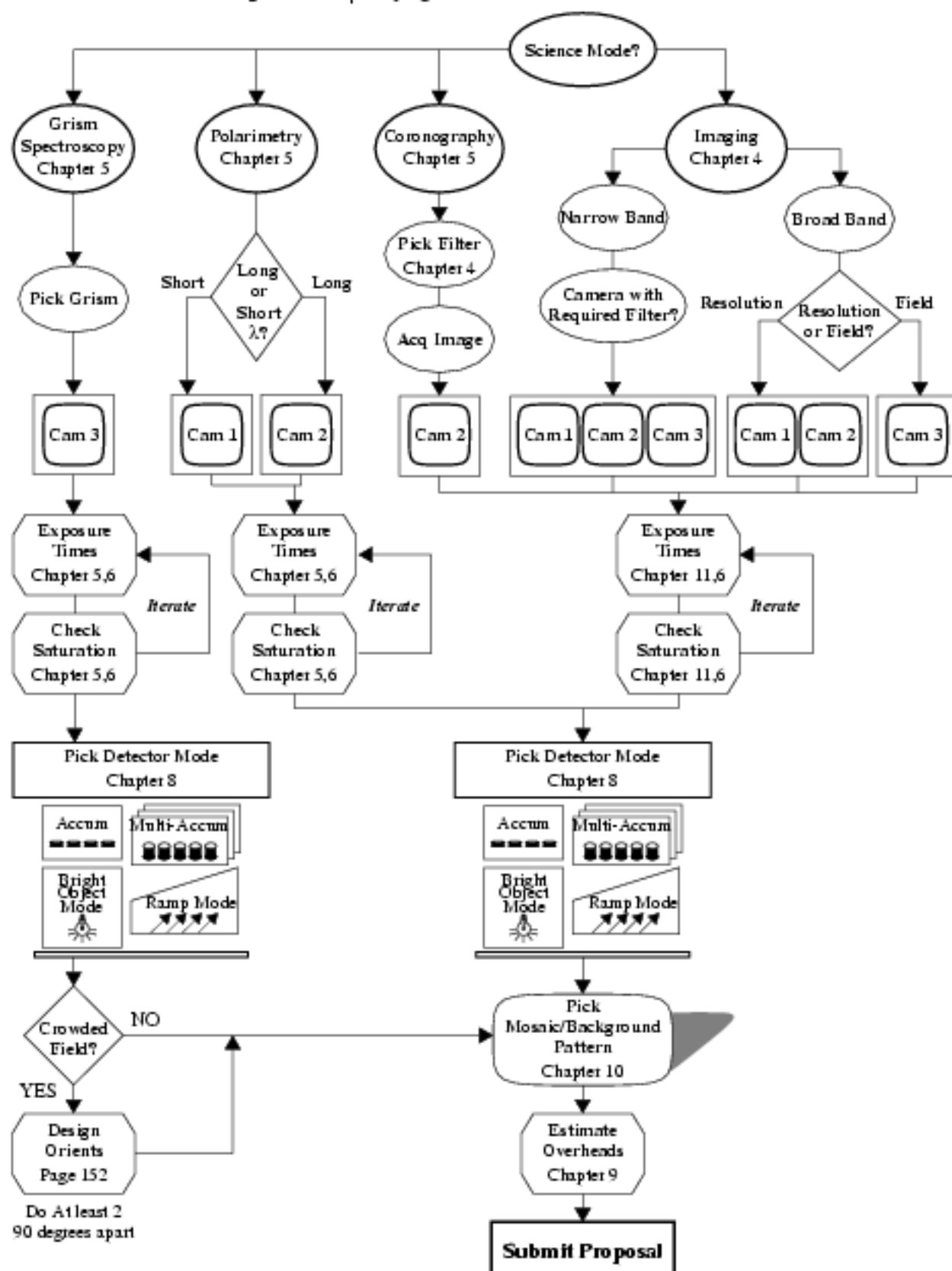
## Designing NICMOS Observations

In the preceding sections, we provided you with an overview of the scientific capabilities of NICMOS and the basic layout and operation of the instrument. Subsequent chapters will provide detailed information about the performance and operation of the instrument. In this section, we describe the conceptual steps you will need to take when designing a NICMOS observing proposal. The basic sequence of steps in defining a NICMOS observation are shown in flow diagram form in Figure 3.7, and are:

- Identify your science requirements and select the basic NICMOS configuration to support those requirements (e.g., imaging, polarimetry, coronagraphy). Refer to the detailed accounts given in Chapter 4 and Chapter 5.
- Select the wavelength region of interest and hence determine if your observations will be Background or Read-Noise limited, see Chapters 4, 6, and 11.
- Establish which detector readout mode you need to use. Detailed descriptions of these are provided in Chapter 8.

- Estimate the exposure time to achieve the required signal to noise ratio and check feasibility (i.e., saturation and bright object limits). To determine your exposure time requirements and assess whether you are close to the brightness and dynamic range limitations of the detectors, refer to the information provided graphically in Chapter 11 for each filter and camera combination.
- If necessary choose a chop and dithering pattern either to measure the background or to enable mapping of areas bigger than the field of view of the NICMOS cameras you plan to use. See Chapter 10.
- If you are doing coronagraphic observations, additional target acquisition exposures will be required to center your target in the aperture to the accuracy required for your scientific aims (e.g., you may wish to center the nucleus of a galaxy in a crowded field behind the coronagraphic spot).
- Calculate the total number of orbits required, taking into account the overheads. In this, the final step, you combine all your exposures (science and non-science, alike) into orbits, using tabulated overheads, and determine the total number of orbits you require. Refer to Chapter 9 when performing this step.

Figure 3.7: Specifying a NICMOS Observation



## CHAPTER 4

# Imaging

### In This Chapter...

Available Filters & Optical Elements /	35
Filter Sensitivity Curves /	42
Out-of-Band Leaks in NICMOS Filters /	44
Point Spread Function /	45
NICMOS Aperture Definitions /	48
NICMOS Coordinate System Conventions /	49
Orients /	49

This chapter provides the information needed to construct an imaging proposal. Filter transmission curves are presented. We have developed sensitivity curves and exclusion curves for each filter. These curves can be used to estimate exposure times. We give examples of how to use these curves, which are contained in full in Chapter 11. Instructions and examples for calculating exposure times and signal to noise ratios are provided in Chapter 6.

---

## Available Filters & Optical Elements

Each camera has 20 filter positions on a single filter wheel: 19 filters and one blank. As a result, not all filters are available in all cameras. Moreover, the specialized optical elements, such as the polarizers and grisms, cannot be crossed with other filters, and can only be used in fixed bands. In general the filters have been located in a way which best utilizes the characteristics of NICMOS, thus at shorter wavelengths the most important narrow band filters are located in Camera 1 so that the diffraction limited performance can be maintained wherever possible, while those in Camera 2 have been selected to work primarily in the longer wavelength range where it will also deliver diffraction limited imaging.

Table 4.1 through Table 4.3 list the available filters and provide an initial general description of each, starting with Camera 1 and working down in spatial resolution to Camera 3. Figure 4.1 through Figure 4.3 show the percentage transmission of each optical element plotted against wavelength.

## Nomenclature

The name of each optical element starts with a letter or group of letters identifying what kind of element it is: filters start with an “F”, grisms with a “G”, and polarizers with “POL”. Following the initial letter(s) is a number which in the case of filters identifies its approximate central wavelength in microns, e.g., F095M implies a central wavelength of 0.95 microns. A trailing letter identifies the filter width, with “W” for wide, “M” for medium and “N” for narrow. In the case of grisms, the initial “G” is followed by a number which gives the center of the free-spectral range of the element, e.g., G206. For the polarizers, a somewhat different notation is used, with the initial “POL” being followed by a number which gives the PA of the principal axis of the polarizer in degrees, and a trailing letter identifying the wavelength range it can be used in, which is either “S” for short (0.8–1.3 microns) or “L” for long (1.9–2.1 microns).

Figures 4.1, 4.2, and 4.3 show the transmission curves of all of the NICMOS filters for Cameras 1, 2, and 3, respectively. The wide, medium, and narrow bandwidth filters are plotted separately for each camera. Only the filter transmission is shown—the efficiency of other optical elements or the detectors has not been included. Different line styles have been used for the different filters only to help differentiate them.

Table 4.1: Camera 1 Filters

Name	Central Wavelength ( $\mu\text{m}$ )	Bandwidth ( $\mu\text{m}$ )	Comment	See also
Blank	N/A	N/A	blank	
F110M	1.025	0.8–1.35		page 166
F140M	1.3	0.8–1.8	Broad Band	page 170
F160M	1.55	1.35–1.75		page 174
F090M	0.9	0.8–1.0		page 156
F110M	1.1	1.0–1.2		page 164
F145M	1.45	1.35–1.55	Water	page 172
F165M	1.6	1.55–1.75		page 178
F170M	1.7	1.6–1.8		page 182
F095M	0.953	1%	[S III]	page 158
F097M	0.97	1%	[S III] continuum	page 160
F108M	1.083	1%	He I	page 162
F113M	1.13	1%	He I continuum	page 168
F164M	1.644	1%	[Fe II]	page 176
F166M	1.66	1%	[Fe II] continuum	page 180
F187M	1.87	1%	Paschen $\alpha$	page 184
F190M	1.90	1%	Paschen $\alpha$ continuum	page 186
POL0S	1.1	0.8–1.3	Short $\lambda$ Polarizer	page 59
POL120S	1.1	0.8–1.3	Short $\lambda$ Polarizer	page 59
POL240S	1.1	0.8–1.3	Short $\lambda$ Polarizer	page 59



Figure 4.1: Filters for Camera 1

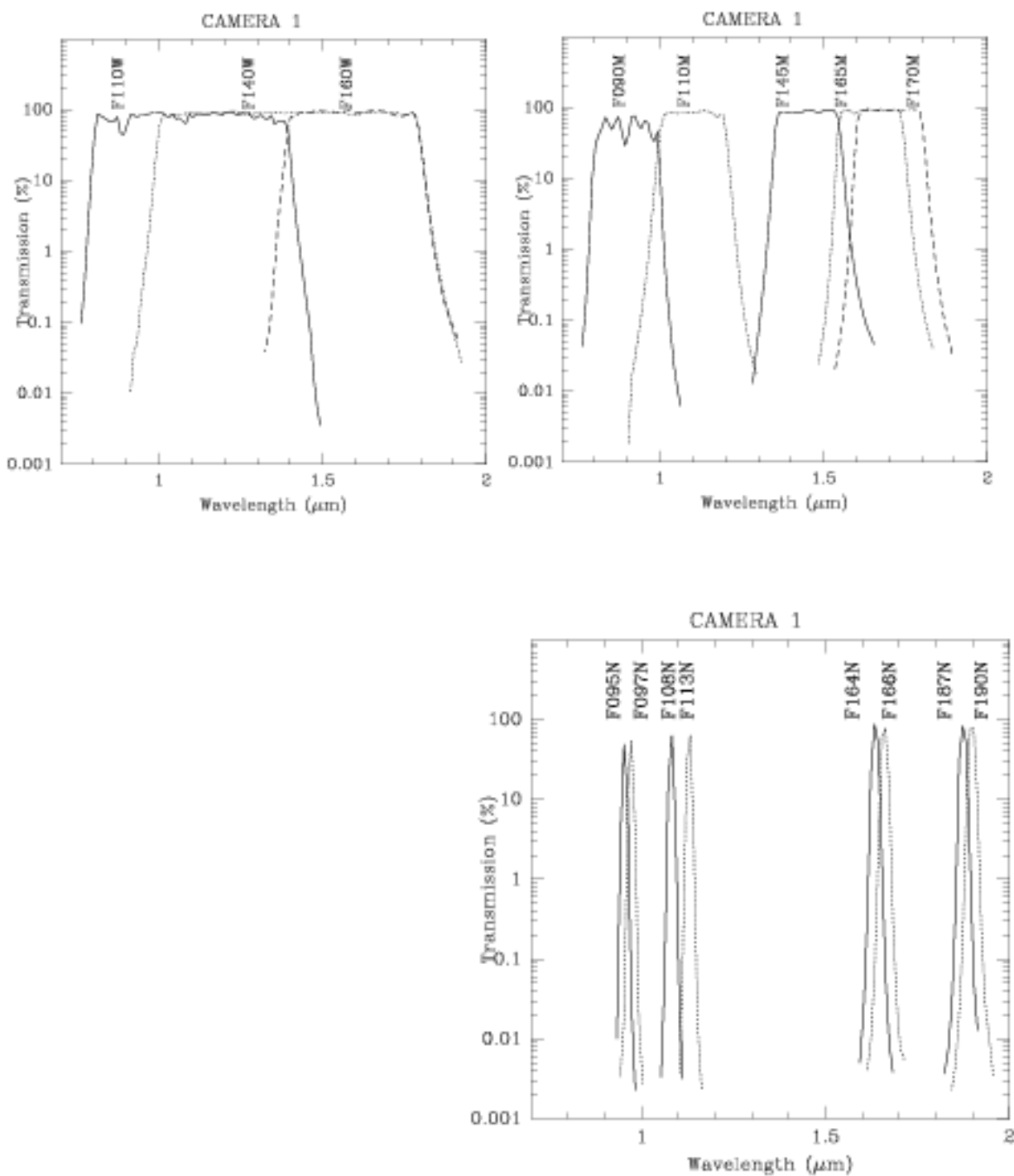


Table 4.2: Camera 2 Filters

Name	Central Wavelength ( $\mu\text{m}$ )	Bandwidth ( $\mu\text{m}$ )	Comment	See also
Blank	N/A	N/A	blank	
F110W	1.1	0.8–1.4		page 188
F160W	1.6	1.4–1.8	Minimum background	page 190
F187W	1.875	1.75–2.35	Broad	page 200
F205W	1.9	1.75–2.0	Broad Band	page 206
F165M	1.7	1.55–1.75	Planetary continuum	page 192
F171M	1.715	1.68–1.75	HCO <sub>2</sub> and C <sub>2</sub> continuum	page 194
F180M	1.80	1.765–1.835	HCO <sub>2</sub> and C <sub>2</sub> bands	page 196
F204M	2.04	1.9–2.09	Methane imaging	page 204
F207M	2.1	2.0–2.15		page 208
F222M	2.3	2.15–2.30	CO continuum	page 216
F237M	2.375	2.3–2.45	CO	page 218
F187H	1.87	1%	Paschen $\alpha$	page 198
F190H	1.9	1%	Paschen $\alpha$ continuum	page 202
F212H	2.121	1%	H <sub>2</sub>	page 210
F215H	2.15	1%	H <sub>2</sub> and Br $\gamma$ continuum	page 212
F216H	2.165	1%	Brackett $\gamma$	page 214
POL0L	2.05	1.9–2.1	Long $\lambda$ polarizer	page 59
POL120L	2.05	1.9–2.1	Long $\lambda$ polarizer	page 59
POL240L	2.05	1.9–2.1	Long $\lambda$ polarizer	page 59

Figure 4.2: Filters for Camera 2

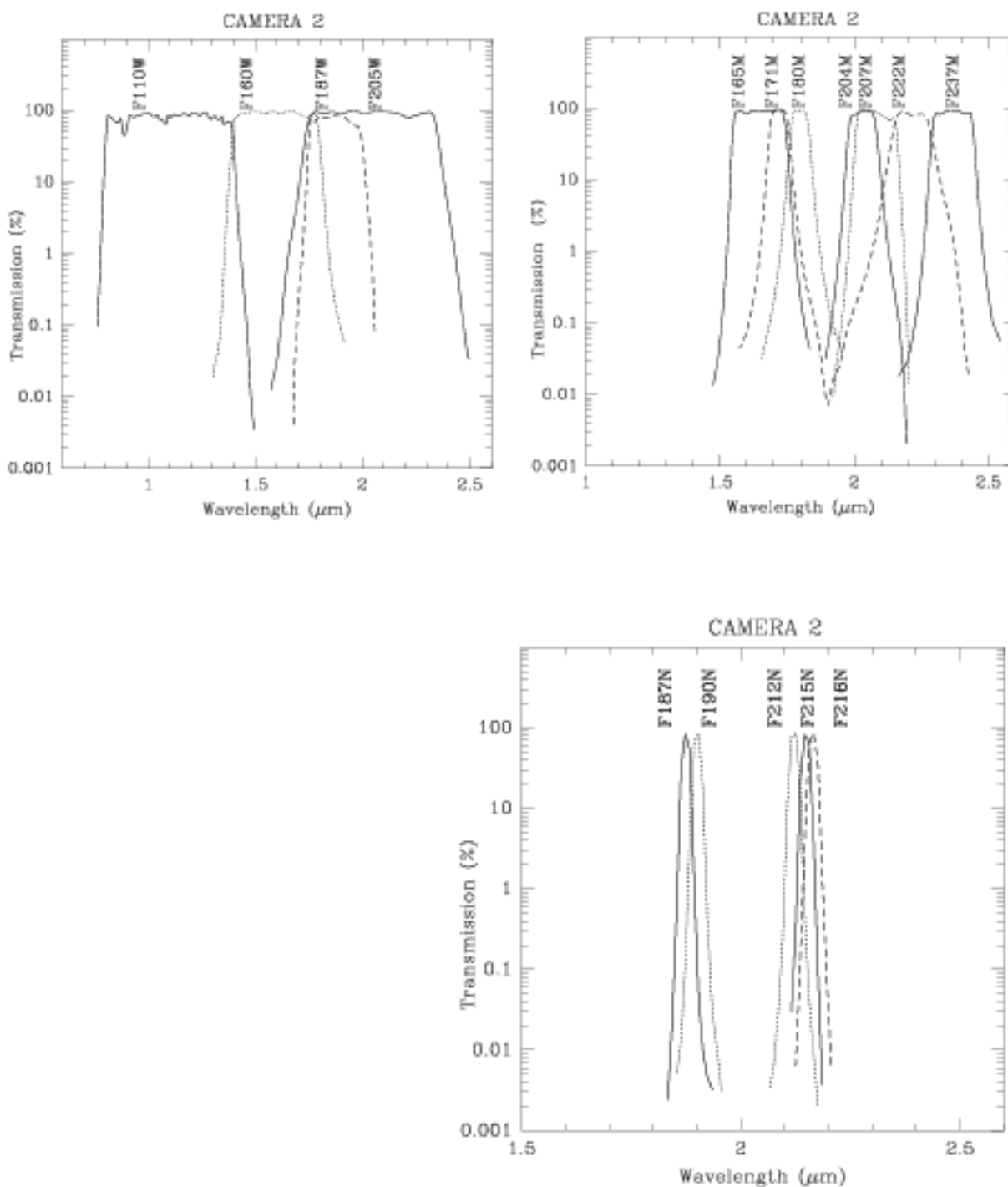
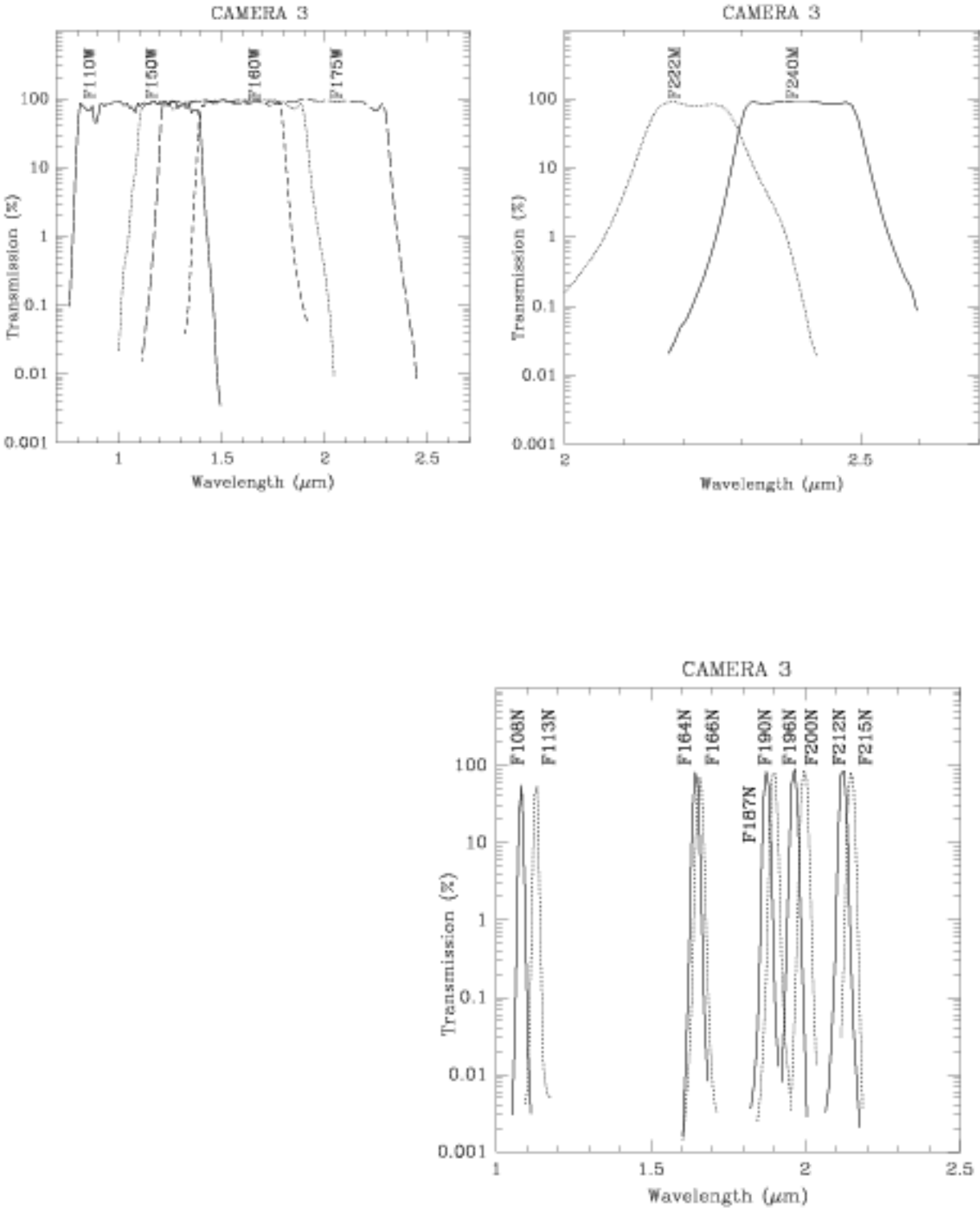


Table 4.3: Camera 3 Filters

Name	Central Wavelength ( $\mu\text{m}$ )	Bandwidth ( $\mu\text{m}$ )	Comment	See also
Blank	N/A	N/A	blank	
F110W	1.1	0.8–1.4		page 222
F160W	1.6	1.4–1.8	Minimum background	page 228
F175W	1.75	1.2–2.3		page 234
F222M	2.3	2.15–2.3	CO continuum	page 248
F240M	2.4	2.3–2.5	CO band	page 250
F10811	1.0830	1%	He I	page 230
F11311	1.13	1%	He I continuum	page 234
F16411	1.644	1%	[Fe II]	page 230
F16611	1.66	1%	[Fe II] continuum	page 232
F18711	1.875	1%	Paschen $\alpha$	page 236
F19011	1.9	1%	Paschen $\alpha$ continuum	page 238
F19611	1.962	1%	[Si VI]	page 240
F20011	2.0	1%	[Si VI] continuum	page 242
F21211	2.121	1%	H <sub>2</sub>	page 244
F21511	2.15	1%	H <sub>2</sub> continuum	page 246
F150W	1.5	1.1–1.9	Grism B continuum	page 226
G096	0.9673	0.8–1.2	GRISM A	page 69
G141	1.414	1.1–1.9	GRISM B	page 71
G206	2.067	1.4–2.5	GRISM C	page 73

Figure 4.3: Filters for Camera 3



## Filter Sensitivity Curves

Detailed information for each filter (Chapter 11) and for the grisms and polarizers (Chapter 5) is provided in the format shown in Figure 4.4. In this section we explain this format and outline the use of these Figures. For many purposes, these Figures may take the place of detailed calculations and permit observers to quickly determine the feasibility or appropriateness of an observation.

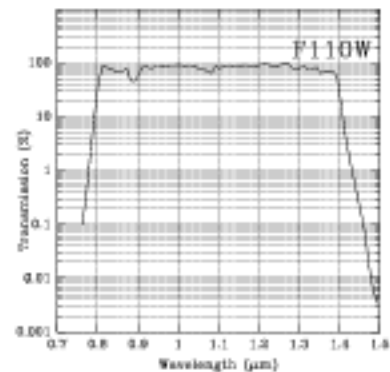
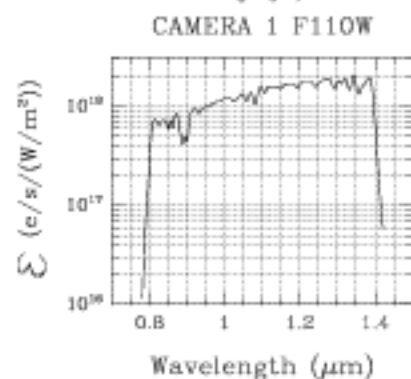
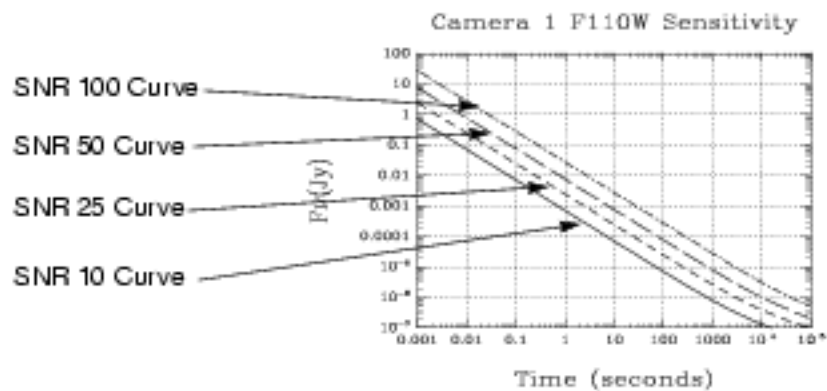
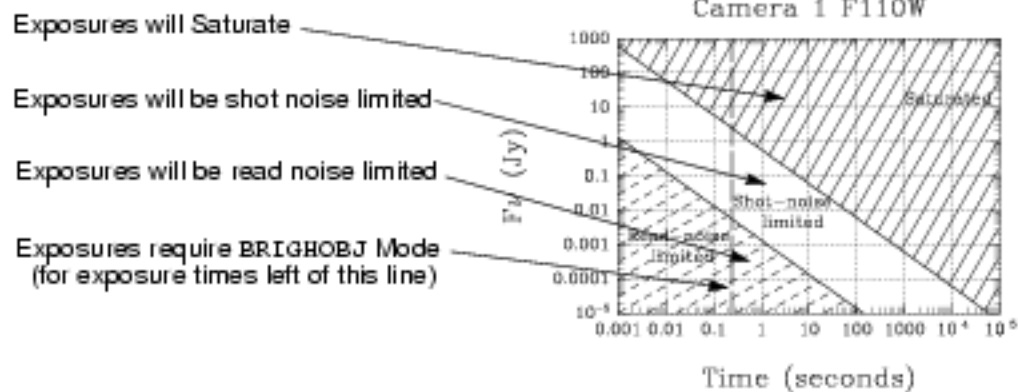


Caution: These Figures are based on preliminary *estimates* of the NICMOS sensitivities, noise characteristics, and backgrounds.

Each figure provides the following:

- A *summary* of the basic filter parameters:
  - Central wavelength
  - Mean wavelength
  - Peak wavelength
  - Full Width at Half Maximum transmission (FWHM)
  - Spectral range
  - Maximum transmission
  - Fraction of light falling on the central pixel for a point source centered on the pixel.
- A *filter transmission curve*. The spectral characteristics of the NICMOS flight filters were measured at cryogenic temperature and normal incidence at Ball Aerospace. All filters had their spectral transmission measured from 0.5 to 2.7 microns with a step size of 0.001 microns.
- An *epsilon diagram*. For each filter we have calculated  $\epsilon(\lambda)$  to permit simple determination of the response of NICMOS to a monochromatic emission line within the filter's useful bandpass. This single parameter encompasses the wavelength dependent DQE, filter transmission, mirror reflectivities (including both the NICMOS fore-optics and the HST primary and secondary mirrors), and dewar window transmission. This parameter is calculated in units of  $e^- s^{-1} (W m^{-2})^{-1} pixel^{-1}$ . Given a line flux in  $W m^{-2}$ , the flux per pixel can be determined using the pixel fraction for point sources or the pixel area for extended sources. Then the  $\epsilon(\lambda)$  parameter provides the count rate in  $e^- s^{-1}$ . Additional discussion and examples of this calculation are provided in Chapter 6.
- *Sensitivity curves for point and extended sources*. These present spectral flux density ( $F_\nu$ ) as a function of time to achieve a signal to noise ratio (S/N) of 10, 25, 50, and 100 (solid, short dash, long dash, and dot-dash lines, respectively). These curves incorporate the expected backgrounds and

Figure 4.4: Example Sensitivity and Exclusion Curves

*Filter Transmission Curve**Epsilon Diagram**Sensitivity Curves**Observational Exclusion Diagrams*

presently understood noise characteristics of the detectors. To use these plots select a camera and filter combination, locate the flux of your source and read across the figure to determine the exposure time for a given S/N.

- *Observational exclusion diagrams* for point and extended sources. These again show flux ( $F_{\nu}$ ) as a function of time. The useful limits of the instrument are shown. Sources falling in the upper right hand region will be saturated (see the discussion of MULTIACCUM mode to observe both bright and fainter sources in the same exposure). Sources falling in the lower left region of the plot will be read noise rather than shot noise limited. Finally, sources to the left of the vertical dashed line at 0.23 seconds must be observed using the BRIGHTOBJ mode.

---

## Out-of-Band Leaks in NICMOS Filters

In order to make use of the high spatial resolution of HST, many observers will wish to use NICMOS to observe very red objects (e.g., protostars) at relatively short wavelengths. By their very nature, these very red objects have very low effective color temperatures. Thus if we observe such an object at a wavelength of 1.0 microns, we can expect that its flux at 2.5 microns will be orders of magnitude larger than its flux at the desired wavelength. In such a case, exceptionally good out-of-band blocking is required from the filter. We have therefore investigated whether the measured filter transmissions would allow any sources with extreme colors to yield erroneous photometry due to out-of-band leaks.

We have calculated the effects of filter leaks for sources with color temperatures from 700K to 10,000K. At this juncture we note that the reddest of the kinds of sources likely to be observed with NICMOS may have color temperatures lower than 400K, while the bluest sources (probably reflection nebulae) can be significantly bluer than a 10,000K blackbody. We find that significant leaks may occur for nine of the filters. No photometric errors as large as 1% were found for any filters using the hottest (i.e., 10,000K) spectrum (however, as noted above some reflection nebulae may have bluer spectra than this, and we cannot rule out the possibility of errors as large as a few percent in this case, for a few filters). For the reddest source considered here (with a color temperature of 700K), the photometric errors might be as large as an order of magnitude in a few filters. There are still some uncertainties regarding the measured transmission curves, and so the information presented here should be regarded only as cautionary. We will release further information as soon as it becomes available, but this is not likely to be before the Cycle 7 Phase 1 deadline.

The nine filters for which these leaks might be a problem are: F090M, F095H, F097H, F108H, F110M, F110W, F113H, F187H, F190H. We recommend that observers using these filters for sources with extremely red colors observe them in a number of filters to minimize the likelihood of filter leaks causing errors.



## Point Spread Function

### Encircled Energy Predictions

The NICMOS I DT have provided *predictions* of the expected encircled energy in the J, H, and K bands (see Figure 4.5). These predictions show that ~90% of the energy will be contained within radii of 0.23, 0.30, and 0.40 arcsecs at wavelengths of 1.25, 1.65, and 2.2 microns, respectively. Using these curves and the present FOC PSF, we estimate in Table 4.4 the fraction of the energy from a point source falling in the central pixel (Pixel Frac.; assuming the PSF to be centered on that pixel) and the area on the detector (in pixels) which encompasses 90% of the energy (Area Pixels).

Table 4.4: Encircled Energy Fractions and Areas in Pixels

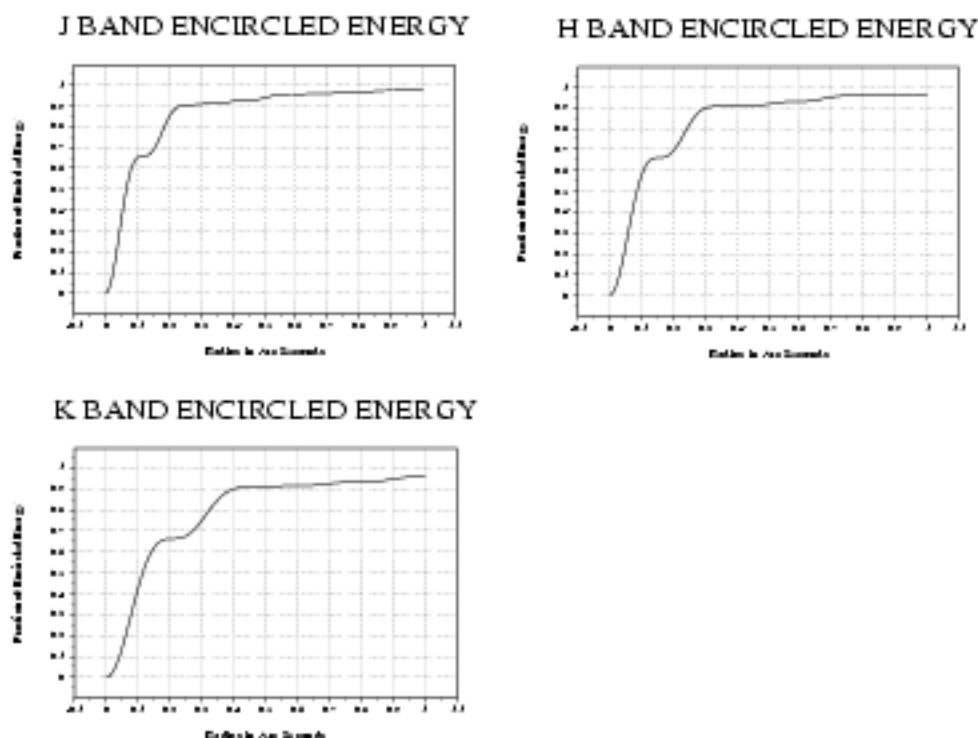
Filter	Camera 1		Camera 2		Camera 3	
	Pixel Frac.	Area Pixels	Pixel Frac.	Area Pixels	Pixel Frac.	Area Pixels
F090M	0.200	49.5				
F095M	0.210	54.8				
F097M	0.220	56.7				
F108M	0.210	68.8			0.840	3.2
F110M	0.160	71.1				
F110M	0.160	70.8	0.340	23.3	0.660	3.3
F113M	0.140	74.5			0.830	3.4
F140M	0.140	110.9				
F145M	0.070	119.3				
F150M					0.780	5.9
F160M	0.070	143.3	0.190	47.0	0.620	6.6
F164M	0.067	150.3			0.760	7.0
F165M	0.081	151.8	0.190	50.0		
F166M	0.069	154.8			0.750	7.1
F170M	0.077	162.6				
F171M			0.200	54.6		
F175M					0.710	8.0
F180M			0.110	59.4		
F187M	0.062	196.9	0.180	64.6	0.710	9.1

Table 4.4: Encircled Energy Fractions and Areas in Pixels (Continued)

Filter	Camera 1		Camera 2		Camera 3	
	Pixel Frac.	Area Pixels	Pixel Frac.	Area Pixels	Pixel Frac.	Area Pixels
F18.7M			0.180	64.5		
F19.0M	0.055	201.9	0.170	66.5	0.700	9.3
F19.6M					0.710	10.0
F20.0M					0.710	10.3
F20.4M			0.170	76.0		
F20.5M			0.180	76.9		
F20.7M			0.110	79.9		
F21.2M			0.140	83.0	0.630	11.7
F21.5M			0.140	85.2	0.620	12.0
F21.6M			0.140	86.4		
F22.3M			0.140	90.7	0.550	12.8
F23.7M			0.120	103.9		
F24.0M					0.490	15.0

The following plots show the predicted encircled energy fraction vs. angular radius under the simplification of a monochromatic wavelength at the center of the J, H, and K bands. These plots should be useful in calculating the amount of flux in any pixel, and are the best available at this time.

Figure 4.5: Predicted Encircled Energy



## Field Dependence

The PSF is at least to some extent a function of position in the OTA field of view. We do not know by how much the PSF will be degraded near the edges of the fields of view of the three cameras. However, our expectation is that only a small degradation will be observed. Movement of the FOM, on the other hand, is expected to have a significant effect on the PSF quality. Since we do not expect to make FOM motions available to the GO community in Cycle 7, we will not discuss the size of this effect at this time.

## NICMOS Aperture Definitions

Each HST Science Instrument requires its own local coordinate system and apertures to support both target acquisition and small angle motions (SAMs). Apertures are calibrated locations in the HST focal plane relative to the FGS frame. All acquisitions and SAMs are relative to apertures. Any location within the field of view of a NICMOS camera can be specified by the POSTARG special requirement (described in the HST Phase II Proposal Instructions).

### Aperture Definitions

The basic philosophy of the NICMOS aperture definitions follows that used by WF/PC-1 and WFPC2. Each NICMOS camera has two primary apertures. One is positioned at the geometric center of the detector and the other at an *optimal* position close to the center. The first of these apertures is anchored to that fixed location, while the second may be moved in the future. In this way the optimal aperture may be shifted to avoid array defects, even if these are time dependent. Observers with large targets which fill the field of view of a particular camera are generally advised to use the first type of aperture, while for observers with smaller targets the second type is recommended.

Additional apertures are defined in Camera 2 for use in the Mode 2 coronagraphic acquisition.

#### Standard Apertures

The names of the defined apertures are listed in Table 4.5 along with a description of their function and their initial location.

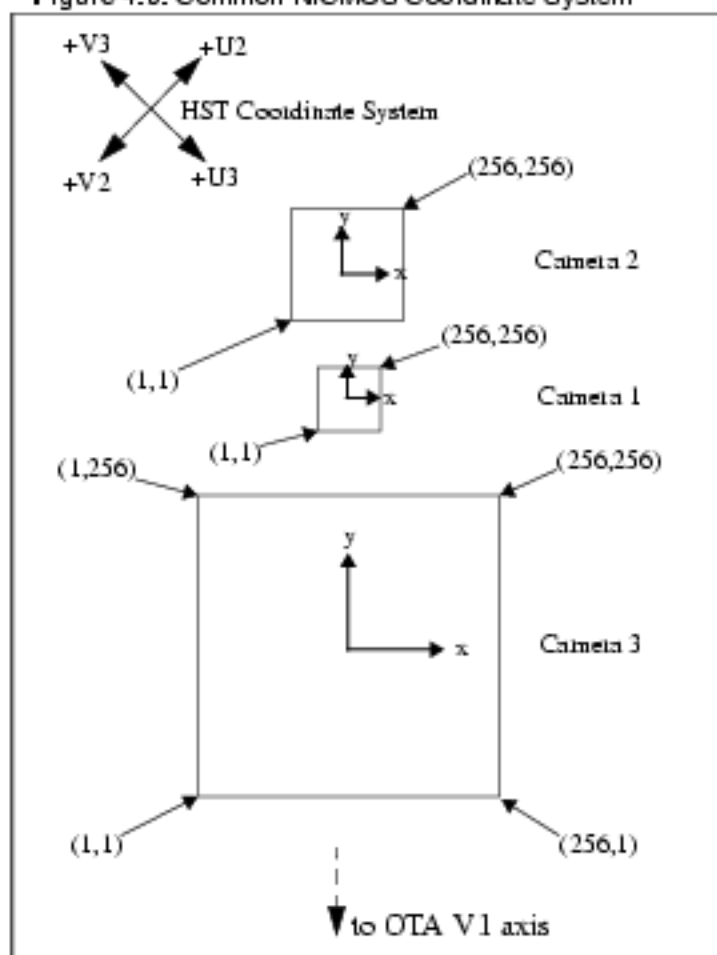
Table 4.5: NICMOS Aperture Definition

Aperture Name	Description	Position (detector pixels)
NIC1	Optimal center of Camera 1	128,128
NIC1-FIX	Geometric center of Camera 1	128,128
NIC2	Optimal center of Camera 2	128,128
NIC2-FIX	Geometric center of Camera 2	128,128
NIC2-CORON	Center of Coronagraphic Mask	
NIC2-ACQ	Center of Mode 2 ACQ region	
NIC3	Optimal center of Camera 3	128,128
NIC3-FIX	Geometric center of Camera 3	128,128

## NICMOS Coordinate System Conventions

Figure 4.7 shows how the NICMOS cameras are arranged in the HST field of view. The alignment of each camera is not exact, and the internal coordinate systems attached to each of them will differ by small rotations (probably  $<2$  degrees). The FITS format data files generated for NICMOS observers will have a World Coordinate System specified appropriately for each camera. The adopted coordinate system for the 3 cameras is summarized in Figure 4.6.

Figure 4.6: Common NICMOS Coordinate System

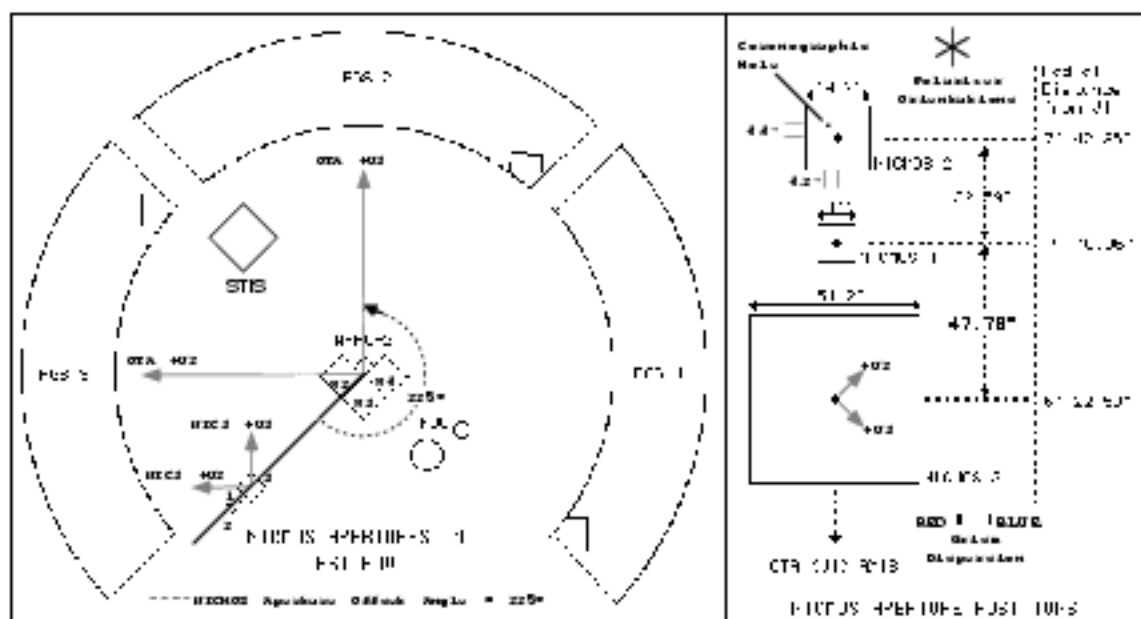


## Orients

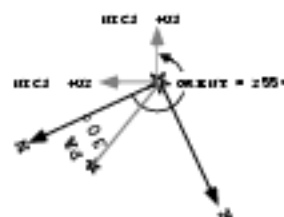
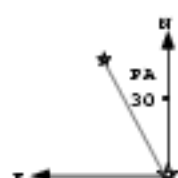
NICMOS orientations are specified relative to the  $+y$  axis shown in Figure 4.6. Eastward rotations are counterclockwise (in the usual astronomical convention). Spacecraft orientations are rotated by 225 degrees from the NICMOS coordinate system.

Due to the linear arrangement of the 3 NICMOS cameras on the sky, it will often be advantageous to consider the specification of a unique telescope orientation. Observers should be aware that such constraints may decrease the duration and number of scheduling opportunities for their observations and, under some circumstances, may make the identification of suitable guide stars impossible.

Figure 4.7: Definition of Orient for NICMOS



Example: Binary Star; PA = 30°



While the Phase II proposal instructions will contain the definitive instructions and examples for specifying the desired orientation for HST. A simple example is shown in Figure 4.7. A binary star with a position angle (PA) 30 degrees measured east from north is to be positioned with the southern star in Camera 3 and the northern star in Camera 2. That is, we want the line connecting the two stars to lie along the NICMOS +y axis. The resulting HST orientation is  $225 + 30 = 255$  degrees. (HST ORIENT = PA + 225 for NICMOS).

## CHAPTER 5

# Coronagraphy, Polarimetry and Grism Spectroscopy

### In This Chapter...

Coronagraphy /	51
Polarimetry /	56
Polarimetric Sensitivity /	59
Grism Spectroscopy /	64
Sensitivity /	68

This chapter provides information on several specialized uses of NICMOS, namely, coronagraphy, polarimetry, and grism spectroscopy. Both the polarimetry and grism spectroscopy sections contain sensitivity and exclusion curves of the type described in Chapter 4 to enable you to estimate exposure times.

---

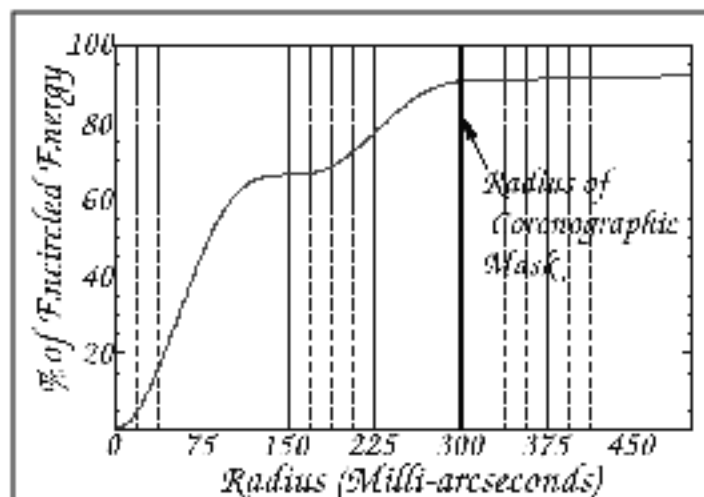
## Coronagraphy

A coronagraphic imaging mode is available in NIC2. This camera has 0.075 arcsec pixels, covering a 19.2 x 19.2 arcsec region of the sky. The coronagraphic spot imaged onto the focal plane provides a circular occulted region 0.3 arcsec in radius. At this radius, in an idealized Point Spread Function, a natural break occurs in the encircled energy profile at 1.6 microns with 93 percent of the energy in the PSF being enclosed (see Figure 5.1). Beyond, the encircled energy profile flattens out toward larger radii. The sky background is expected to be a minimum near 1.6 microns.

The Camera 2 coronagraph comprises two elements. A 170 micron diameter hole has been laser ablated out of the Camera 2 mirror in the NICMOS field

divider assembly, which is at the image plane. (Small irregularities within a 10 microns annulus at the edge of the hole may be a source of residual scattered light in the images.) An oversized cryogenic pupil-plane mask screens out residual radiation from the edges of the HST primary and secondary mirrors and the secondary mirror support structures (pads, spider, and mounts.). This mask obscures approximately 15% of the primary mirror area. (Scattering by dust on the primary mirror may affect the overall image contrast, and while this is expected to be a small effect it can only be quantified on-orbit.)

Figure 5.1: Relationship Between the Radius of the Coronagraphic Spot and the Encircled Energy in the HST PSF at 1.6 microns



## Coronagraphic Acquisitions

Coronagraphic imaging requires an acquisition sequence at the beginning of the observation to center the target onto the occulting spot since the size of the occulting spot is smaller than typical HST blind-pointing errors. The procedure for a coronagraphic observation is to first acquire the target on the NIC2-ACQ aperture using an onboard, reuse target offset, or interactive acquisition.

The science exposures are then specified using any of the NICMOS observing modes with the target positioned on the NIC2-CORON aperture (which is behind the coronagraphic spot).

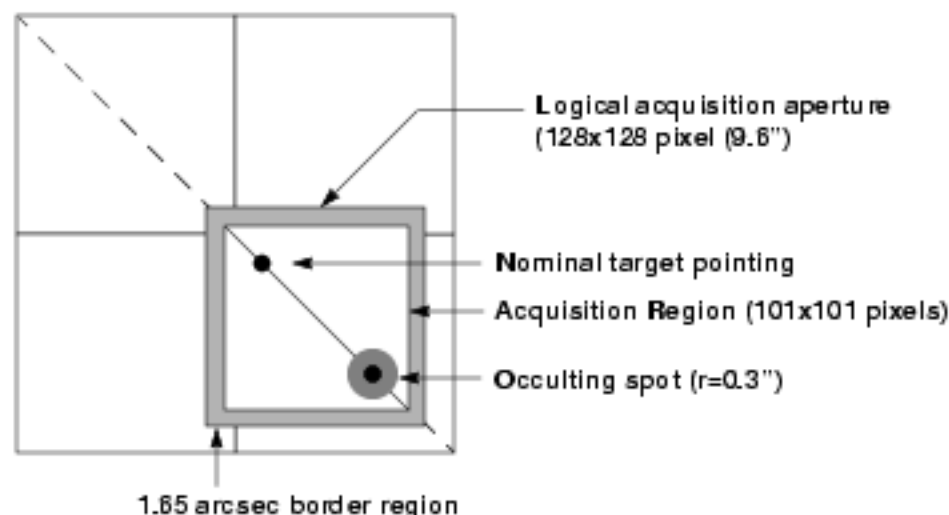
### Onboard Acquisition (ACQ mode)

The NICMOS flight software includes an automatic target acquisition mode. A coronagraphic acquisition is requested through the proposal interface (exposure logsheet), as an ACQ exposure using the NIC2-ACQ aperture as described in the NICMOS Phase II Proposal Instructions. In this process, after pointing to the field and acquiring guide stars, two images of the target are taken (for cosmic ray removal), and the brightest object is located in a 128 x 128 pixel sub-array in the coronagraphic acquisition aperture (see Chapter 8). The NICMOS flight software will then request a vehicle slew to move the spacecraft to place this object in the



center of the occulting spot. This is illustrated in Figure 5.2 which shows a schematic representation of the Camera 2 acquisition aperture. The observer must select the filter type and the exposure time (see the flow chart in Figure 5.4). The telescope is pointed so that the target nominally appears at the aperture **NIC2-ACQ** which is located in a  $128 \times 128$  logical acquisition aperture. The acquisition software, analyzes this aperture, locates the center of the target, and offsets the telescope so that the target is placed behind the occulting spot.

Figure 5.2: Acquisition Process



Very bright targets might cause saturation, leading to poor results in the centroid solution, and in the subsequent placement behind the occulting spot. To avoid this, a narrow band filter may have to be used to cut down the target flux. Since the NCMOS filters are in the pupil plane there should not be a shift introduced by using a different filter than needed for the science observations.



For observations longer than ~5 minutes the probability of cosmic ray hits occurring in the same pixel in each of the two acquisition images is sufficiently high that observers must instead use an early acquisition image to avoid their observation failing due to a false center determination. Early acquisitions are described in the next section. In practice, this should not be a severe restriction as in the **F160W** filter one will reach a signal-to-noise of 50 at  $H=17$  in only 2–3 minutes.

## Reuse Target Offset and Interactive Acquisitions

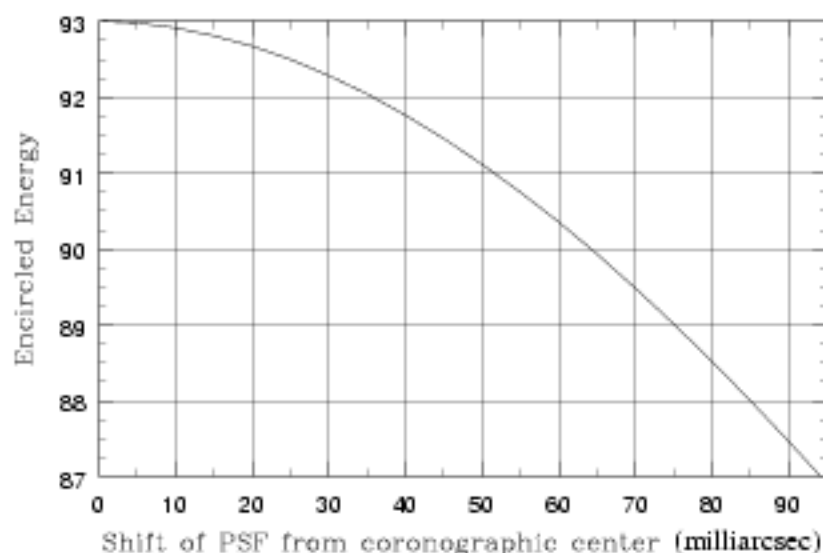
In crowded fields, or for extended objects, the coronagraphic acquisition should not be relied on, since by necessity the on-board centering algorithm is rather simple. Whenever you know *a priori* that this is the situation, or the complexity of the field is unknown, we recommend obtaining an acquisition image before the scientific observation instead, even though this will require

slightly more HST observations to accomplish your program. The telescope control system has the ability to re-use the same pair of guide stars as were used for the acquisition exposure, and from the accurate coordinates you have obtained, it is then possible to blind-offset the source onto the coronagraphic spot (RE-USE TARGET OFFSET). This can be obtained a few orbits or days prior to the science exposure. Alternatively, a real-time, interactive acquisition (INT-ACQ) can be obtained although the number of these are limited and must be justified in the Phase 1 proposal. This will mainly be necessary for time critical observations.

## PSF Centering

Both the total encircled energy rejection (from the occulted core of the PSF) and the local contrast ratio obtainable in a coronagraphic image depend on the accuracy of the target centering on the occulting spot. The goal is to center the PSF of the occulted source to a precision of a quarter pixel. The decrease in the fractional encircled energy due to imprecise centering of the core of an idealized PSF in the occulting spot is 0.3 percent for a 1/4 pixel offset, and 4.4 percent for a 1 pixel (75 milliarcsecs) offset at 1.6 microns. The fractional decrease in the encircled energy relative to that for a perfectly centered PSF is plotted against the shift of the center of the PSF from the center of the hole in Figure 5.3.

Figure 5.3: Contrast Decrease Due to PSF De-centering

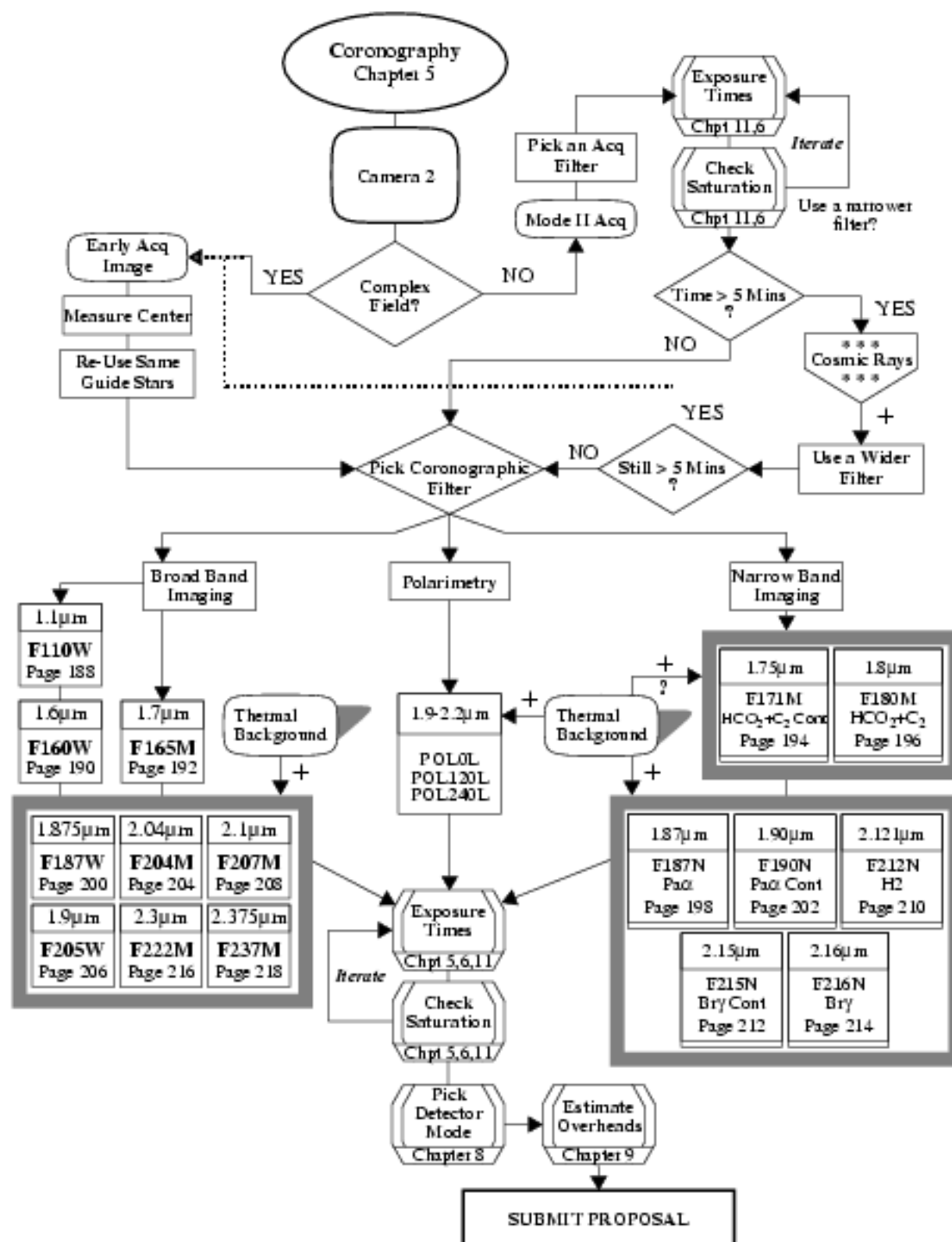


However, a small error in target centering will create an asymmetric displacement of the PSF zonal structures both in and out of the occulting spot, leading to position dependent changes in the local image contrast ratios.

## Coronagraphic Decision Chart

The decision chart given in Figure 5.4 leads you through the selection process to construct a coronagraphic observation.

Figure 5.4: Coronagraphic Decision Chart



## Polarimetry

Cameras NIC1, and NIC2, each contain 3 polarizers, whose principal axes of transmission are separated by 120 degrees. Observations in all three polarizers will provide the Stokes parameters of linearly polarized light. The spectral coverage is fixed for each camera, and the polarizers cannot be crossed with other optical elements. For Camera 1, the polarizers cover the wavelength range 0.8 to 1.3 microns, and for Camera 2, 1.9 to 2.1 microns.

### Instrumental Polarization

Since there are a number of internal reflections in NICMOS prior to reaching the polarizers there will be instrumental polarization, estimated to be 1 to 2 percent. It should, however, be quite stable. Measurements of polarized and unpolarized standard stars will be obtained as part of the Cycle 7 calibration program and these will be used to measure the instrumental polarization and the zero position angle for each polarizer (remember the actual zero point will depend on your spacecraft orient).

### Theory

The raw polarimetric images obtained through the three polarizers will be routinely processed by the first stage of the pipeline like any other exposure. The resulting images will have been placed onto a common intensity scale by correcting for the relative transmissions of each of the polarizers. If we define the intensity and statistical uncertainties (including read-noise) obtained in the 3 polarizers after processing by the pipeline to be  $I_0$ ,  $I_{120}$  and  $I_{240}$  and  $\sigma_0$ ,  $\sigma_{120}$ ,  $\sigma_{240}$  respectively, then we may obtain the total intensity  $I$  from:

$$I = \frac{2}{3}(I_0 + I_{120} + I_{240})$$

and the Stokes parameters  $Q$  and  $U$ :

$$Q = \frac{2}{3}(2I_0 - I_{240} - I_{120})$$

$$U = \frac{2}{\sqrt{3}}(I_{240} - I_{120})$$

The statistical uncertainties are obtained by straightforward propagation of errors:

$$\sigma_I = \frac{2}{3} \sqrt{[\sigma_0^2 + \sigma_{240}^2 + \sigma_{120}^2]}$$

$$\sigma_U = \frac{2}{\sqrt{3}} \sqrt{[\sigma_{240}^2 + \sigma_{120}^2]}$$

$$\sigma_Q = \frac{2}{3} \sqrt{[4\sigma_0^2 + \sigma_{240}^2 + \sigma_{120}^2]}$$

The Stokes parameters can then be combined to yield the polarized intensity,  $I_p$ :

$$I_p = [Q^2 + U^2]^{1/2}$$

and the degree,  $P$ , and position angle of polarization,  $\theta$ , using:

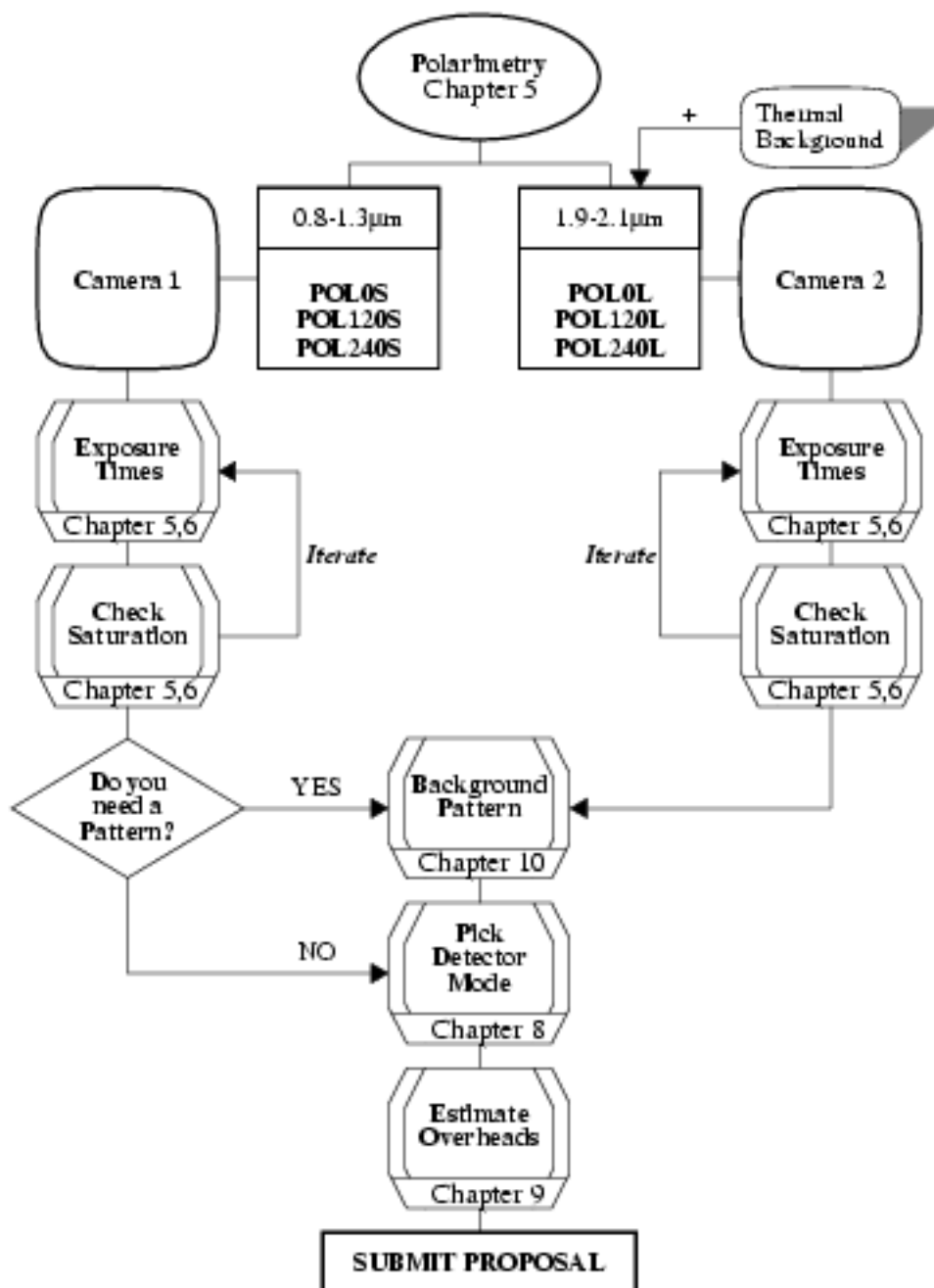
$$P = \frac{I_p}{I}$$

$$\theta = 28.648 \tan\left(\frac{U}{Q}\right)$$

## Polarimetry Decision Chart

The decision chart given in Figure 5.5 leads you through the selection process to construct a polarimetry observation.

Figure 5.5: Polarimetry Decision Chart



---

## Polarimetric Sensitivity

In Figure 5.6 through Figure 5.8 we provide sensitivity information for the two sets of polarizers. We give the same information as was described in Chapter 4: namely a sensitivity curve, plotted as flux against time for a constant S/N ratio and an exposure *exclusion* curve for both point and extended sources. To use these, look up the integration time required for your source flux on the sensitivity curve for the signal to noise you want (see Chapter 12 if you need to convert the units). Then go to the associated *exclusion* curve and check that you are not in the shaded areas. If you are, adjust your integration time appropriately until you are in the clear area. If you are to the left of the vertical dashed line then you must use bright object mode. Work out how many integrations you need to get your desired S/N. To get the total exposure time required for a polarimetric observation multiply your final answer by 3 to account for the fact that you need to use 3 polarizers to get a measurement. Note that the transmission curves are for a 100% polarized source while all the sensitivity information here is calculated for a single polarizer image, assuming an unpolarized source.

### Camera 1, Polarizers

The polarizers consist of 3 identical elements at relative angles of 0, 120, and 240 degrees.

Central (microns)	Mean (microns)	Peak (microns)	FWHM (microns)	Range (microns)	Principal Tr percent	Pixel fraction
1.0450	1.0384	1.0245	0.4750	0.8–1.3	77.60	0.048

Figure 5.6: Throughput of Short Wavelength Polarizers

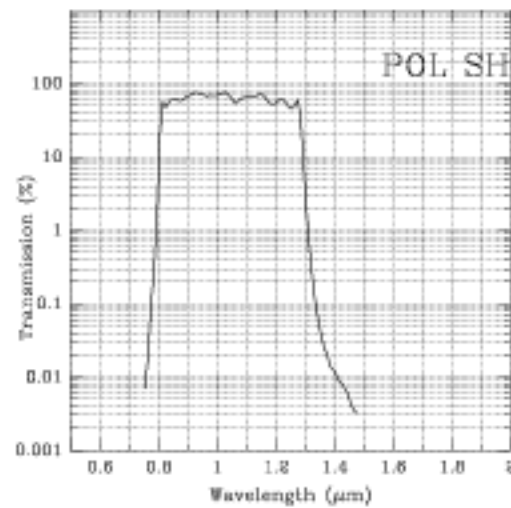
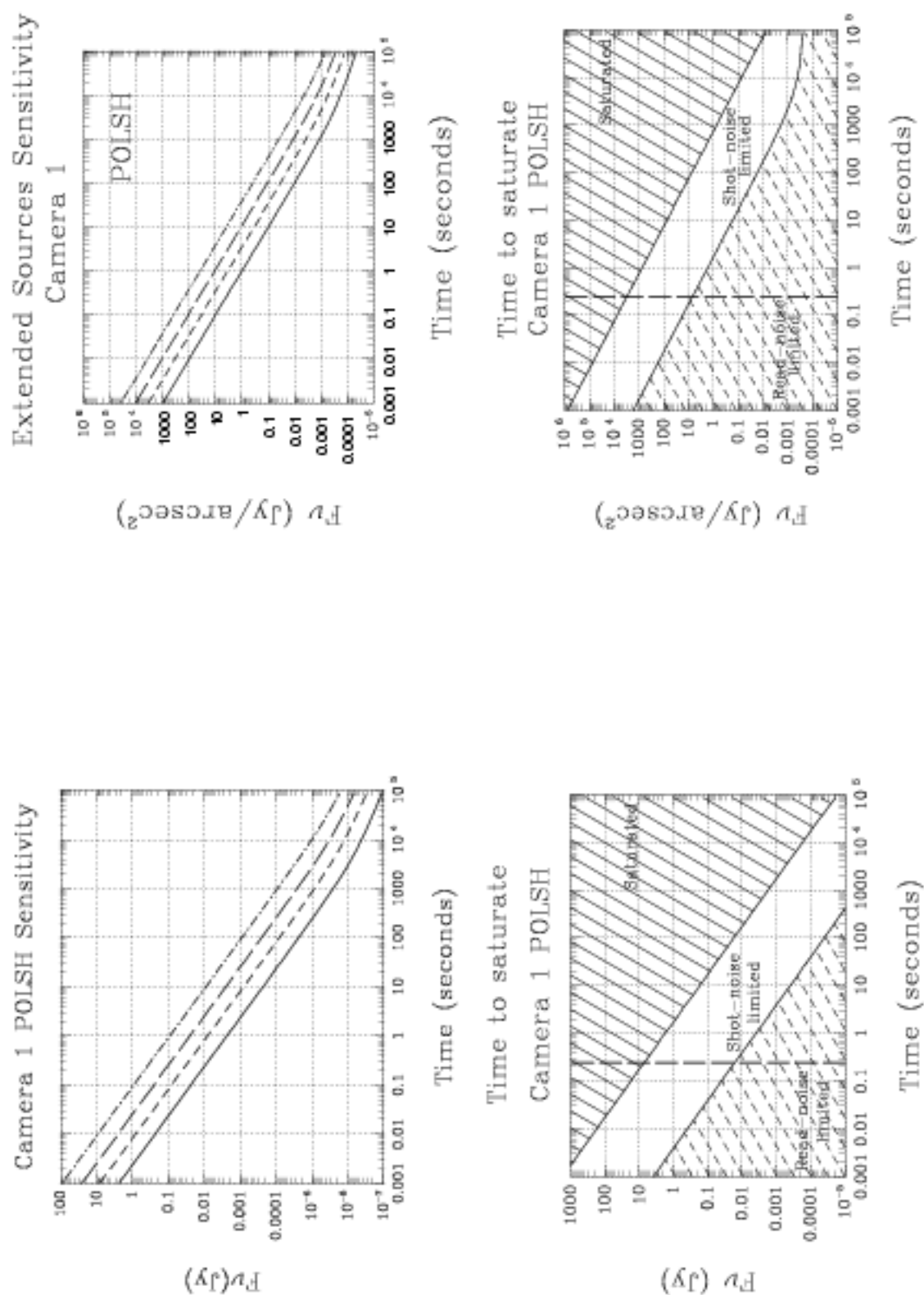




Figure 5.7: Sensitivity and Exclusion Plots for Short Wavelength Polarizers

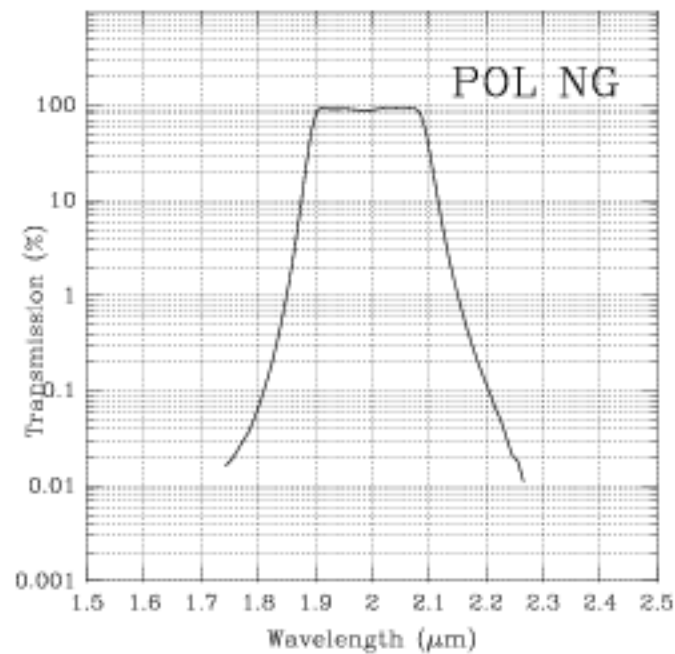


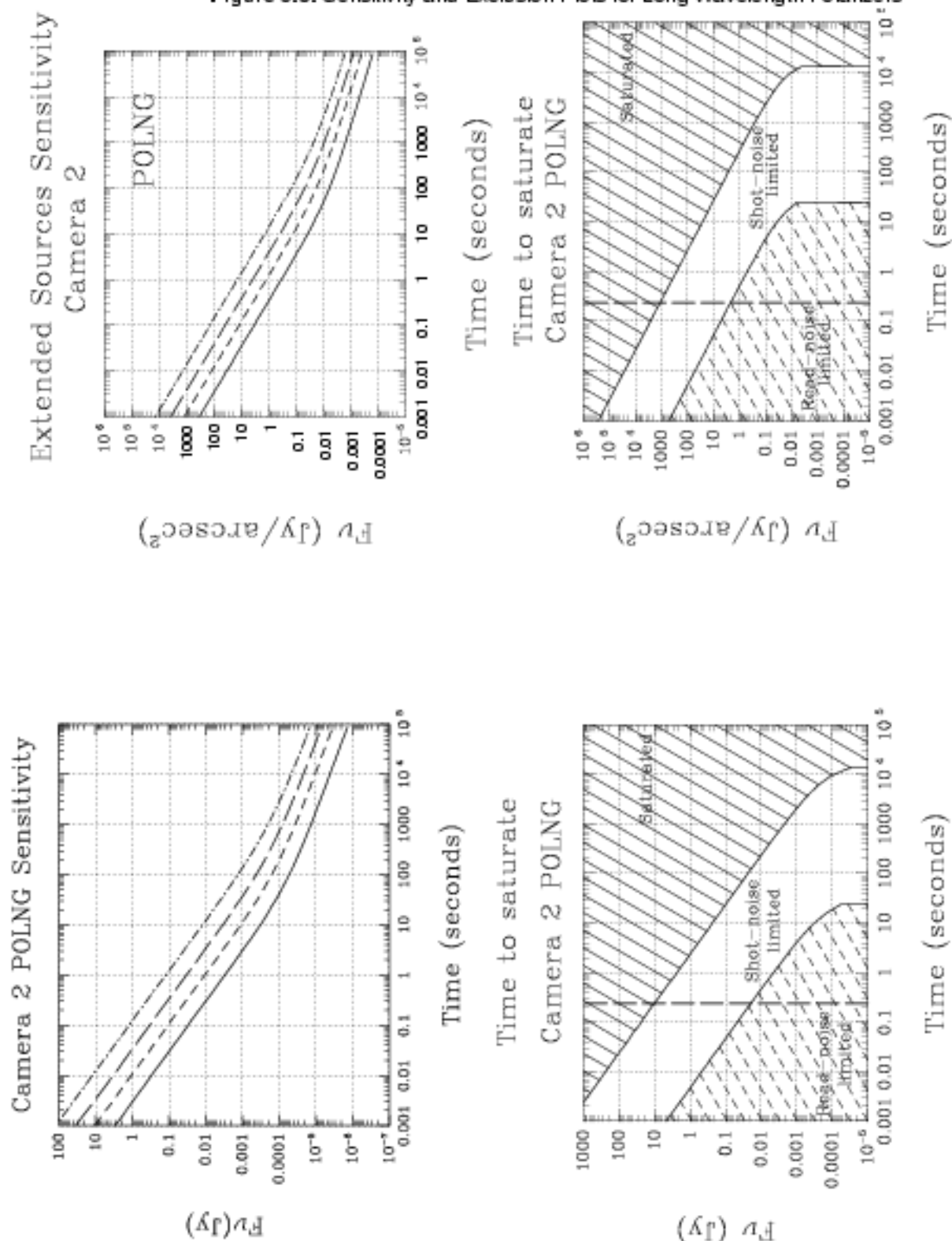
### Camera 2, Polarizers

The polarizers consist of 3 identical elements at relative angles of 0, 120, and 240 degrees. Thermal background is important.

Central (microns)	Mean (microns)	Peak (microns)	FWHM (microns)	Range (microns)	Principal Tr	Pixel Fraction
1.9943	1.9946	1.9100	0.2025	1.9—2.1	96.67	0.33

Figure 5.8: Throughput of Long Wavelength Polarizers





## Grism Spectroscopy

A grism is a combination of a prism and grating arranged to keep light at a chosen central wavelength undeviated as it passes through the grism. Grisms are normally used to create spectra in a camera by inserting the grism into the normal camera beam. The grism then creates a dispersed spectrum centered on the location of the object in the camera field of view. The resolution of a grism is proportional to the tangent of the wedge angle of the prism in much the same way as the resolution of gratings are proportional to the angle between the input and the normal to the grating.

NICMOS uses this mode of operation without any slit or aperture at the input focus so that all objects in the field of view display their spectra for true multi-object spectroscopy. The NICMOS grisms operate in the spectral range between 0.8 and 2.5  $\mu\text{m}$ . The grisms reside in the filter wheel for Camera 3, therefore the spatial resolution of the spectroscopy is similar to the spatial resolution of Camera 3. The filter wheel contains three grisms, of infrared grade fused silica, which cover the entire NICMOS wavelength range with a spectral resolving power of  $\sim 200$  per pixel.

The two shorter wavelength grisms exploit the low natural background of HST while the longest wavelength grism is subject to the thermal background emission from HST.

The NICMOS grisms have an interference filter coated on their entrance faces to limit the bandpass of the spectrum. This is necessary to prevent overlap of orders and reduce thermal background from the telescope. Since the NICMOS grisms do not have an input slit or aperture, there is not a reduction of the background flux found in slit dispersing systems. This is not a significant problem in the shorter wavelengths, but the long wavelength grism has a high background flux.

The basic parameters of the NICMOS grisms are given in Table 5.1.

Table 5.1: Grism Characteristics

Grism	Resolution per Pixel	Central Wavelength	Wedge Angle	Bandpass	Lines per mm
A	200	0.964	5.219	0.8 - 1.2	45.0
B	200	1.401	5.5889	1.1 - 1.9	30.769
C	200	2.058	5.6944	1.4 - 2.5	21.05

### Relationship Between Wavelength and Pixel

Table 5.2 gives the dispersion relationship in the form:

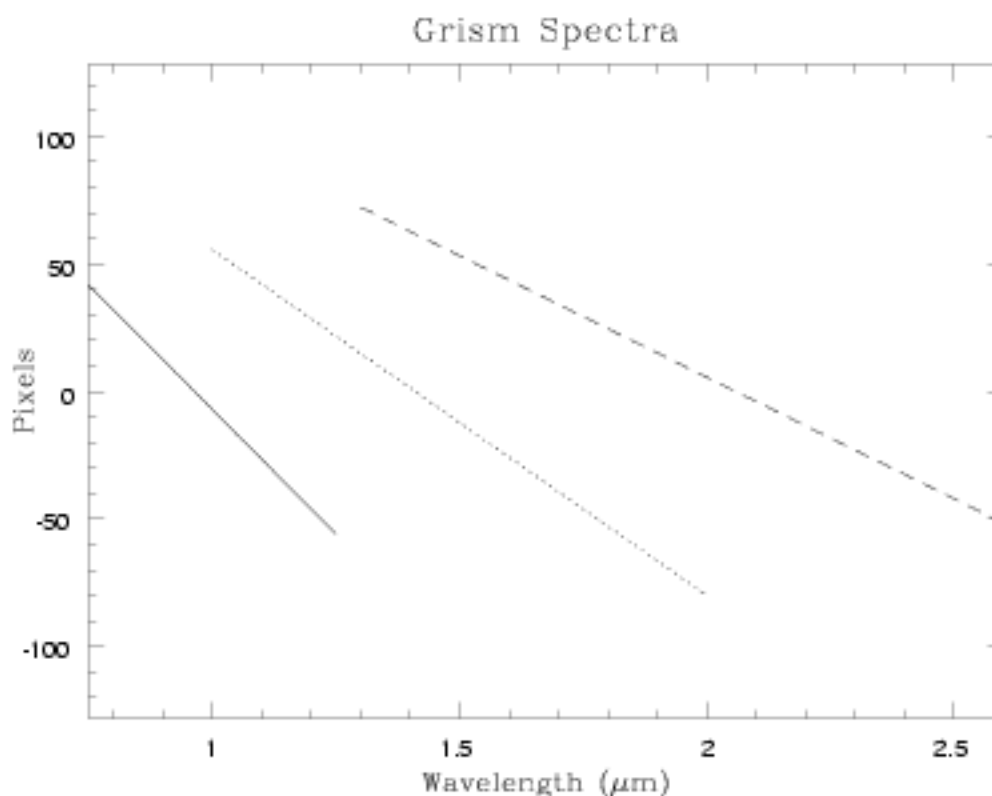
$$\text{wavelength} = m \cdot \text{pixel} + b,$$

where wavelength is in microns and the 0 pixel is at the central wavelength. The relationship is plotted in Figure 5.10. The actual location of the plus and minus pixels will be dependent on the grism orientation and the location of the source in the image. The grisms will be aligned as accurately as possible along a row or column of the array. We do not expect any distortion or curvature in the spectrum.

**Table 5.2: Wavelength to Pixels Relationship**

Grism	m	b
1	-0.005126312	0.9638530
2	-0.007379983	1.4098832
3	-0.010506387	2.0583025

**Figure 5.10: Wavelength Versus Pixel Number for each Grism.** Note that the actual location of the central wavelength on the detector depends on the position of the source.



## Multi-Object Spectroscopy

Grism observations are carried out in the same manner as any of the imaging operations discussed earlier. In multi-object spectroscopy one of the grisms in the filter wheel for NIC3 will be selected. The observations then proceed via one of the readout and operation modes discussed later.

Although multi-object spectroscopic observations can stand alone with no supporting observations, we recommend pairing them with an image in Camera 3, through an appropriate filter, at the same pointing. This provides the location of each object in the field and aids in the identification of their individual spectra. Because of this natural pairing it is anticipated that most spectroscopy observations will be in at least a two image sequenced observation.

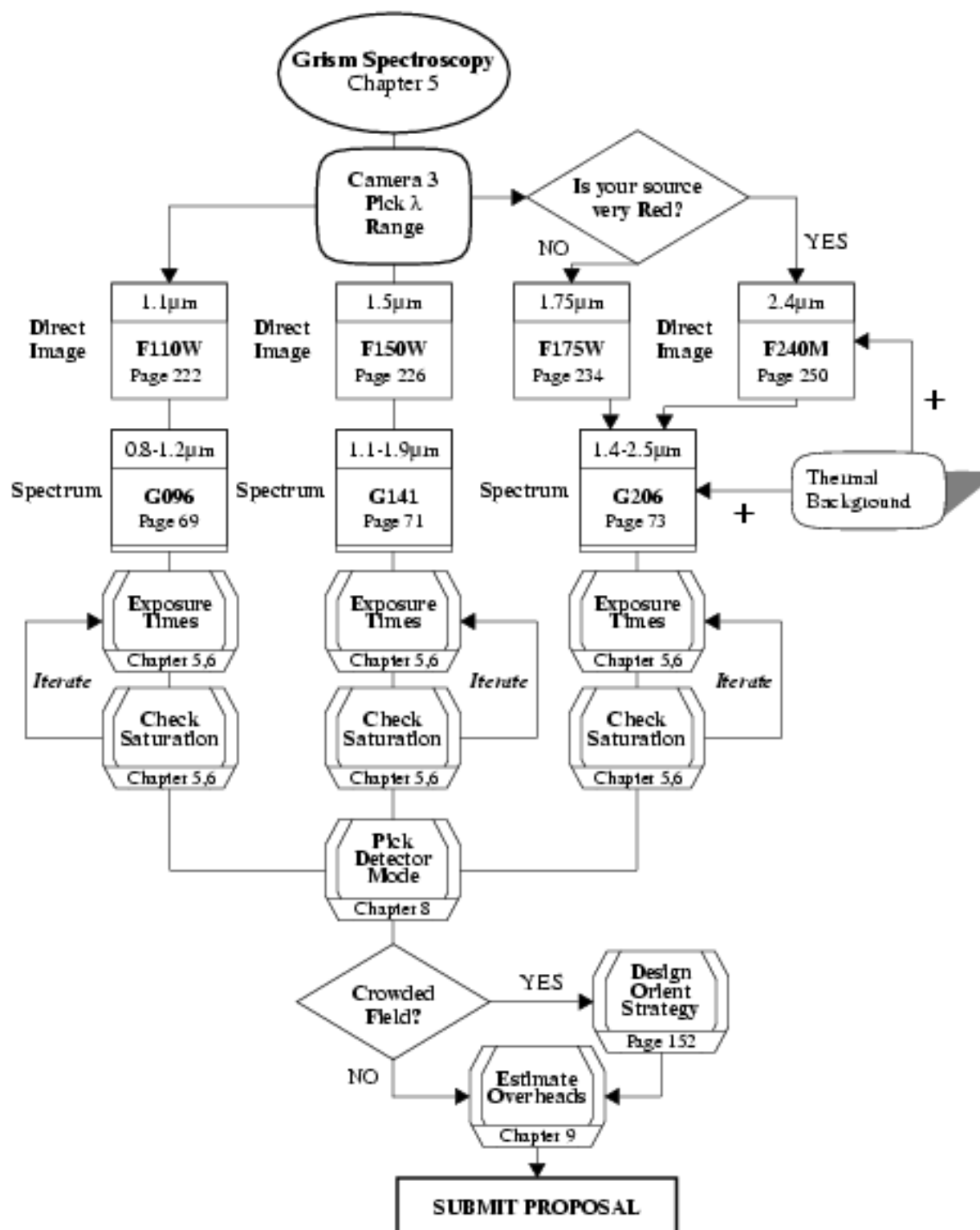
The direction of dispersion is perpendicular to the radial direction in Camera 3 where the radial direction is defined by a vector originating at the center of the field of view for Camera 3 and pointing toward the center of the OTA axis. In complex fields, such as extended objects and crowded fields, individual spectra of targets may overlap and cause confused images. In such cases, it may be possible to alleviate the superposition of spectra by requesting a specific orientation of the telescope during the Phase II Proposal submission. For complex fields, several different orientations may be necessary so that the individual spectra can be deconvolved from those of other sources in the field. It should be recognized that specifying an orientation for a grism observation creates constraints on the number of visibility windows available for scheduling. If different orientations are needed to unscramble the source spectra, then this will make telescope scheduling difficult.

Software is being developed at the ST-ECF for the analysis of grism observations. Using this, the observer will be able to fully extract spectra of single objects from the images, including the disentanglement of overlapping spectra and extended sources. To obtain the best results it is recommended in fields with multiple or extended sources that grism images be obtained at more than one spacecraft roll angle (preferably 3 or more), and it is essential that the image spectrum pair be obtained as described. If the matching image is not obtained, reduction and analysis of the grism data may be very difficult.

## Grism Decision Chart

The decision chart given in Figure 5.11 leads you through the construction of a grism observation.

Figure 5.11: Grism Decision Chart



## Sensitivity

Background radiation will be a worse problem for grisms than for imaging observations. Every pixel on the array will receive background radiation over the spectral bandpass of the particular grism, while the source spectrum will be dispersed over many pixels. Therefore, the ratio of the source to background flux will be much lower for the grisms than for the regular imaging mode filters. The expected detected background rate per pixel is shown in Table 5.3 below for the three grisms. The increase in the background flux for grism C is dramatic. Use grisms A and B when possible. Grism C is for the longer wavelengths only.

Table 5.3: Grism Background Radiation

Grism	Wavelength range microns	Background (e <sup>-</sup> /sec/pixel)	Background (Jansky/pix)
A	0.8-1.2	0.70	$5.4 \times 10^{-5}$
B	1.1-1.9	8.8	$5.6 \times 10^{-4}$
C	1.4-2.5	3000	0.10

## Grism Sensitivity Curves

Figures 5.12 through 5.17 present the sensitivity information for the three NLCMOS grisms. We provide basically the same information as presented earlier, namely a sensitivity curve, plotted as flux against time for a constant signal to noise ratio, and an *exclusion* curve. In the former case, the grisms are a little more complicated than the imaging filters, because the signal to noise is obviously now a function of wavelength. We have therefore picked three wavelengths across the bandpass of each of the grisms, and plotted a curve for each of these wavelengths. In practice, it turns out that there is rather little variation in sensitivity with wavelength within the bandpass of each grism. Note that for Grism C, the large thermal background means that exposures can never be longer than about one minute, even for faint sources, because the detector will be saturated by the background. Thus, in order to obtain spectra of faint sources with Grism C, it will be necessary to obtain a large number of single ACCUM mode exposures.

We also present a line correction factor curve. To use this, find the wavelength of your line and read off the correction factor  $\epsilon_G$  from the graph. As described in Chapter 4 multiply the line flux by this factor and add to the continuum flux. The integration time may now be calculated from the sensitivity curve as if you had a pure continuum source. To use the sensitivity curves look up the integration time required for your source flux on the sensitivity curve for the signal to noise you want. Then go to the associated *exclusion zone* curve and check that you are not in the shaded areas. If you are, adjust your integration time appropriately until you



are in the clear area. If you are to the left of the vertical dashed line then you must use bright object mode.

Grism A: G096

Central (microns)	Mean (microns)	Peak (microns)	FWHM (microns)	Range	Max T r (percent)
0.9673	0.9911	1.0010	0.4029	0.8–1.2	69.8
Continuum Filter F110W					
1.0998	1.1035	1.1035	0.5915	0.8–1.4	94.9

Figure 5.12: Grism A Throughput and Line Correction Curve. To use the latter find the wavelength of your line and read off the correction factor  $\epsilon_G$  from the graph (described in Chapter 4) multiply the line flux by this factor and add to the continuum flux. The integration time may now be calculated from the sensitivity curve.

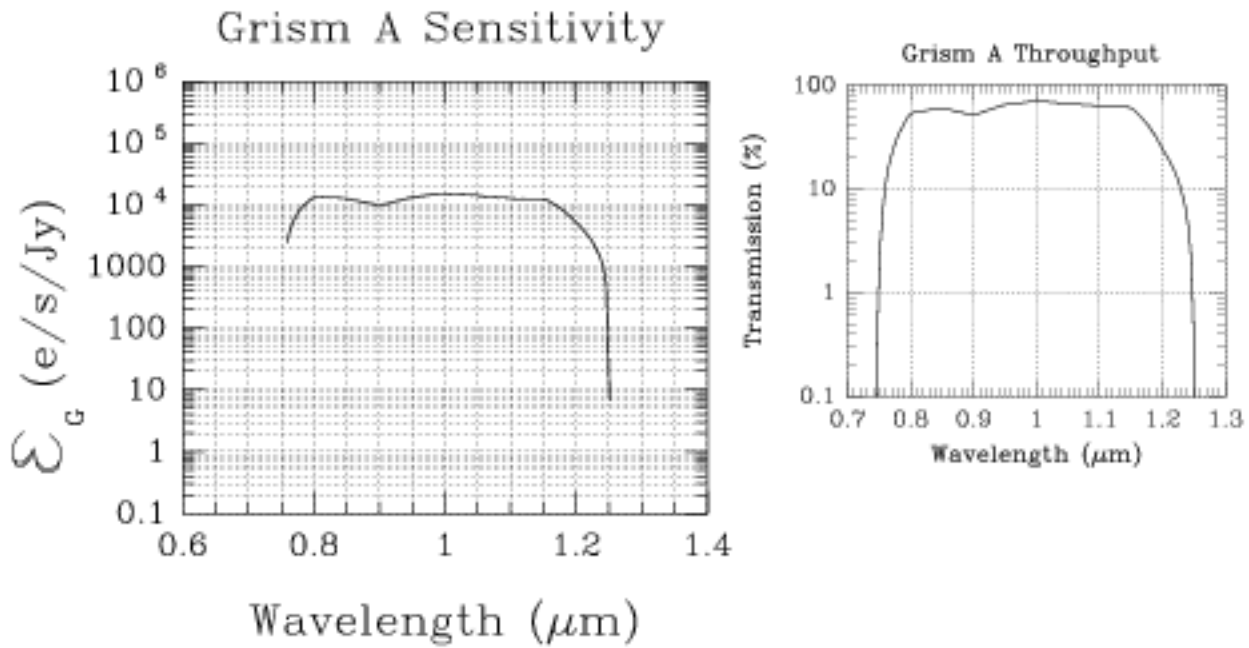
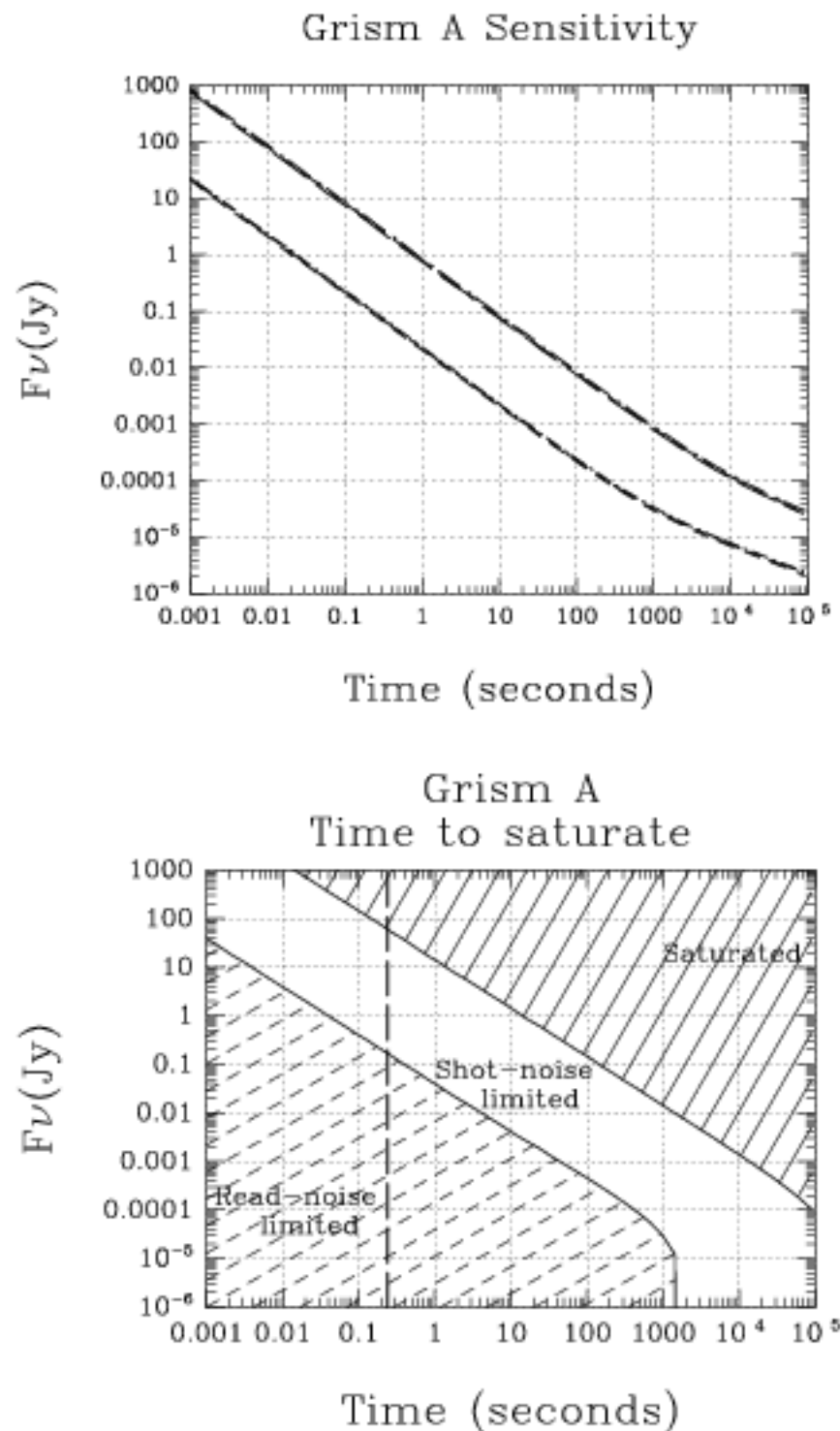


Figure 5.13: Sensitivity Plot Grism A. Curves are plotted for two choices of S/N, 10 (lower) & 100 (upper). As described in the text curves have been plotted at three wavelengths (0.836  $\mu\text{m}$ , 0.969  $\mu\text{m}$ , and 1.138  $\mu\text{m}$ ) covering the free-spectral range of the grism for each S/N, but they are so close as to be indistinguishable at this scale.



**Grism B: G141**

Thermal background is important.

Table 5.4: Grism B: G141

Central (microns)	Mean (microns)	Peak (microns)	FWHM (microns)	Range (microns)	Max Tr (percent)
1.414	1.5100	1.4020	0.7914	1.1–1.9	74.7
<i>Continuum Filter F150W</i>					
1.5035	1.5069	1.6355	0.8020	1.1–1.9	97.7

Figure 5.14: Grism B Throughput and Line Correction Curve. To use the latter find the wavelength of your line and read off the correction factor  $\epsilon_G$  from the graph (described in Chapter 4) multiply the line flux by this factor and add to the continuum flux. The integration time may now be calculated from the sensitivity curve.

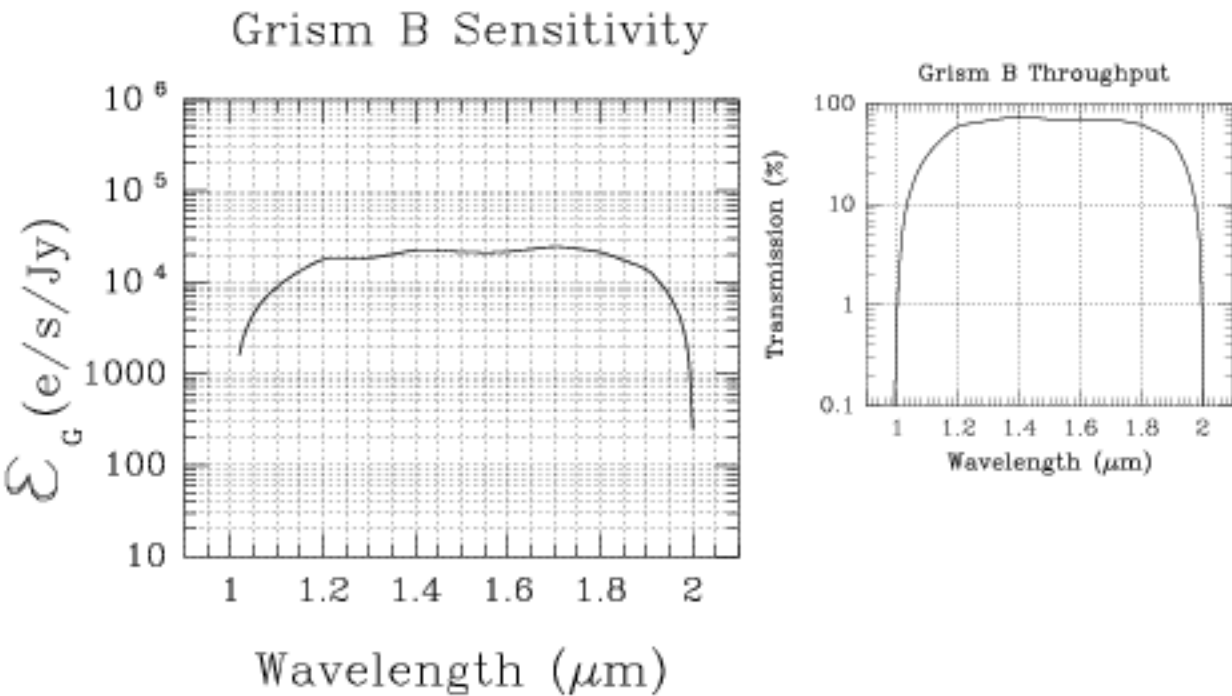
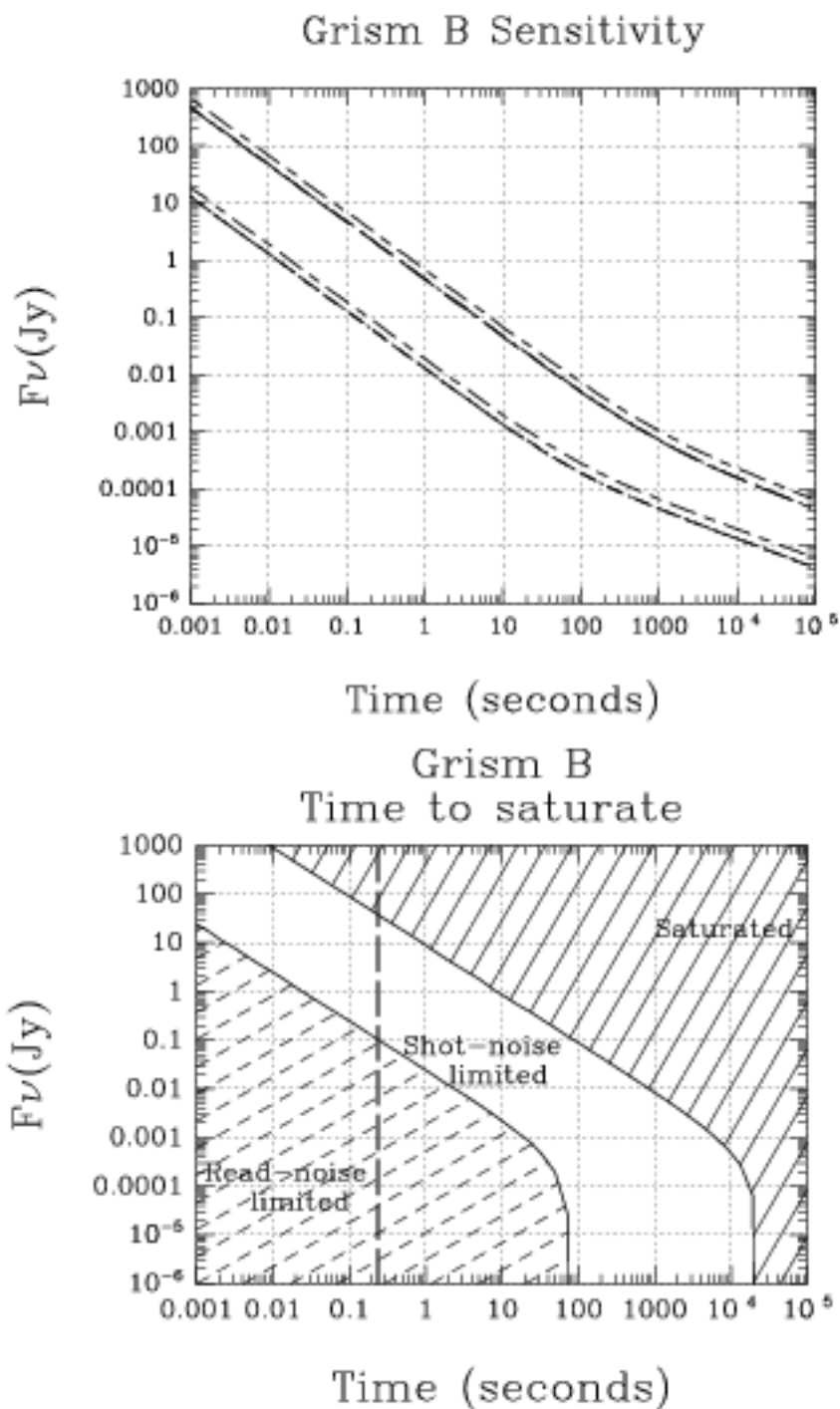


Figure 5.15: Sensitivity Plot Grism B. Curves are plotted for two choices of S/N, 10 (lower) & 100 (upper). As described in the text, curves have been plotted at three wavelengths (1.174  $\mu\text{m}$ , 1.417  $\mu\text{m}$ , and 1.772  $\mu\text{m}$ ) covering the free-spectral range of the grism for each S/N, but the two short-wavelength curves are indistinguishable.



**Grism C: G206**

High thermal background. Use only for bright sources.

Table 5.5: Grism C: G206

Central (microns)	Mean (microns)	Peak (microns)	FWHM (microns)	Range (microns)	Max Tr (percent)
2.067	1.9523	2.0880	1.1575	1.4 - 2.5	73.4
<i>Continuum Filters F175W, F240M</i>					
1.7530	1.7508	1.9070	1.0940	1.2-2.3	96.6
2.3978	2.3977	2.3155	0.1975	2.3-2.5	92.4

Figure 5.16: The Grism C Throughput and Line Correction Curve. To use the latter find the wavelength of your line and read off the correction factor  $\epsilon_G$  from the graph (described in Chapter 4) multiply the line flux by this factor and add to the continuum flux. The integration time may now be calculated from the sensitivity curve.

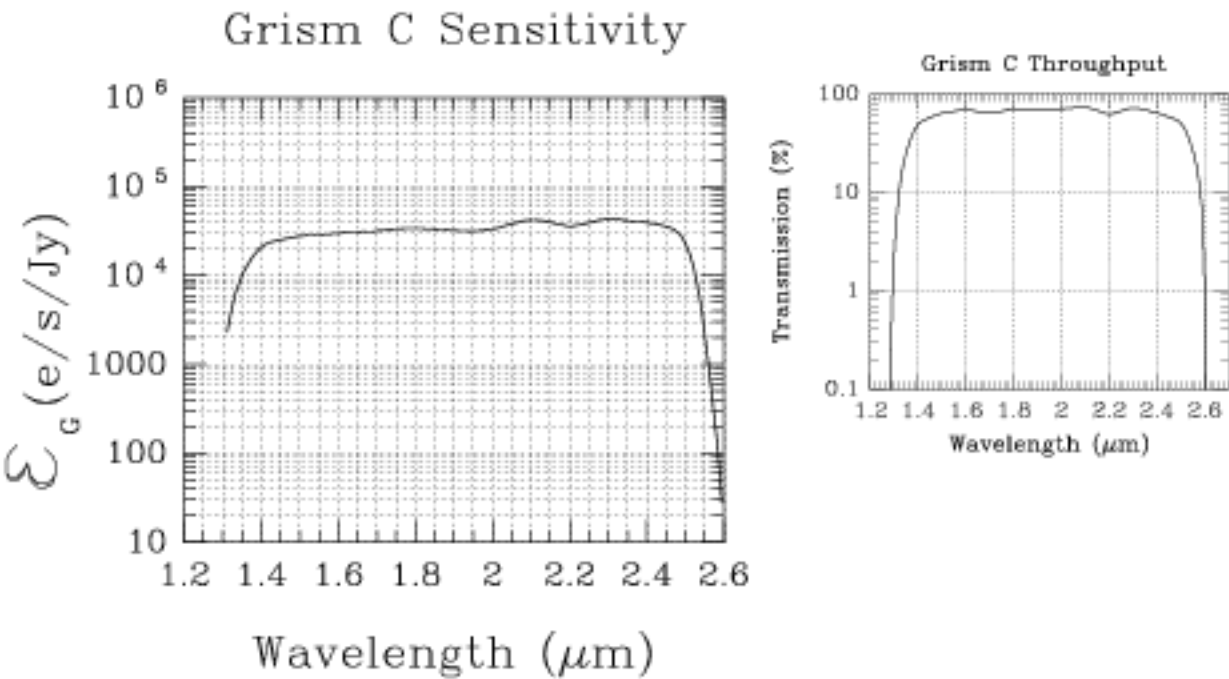
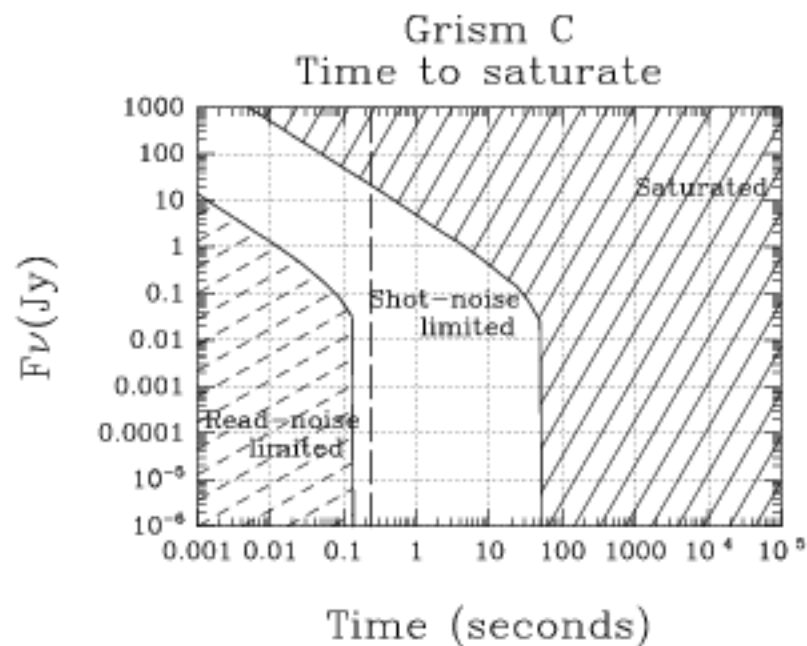
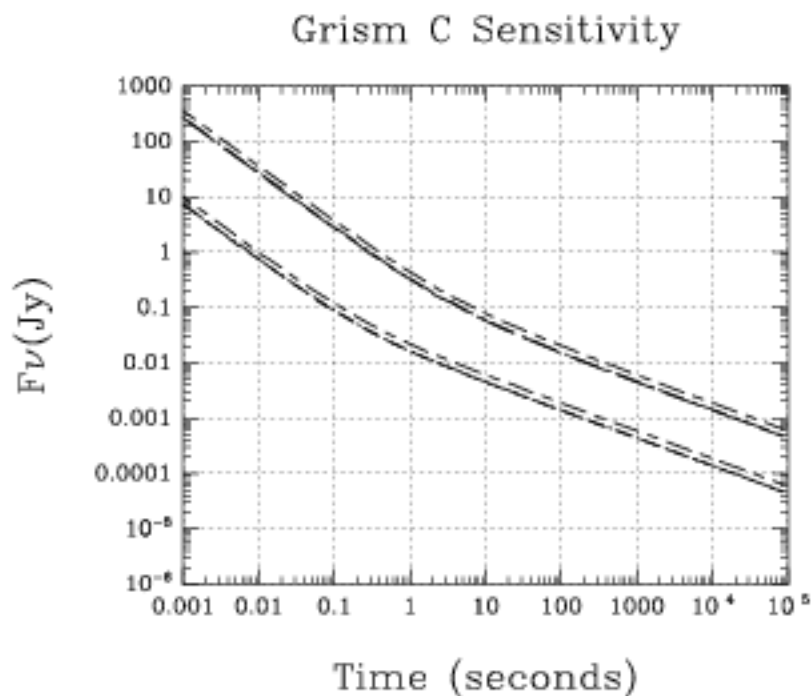


Figure 5.17: Sensitivity Plot Grism C. Curves are plotted for two choices of S/N, 10 (lower) & 100 (upper). As described in the text, curves have been plotted at three wavelengths (1.607  $\mu\text{m}$ , 2.069  $\mu\text{m}$ , and 2.395  $\mu\text{m}$ ) covering the free-spectral range of the grism for each S/N, but the two short-wavelength curves are indistinguishable.



## CHAPTER 6

# Exposure Time Calculations

### In This Chapter...

Overview / 75

Calculating NICMOS Imaging Sensitivities / 78

WWW Access to Imaging Tools / 83

Examples / 84

In this chapter we provide NICMOS-specific performance information needed to prepare a NICMOS Phase I proposal for Cycle 7. First, we discuss various parameters that affect performance, and the extent to which they are known. Next, we describe how to determine the system sensitivity. We then describe the ways in which you can determine the exposure time required for a given observation and the signal to noise that will be achieved; examples are provided. We describe several computer programs that will perform these calculations and which are available on the WWW. These programs have been used to calculate the sensitivity and exclusion curves for the NICMOS filters, polarizers, and grisms, presented elsewhere in this Handbook. We also describe how to calculate signal to noise ratios and exposure times by hand for NICMOS.

---

## Overview

At the time of writing, many of the factors that contribute to the throughput of NICMOS are not fully defined. Construction of the instrument is complete, but the System Level Thermal Vacuum (SLTV) testing phase, during which many aspects of the instrument performance will be determined, has not yet begun. The sensitivities presented in Chapters 11 and 5 have been calculated using the best information currently available for each parameter. In some cases this means preliminary measurements made using NICMOS subsystems in the laboratory, while in others we are only able to make estimates. General Observers should

watch the NICMOS web pages in mid-August, where we will provide updates as new information becomes available, as discussed in Chapter 1. Some performance aspects cannot be tested until the instrument is installed on HST, and in these cases the performance will not be well established until the first few months of NICMOS's orbital lifetime. Some observers will need this information to prepare Phase II proposals, and this information will be found on the NICMOS web pages. In summary, the information provided in this chapter is preliminary, and observers should be prepared for some of it to change substantially.

## Instrumental Factors

### Detectors

The detector properties which will affect the sensitivity are simply those familiar to ground-based optical and IR observers, namely dark current and read noise, and the detector quantum efficiency (DQE). Laboratory measurements have determined the read noise for the three NICMOS flight arrays to be ~30 electrons. The measured numbers are given in Table 7.1 on page 92.

### Optics

NICMOS is a relatively simple instrument in layout, and thus contains a fairly small number of elements which affect the sensitivity. These are the filter transmission, the field of view (determined by the NICMOS optics external to the dewar, in combination with the HST mirrors), the reflectivities of the various external mirrors and the transmission of the dewar window.

The filter transmissions as functions of wavelength were measured in the laboratory, and the resulting curves were presented earlier. Some filters may have minor leaks outside the primary filter bandpass; the reality of these has not yet been established, and we assume here for the purposes of sensitivity calculations that the transmission is zero outside the primary bandpass.

NICMOS contains a total of seven mirrors external to the dewar, each of which reduces the signal received at the detector. The mirrors are gold coated for maximum reflectivity, and are expected to achieve about 95% reflectivity. The dewar window has a transmission of roughly 90%. Therefore, the combination of optical elements is expected to transmit ~63% of the incoming signal from the OTA.

The sensitivity will obviously be affected by the pixel field of view. The smaller the angular size of a pixel, the smaller the fraction of a given source that will illuminate the pixel. Finally, the optical efficiency will be degraded further by the reflectivities of the aluminum with  $\text{MgF}_2$  overcoated HST primary and secondary mirrors. These are given as exactly one minus the emissivities.

### Background Radiation

At long wavelengths the dominant effect limiting the NICMOS sensitivity will be the thermal background emission from the telescope. How large this will be depends on the areas of the primary and secondary mirror and their optical



configuration, temperatures, and emissivities. We discussed the issue of thermal background and its stability in Chapter 3.

For the purposes of sensitivity calculations, we used the values listed in Tables 6.1 and 6.2 and assumed that the effects of debris on the mirrors can be ignored.

**Table 6.1: Optical Efficiency**

Optical Element	Efficiency
First bending mirror	0.95
Re-imaging mirror	0.95
Pupil mirror	0.95
Image mirror	0.95
First paraboloid	0.95
Second paraboloid	0.95
Bending mirror	0.95
Dewar window	0.9
Total	0.63

**Table 6.2: HST Infrared and Optical Properties**

Property	Assumed Value
Primary mirror collecting area	38993 cm <sup>2</sup>
Primary mirror temperature	293 K
Primary mirror emissivity	0.2
Secondary mirror collecting area	684.4 cm <sup>2</sup>
Secondary mirror pupil clear fraction	0.86
Secondary mirror temperature	293 K
Secondary mirror emissivity	0.2
Focal plane image scale	35.8 arcsec/cm
Back focal distance	640.6 cm

At shorter NUCMOS wavelengths, sensitivities will be affected by the zodiacal background which is given by the equation in Chapter 3; the overall expected background is shown in Figure 3.6.

Background radiation will be a slightly worse problem in the case of Multi-Object Spectroscopy (MOS) than in the case of imaging observations. Every pixel on the array will always see the entire background radiation integrated over the grism bandpass. The expected detected background rate per pixel is shown in Table 5.3.

## Calculating NICMOS Imaging Sensitivities

The sensitivity curves presented in Chapters 11 and 5 allow one to estimate the exposure times from a given source flux. In some situations it may be desirable to go through each step of the calculation. One example would be the case of a source with strong emission lines, where one wants to estimate the contribution of the line(s) to the signal. This could include the case of a strong emission line which happens to fall in the wing of a desired filter's bandpass. To facilitate such calculations, we provide in this section recipes for determining the signal to noise or exposure time by hand.

### Signal to noise Calculation

The signal generated by a continuum source with a flux  $F_j$  [Jansky] falling on a pixel is:

$$\begin{aligned} C_c &= F_j \gamma_{\text{opt}} \gamma_{\text{det}} \gamma_{\text{fil}} h A_{\text{prim}} E \\ &= F_j \eta_c \text{ [e}^-/\text{sec]} \end{aligned} \quad (1)$$

where:

- $\gamma_{\text{opt}}$  is the efficiency of the optics, including the HST mirrors and the NICMOS optics.
- $\gamma_{\text{det}}$  is the detector quantum efficiency.
- $\gamma_{\text{fil}}$  is the filter transmission.
- $A_{\text{prim}}$  is the HST primary mirror collecting area.
- $E$  is a constant given by:

$$E = 10^{-26} / (h\lambda) \quad (2)$$

where  $h$  is Planck's constant and  $\lambda$  the wavelength.

The expression for  $C_c$  has to be integrated over the bandpass of the filter, since some of the terms vary significantly with wavelength. The value for  $\eta_c$  is listed for each filter in Tables 6.3, 6.4, and 6.5, so that the signal in  $\text{e}^-/\text{sec}$  can be estimated. It should be noted that to determine  $C_c$  more accurately, the source flux  $F$  should be included in the integral over the filter bandpass, since the source flux is bound to be a function of wavelength. In the sensitivity curves plotted in the previous section, this has been done, assuming a source effective temperature of 5,000K.

If an emission line falls in the bandpass of the filter, we need to take account of its effect on the signal (in some cases the emission line may generate almost all the detected signal). The line signal can be determined as:

$$\begin{aligned} C_l &= I_{ij} \gamma_{\text{opt}} \gamma_{\text{det},\lambda} \gamma_{\text{fil},\lambda} h A_{\text{prim}} E \\ &= \epsilon_\lambda I_{ij} \text{ [e}^-/\text{sec]} \end{aligned} \quad (3)$$

where  $E$  is defined as before. However, on this occasion it is necessary to use a line flux  $I$  (in  $\text{Wm}^{-2}$ ), and the detector quantum efficiency and filter transmission are determined for the wavelength  $\lambda$  of the emission line.

The factor  $E_\lambda$  is plotted for every filter in Chapter 11, and a similar factor for the grisms in Chapter 5. Thus one only needs to pick the wavelength of interest, read off  $E_\lambda$ , and multiply your flux,  $I_{ij}$ , by this to get the line contribution to the flux in the filter. The maximum value of  $E_\lambda$ , denoted as  $\hat{E}$ , is also listed in Tables 6.3, 6.4, and 6.5. Note that for the grisms, where both lines and continuum will frequently be present, we have plotted  $E_\lambda$  in units of  $e^-/\text{sec}/\text{Jansky}$ . Thus, in this case it is necessary to estimate the spectral flux density of any line emission in Janskys, which is done simply by using the line strengths and the spectral resolution of the grisms.

The total signal generated by the pixel is the sum of the continuum and line signals calculated above.

Next the background signal must be calculated. This is particularly important in the infrared, since *in some situations* the signal to noise in the final observation is determined largely by the photon noise in the background signal, rather than that in the source signal. At wavelengths longer than 1.6 microns in particular, the thermal background emission will very often be brighter than the target source, in many cases perhaps by several orders of magnitude. The expected background as a function of wavelength for each of the three NICMOS cameras is plotted in Figure 3.6. This has been used to derive the background signal which is listed for each filter in Table 6.3 to Table 6.5 in  $e^-/\text{sec}$  as  $B$ .

The final ingredients needed to calculate the signal to noise for the observation are the read noise  $N_r$  and dark current  $I_d$ . The read noise can be taken from Table 7.1. The dark current has not been very well determined at the time of writing, but we recommend that the upper limits listed in Table 7.1 should be adopted.

It is now possible to calculate the signal to noise ratio expected for an exposure of duration  $t$  seconds, where a number  $N_{\text{read}}$  of reads are taken before and after the integration. It is:

$$SNR = \frac{C_s t}{\sqrt{(C_s + B + I_d)t + \frac{N_r^2}{N_{\text{read}}}}} \quad (+)$$

Where  $C_s$ , the count rate in  $e^-/\text{sec}$ , is the sum of  $C_c$  plus  $C_l$ .

It is important to note that in these equations, the flux to be entered (either  $F_{ij}$  or  $I_{ij}$  or both) is *not* the total source flux, but the flux falling on a pixel. In the case of an extended source this can easily be worked out from the surface brightness and the size of the pixel. For a point source, it will be necessary to determine the fraction of the total flux which is contained within the area of one pixel, as listed in Table 4.4, and scale the source flux by this fraction. For Camera 1 in particular, this fraction may be quite small, and so will make a substantial difference to the outcome of the calculation.

## Exposure Time Calculation

The other situation frequently encountered is when the required signal to noise is known, and it is necessary to calculate from this the exposure time needed. In this case the same elements must be looked up as described above, and the required time can be calculated as:

$$t = \frac{(SNR)^2(C_s + B + I_d) + \sqrt{(SNR)^4(C_s + B + I_d)^2 + 4(SNR)^2 C_s \frac{N_r^2}{N_{read}}}}{2C_s^2} \quad (5)$$

**Table 6.3:** Camera 1 Filter Sensitivity Parameters

Filter name	$\eta_c$ [e <sup>-</sup> /sec/Jy]	$\mathcal{E}$ [e <sup>-</sup> /sec/(W/m <sup>2</sup> )]	B [e <sup>-</sup> /sec]
F090M	$4.82 \times 10^{-5}$	$8.6 \times 10^{17}$	0.015
F095N	$3.45 \times 10^{-4}$	$7.0 \times 10^{17}$	$1.04 \times 10^{-3}$
F097N	$3.83 \times 10^{-4}$	$8.0 \times 10^{17}$	$1.14 \times 10^{-3}$
F108N	$4.29 \times 10^{-4}$	$1.3 \times 10^{18}$	$1.18 \times 10^{-3}$
F110M	$8.16 \times 10^{-5}$	$1.6 \times 10^{18}$	0.0223
F110W	$2.18 \times 10^{-6}$	$2.0 \times 10^{18}$	0.0604
F113N	$5.0 \times 10^{-4}$	$1.5 \times 10^{18}$	$1.34 \times 10^{-3}$
F140W	$3.45 \times 10^{-6}$	$4.9 \times 10^{18}$	0.17
F145M	$8.21 \times 10^{-5}$	$3.1 \times 10^{18}$	0.0196
F160W	$1.86 \times 10^{-6}$	$4.8 \times 10^{18}$	0.13
F164N	$8.62 \times 10^{-4}$	$3.7 \times 10^{18}$	$3.77 \times 10^{-3}$
F165M	$9.41 \times 10^{-5}$	$4.6 \times 10^{18}$	0.0595
F166N	$8.75 \times 10^{-4}$	$3.8 \times 10^{18}$	$4.80 \times 10^{-3}$
F170M	$1.01 \times 10^{-6}$	$5.0 \times 10^{18}$	0.12
F187N	$9.18 \times 10^{-4}$	$4.8 \times 10^{18}$	0.0664
F190N	$9.55 \times 10^{-4}$	$5.2 \times 10^{18}$	0.0912

**Table 6.4:** Camera 2 Filter Sensitivity Parameters

Filter Name	$\eta_c$ [e <sup>-</sup> /sec/Jy]	$\hat{\epsilon}$ [e <sup>-</sup> /sec/(W/m <sup>2</sup> )]	B [e <sup>-</sup> /sec]
F110W	$2.20 \times 10^6$	$2.2 \times 10^{18}$	0.19
F160W	$1.86 \times 10^6$	$5.2 \times 10^{18}$	0.39
F165M	$9.40 \times 10^5$	$5.0 \times 10^{18}$	0.18
F171M	$4.02 \times 10^5$	$5.2 \times 10^{18}$	0.14
F180M	$3.80 \times 10^5$	$5.5 \times 10^{18}$	0.33
F187N	$9.26 \times 10^4$	$5.3 \times 10^{18}$	0.20
F187W	$1.02 \times 10^6$	$5.4 \times 10^{18}$	3.0
F190N	$9.44 \times 10^4$	$5.8 \times 10^{18}$	0.27
F205W	$3.57 \times 10^6$	$1.2 \times 10^{19}$	175
F207M	$8.72 \times 10^5$	$8.5 \times 10^{18}$	20.0
F212N	$1.43 \times 10^5$	$9.4 \times 10^{18}$	4.4
F215N	$1.29 \times 10^5$	$8.9 \times 10^{18}$	5.1
F216N	$1.39 \times 10^5$	$9.5 \times 10^{18}$	6.4
F222M	$9.26 \times 10^5$	$9.8 \times 10^{18}$	74.0
F237M	$1.06 \times 10^6$	$1.4 \times 10^{19}$	279

Table 6.5: Camera 3 Filter Sensitivity Parameters

Filter Name	$\eta_c$ [e <sup>-</sup> /sec/Jy]	$\xi$ [e <sup>-</sup> /sec/(W/m <sup>2</sup> )]	B [e <sup>-</sup> /sec]
F108N	$3.78 \times 10^6$	$1.2 \times 10^{18}$	0.0225
F110W	$2.04 \times 10^6$	$2.1 \times 10^{18}$	1.2
F113N	$4.33 \times 10^6$	$1.4 \times 10^{18}$	0.025
F150W	$3.33 \times 10^6$	$5.2 \times 10^{18}$	10.0
F160W	$1.78 \times 10^6$	$5.1 \times 10^{18}$	2.7
F164N	$8.13 \times 10^6$	$3.9 \times 10^{18}$	0.0767
F166N	$8.12 \times 10^6$	$4.0 \times 10^{18}$	0.0964
F175W	$5.23 \times 10^6$	$9.5 \times 10^{18}$	71.7
F187N	$8.87 \times 10^6$	$5.1 \times 10^{18}$	1.4
F190N	$9.05 \times 10^6$	$5.6 \times 10^{18}$	1.9
F196N	$9.74 \times 10^6$	$5.9 \times 10^{18}$	4.3
F200N	$1.07 \times 10^5$	$6.4 \times 10^{18}$	6.7
F212N	$1.36 \times 10^5$	$9.1 \times 10^{18}$	30.0
F215N	$1.25 \times 10^5$	$8.7 \times 10^{18}$	35.0
F222M	$9.05 \times 10^5$	$9.7 \times 10^{18}$	51.7
F240M	$1.32 \times 10^6$	$1.3 \times 10^{19}$	30.70

## Software Tools

Rather than going through all the above calculations by hand for every source on an observing list, software tools can be used. These tools created the figures in Chapters 11 and 5. The tools are available on the NICMOS World Wide Web page, and can be found by following the Software Tools link.

Some of the parameters used by these tools are, at the time of writing, still uncertain. Chief amongst these are the dark current and the thermal background. As described earlier, the dark current should be less than 0.1 e<sup>-</sup>/sec, so this is what we currently use in the code; it will be updated as soon as better information becomes available. For the thermal background calculation we have used the values listed in Tables 6.3, 6.4, and 6.5. Both of these parameters will hopefully prove on orbit to be better than we have assumed here, so that the sensitivities we calculate are likely to be a little pessimistic.

## Filter Sensitivity Curves

The first of the tools available will calculate the flux required as a function of time to achieve a given signal to noise for any NLCMOS filter. Two versions of this tool are available, one for point sources and one for extended sources.

Calculations are carried out on a grid of wavelengths across the bandpass of the chosen filter. At each wavelength we determine the filter transmission, detector quantum efficiency, optical efficiency of the NLCMOS+HST system, and source flux. In the case of a point source we determine the fraction of the total source flux which is expected to land on the central pixel, assuming that the source lies directly in the center of a pixel, while for the extended source case we merely have to multiply the surface brightness by the pixel area. For a wide range of integration times we use the above data, plus the dark current, read noise and background radiation (both zodiacal and thermal backgrounds as discussed earlier in this chapter), to calculate the point source flux, or surface brightness, required to achieve a range of signal to noise ratios (in the current version of the software values of 10, 25, 50 and 100 are adopted).

## Signal to Noise for a Source

For a particular source, with a known flux density or surface brightness, there are a pair of tools. These perform very similar calculations to those described above, with the output being signal to noise against time. Currently the source flux must be for the wavelength of the filter; eventually bells and whistles will be added so that you can enter the flux at one of the standard IR photometric bands (I, J, H or K).

## Saturation and Detector Limitations

The signal to noise which can be achieved in a given time is one indication of how useful an observation is likely to be. However, there are two further pieces of information which are important to know, and which are not readily apparent from the mere knowledge of signal to noise: firstly, is the detector operating in its linear response range, and secondly, what is limiting the signal to noise? A further pair of programs generate this information for each filter. These generate both the flux (or surface brightness, as appropriate) above which the observation is limited by photon noise (either from the source or the background) rather than detector noise, and the flux above which the observation enters the non-linear detector operation regime, which we refer to as saturated.

---

## WWW Access to Imaging Tools

The tools described above can be accessed via the WWW pages already mentioned. To run the tools, you will have to first select whether you want to image point sources or extended sources, or obtain grism data. This choice will

take you to another window where you will click on buttons to select the camera and filter, and then you will need to enter a number of reads, source color, temperature, and source flux (in Janskys). The latter is optional, and only used if you want to obtain signal to noise vs. time for a particular source. You can then click the “Submit simulation” button and you will be offered a set of outputs. All three of the tools described above are run simultaneously, so you can choose which of the types of output you want. The “input info” output reminds you what inputs were used and supplies warnings where necessary. “Get the tables” retrieves the ASCII output files generated by the code, and the “Get the plots” option retrieves a graphical display of the output, which you can save for later reference if desired.

---

## Examples

### Using Exposure Time and Signal to noise Calculators

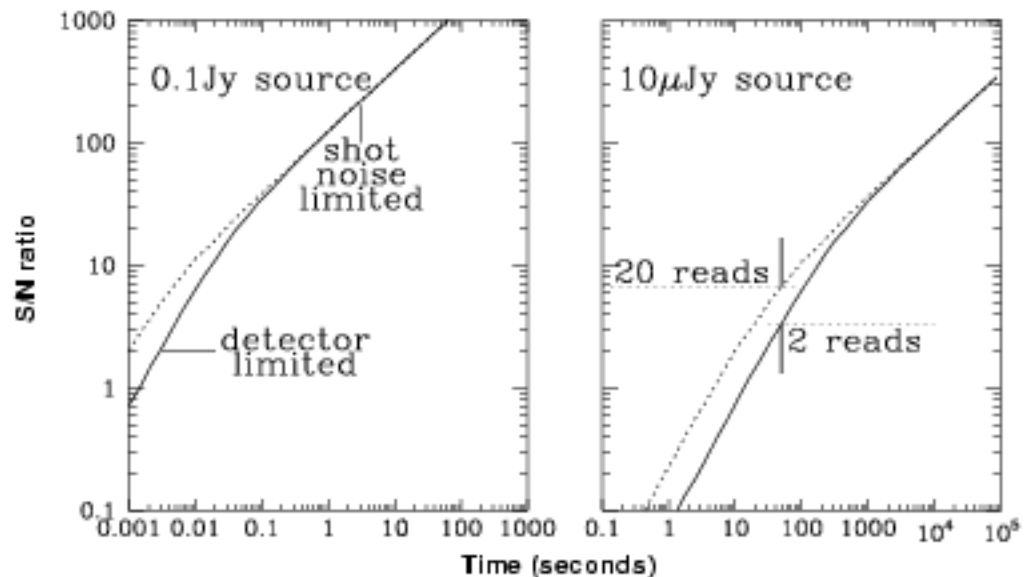
In this section we describe how to use the programs found on STScI’s NICMOS WWW pages, in order to determine the signal to noise for a particular source, or to determine the integration time needed to achieve a given signal to noise.

#### Example 1: Signal to noise with Low Background

Here, the program has been used to model two sources being observed using Camera 1 through the F160W filter, see Figure 6.1. In the left panel we see the case of a 0.1 Jansky ( $H=10.0$ ) source. For a source this bright, we see that whenever it is observed in any mode other than Bright Object Mode (i.e., integration times longer than about 0.2 seconds), the signal to noise obtained is always the same however many readouts are made at the beginning and end of the integration.



Figure 6.1: Signal to Noise with Low Background

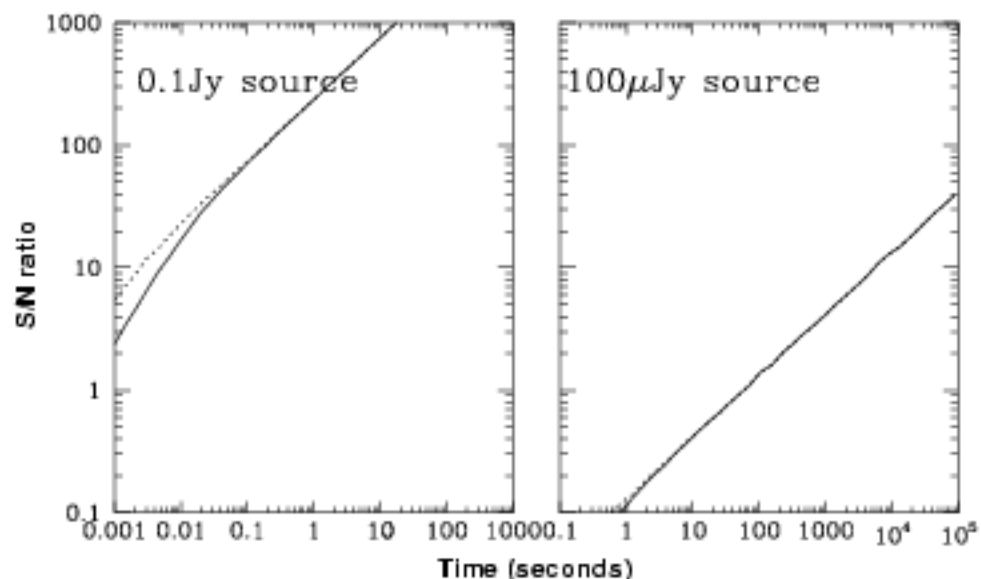


In these modes (ACCUM, or MULTIACCUM), the observation of the source in question is always photon-noise limited, and so the read noise of the detector is irrelevant, and the signal to noise increases roughly as the square root of the integration time. In the right panel is shown the case of a 10  $\mu$  Jansky source (observed through the same filter). In this case, the number of readouts does have an effect on the signal to noise obtained for integration times less than about 1000 seconds. Where the signal to noise obtained is about 5 (integration times of a little less than a minute), increasing the number of readouts by a factor of ten can improve the signal to noise obtained by up to a factor of three or thereabouts. This example illustrates an important point: so long as the background is relatively faint, then if the signal to noise obtained is low, it is probably possible to improve it without increasing the integration time, by increasing the number of readouts. A balance should be sought between the integration time saved by doing this and any extra overhead incurred by making multiple readouts.

### Example 2: Signal to noise with high background

Figure 6.2 shows what happens at longer wavelengths. Here we see two sources, with fluxes of 0.1 Jansky ( $K=9.5$ ) and 100  $\mu$  Janskys observed through the F237M filter with Camera 2. Here the background radiation is so bright that even at very short exposure times the number of readouts makes little difference to the signal to noise obtained. For the 100  $\mu$  Jy source, even when the signal to noise has dropped so low that the source is no longer detected, the number of readouts makes no difference. When the background is bright compared to the source, the observations will invariably be photon-noise limited, and so the only means of improving the signal to noise is to increase the integration time. Multiple initial and final reads are pointless in such cases.

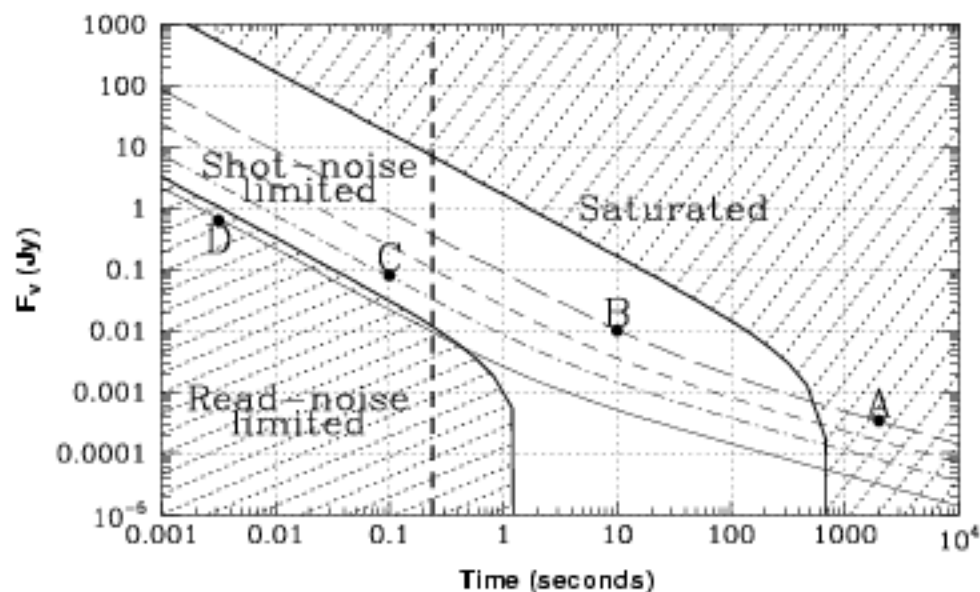
Figure 6.2: Signal to noise with High Background



### Example 3: Exposure Time Determination

Figure 6.3 illustrates the various parameters that are important in constructing a NICMOS observation, using output from the tools. We plot the flux required to obtain a signal to noise of 10, 25, 50 and 100 on a point source against integration time. Four cases are considered, and plotted in the Figure; these cases are identified as A, B, C, and D.

Figure 6.3: Effect of Parameters on NICMOS Observation



In case A, we see that we can obtain a signal to noise of 100 in an integration time of about 2000 seconds. However, the exclusion curves reveal that with such a long integration time the detector is saturated. This does not mean, however, that a signal to noise of 100 cannot be achieved for this source: it simply means that such a signal to noise cannot be achieved *in a single exposure*. Instead, to achieve such a high signal to noise it will be necessary to make a number of separate exposures (ACCUM or MULTIACCUM mode) and co-add the results. If the source of interest is actually fainter than this, and we merely needed to get a signal to noise of 100 on this bright target in order to get sufficient signal to noise on some nearby or surrounding fainter target, we could use MULTIACCUM mode, and repair the saturated core of this bright source.

Case B shows an observation which is optimal: this source can be observed to a signal to noise of 100 in a reasonable integration time (10 seconds), and there are no problems or complications.

Case C shows that it can actually be quicker to obtain *more* signal to noise. A signal to noise of 25 was deemed sufficient, but it transpires that for this source an integration time of 0.1 seconds is required for this signal to noise. This would require Bright Object mode, and to obtain a 0.1 second exposure for every pixel would require about 1600 seconds. However, by increasing the exposure time to about 0.6 seconds a signal to noise of about 90 is obtained, and this integration time is long enough that a standard ACCUM exposure can be made.

Case D shows a source being observed in Bright Object mode, where a relatively short exposure obtains a signal to noise of 10, and the total integration time is a little less than a minute. In this case the signal to noise is dominated by the detector read-noise, however.

#### **Example 4: Exposure Time Calculation for the Calibration Star P041-C**

In this example we derive exposure times for the calibration star P041-C (see Table 15.3) for the purpose of characterizing the medium band filters F222M and F237M (CO band and continuum), and the narrow band filters F215H and F216H (Br  $\gamma$  and continuum) in Camera 2. This example will be used in Chapter 8, where the observing strategy and the overhead estimates will be carried out.

The K magnitude of P041-C is 10.56, corresponding to 0.037 Jansky at 2.2 microns. The star is a solar analog and we assume its color temperature to be 5800 K. The saturation diagrams produced for each filter by the WWW NICMOS exposure time calculator (see also Chapter 11) show that the source will saturate the two medium band filters after only 40 seconds of exposure, due to the high background which affects the 2 micron wavelength window. In the two narrow band filters, the saturation limit will be reached after an exposure of about 300 seconds. Since we want to remain well within the linear response regime of the detector, we choose exposure times which are a half of the saturation limit, namely, 20 seconds for the medium band filters and 150 seconds for the narrow band filters. With these times, the signal to noise ratio versus time diagram produced by the calculator indicates that SNR=280 in the F222M and F237M filters and SNR=315 in the F215H and F216H filters will be obtained. Such high signal to noise ratios are unlikely to be achievable, due to calibration limitations

(such as flat field response and dark current); we expect, however, to be able to reach SNRs around 50–100.

## Examples of Calculations by Hand

### Example 1: Exposure Time for an Emission Line Source

We consider here the example of a diffuse Planetary Nebula with a diameter of 3.0 arcsecs, a Br  $\gamma$  emission line determined from the ground to have a strength of  $10^{-13}$  W/m<sup>2</sup> and negligible continuum. The surface brightness of the nebula in the line is assumed to be uniform, and the observation will be made with Camera 2 in the F21611 filter. We wish to obtain a signal to noise of 20 on each pixel. Two reads at the beginning and end of the exposure will be made.

First of all we determine that the surface brightness in the line is  $1.5 \times 10^{-14}$  W/m<sup>2</sup>/arcsec<sup>2</sup>. The size of a pixel in Camera 2 is 0.075 arcsec, and so the flux falling on a pixel is  $8.3 \times 10^{-17}$  W/m<sup>2</sup>.

The signal generated by this line flux will be calculated using equation (3), in which  $I_{\lambda}$  is  $8.3 \times 10^{-17}$  W/m<sup>2</sup>, as determined above.  $e_{\lambda}$  we read off Figure 11.60 on page 215 is  $9.5 \times 10^{18}$  e<sup>-</sup>/sec/(W/m<sup>2</sup>). We therefore determine the signal generated in the detector is  $C_1 = 2.0 \times 10^{-5} \times 0.62 \times 0.85 \times 1.6 \times 10^5 = 4.4$  e<sup>-</sup>/sec.

Now to determine the exposure time needed we will use equation (5).  $C_1$  we have just determined, and  $C_c$  for this source is negligible. The background emission for this filter we find in Table 6.4 is 6.4 e<sup>-</sup>/sec. At this point we note that the background emission is actually brighter than the source emission. Therefore, we will require a background image in order to remove the background from our image of the source. For a chopped observation, the time on source must equal the time on background. The ratio of the signals from source-plus-background to background-only is 1.69. In this background limited observation the signal to noise will be determined by photon statistics in the signal: the detector noise will be more or less irrelevant. It is easy to show in this case that if we require a signal to noise  $SN_s$  on our background-subtracted image, we must obtain a signal to noise of  $(SN_s^2 \times (1 + 1/1.69))^{0.5}$  on the image with the source in it, which in this case translates to a signal to noise of 25.2.

The dark current we take to be 0.1 e<sup>-</sup>/sec, from Table 7.1. The read noise from Table 7.1 is 28 e<sup>-</sup> for this detector. The required signal to noise is 25.2. We can now use equation (5), and we find that the time required is 507 seconds. It must be borne in mind that this is only the on source time, and that another 507 seconds observation of the background will be required.

### Example 2: Exposure Time for a Line Plus Continuum Source

In this example we consider the case of a galaxy which is to be observed with Camera 1 using the F09511 and F09711 filters. It is expected to have a uniform surface brightness of 0.2 Jansky/arcsec<sup>2</sup> in the continuum and  $4.2 \times 10^{-15}$  W/m<sup>2</sup>/arcsec<sup>2</sup> in the line. The redshift of the galaxy is 0.005. A signal to noise of 20 is required in the [SIII] line image after the continuum has been subtracted. The continuum spectral energy distribution is flat enough in this wavelength

region that differences in continuum level between 0.95 and 0.97 microns can be ignored.

In order to generate the [SIII] line image, we will have to subtract the F09711 image from the F09511 image, assuming that the continuum at the two wavelengths is identical (for sources with very low line-to-continuum ratio, this assumption might be dangerous for the post-observation image analysis). We will assume for simplicity that these observations are all photon-noise limited, so that the signal to noise varies roughly as the square of integration time. The noise in the final line image will be the square root of the sum of the squares of the noise in the two observed images.

The continuum surface brightness is  $0.2 \text{ Jansky/arcsec}^2$ , and the constant  $\eta_c$  from Table 6.3 is  $3.83 \times 10^4$  for the [SIII] continuum filter. The pixel surface area is  $1.85 \times 10^{-3} \text{ arcsec}^2$ . Therefore the continuum signal in the F09711 filter is  $C_c = 0.2 \times 3.83 \times 10^4 \times 1.85 \times 10^{-3} = 0.14 \text{ e}^-/\text{sec}$  (from equation 1 on page 78).

In the line filter we have to consider the contributions both from the line and from the continuum. The continuum surface brightness is as used above, and the efficiency constant  $\eta_c$  is  $3.45 \times 10^4$  from Table 6.3. This gives us a continuum signal of  $0.2 \times 3.45 \times 10^4 \times 1.85 \times 10^{-3} = 0.13 \text{ e}^-/\text{sec}$ . The line efficiency factor  $\epsilon_\lambda$  is  $4 \times 10^{17} \text{ (e}^-/\text{sec)/(W/m}^2\text{)}$ . Therefore, the signal generated by the line is  $C_l = 4.2 \times 10^{-15} \times 4 \times 10^{17} \times 1.85 \times 10^{-3} = 3.1 \text{ e}^-/\text{sec}$ . Thus the combined signal in the F09511 filter should be  $0.16 \text{ e}^-/\text{sec}$ .

The signal rates are roughly the same for the two images, so each will contribute roughly equal amounts of noise to the final image. (Note that if the continuum was much fainter than the line emission, the continuum image would contribute much less noise to the final result than the F09511 image. If the item of interest is the resulting line image, it does not make sense to integrate for a long time to obtain good signal to noise on the continuum image, since it will not significantly affect the signal to noise in the final image. In our example here, both images contribute similar amounts of noise to the result, and so it is equally important to obtain high signal to noise for both images.) Therefore the signal to noise required in each image is roughly  $(16/31) \times 20 \times 2^{0.5}$ , or 146.

For the F09511 filter, the background is  $1.04 \times 10^{-3} \text{ e}^-/\text{sec}$  (Table 6.3), the number of reads is 2, and the dark current is taken to be  $0.1 \text{ e}^-/\text{sec}$  as before. The required exposure time for this image is therefore roughly 1360 seconds. For the F09711 filter, the background is slightly higher, and the count rate slightly lower; the required exposure time turns out to be 1550 seconds. The two images thus require of order one orbit.

Finally, we should comment on two aspects of this proposal. First, the signal to noise being requested is very high. It is far from clear that the various calibration data needed will be of sufficiently high signal to noise to allow a signal to noise of 146 in the final product. In practice, a signal to noise of 100 is probably an impressive goal to aim for. Second, although the redshift of this galaxy is rather low, the line is on the edge of the filter curve. For sources with large redshifts, care is needed to check whether emission lines of interest fall into any of the available filters.

## NICMOS Grism Sensitivity on the Web

As already mentioned, software tools are available on the NICMOS WWW pages to assist in the preparation of grism observations and proposals. These tools are exactly analogous to the tools previously described for imaging observations, and the same caveats apply. Since grism data will be difficult to interpret in the case of extended sources, these tools currently only deal with point sources.

### Grism Sensitivity Curves

This tool is exactly analogous to the imaging tool described earlier. The same calculations are carried out in the same manner. The differences are that in this case the PSF is considered to be one dimensional only, and calculations must be carried out separately for various wavelengths inside the grism bandpass. In practice, we choose 3 wavelengths inside the grism bandpass, and carry out calculations at each of the three wavelengths for signal to noise ratios of 10 and 100. The results of this calculation were plotted in the previous section.

### Signal to noise for a Particular Source

To obtain a signal to noise ratio for a particular source, with known flux density and color temperature, another tool is available. Currently the source flux must be for the central wavelength of the grism bandpass; eventually it will be possible to enter the flux at one of the standard IR photometric bands. The source currently is represented by a blackbody spectrum; eventually it may be possible to adopt a model atmosphere spectrum, or enter a user-supplied spectrum. The output from this code is time against wavelength for a set of signal to noise ratios (currently 10, 25, 50 and 100).

### Saturation and Detector Limitations

Again, this tool is analogous to the corresponding image mode tool. It generates the fluxes required to saturate the detector and for the photon noise to exceed the detector noise as a function of time. In principle this information should be calculated as a function of wavelength; however, since the sensitivity inside the grism passbands is only very weakly a function of wavelength, we carry out the calculations only for the central wavelength. Departures from this value will only be significant for wavelengths near the ends of the spectrum where the grism throughput is changing rapidly.

### WWW Access to Grism Tools

If you select the grism spectra option, you will be offered choices almost identical to those for the imaging tools, except that now only one camera (Camera 3) is available.

## CHAPTER 7

# NICMOS Detectors

### In This Chapter...

Physical Characteristics / 91  
Flat Field Response / 97

NICMOS uses three  $256 \times 256$  HgCdTe Rockwell arrays, one in each camera. We report on their measured detector quantum efficiency (DQE), read-noise, and dark current which have been determined at the unit test level prior to this summer's thermal vacuum characterization. Other aspects of their expected performance are discussed here, including shading, linearity and saturation, cosmic ray susceptibility and flat fielding.

---

## Physical Characteristics

Each detector array comprises  $256 \times 256$  square pixels and is divided into 4 quadrants of  $128 \times 128$  pixels, each of which is read out independently. The basic performance of the nominal flight detectors is summarized in Table 7.1. Typically, the read-noise is  $\sim 30e^-/\text{pixel}$ , and the dark current  $< 0.2e^-/\text{sec}/\text{pixel}$ . (The dark current is probably closer to a tenth of this upper limit, but this is currently the limit of our measurement accuracy. We expect to obtain better measurements from SLTV and on orbit.) Only a few tens of bad pixels (i.e., very low response) are expected. The current gain figures,  $\sim 10 e^-/\text{ADU}$ , have been set so as to map the full useful dynamic range of the detectors into the 16-bit precision used for the output science images.

### Detector Response Curves

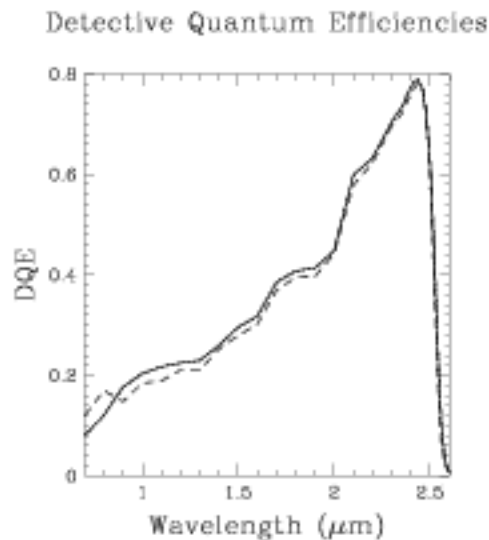
Preliminary measurements of the wavelength-dependent detector quantum efficiencies, averaged over the detector, are shown in Figure 7.1.

Table 7.1: Flight Array Characteristics

Characteristics	Camera 1	Camera 2	Camera 3
Dark Current ( $e^-$ /second)	<0.2	<0.1	<0.2
Read Noise ( $e^-$ ) <sup>a</sup>	30	28	33
Bad Pixels	86(0.1%)	74(0.1%)	37(0.1%)
Conversion Gain ( $e^-$ / ADU)	10.32	10.23	12.83
SATURATION ( $e^-$ ) (98% Linearity)	184000	173000	205000
50% DQE Cutoff Wavelength (microns)	2.55	2.53	2.52

a. The quoted readout noise is the realized noise from a pair of readouts (i.e., the quadrature sum of a single initial and final readout).

Figure 7.1: DQE Versus Wavelength for Flight Arrays (solid line is IIC1, broken line IIC2, IIC3 is not plotted but is similar to the other two)



The fine details in these DQE curves should not be interpreted as detector features, as they may be artifacts introduced by the test set-up used to measure them. At the blue end, near 0.9 microns, the DQE is  $\sim 15\%$ , and rises quasi-linearly up to a peak DQE  $\sim 80\%$  at 2.4 microns, after which there is a rapid decrease to zero at 2.6 microns. The NICMOS arrays are blind to longer wavelength emission. When looking at these DQE curves, the user should bear in mind that this is not the only criterion to be used in determining one's sensitivity in the near-IR. For example, significant thermal emission from the telescope starts to be a problem beyond  $\sim 1.6$  microns. The shot-noise on this bright background



significantly degrades the signal to noise obtained at long wavelengths, negating the advantage offered by the increased DQE.

It is very important, especially for observations of very faint targets where the expected signal to noise is low, to note that the DQE presented here is only the average for the entire array. The flat field response described in detail later is non-uniform, and thus the DQE curves for individual pixels may be rather different.

The individual pixels in the NICMOS arrays are completely independent, and they do not suffer from the charge transfer effects present in CCDs, or from *bleeding* if the wells are filled due to over exposure. They do however have read-noise as well as their own special detector artifact, shading.

## Shading—a Detector Artifact

The NICMOS arrays exhibit a noiseless signal gradient, a kind of pixel-dependent bias, orthogonal to the direction of primary clocking, called *shading*.

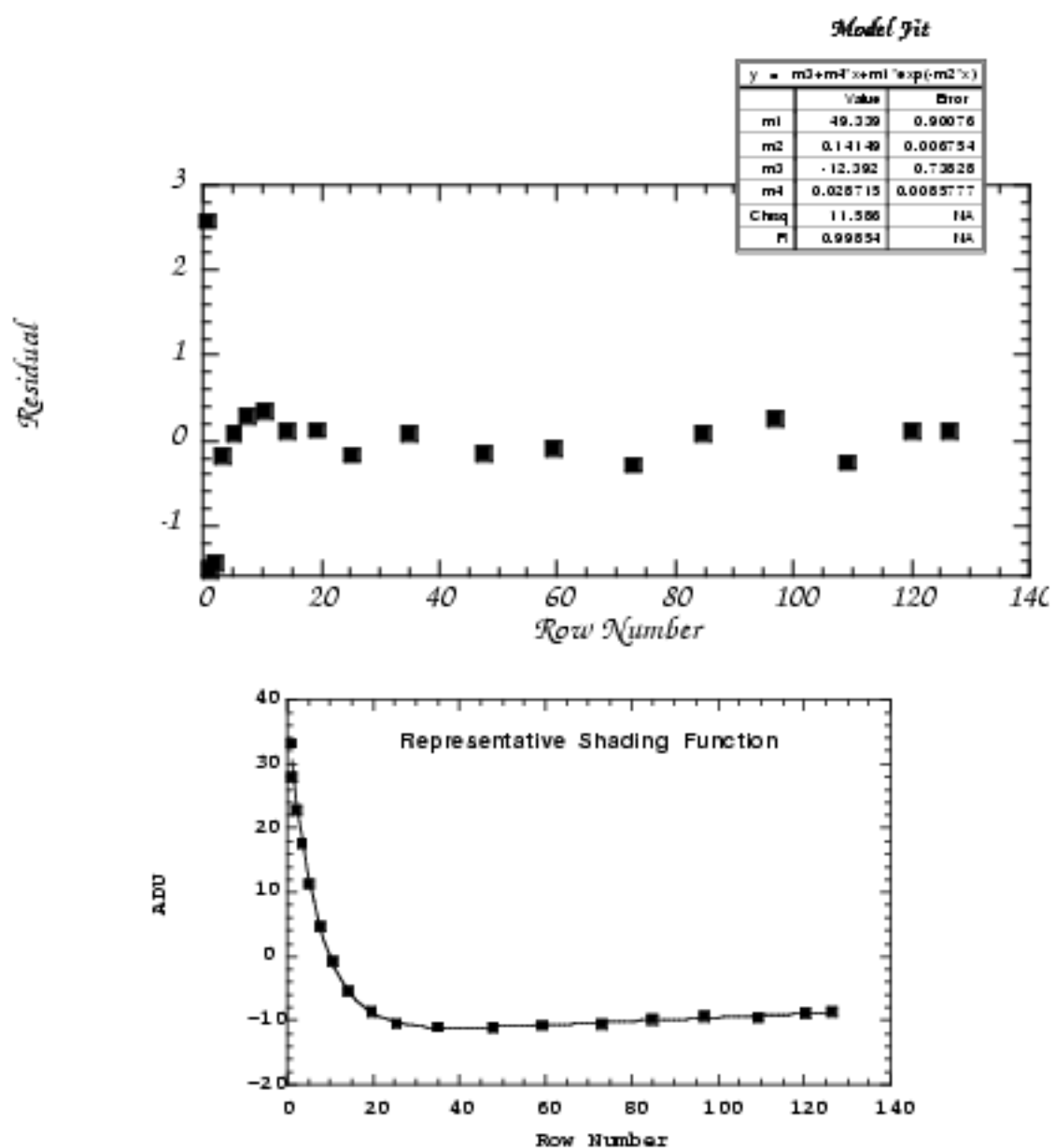
The shading effectively changes the bias level for the pixels as a function of time. The amplitude of the shading is as large as several hundred electrons for some pixels for very short integration times, but becomes negligible after only a minute or two. We will obtain dark observations for a number (probably of order 30) of integration times, which will allow accurate removal of the shading in the calibration pipeline software. The integration times that we will use for these calibration exposures will be published in a handbook update in mid-August, and our current list of expected times is in Table 8.2. We recommend that observers use one of these times. For all other integration times the pipeline will interpolate between the calibration exposures to remove the shading. We expect, but cannot guarantee, that this will work well.

The magnitude of the shading signal is dependent upon:

1. Time between a pixel read and the last reset in its row.
2. Pixel clock rate (the readout duration).
3. Array column number (similar functional forms, but different scaling).

Shading is repeatable for image frames clocked in exactly the same manner. The typical functional form of the shading for one of the flight spare arrays is shown in Figure 7.2. There is a rapid initial exponential decay (e-folding length  $\sim 0.2$  pixels) over the first  $\sim 32$  rows of the detector, after which it is almost flat. The results of a model fit of the form given in the figure is shown in the lower panel as a solid line. The bottom panel shows the observed shading (in ADU) versus row number (squares). The solid line shows a least-squares fit of an exponential function of the form shown in the insert to the top panel. The top panel shows the residuals from this fit, which are small.

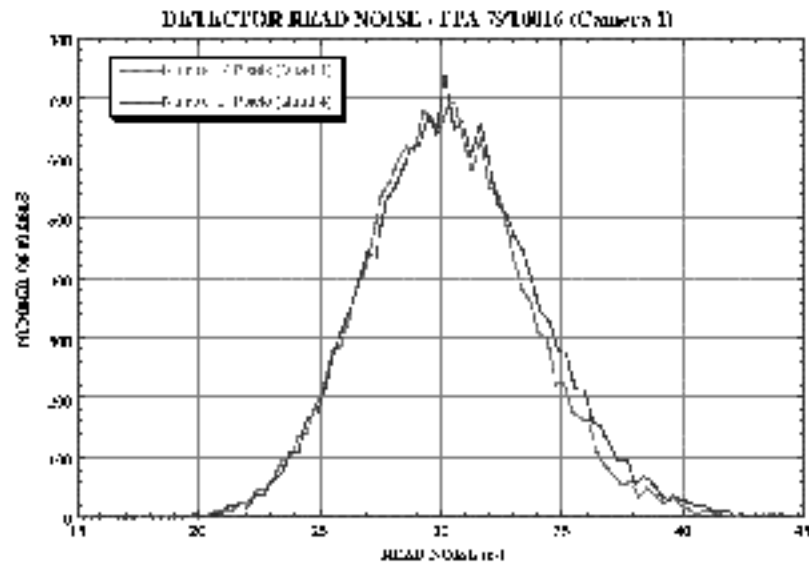
Figure 7.2: Shading Characteristics



## Read-Noise

Each detector has four independent readouts, each of which reads a  $128 \times 128$  quadrant. The four different readouts each generate very similar amounts of read noise to one another—this is illustrated in Figure 7.3, where the read noise distributions for the 1st and 4th quadrants of the Camera 1 array are compared. The distribution of read noise values for all the pixels in a given quadrant is relatively narrow (see Figure 7.3; a FWHM of 8 electrons is measured), so that there are very few very noisy pixels in these arrays (if the distribution were very broad, calculations of expected signal to noise values, which were critically dependent on the read noise, would be misleading).

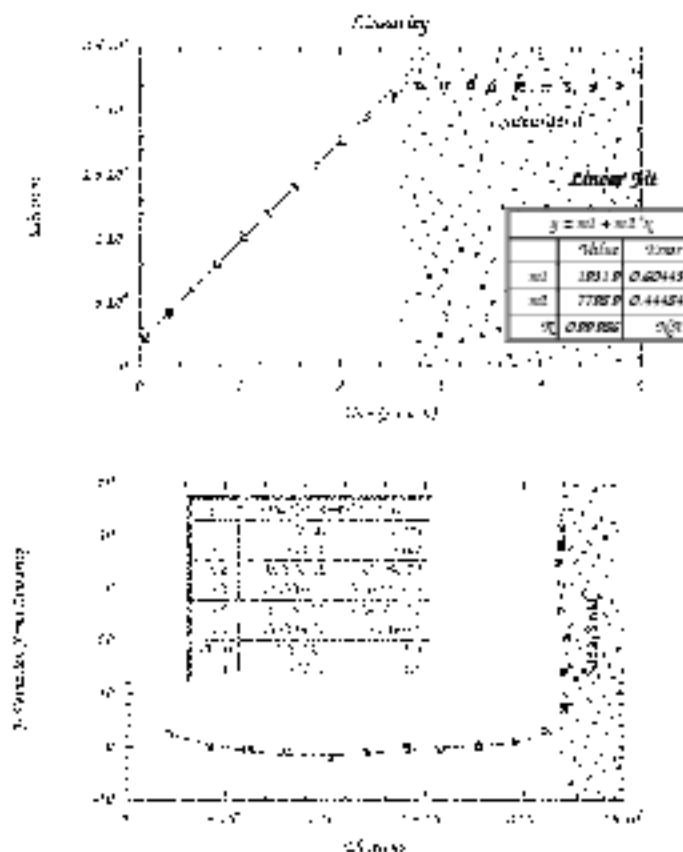
Figure 7.3: Read Noise Characteristics for Two Quadrants on Camera 1 Detector



## Linearity and Saturation

The NCMOS arrays exhibit an essentially linear response over much of their useful dynamic range. Figure 7.4 illustrates the regimes of non-linearity and saturation for a representative small region of one of the arrays. A linear regression fit to the data (solid squares) is shown in the top panel. In both the very low flux regime, and in the high flux regime, departures from linearity occur (lower panel of Figure 7.4). The non-linear portions of the response curves are highly repeatable and will be characterized on a pixel-by-pixel basis. Linearity corrections, based upon this characterization, will be performed in the calibration pipeline.

Figure 7.4: Linearity of NICMOS Arrays



## Effect of Cosmic Rays

As with CCDs, cosmic ray hits will produce unwanted signal in the output images, but hot pixels are not expected to develop from such hits. The NICMOS arrays have been subjected to radiation doses much higher than expected in their entire lifetime in accelerator tests without sustaining any long-term damage or measurable depreciation in DQE. Hence, cosmic rays should have little impact on the long-term array performance in orbit.

The expected frequency of cosmic ray hits is large enough that we recommend the use of MULTIACCUM for all exposures longer than 10 minutes, in order to filter out cosmic rays or multiple ACCUM images. MULTIACCUM provides a series of intermediate non-destructive reads as well as the final image (see Chapter 8). These intermediate reads can be used to identify cosmic ray hits, analogous to the use of CRSPLITS in WFPC2 or STIS observations. The calibration pipeline, described in Chapter 13, can identify and remove cosmic ray hits from MULTIACCUM observations.

## Intra-Pixel Sensitivity Variations

As with many other modern array detectors, the sensitivity of the NICMOS detectors is lower near the edges of pixels than in their centers. It is as though there were very small regions of reduced sensitivity along the intra-pixel boundaries. This means that the response of a pixel to a source whose flux changes rapidly on a size scale comparable with or smaller than the pixel size will depend on where the center of the source lies with respect to the center of the pixel. Since the latter is not known a priori, this effect will introduce some uncertainty in the flux calibration for a point source. This uncertainty will be largest for Camera 3 at short wavelengths, for which the PSF is undersampled. We will try to measure the size of this effect on orbit, but we expect it to be no more than a few percent uncertainty for Camera 3.

---

## Flat Field Response

Flat field frames taken with the NICMOS arrays show significant large-scale non-uniformity as well as pixel-to-pixel fluctuations. We shall correct these fluctuations in the normal way by flat fielding, which is an essential part of the calibration pipeline.

### Characteristics of the Flat Fields

In conjunction with the NICMOS science team we carried out a number of flat field tests using a flight spare detector array, and report here on our results. (Detailed results are given in two technical reports LSR 5 and 6, see the NICMOS WWW pages.) The flat field calibrations for the flight detectors themselves will be performed in July 1996 and these data will complement the earlier study. Figure 7.5 shows the measured flat field response at a number of wavelengths. (We estimate that the likely uncertainties of the flat field response measurements are ~4%.) At 0.8 microns, the most sensitive areas on the array are > 2 times more sensitive than the mean, and the least sensitive areas < 1/2 as sensitive (i.e. there is variation by a factor of ~ 5 in the relative response across the array). This declines to a factor of ~ 3 at a wavelength of 2.2 microns, and at 2.5 microns the array is almost flat. To quantify the large scale variations we have binned the data into 10 x 10 pixel regions. Variations of almost a factor of 4 occur between the most and least sensitive regions in the array at intermediate wavelengths and this rises to a factor of eight at the shortest wavelengths.

In order to assess the amplitude of pixel-to-pixel variations in response, we generated a version of the flat field response smoothed by a 4 x 4 pixel kernel, then divided the original flat field response by this. The result is displayed in several ways in Figure 7.6, for a wavelength of 1.5 microns, and shows that the variations are essentially random with position on the array, and have a typical 1 $\sigma$  amplitude ~8% and that the pixel-to-pixel variations are independent of the global response.

**Figure 7.5:** Flat Field Response Images Using 10% Bandwidth Filters on a Flight Spare Array. Wavelengths used include (a)  $0.8\mu\text{m}$ , (b)  $1.5\mu\text{m}$ , (c)  $2.1\mu\text{m}$  and (d)  $2.5\mu\text{m}$ . The images have been normalized to the mean response for each wavelength. The contours and greyscale are linearly spaced in each image between normalized responses of 0.4 and 2.2. Significant areas of the array span this whole range at  $0.8\mu\text{m}$ , while at  $2.5\mu\text{m}$  the array is almost flat.

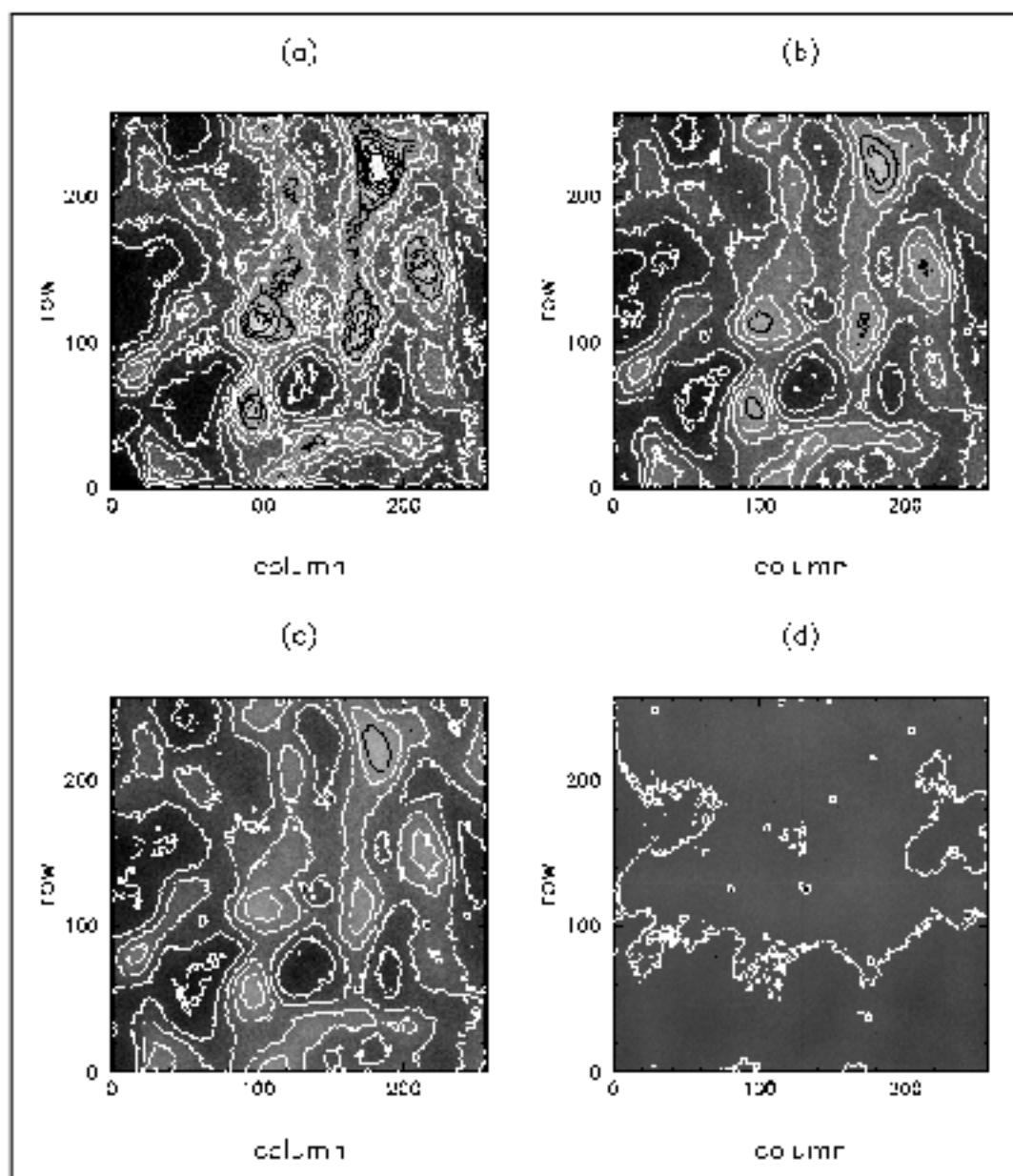
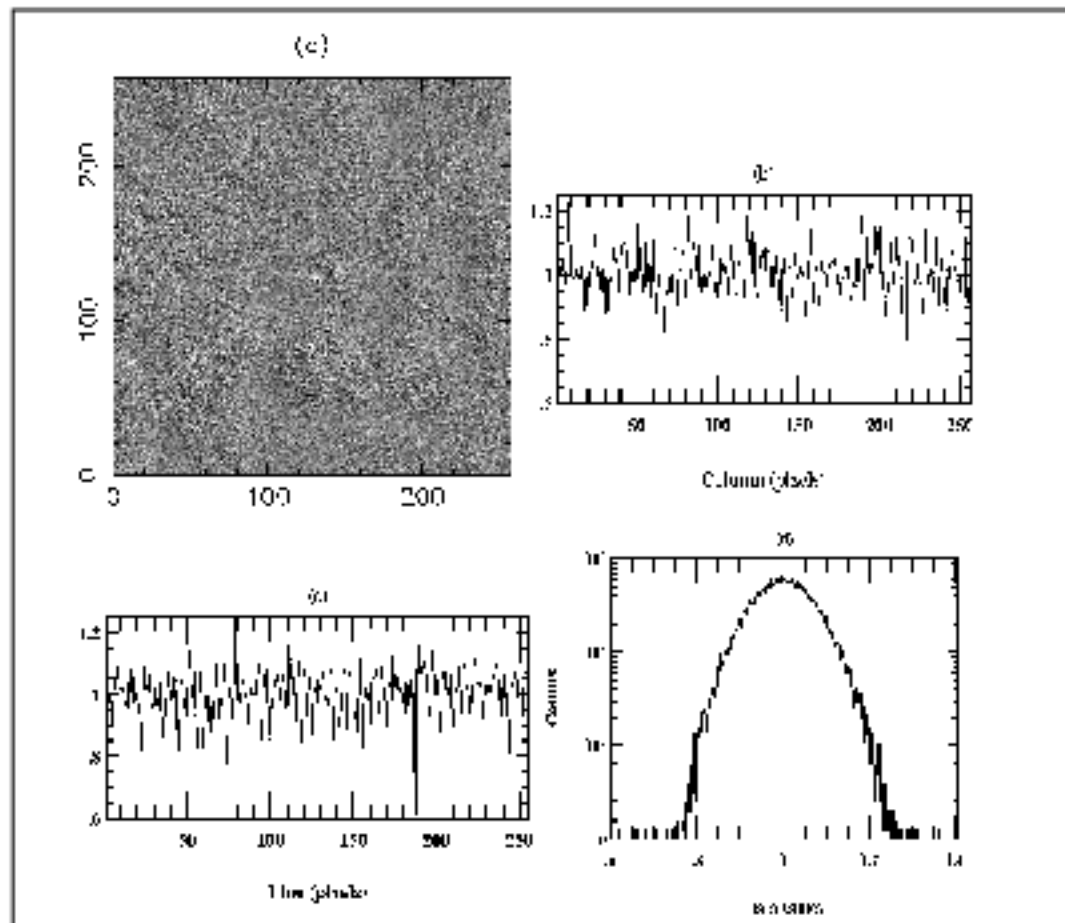


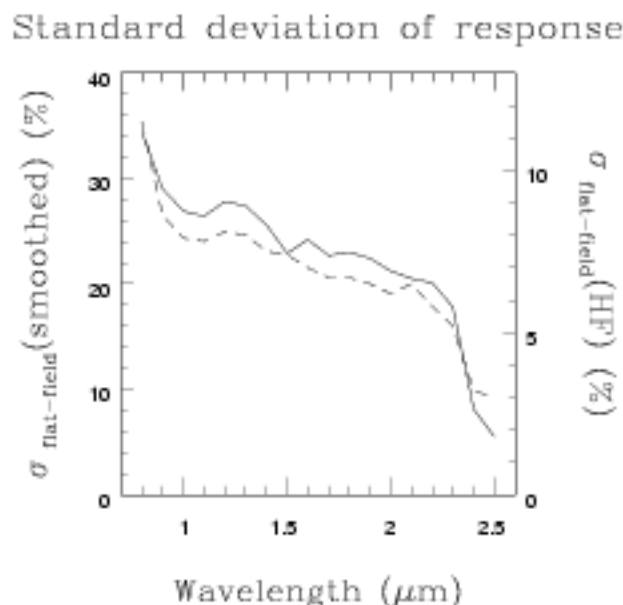
**Figure 7.6:** High Spatial Frequency Noise at 1.5 $\mu$ m. This was measured by dividing the image in Figure 7.5, (b) by a smoothed version of itself (see text). The grey-scale version in (a) is scaled between 0.9 and 1.1. Slices through the image are plotted in (b) along row 100 and in (c) along column 100. The distribution of data is plotted as a histogram in (d).



## Wavelength Variations—Details

The size of the pixel-to-pixel sensitivity variations with wavelength is similar to that measured for spatial variations in the global flat field response. At 0.8 microns the standard deviation of the pixel-to-pixel sensitivity variations is ~11%, at 1.5 microns it is ~7%, at 2.1 microns ~6% and at 2.5 microns it is less than the uncertainties on our measurements. While it is difficult to define a single number which adequately quantifies the behavior of the flat field response over the entire array, the standard deviation plot in Figure 7.7 gives a reasonable representation of the general manner in which the flat field response varies with wavelength. Inspecting this figure we see that the patterns of variation in sensitivity with wavelength are rather similar on small and large scales.

Figure 7.7: Amplitude of Flat Field Response Variations as a Function of Wavelength. The solid line shows the global flat field response, defined as the standard deviation of the individual pixel responses, while the dashed line shows the pixel-to-pixel variations. The two follow the same behavior very closely.

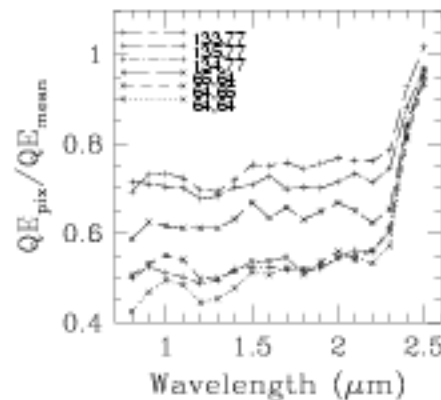


The relative response of four selected areas of three pixels is displayed in Figure 7.8. Each area plotted consists of adjacent pixels, either in a line or in an “L” shape. Two of the areas are from regions which were clearly of relatively high sensitivity, and the other two in regions of relatively low sensitivity. The ratio of the pixel sensitivity over the mean for the array at that wavelength is plotted against wavelength, using all of our 10% bandwidth measurements. The results show clearly that for many pixels, at wavelengths between 1.0 and 2.2 microns the variation in response changes fairly slowly, but that at a wavelength near 2.25 microns there is a turnover, past which the change with wavelength is dramatic.

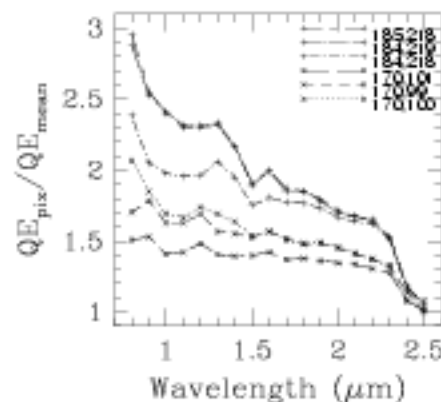


**Figure 7.8: Relative Response as a Function of Wavelength of Three-Pixel Groups.** These diagrams basically show the response of a given pixel relative to the mean for the array at each wavelength, for groups of pixels in regions of low sensitivity (top panel) and high sensitivity (bottom panel). These figures show that the response flattens rapidly longward of 2.2 microns.

Relative Response In Cool Spots



Relative Response In Hot Spots



The rather dramatic change in the flat field response near 2.25 microns is likely to degrade the photometric accuracy of observations in the longest wavelength NICMOS filters. To estimate the magnitude of these effects we can make a number of comparisons of data in this wavelength region. First, we compare the broad band (K) flat field response with the 10% bandwidth 2.2 microns flat field response. The two flat field images differ by almost 10%, which emphasizes how rapidly the response is changing inside the K bandpass. Secondly, we have compared the flat field response images obtained using 2 filters: the 10% bandpass filter at 2.4 microns and the narrow bandpass filter at 2.415 microns. We find that they differ by about 4%, close to the uncertainties in the data. These results suggest that the change in the flat field response between 2.3 microns and 2.5 microns is more or less linear.

Overall, present indications are:

- The flat field response variations are large and wavelength dependent. The difference in response between the most and least sensitive areas is almost a factor of five at the shortest wavelengths and a factor of 1.1 at the longest wavelengths.
- The variation with wavelength is not linear, the largest variations occurring in small wavebands shortward of 1.1 microns and longward of 2.2 microns. The variations in response longward of about 2.2 microns are much more extreme than those shortward of 1.1 microns.
- The arrays exhibit wavelength dependent pixel-to-pixel response variations, ranging from an amplitude of order 10% at the shorter wavelengths to less than our measurement uncertainties at the longest wavelengths. The variation with wavelength of the pixel-to-pixel response variations is almost identical to the behavior of the global flat field response variations.

Despite these results, we expect to be able to flat field on-orbit astronomical data to high precision because the non-uniformities should be very stable with time.

## Special Situations

### Sources with Extreme Colors

We have carried out tests to establish the likely impact on photometric observations of sources of extreme colors induced by the wavelength-dependent flat field. For each filter, we used two sources with different colors assuming spectral energy distributions were black-body functions. The first case had a color temperature of 10,000K, and thus is typical of stellar photospheres and the resultant color is representative of the bluer of the sources that will be seen with NICMOS. (It is worth noting that for reflection nebulae illuminated by hot stars, a significantly bluer spectrum is often seen.) The second source had a color temperature of 700K which in ground-based terms corresponds to  $[J - K] = 5$ , a typical color encountered for embedded sources, such as Young Stellar Objects (YSOs). (Again, there are sources which are known to be redder. The Becklin-Neugebauer object, for example, has no published photometry at J, but has  $[H - K] = 4.1$ , and the massive YSO AFGL2591 has  $[J - K] = 6.0$ . YSOs with  $[J - K] = 7$  are known, although not in large numbers.)

An example of a pair of the simulated spectra is shown Figure 7.9, for the F110W filter. In this filter an image of a very red source will be dominated by the flat field response in the 1.2 to 1.4 micron interval, while for a blue source the most important contribution will come from the 0.8 to 1.0 micron interval. The results of our study for the worst affected filters are shown in Table 7.2.

- Even for the broadest NICMOS filters the wavelength dependence of the flat field response generates only small photometric errors, typically less than 3% for sources of unknown color. Not surprisingly, the largest errors arise in the 3 broadband filters whose bandpasses include some part of the regions where the flat field response changes most rapidly.

- The same results hold true even for filters at the most extreme wavelengths (e.g., F090M, F222M and F240M) because of their small bandwidth.
- It will probably be difficult to obtain photometry to better than the limits shown in Table 7.2 for the F090M, F110W, F140W, F205W and F240M filters, and observers requiring higher accuracy should contact the Help Desk at STScI for guidance.
- These errors can probably be corrected if more accurate photometry is needed, by taking multi-wavelength observations and using an iterative correction technique.
- For observers requiring high precision photometry, these represent non-trivial limits beyond which it will not be possible to venture without obtaining multi-wavelength images. In order to obtain 1% precision using the F110W filter, for instance, observers should observe at a minimum of one other wavelength. The color information derived from the pair (or group) of images could then be used to construct a more appropriate flat field image, which could then be applied to improve the color information, and so on.

Figure 7.9: Detected Source Spectrum. These are for sources with color temperatures of 700K (solid line) and 10,000K (dashed line). It is easy to see that the detected image will be dominated by the flat field response in the 1.2-1.4 $\mu$ m region for a 700K source, while for a 10,000K source the detected image will be affected by the flat field response throughout the filter bandpass.

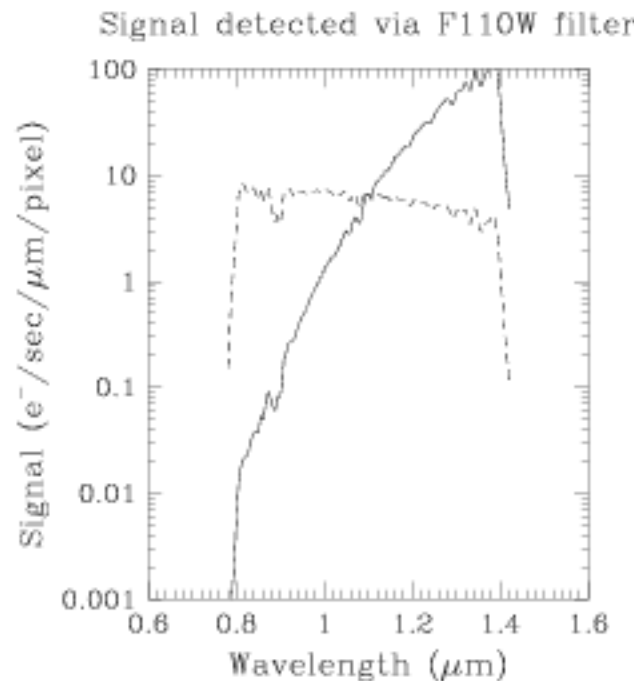


**Table 7.2:** Filters with Largest Photometric Errors for Sources of Extreme Color

Filter	10,000K model. Error (percent)	700K model. Error (percent)
F090M	<0.1	1.9
F110W	1.1	2.9
F140W	0.7	3.1
F160W	<0.1	0.3
F187W	<0.1	0.3
F205W	0.4	2.1
F222W	<0.1	0.1
F240M	1	0.9

## Extended Sources with Extreme Spatial Color Variations

Our analysis has been limited to point sources, but some mention should be made of the situation for extended objects. A good example is the YSO AFGL2591. This has an extremely red core, whose  $[J - K] = 6$  and which is entirely undetected optically. However, it also has a large IR nebula which is quite prominent at J and K, and in the red visual region, but much fainter at L, and which is probably a reflection nebulosity. Spatially, the nebula has highly variable color, some parts of it having fairly neutral or even slightly blue colors in the NICMOS waveband, while other parts are extremely red. Obtaining very accurate measurements of the color of such a source would again require the use of images at more than one wavelength and an iterative tool of the kind described earlier. A further example of this kind of complicated object is the prototypical post-AGB object CRL2688, the Cygnus Egg Nebula, which has an extremely blue bipolar reflection nebula surrounding an extremely red core. Techniques which require very accurate measurements of the surface brightness of extended objects, such as the brightness fluctuation technique for distant galaxies, will need to be applied with care given to the photometric uncertainties such as those discussed here.

## Multi-Object Grism Spectroscopy

Flat fielding will be a problem because of the combined effect of the source spectrum and sky background falling on individual pixels. Astronomical sources well above the background should be measurable. Spectra of very faint sources are likely to be severely modulated by the flat field.

## CHAPTER 8

# Detector Readout Modes

### In This Chapter...

Introduction / 105
Accumulate Mode / 107
Multiple-Accumulate Mode / 110
Read Times & Dark Current in ACCUM & MULTIACCUM / 112
Bright Object Mode / 114
Acquisition Mode / 116
NICMOS Science Data / 117
Summary and Quick Reference / 118

The NICMOS flight software supports several detector readout modes which take advantage of the non-destructive read capabilities of the detectors to yield the optimum signal to noise for your science observations. These are described in detail in this chapter. In describing these we introduce the nomenclature used to command each of the modes in the Phase II proposal instructions. Finally we give recommendations about when to use of each of these readout modes.

---

## Introduction

NICMOS has four detector readout modes that may be used to take data. After observing time has been approved the choices of readout mode can be selected by the observer during the completion of their Phase II proposal entry. However, a potential observer must understand the advantages and limitations of each of the readout modes in order to properly design their Phase I proposal.

There are three available readout options within this general framework:

1. Accumulate Mode.
2. Multiple-accumulate Mode.

## 3. Bright Object Mode.

The basic scientific rationale behind each of these modes, and a summary of their capabilities is outlined in the Table 8.1, along with a recommendation regarding their use. The Phase II proposal instruction needed to identify the operation mode is given in brackets under the mode name.

Table 8.1: Readout Modes and their Functions

Mode	Use	Functionality	Recommendation
Accumulate (ACCUM)	High signal to noise targets Simplest observing mode producing single image Long wavelengths	When read noise > dark current + photon noise Can reduce noise by performing and averaging multiple initial and final readouts S/N gains from multiple reads is limited ~ factor 3. $t > 0.57$ seconds Limited to 173 tabular integration times, 32 of which will have matched dark current calibrations.	Suitable for most programs.
Multiple-Accumulate (MULTIACCUM)	Faint targets Large dynamic range Optimal image construction. Ground processing of cosmic rays and saturation. Long wavelength integrations	Multiple readouts at specific times during an integration $8590 > t > 0.215$ seconds Number of readouts $\leq 25$	Suitable for most programs. Use whenever high dynamic range need e.g., source with bright core and faint extended emission or long integrations times.
Bright Object (BRIGHTOBJ)	For bright targets which would saturate the arrays in the other modes with the shortest integration time allowed	reset/read/wait/read each pixel sequentially in a quadrant $t < 0.2$ seconds	When possible use a narrow filter with ACCUM instead
Onboard Acquisition (ACQ)	Locate brightest source in a subarray and reposition telescope to place source behind coronagraphic spot	Two ACCUM exposures are obtained, combined with cosmic ray rejection, sources located, and centered.	Reasonably bright sources on uncrowded fields.
Ramp (RAMP)	Faint targets Large dynamic range Uncertain target flux On-board cosmic ray removal On-board saturation detection	Slope computation Reduces Data Volume Provides Variance and valid samples array $t > 50$ seconds number of readouts $\leq 50$	MULTIACCUM superior. Only use this if data volume becomes an issue



Ramp mode is not supported for Cycle 7. See Appendix.

## Detector Resetting as a Shutter

It is important to remember that NCMOS *does not have a physical shutter mechanism*. Instead, the following sequence of operations are performed to obtain an exposure:

- *Array reset*: All pixels are set to zero—the bias level.
- *Array read*: The charge in each pixel is measured and stored in the on-board computer's memory. This happens as soon as practical after the array reset. In effect, a very short exposure image is stored in memory. Note that it takes a different, but reproducible time from the array reset to access each pixel during the read.
- *Integration*: NCMOS waits for the period specified for the integration.
- *Array read*: The charge in each pixel is measured and stored in the on-board computer's memory.

## Fast and Slow Readout Modes

The NCMOS detectors have two readout speeds: **FAST** and **SLOW**. While it is possible that **SLOW** mode will result in improved detector performance (e.g., read noise), it is presently expected that **FAST** mode will be the default. There *may* be significant advantages to **SLOW** mode for *readout noise limited observations* but this remains to be determined during the ground testing of NCMOS. If that is the case then this mode will be made available and calibrated for Cycle 7.

The use of **SLOW** mode imposes a 3 second readout overhead which increases the minimum possible integration time (to slightly more than 3 seconds). When multiple readouts are obtained in **ACCUM** mode, the readout overhead becomes rather large (e.g., 30 seconds for **1READ=10**).



At this time we advise observers to plan on using the **FAST** readout mode. Depending upon the results of the ground testing program, STScI may update this advice in mid-August 1996.

---



---

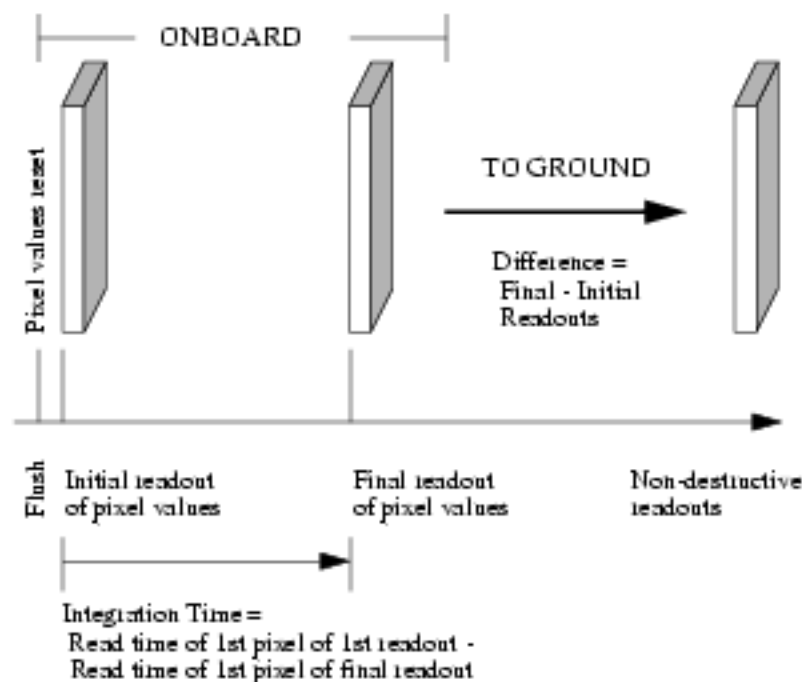
## Accumulate Mode

The *Accumulate Readout Mode* (**ACCUM**) generates the simplest basic exposure. In its simplest incarnation, *two sample readout*, illustrated in Figure 8.1 it is analogous to a WFPC2 readout. This simple two sample readout strategy is the one to use for short integrations of relatively bright objects, and when you are observing in the background limited regime, at long wavelengths. This section is therefore a good place to start to get familiar with the concepts inherent in the operation of the NCMOS arrays, including their *non-destructive readout capabilities*. The allowed **ACCUM** mode integration times are restricted to 173

tabular values. Furthermore, as described on page 112, only 32 of these will have matched dark calibration frames.

The first action of an ACCUM exposure is three passes through the detector *resetting* each of the pixels. The *reset* is immediately followed by a fourth pass through the detector *non-destructively reading* and storing the pixel values. This marks the beginning of the integration. The final action is a second non-destructive reading of the detector, which marks the end of the integration. *The returned image is the difference between the second and the first pass pixel values, and the integration time is defined as the time between the first and second read of the first pixel.* The minimum exposure time is ~ 0.6 sec, and the minimum time between successive exposures is ~ 8-12 seconds. It has the minimum time for output amplifier operation which minimizes the amplifier glow contribution to the image (see below). This method does not discriminate against cosmic ray events and does not check for saturation levels in the image.

Figure 8.1: Basic NICMOS Readout—Simple Two-Sample Readout



Flush time is 0.615s or 3.69s (depending on the detector read speed) and is followed immediately by the Initial Readout.

### Multiple Initial and Final Sample Readout

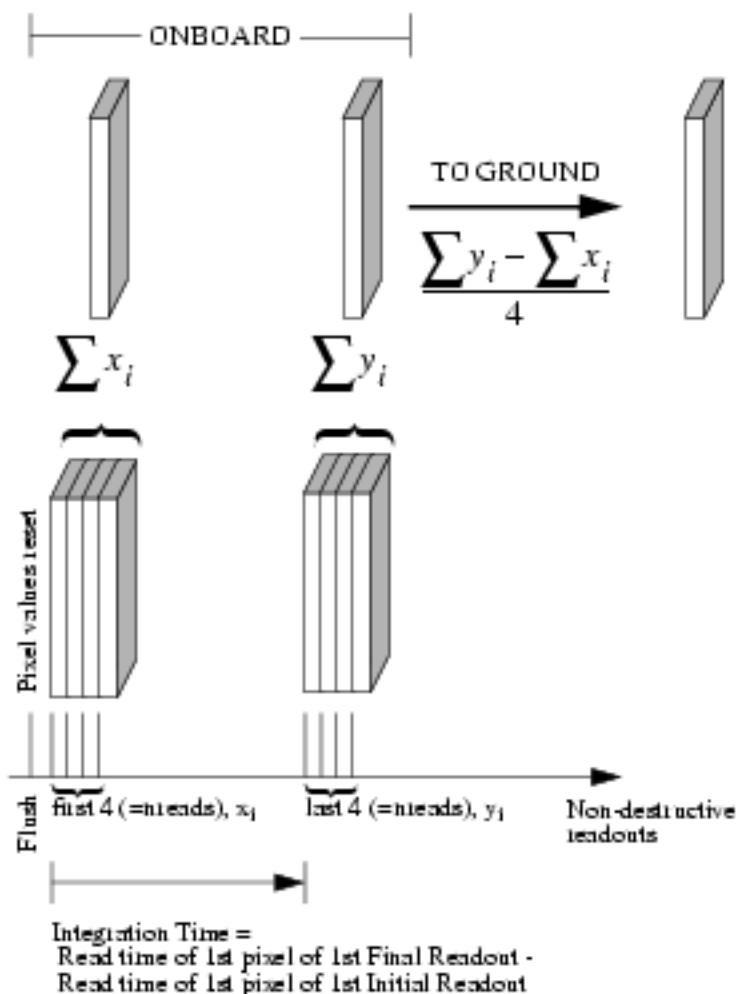
The observer has the option of requesting *multiple reads* in place of the single initial and final readouts in ACCUM mode. In this case after the detector array is reset it will be followed by 1–25 (specified by the NREAD parameter) reads of the initial pixel values which are averaged onboard to define the initial signal level. After the exposure time has elapsed, the final pixels values are again read NREAD times and averaged onboard. The data downlinked is the difference between the



initial and final average signal levels for each pixel. The integration time is defined as the time between the first read of the first pixel in the initial NREAD passes and the first read of the first pixel in the final NREAD passes. The use of multiple reads in ACCUM mode is illustrated in Figure 8.2 for the case of NREAD = 4.

The advantage of this method is a reduction in the read noise associated with the initial and final reads, which can reduce the noise in intermediate time integrations on faint sources. In theory the read noise should be reduced by  $1/(n)^{1/2}$  where  $n$  is the number of reads. For integrations where source photon noise or dark current noise exceeds the detector read noise the multiple readouts may not offer much advantage. This option puts a higher burden on the CPU and requires an additional time per readout of 0.3 seconds in FAST mode. This mode does not discriminate against cosmic ray events and does not check for saturation. An effect known as amplifier glow, which adds extra signal and associated noise close to the corners of the array, becomes important when the number of readouts exceeds 10. Amplifier glow is an additive noise source. Since this only effects a small area of the array this will not be important for many programs, and higher numbers of reads can be useful in further reducing the noise.

Figure 8.2: ACCUM Mode with Four Initial and Final Readouts



## Multiple-Accumulate Mode

Normally a single integration on a target results in a single 256x256 image at the termination of the exposure. The non-destructive nature of the NICMOS readout offers more elaborate methods of using the instrument which aim to optimize the scientific content of the results. In particular it is possible to read-out images at intermediate stages of an integration and *return both these and the final image to the ground*. In this mode of operation, known as *Multiple-Accumulate* (MULTIACCUM) each intermediate readout can only consist of a single readout. The observer uses this capability by creating a list of times, specified by the SAMP-TIME parameters, at which the detector pixels are read out non-destructively creating images of various integration times. The choice of the times during the integration in which the observer can create these reads is very

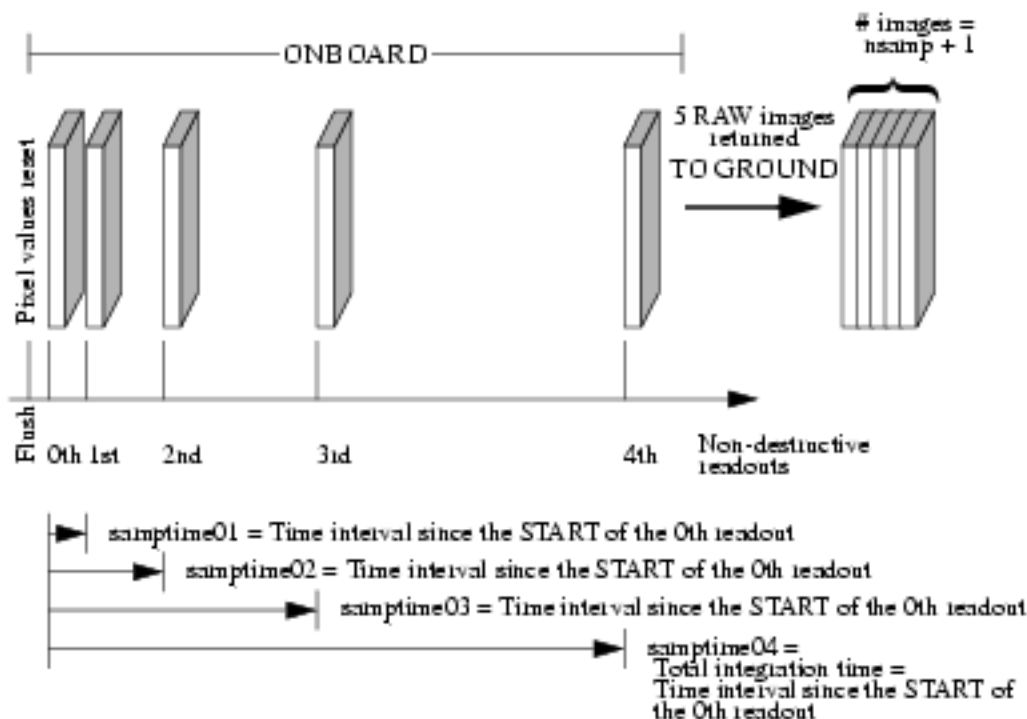
flexible, for example they might be linearly spaced or logarithmically spaced. Linearly spaced exposures may be useful for very faint targets where cosmic ray filtering is important while logarithmically spaced exposures permit the observation of a very wide dynamic range. The process is shown schematically in Figure 8.3 for the case of logarithmically spaced intervals with  $N_{\text{SAMP}}=4$ . In **MULTIACCUM** the detector reset is followed by a single read of the initial pixel values. Then a sequence of non-destructive array readouts are obtained at observer specified times. Up to 25 readouts can be specified spanning a total integration time from 0.215 seconds to 8590.0 seconds. The last read of the detector array ends the exposure and thus the last **SAMP-TIME** will be equal to the total exposure time. All of the readouts, including the initial readout, are stored and downlinked without any onboard processing. This is different to **ACCUM** mode as the initial read is also returned and no on board subtraction occurs. For  $N$  readouts, this mode requires the storage and transmission (downlink) of  $N+1$  times the data volume as the **ACCUM** mode. However, current estimates of the anticipated **NICMOS** observing volume indicate that, with the availability of the 1 gigabit Solid State Recorder (SSR) after the Second Servicing Mission, unrestrained usage of **MULTIACCUM** mode for the primary **NICMOS** camera will be sustainable.

While consuming considerably larger quantities of commanding data volume, internal data storage, and downlink bandwidth than the other **NICMOS** modes, **MULTIACCUM** mode arguably provides the highest quality scientific data in return. The benefits of obtaining observations in **MULTIACCUM** mode fall into two areas.

- The dynamic range of the observation is greatly increased. Rather than being limited by the charge capacity of a **NICMOS** pixel (a few  $\times 10^5$  electrons), an observation's dynamic range is in principle limited by the product of the pixel capacity and the ratio of the longest and shortest exposures (8590.0 and 0.215 seconds). In practice, the PSF and internal stray light will probably be the limiting factors.
- An image can be reconstructed by processing of the stack of readouts to cope with the effects of cosmic ray particle events, as well as saturation.

**MULTIACCUM** provides the best choice for deep integrations or integrations on fields with objects of quite different brightness except when the signal is readnoise limited or the background signal is so bright that it requires the use of short exposures where the background of the telescope dominates the signal.

Figure 8.3: Example MULTI-ACCUM with NSAMP = 4



## Read Times and Dark Current Calibration in ACCUM and MULTIACCUM Modes

Because of the effects of shading, and the possibility that the underlying dark current may vary with time since reset, the removal of dark current (for calibration purposes, we implicitly assume shading is a part of the time variable “dark current”) from data is more complicated than for many other instruments. The most accurate way to accurately remove the dark current from any observation is a measurement of the dark current with an identical integration time. This would also apply to every individual read-out in a MULTIACCUM observation. Of course, this would be prohibitively expensive in on-orbit calibration time. Instead, we have adopted two strategies. First, for ACCUM observations we will make dark current calibration observations for a set of 32 exposure times for a single initial and final read (listed below) and 21 exposure times for 10 initial and final reads. As for WFPC2, only a certain set of exposure times are allowed in ACCUM mode (173 times are specified currently, ranging from 0.57 seconds to 3600 seconds), and in Phase II proposals any user selected exposure time will be rounded down to the nearest available option from the 173 available times. If you select one of the times listed below (this list will be published with the Phase II Proposal Instructions), then the calibration database used by the calibration pipeline software will contain dark current calibration files which are an exact match to

your exposure times. On the other hand, if you must use any other one of the 173 allowed exposure times in *ACCUM* mode, the calibration pipeline will interpolate between the various files in the database to determine the dark current for your exposure time. Based on our current understanding, we expect this to be a very accurate technique, and to be limited by the signal to noise in the dark observations rather than by the interpolation accuracy. For *MULTIACCUM* mode, the individual read-out times can be set to match some of the 32 calibrated times. Finally, we note that the effect of the *FAST* or *SLOW* read-out rate parameter on the dark current and shading will not be known until after SLTV, and at present we are only expecting to support the *FAST* read-out rate. If after SLTV we adopt the *SLOW* rate instead, some of the times listed here will be unavailable. Therefore, we urge all observers to treat the times listed here as provisional only.

**Table 8.2:** Preliminary Exposure Times with Dark Current Calibration

Time (seconds) (NREAD=1)	Time (seconds) (NREAD=10)
0.57	
0.65	
0.73	
0.80	
0.90	
1.05	
1.26	
1.57	
2.01	
2.86	
3.59	
4.96	10.1
6.88	12.1
9.69	14.9
12.6	17.8
18.0	23.1
25.7	30.9
40.4	45.6
58.2	63.3
83.8	88.9
110.	116.
160.	165.

Table 8.2: Preliminary Exposure Times with Dark Current Calibration (Continued)

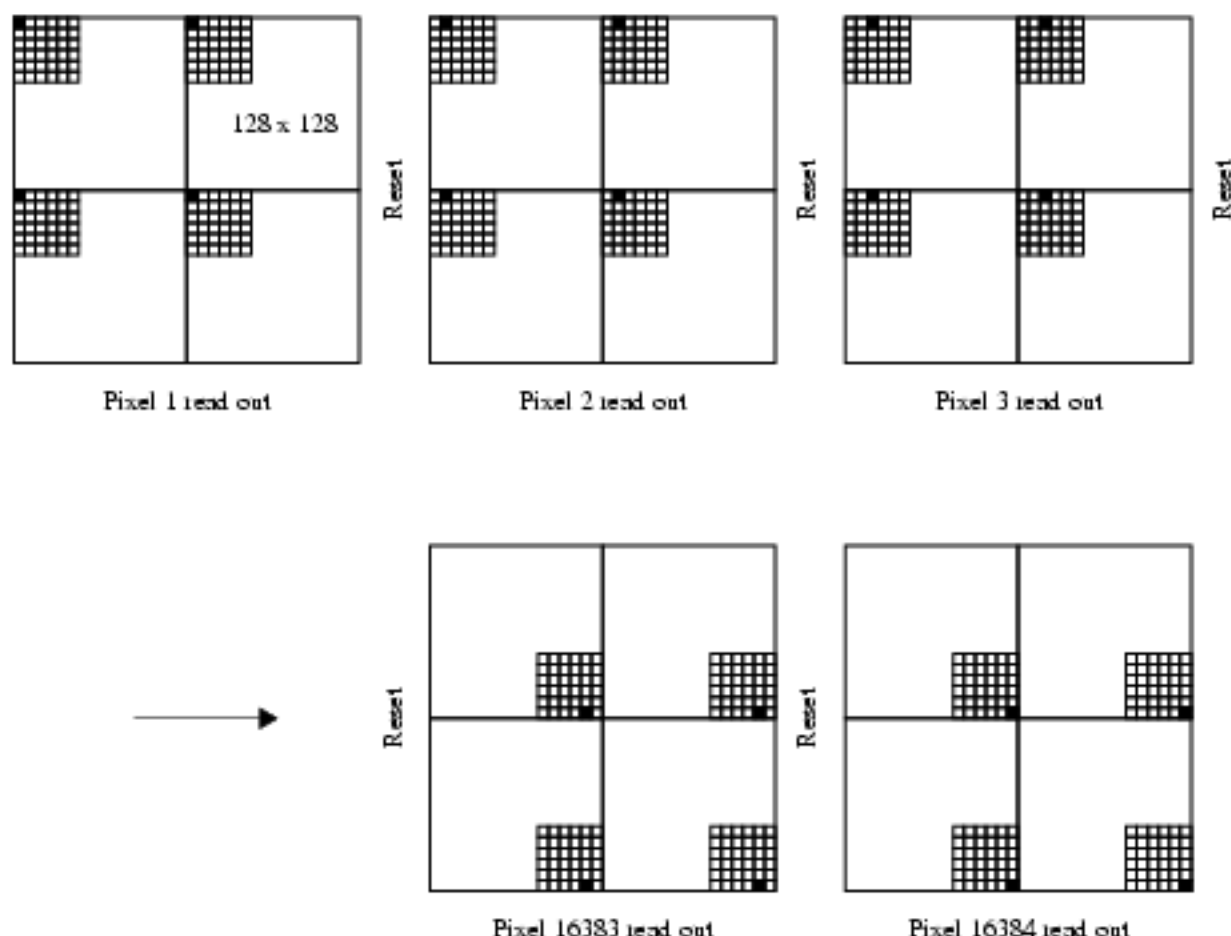
Time (seconds) (NREAD=1)	Time (seconds) (NREAD=10)
230.	235.
361.	366.
481.	486.
577.	582.
961.	966.
1203.	1208.
1447.	1452.
1861.	1866.
2701.	2706.
3601.	3606.

## Bright Object Mode

The time taken to read through a quadrant on the array sets a fundamental limit on the fastest electron collection rate which can be achieved by resetting all the pixels. An inherent consequence of the methods of operating the NCMOS array detectors in the ACCUM, MULTIACCUM, and RAMP modes is therefore that there is a minimum possible exposure time,  $\sim 0.6$  seconds, set by the time required to read the array. For a very bright object, such as the disk of Jupiter, the time between the reset of a pixel, and its final read is sufficiently long that the pixel saturates. Although the detector arrays are multiplexed by division into four quadrants, each pixel in a  $128 \times 128$  pixel quadrant must be sampled in some order (note that there is no transfer of charge as is done in a CCD).

The solution adopted to this problem for NCMOS is the provision of a *bright object* mode which enables targets to be observed which are  $\sim 600$  times brighter than is possible in the other modes without saturating. In BRIGHTOBJ mode, an ACCUM sequence of operations is performed on *one* pixel in each quadrant at a time. That is, the pixel is reset, read, integrated, and read again with the difference between the final and initial readouts being stored as the measured signal and the interval between the reads being the exposure time. This process is repeated sequentially for all pixels in each quadrant. Users can think of this as integrating on a single pixel at a time. The smallest integration time which can be used is 1.024 milliseconds. Figure 8.4 illustrates the operation of bright object mode. Initially the detector is reset and the first pixel (solid shading) in each quadrant is read. A reset is then made and the second pixel in each quadrant is read. The process continues until all 16,384 pixels in each quadrant have been read.

Figure 8.4: Bright Object Mode Operation



The time required to take a BRIGHTOBJ mode exposure can be rather long. Since photons are only collected in one pixel per quadrant at an time, the time associated with obtaining the frame is  $0.206 + (EXPTIME \times 16384)$  where *EXPTIME* is the integration time per pixel (i.e. the observation time is approximately  $(128^2) \times$  the exposure time). For example, if an integration time of 0.1 seconds is used to observe a bright target then the actual time required to complete the observation would be around 27 minutes! This means that allowing for acquisition time only two such exposures could be obtained in an a single target visibility period. However, it is not always so serious. In the case of Jupiter for example the integration times required per pixel are only of the order of milliseconds and so the total integration time will only be around 20 seconds.

The longest exposure time which is possible in BRIGHTOBJ mode is 0.261 seconds, requiring 4278 seconds in total. Thus it is possible, in the worst case, for a single BRIGHTOBJ mode exposure to use most of an orbit. In general observers are strongly advised to consider the trade-off between relatively long BRIGHTOBJ mode exposures (which take the longest time) and short ACCUM

mode exposures (perhaps using a filter and camera combination with lower throughput).

One of the obvious uses of BRIGHTOBJ mode is for solar system targets. Due to the limitations of the Track 51 capability (linear tracking with orbital or planetary parallax correction) HST can only follow a moving target for 2048 seconds, of which 1980 seconds is available for an exposure. This therefore sets the longest integration time that is possible for a moving target in BRIGHTOBJ mode. Proposers will need to judge the real integration time and signal to noise ratio required for the observation time and adjust accordingly.

The advantage of this mode of operation is the ability to observe objects significantly brighter than the normal saturation limit of the detector.

The disadvantages are several:

- Due to the extremely large time penalties involved in this mode operation, *it cannot be used to accomplish time resolved observations on shorter time intervals than ACCUM mode.*
- Some observations will take a long time. BRIGHTOBJ mode exposures are therefore very sensitive to the quality of the pointing of HST. They should not be obtained using GYRO guiding mode. In addition, if the object changes (planetary rotation) or if the telescope pointing changes it will affect different parts of the image differently.
- The D.C. offset of the detector output is not removed in this mode of operation. In general, the signal is very high and the offset does not matter. In some cases it will and this can be a detriment to the signal accuracy.
- There is also no cosmic ray correction or saturation detection in this mode of operation. Although they are still susceptible to cosmic rays, events should be very rare as the integration time *per pixel* is very short.

---

## Acquisition Mode

Images obtained using the coronagraph in Camera 2 may be taken using any of the detector read-out modes. An ACQ mode observation performs an autonomous on-board acquisition (mode 2 acquisition) for subsequent coronagraph images.

In this mode the target is first acquired in the Coronagraphic Acquisition Aperture (see Figure 5.2). The ACQ mode image is now obtained, with an integration time specified by the observer, which should be long enough to determine the centroid of the target image accurately. An ACQ mode exposure actually results in two images. Each image is analogous to an ACCUM mode image (i.e., it has a single reset and read before and after each integration period). The two images are flat fielded and corrected for the “shading” effect (see Chapter 3) using the on-board NICMOS computer, and then compared in order to filter out any CR hits. The brightest object common to both images and located inside the coronagraphic acquisition aperture is found. This object is assumed to be the desired target. A simple (and of undemonstrated reliability for anything other than



a point or circular source) algorithm is now used to determine the position of the centroid of this source, and the telescope is moved such that this position is centered in the coronagraphic hole. The expected accuracy of this procedure for point sources is better than one quarter of a Camera 2 pixel (i.e., 0.013 arcsec), assuming all cosmic rays are successfully removed on-board. The instrument is now ready to acquire more data, and the ACQ mode procedure finished.

Problems to beware of in the ACQ process include cosmic rays and coronagraph centering accuracy. It is expected, as mentioned above, that the target should be centered behind the hole with an accuracy of better than one quarter of a pixel. How much better remains to be seen. Observers should note that in order to compare library PSFs with coronagraphic images for the purposes of determining source extensions or morphology, an accuracy of one quarter of a pixel may not be sufficient at long wavelengths. The two separate images obtained in ACQ mode will filter out most cosmic rays in short exposures, but if an ACQ mode exposure longer than about 10 minutes (i.e., 5 minutes for each of the CRSPILT images) is required, observers should seriously consider a REUSE TARGET OFFSET or INT-ACQ observation, because the probability of a CR hit not being filtered out on-board becomes larger the longer the exposure. In this case it is likely that the acquisition procedure will fail because the brightest source will be a CR hit, and the intended target will not be hidden behind the coronagraph during the subsequent integrations. If the target is bright enough to saturate the detector during the ACQ mode exposure, this is likely to cause poor centering. A failed or unsatisfactory acquisition will probably cause the subsequently acquired images to be useless to the observer.

The data which are returned to the ground will be formatted as a hybrid between ACCUM and MULTIACCUM mode data. The two individual images will each be returned (not flat fielded or reduced in any way) to the ground, and will be reduced in the calibration pipeline exactly as if they were two separate ACCUM mode images. However, they are stored in a single FITS data file, similar to a 2-read MULTIACCUM observation, except that there will be no zeroth read returned to the ground.

---

## NICMOS Science Data

One of the major differences the user will find compared to existing instruments on-board HST is that NICMOS (and STIS) data delivered to the observer contains not only the images obtained, but also have variance and quality arrays for each of them. On a pixel by pixel basis these give the statistical uncertainty in the data, and flags identifying any abnormalities in the data respectively. In the case of RAMP mode, as we describe in the Appendix, the variance array is created on board. For the other three modes of operation, these arrays are constructed in the analysis in the ground processing systems (pipelines). For NICMOS data there will be an integration time and a number of valid sample images for each dataset. All the data the user will see will contain all five of these components for each image in a dataset.

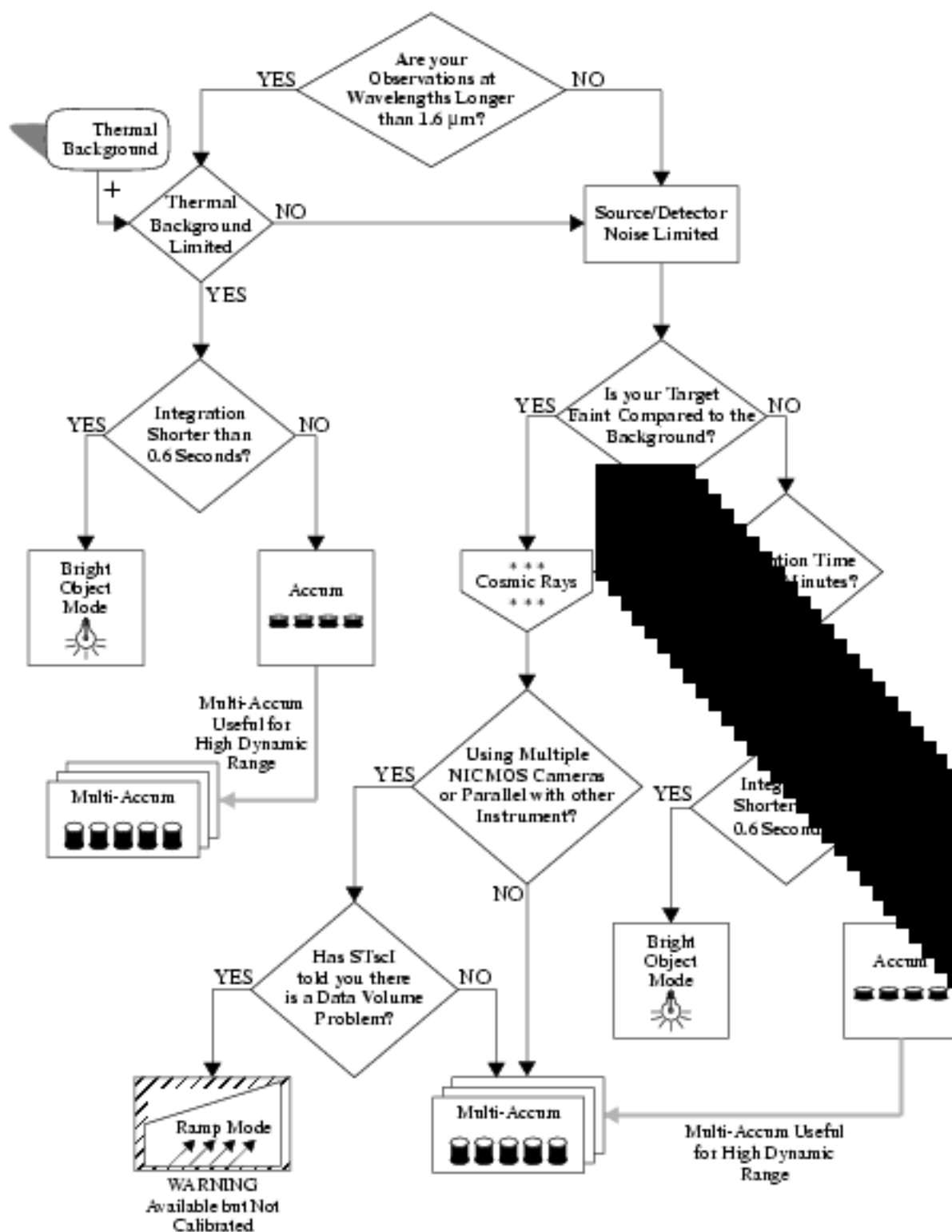
See Chapter 13 for a detailed discussion of the NICMOS data products.

---

## Summary and Quick Reference

Rounding off this chapter, we give the decision tree the user has to navigate in choosing which detector mode is right for their program in the flow chart shown in Figure 8.5. To use this as a quick reference start at the top of the diagram and branch along the path indicated according to the answer to each of the questions you are asked until you reach the bottom of the tree.

Figure 8.5: Decision Flow for Choosing Detector Mode





# Overheads and Orbit Time Determination

**In This Chapter...**

Overview / 121

NICMOS Overheads / 126

Examples / 129

In this chapter we describe the overheads associated with NICMOS observations and give examples of how to determine the number of orbits that your program will require.

---

## Overview

Once you have determined the set of science exposures and any additional target acquisition or calibration exposures you may require for your science program, you are ready to determine the total number of orbits to request. Generally, this is a straightforward exercise involving tallying up the overheads on the individual exposures and on the selected pattern (see Chapter 10), and packing the exposure and overhead times into individual orbits, and tallying up the results to determine your total orbit request. This process may need to be iterated, in order to seek the most efficient use of the orbit time.

We refer you to the CP/Phase 1 Proposal Instructions for information on the Observatory policies and practices with respect to orbit time requests and for the orbit determination work sheets. Below, we provide a summary of the NICMOS specific overheads, and give several examples to illustrate how to calculate your orbit requirements for Phase 1 Proposals.

## NICMOS Exposure Overheads

Estimates of the overheads on exposures are summarized in Table 9.1. All numbers given are preliminary, approximate, rounded where appropriate to the nearest half minute and do not attempt to differentiate in detail the overheads for different NICMOS modes and configurations. They are subject to change prior to the actual scheduling of Cycle 7 proposals (i.e., prior to Phase II). They represent our current best, conservative, but still very uncertain predictions. These overhead times are to be used (in conjunction with the actual exposure time and the Cycle 7 Phase I Proposal Instructions) to estimate the total time in orbits for your Cycle 7 proposal time request. After your HST proposal is accepted, you will be asked to submit a Phase II proposal to allow scheduling of your approved observations. At that time you will be presented with actual, up to date overheads by the scheduling software. Allowing sufficient time for overhead in your Phase I proposal is important; additional time to cover unplanned overhead will not be granted later.

We note the following important points.

- *Generic (Observatory Level) Overheads:*
  - The first time you acquire an object you must include the overhead for the guide star acquisition.
  - In subsequent contiguous orbits you must include the overhead for the guide star re-acquisition; if you are observing in the continuous viewing zone (CVZ, see the CP/Phase I Proposal Instructions), no guide star *re-acquisitions* are required.
  - The re-acquisitions can be assumed to be accurate to  $\leq 10$  milli-arcsecs; thus additional target acquisitions or pickups are not needed following a re-acquisition.
  - Time must be allowed for each deliberate movement of the telescope; e.g., if you are performing a target acquisition exposure on a nearby star and then offsetting to your target or if you are taking a series of exposures in which you move the target relative to the camera, you must allow time for the moves.
- *NICMOS Specific Overheads:*
  - The 12 second set-up time at the beginning of each orbit or at each different telescope pointing is inclusive of the filter selection. There is no additional set-up time for new telescope pointings due to dithering or chopping with the same instrument configuration.
  - Overheads are operating-mode dependent. In particular, the overhead for the BRIGHTOBJ mode is particularly onerous, since this mode resets and reads each pixel, one pixel at a time.
  - The target acquisition overhead of 98 seconds for coronagraphy needs to be accounted for the first time an object is acquired under the coronagraphic spot. No re-acquisition is required for observing the same target in different filters, or from one orbit to the next.

- Overhead times for changing cameras equal to the slew time for the physical distance between the centers of the cameras in arcsecs + 10 seconds. In addition, the observer must include 12 seconds for set-up which includes filter selection.
- The amount of time required to chop depends on the chop throw, and whether an on-target guide star re-acquisition is desired. The telescope can maintain lock on the guide stars if the chop throw is smaller than 2 arcminutes. If it is larger, then the observer can choose to maintain pointing through the gyros (drop-to-gyro) or re-acquire the guide stars (3 minute overhead per re-acquisition—note that this is not the 6-minute orbit re-acquisition) every time the telescope goes back to the target; with the first option the pointing uncertainty is about 1 milliarcsec/second due to telescope drift. The drop-to-gyro option can be adopted for background pointings, where telescope drift is not a concern.
- In most cases, the data management overhead of 2 minutes will be hidden inside the orbit occultation time. However, if a total of (summed over the three cameras) 100 or more read-outs occur within the visibility period of one orbit, the observer must include 2 minutes overhead every 100 read-outs.

Table 9.1: NICMOS Overheads

Action	Overhead
<i>Generic (Observatory Level)</i>	
Guide star acquisition	Initial acquisition 9 minutes re-acquisitions on subsequent orbits = 6 minutes per orbit
Spacecraft POSTARG moves	for offsets less than 1 arcminute and more than 10 arcsecs = 1 minute, for offsets between 10 arcsecs and 1 arcsec = 0.5 minute; for offsets less than 1 arcsec in size = 10 seconds
Slew of $x$ arcsecs to new target within an orbit (slew < 2 arcmin, same guide stars)	$(x + 10)$ seconds
Type 2 Slew to new target within an orbit (slew > 2 arcmin, new guide stars)	<1 degree slew: 2.5 min. + 9 min. guide star acq. 1 degree < slew < 10 degrees: 5.0 min. + 9 min. guide star acq. 10 degrees < slew < 100 degrees: 13 min. + 9 min. guide star acq.
<i>Provisional NICMOS Specific Overheads</i>	
Set-up at beginning of each orbit or at each different telescope pointing - always required. (other than dither/chop maneuvering)	12 seconds
Filter change	12 seconds
Exposure overheads:	
ACCUM	$(6 + \text{HREAD} \times 0.705)$ seconds in FAST readout
MULTIACCUM	$(9 + \text{HREAD} \times 3.78)$ seconds in SLOW readout
BRIGHTOBJ	12 seconds
	$(\text{exptime} \times 16.384 + 10)$ seconds
Target acquisition (for coronagraphy)	98 seconds

Table 9.1: NICMOS Overheads (Continued)

Action	Overhead
Change of camera: from 2 to 3 or vice versa	90 seconds + 12 seconds for set-up
from 1 to 2 or vice versa	43 seconds + 12 seconds for set-up
from 1 to 3 or vice versa	58 seconds + 12 seconds for set-up
Dithering/Chopping of $x$ arcsecs ( $< 2$ arcmin)	$(x + 10)$ seconds
Chopping of $x$ arcsec ( $> 2$ arcmin, using drop-to-gyro)	$(x + 31)$ seconds
Chopping of $x$ arcsec ( $> 2$ arcmin, with guide star re-acquisition)	$(x + 31)$ seconds + 3 minutes for each guide star re-acq
Data management (for every 100 read-outs within an orbit)	2 minutes

## Orbit Use Determination

The easiest way to learn how to compute total orbit time requests is to work through a few examples. We provide below seven examples of how to use the information in Table 9.1 to determine your orbit requirements. The overhead examples cover the following cases:

- Example 1: Coronagraphic observation, with the **TWO-CHOP** pattern.
- Example 2: Polarimetric observation, with the **FOUR-CHOP** pattern.
- Example 3: Emission-line mapping of an extended object, with the **SQUARE-WAVE-DITH** pattern.
- Example 4: General observation with switch of camera and pattern.
- Example 5: Spectroscopic observation, with the **YSTRIP-DITH-CHOP** pattern.
- Example 6: Mapping of an extended object with the **SPIRAL-DITH-CHOP** pattern.
- Example 7: Observing calibration star (P0+1-C).

Unless otherwise specified, we assume in the examples that the target declination is 50 degrees, which implies that its visibility period during one orbit is 56 minutes (see the Phase 1 Proposal Instructions).

### Example 1: A Two-Chop Pattern Using Multi-Accum and the Coronagraph

The proposed science is to observe the extended nebulosity around an IR-bright source at  $\lambda = 2.1$  microns. Since the source would saturate the cameras, the observer decides to hide it behind the coronagraphic spot in NIC2. Coronagraphic observations require an onboard acquisition of the target under the



coronagraphic spot (see Chapter 5). The two acquisition exposures, which are needed to locate the target in the Camera 2 field of view are assumed here to require 10 seconds integration each in the selected filter (F207M for this observation). The total overhead for reading the two images, calculating the position of the target, and moving it under the coronagraphic spot is 98 seconds. The long wavelength observations are affected by non-negligible background, and the observer chooses the TWO-CHOP pattern with a chopping throw of 19 arcsec for background subtraction. The overhead for slewing between the target and each of the two backgrounds is 29 (19+10) seconds, and the same guide stars can be maintained for such small slews (Table 9.1). The sequence for the TWO-CHOP pattern is: target-background-target-background, with the two background fields positioned on opposite sides of the target (see Chapter 10).

The observer wishes to use the F207M filter in MULTIACCUM mode for the observation, and specifies exposure times of 15 minutes at each pointing, for a total exposure time target+background of 60 (i.e., 15 x 4) minutes, half of which is spent on the target. The orbit requirements are summarized in Table 9.2 below:

Table 9.2: Orbit Determination for Example 1

Action	Time (minutes)	Explanation
<i>Orbit 1</i>		
Initial Guide Star Acquisition	9.0	Needed at start of observation of new target
Target Acquisition (under the coronagraphic spot)	2.0	98 seconds overheads 10 seconds for first acquisition exposure 10 seconds for second acquisition exposure
Science exposure, NIC2 F207M	15.4	12 seconds for instrument set-up 900 seconds exposure time on target 12 seconds for MULTIACCUM readout
Science exposure, NIC2 F207M	16.2	29 seconds chopping slew 900 seconds exposure time on background 12 seconds for MULTIACCUM readout
<i>Orbit 2</i>		
Guide star re-acquisition	6.0	Start of new orbit
Science exposure, NIC2 F207M	15.4	29 seconds chopping slew 12 seconds for instrument set-up 900 seconds exposure time on target 12 seconds for MULTIACCUM readout
Science exposure, NIC2 F207M	15.7	29 seconds chopping slew 900 seconds exposure time on background 12 seconds for MULTIACCUM readout

After the second exposure, the total time spent on the target is  $(9.0 + 2.0 + 15.4 + 16.2) = 42.6$  minutes, with a visibility period of 56 minutes. The third and fourth exposures in the F207M filter must be done during the second orbit, following the guide star re-acquisition and the instrument set-up,

since NICMOS exposures cannot be paused across orbits, and the third exposure would not fit in what remains of the first visibility window. The user requests two orbits to accomplish the proposed science observation. (The observer should develop their program by including additional exposures through the same or other appropriate filters to make more efficient use of what is left of the orbits).

## Example 2: Polarization Observations Using a Chop Pattern and MULTI-ACCUM

Polarimetric observations at long wavelengths will be obtained for target A. The NIC2 filters POL0L, POL120L, and POL240L will provide information on the three Stokes parameters. The observer requires exposure times of 20 minutes in each polarizer, in MULTIACCUM mode. The long wavelength filters are affected by background, and the observer chooses to chop, using the FOUR-CHOP pattern with 150 arcsec chopping throw. With this pattern, the sequence target-background is repeated four times with four different background fields. Since the chopping slew is greater than 2 arcmin, the overhead for chopping will be  $(150 + 31) = 181$  sec. Every time the telescope goes back to the target, there is the additional 6 minutes overhead for the guide star re-acquisition.

The total exposure time for the observation is 20 minutes in each of the three polarizers, times the 8 pointings of the FOUR-CHOP pattern, or  $T = (20 \times 3 \times 8) = 480$  minutes, without including the overheads.

The declination of the source is 30 degrees, so the visibility period during one orbit is 53 minutes. The orbit requirement is summarized in Table 9.3 below.

Table 9.3: Orbit Determination for Example 2

Action	Time (minutes)	Explanation
<i>Orbit 1</i>		
Initial Guide Star Acquisition	9.0	Needed at start of observation of new target
Science exposure, NIC2 POL0L	20.4	12 seconds for instrument set-up 1200 seconds exposure time on target 12 seconds for MULTIACCUM readout
Science exposure, NIC2 POL120L	20.4	12 seconds for filter change 1200 seconds exposure time on target 12 seconds for MULTIACCUM readout
<i>Orbit 2</i>		
Guide Star re-acquisition	6.0	Start of new orbit
Science exposure, NIC2 POL240L	20.4	12 seconds for instrument set-up 1200 seconds exposure time on target 12 seconds for MULTIACCUM readout
Science exposure, NIC2 POL240L	23.2	181 seconds chopping slew 1200 seconds exposure time on background # 1 12 seconds for MULTIACCUM readout

Table 9.3: Orbit Determination for Example 2 (Continued)

Action	Time (minutes)	Explanation
<i>Orbit 3</i>		
Guide Star re-acquisition	6.0	Start of new orbit
Science exposure, NIC2 POL1 20L	20.4	12 seconds for instrument set-up 1200 seconds exposure time on background # 1 12 seconds for MULTIACCUM readout
Science exposure, NIC2 POL0L	23.2	12 seconds for filter change 1200 seconds exposure time on background # 1 12 seconds for MULTIACCUM readout 181 seconds chop slew
<i>Orbit 4</i>		
Guide Star re-acquisition	6.0	Start of new orbit
Science exposure, NIC2 POL0L	20.4	12 seconds for instrument set-up 1200 seconds exposure time on target 12 seconds for MULTIACCUM readout
Science exposure, NIC2 POL1 20L	20.4	12 seconds for filter change 1200 seconds exposure time on target 12 seconds for MULTIACCUM readout
<i>Orbit 5</i>		
Guide Star re-acquisition	6.0	start of new orbit
Science exposure, NIC2 POL2 40L	20.4	12 seconds for instrument set-up 1200 seconds exposure time on target 12 seconds for MULTIACCUM readout
Science exposure, NIC2 POL2 40L	23.2	181 seconds chopping slew 1200 seconds exposure time on background # 2 12 seconds for MULTIACCUM readout
-	-	-
-	-	-
-	-	-
and so on, until the entire sequence target-background is completed.		

### Example 3: Making a Map using SQUARE-WAVE-DITH

The proposer wants to map an extended region in the light of [FeII] ( $\lambda$  1.644 microns). The choice is to use the F16411 (line) and F16611 (continuum) filters of NIC1, MULTIACCUM mode, and the SQUARE-WAVE-DITH pattern. The selected dithering step is 4 arcsec, with a total of 20 positions. The slewing overhead between each position will be 14 (i.e., 4 + 10) seconds. The requested exposure time at each position is 10 minutes in each filter, implying that the

exposure time for the observation is:  $T = (10 \times 2 \times 20) = 400$  minutes, exclusive of overheads. The orbit requirements are summarized in Table 9.4.

Table 9.4: Orbit Determination for Example 3

Action	Time (minutes)	Explanation
<i>Orbit 1</i>		
Initial Guide Star Acquisition	9.0	Needed at start of observation of new target
Science exposure, NIC1 F1 6411	10.4	12 seconds for instrument set-up 600 seconds exposure time on position # 1 12 seconds for MULTIACCUM read out
Science exposure, NIC1 F1 6611	10.4	12 seconds for filter change 600 seconds exposure time on position # 1 12 seconds for MULTIACCUM read out
Science exposure, NIC1 F1 6611	10.4	14 seconds dither 600 seconds exposure time on position # 2 12 seconds for MULTIACCUM read out
Science exposure, NIC1 F1 6411	10.6	12 seconds for filter change 600 seconds exposure time on position # 2 12 seconds for MULTIACCUM read out 14 seconds dither
<i>Orbit 2</i>		
Guide Star re-acquisition	6.0	Start of new orbit
Science exposure, NIC1 F1 6411	10.4	12 seconds for instrument set-up 600 seconds exposure time on position # 3 12 seconds for MULTIACCUM read out
Science exposure, NIC1 F1 6611	10.4	12 seconds for filter change 600 seconds exposure time on position # 3 12 seconds for MULTIACCUM read out
-	-	-
-	-	-
-	-	-

and so on, until the 20 positions of the dithering pattern have been covered.

### Example 4: Changing Cameras and Pattern

The proposed science is to observe a target taking:

- Exposures in the NIC1 F10811 and F11311 filters, using the MULTIACCUM mode and the XSTRIP-DITH pattern, with 5 arcsecs dithering step; the exposure time is  $T=900$  seconds in each filter, at each position.
- Exposures in the NIC2 F205W filter, using the ACCUM mode with NREAD=5 and FAST readout. The TWO-CHOP pattern with chopping throw of 150 arcsecs and guide star re-acquisition on the target (see Exam-

ple 1) is selected to remove the background. The exposure time is  $T=250$  seconds at each pointing, implying a total on-source exposure time of 500 seconds.

Table 9.5 lists the orbit requirements.

Table 9.5: Orbit Determination for Example 4

Action	Time (minutes)	Explanation
<i>Orbit 1</i>		
Initial Guide Star Acquisition	9.0	Needed at start of observation of new target
Science exposure, HIC1 F108N	15.4	12 seconds for instrument set-up 900 seconds exposure time on position # 1 12 seconds for MULTIACCUM readout
Science exposure, HIC1 F113N	15.4	12 seconds for filter change 900 seconds exposure time on position # 1 12 seconds for MULTIACCUM readout
Science exposure, HIC1 F113N	15.4	15 seconds dither 900 seconds exposure time on position # 2 12 seconds for MULTIACCUM readout
<i>Orbit 2</i>		
Guide Star re-acquisition	6.0	Start of new orbit
Science exposure, HIC1 F108N	15.4	12 seconds for instrument set-up 900 seconds exposure time on position # 2 12 seconds for MULTIACCUM readout
Science exposure, HIC2 F205W	5.2	(43+12) seconds for camera change + set-up 250 seconds exposure on target 9.5 seconds ACCUMFAST readout for HIC2=5
Science exposure, HIC2 F205W	7.3	181 seconds chop 250 seconds exposure on background # 1 9.5 seconds ACCUMFAST readout
Science exposure, HIC2 F205W	13.3	181 seconds chop 360 seconds guide star re-acquisition 250 seconds exposure on target 9.5 seconds ACCUMFAST readout
Science exposure, HIC2 F205W	7.3	181 seconds chop 250 seconds exposure time on background # 2 9.5 seconds ACCUMFAST readout

After the initial guide star acquisition, and the instrument set-up of 12 seconds, the first science exposure of 900 seconds in the first filter (F108N in our case) is obtained on the first pointing (position # 1). An exposure of 900 seconds with the second filter (F113N) on the same position follows. The telescope slew to reach position # 2 requires (5+10) seconds = 15 seconds, and the exposures in both the F113N and F108N filters are repeated. For the second part of the observation, the switch from HIC1 to HIC2 requires 43 seconds to which 12 seconds for

instrument set-up must be added. The on-target exposure time requested in the F205W filter is  $T=500$  seconds, split between the two target visits of the TWO-CHOP pattern. After the first exposure on the target and after the camera read-out ( $6 + 5 \times 0.705 = 9.5$  seconds in FAST readout and NREAD=5), the telescope slews to the background in  $150 + 31 = 181$  seconds (see Table 9.1). The subsequent slew, back onto the target, is followed by a guide star re-acquisition of 6 minutes. The sequence continues, alternating target and background, until the pattern is completed.

### Example 5: Use of the Grism and ACCUM Mode

The proposed science is to obtain multiobject spectroscopy of a field using Grism C in NIC3, and the ACCUM mode. Grism C covers the wavelength range 1.4–2.5 microns, which is affected by a non-negligible background. The observer chooses to remove the background by chopping, and to place the objects of interest in different locations of the camera. The YSTRIP-DITH-CHOP pattern is therefore selected, with 3 on-target positions, dithering step = 15 arcsecs, and chopping throw = 60 arcsecs. The YSTRIP-DITH-CHOP pattern dithers the camera in the direction orthogonal to the dispersion axis of the grism, and chops along the dispersion axis. We will denote the on-target positions #1 through #3. The exposure time at each pointing is 360 seconds, split into 12 ACCUM mode exposures of 30 seconds each, to prevent saturation on the thermal background (see Figure 5.17).

When using the NICMOS grisms, it is advisable to associate the spectroscopic observation with an image in the appropriate filter at the same pointing to get the location of each object in the field, and to identify the spectrum. For Grism C, a possible choice is F175W. The observer calculates that exposures of 25 seconds in this filter at each position will suffice for producing high signal to noise images. The orbit requirements are listed in Table 9.6 below.

Table 9.6: Orbit Determination for Example 5

Action	Time (minutes)	Explanation
<i>Orbit 1</i>		
Initial Guide Star Acquisition	9.0	Needed at start of observation of new target
Science exposure, NIC3 GRISM C	7.5	12 seconds for instrument set-up 360 seconds exposure time on-target (posn # 1) 12 reads X 6.7 seconds for ACCUM
Science exposure, NIC3 F175W	0.7	12 seconds for filter change 25 seconds exposure time on-target (posn # 1) 12 seconds for ACCUM readout
Science exposure, NIC3 F175W	1.7	70 seconds chop 25 seconds exposure time on background 6.7 seconds for ACCUM readout

Table 9.6: Orbit Determination for Example 5 (Continued)

Action	Time (minutes)	Explanation
Science exposure, 11 IC3 GRISM C	7.5	12 seconds for filter change 360 seconds exposure time on background 12 reads X 6.7 seconds for ACCUM
Science exposure, 11 IC3 GRISM C	14.5	72 seconds chop 360 seconds for guide star re-acquisition 360 seconds exposure time on-target (posn # 2) 12 reads X 6.7 seconds for ACCUM
Science exposure, 11 IC3 F1 75W	0.7	12 seconds for filter change 25 seconds exposure time on-target (posn # 2) 6.7 seconds for ACCUM readout
Science exposure, 11 IC3 F1 75W	1.7	70 seconds chop 25 seconds exposure time on background 6.7 seconds for ACCUM readout
Science exposure, 11 IC3 GRISM C	8.7	12 seconds for filter change 360 seconds exposure time on background 12 reads X 6.7 seconds for ACCUM 72 seconds chop
<i>Orbit 2</i>		
Guide Star re-acquisition	6.0	Start of new orbit
Science exposure, 11 IC3 GRISM C	7.5	12 seconds instrument set-up 360 seconds exposure time on-target (posn # 3) 12 reads X 6.7 seconds for ACCUM
Science exposure, 11 IC3 F1 75W	0.7	12 seconds for filter change 25 seconds exposure time on-target (posn # 3) 6.7 seconds for ACCUM readout
Science exposure, 11 IC3 F1 75W	1.7	70 seconds chop 25 seconds exposure time on background 6.7 seconds for ACCUM readout
Science exposure, 11 IC3 GRISM C	7.5	12 seconds for filter change 360 seconds exposure time on background 12 reads X 6.7 seconds for ACCUM

Since the chop throw is less than 2 arcmin, the formula used to calculate the chopping slew is  $(60 + 10) = 70$  seconds (see Table 9.1). In our example, slewing away from the target costs less time than slewing back onto the target (70 seconds versus 72 seconds), because the latter is a combination of the dithering step, 15 arcsec, with the chopping throw, 60 arcsec:  $[10 + \text{sqrt}(15^2 + 60^2)] = 72$  seconds.

### Example 6: Another Example of Mapping

The observer wants to map an extended object, for instance a galaxy, with NIC2 and the F187W filter. The wavelength chosen is long enough that the observation may be affected by background emission, and the

`SPIRAL-DITH-CHOP` is selected for background removal. The dithering step is set equal to the size of `NIC2`, 19.2 arcsec, and the chopping throw is set to 180 arcsec. The `SPIRAL-DITH-CHOP` pattern will start at the center of the target and move outward. The galaxy has a bright core and relatively faint extended emission, so `MULTIACCUM` mode will be used. The proposed exposure time is 3 minutes per pointing, and the galaxy will be covered with 9 different pointings. The orbit requirements are summarized in Table 9.7.

Table 9.7: Orbit Determination for Example 6

Action	Time (minutes)	Explanation
<i>Orbit 1</i>		
Initial Guide Star Acquisition	9.0	Needed at start of observation of new target
Science exposure, <code>NIC2 F1.87W</code>	3.4	12 seconds for instrument set-up 180 seconds exposure time on target position # 1 12 seconds for <code>MULTIACCUM</code> read out
Science exposure, <code>NIC2 F1.87W</code>	6.7	211 seconds chop 180 seconds exposure time on background # 1 12 seconds for <code>MULTIACCUM</code> read out
Science exposure, <code>NIC2 F1.87W</code>	12.4	192 seconds chop 360 seconds guide star re-acquisition 180 seconds exposure time on target position # 2 12 seconds for <code>MULTIACCUM</code> read out
Science exposure, <code>NIC2 F1.87W</code>	6.7	211 seconds chop 180 seconds exposure time on background # 2 12 seconds for <code>MULTIACCUM</code> read out
Science exposure, <code>NIC2 F1.87W</code>	16.3	212 seconds chop 360 seconds guide star re-acquisition 180 seconds exposure time on target position # 3 12 seconds for <code>MULTIACCUM</code> read out 211 seconds chop
<i>Orbit 2</i>		
Guide Star re-acquisition	6.0	Start of new orbit
Science exposure, <code>NIC2 F1.87W</code>	3.4	12 seconds for instrument set-up 180 seconds exposure time on background # 3 12 seconds for <code>MULTIACCUM</code> read out
Science exposure, <code>NIC2 F1.87W</code>	13.0	230 seconds chop 360 seconds guide star re-acquisition 180 seconds exposure time on target position # 4 12 seconds for <code>MULTIACCUM</code> read out
Science exposure, <code>NIC2 F1.87W</code>	6.7	211 seconds chop 180 seconds exposure time on background # 4 12 seconds for <code>MULTIACCUM</code> read out



Table 9.7: Orbit Determination for Example 6 (Continued)

Action	Time (minutes)	Explanation
Science exposure, NIRC2 F1.87W	13.0	230 seconds chop 360 seconds guide star re-acquisition 180 seconds exposure time on target position # 5 12 seconds for MULTIACCUM read out
Science exposure, NIRC2 F1.87W	10.3	211 seconds chop 180 seconds exposure time on background # 5 12 seconds for MULTIACCUM read out 212 seconds chopping slew
<i>Orbit 3</i>		
Guide Star re-acquisition	6.0	Start of new orbit
Science exposure, NIRC2 F1.87W	3.4	12 seconds for instrument set-up 180 seconds exposure time on target position # 6 12 seconds for MULTIACCUM read out
Science exposure, NIRC2 F1.87W	6.7	211 seconds chop 180 seconds exposure time on background # 6 12 seconds for MULTIACCUM read out
Science exposure, NIRC2 F1.87W	12.7	212 seconds chop 360 seconds guide star re-acquisition 180 seconds exposure time on target position # 7 12 seconds for MULTIACCUM read out
Science exposure, NIRC2 F1.87W	6.7	211 seconds chop 180 seconds exposure time on background # 7 12 seconds for MULTIACCUM read out
Science exposure, NIRC2 F1.87W	12.4	192 seconds chop 360 seconds guide star re-acquisition 180 seconds exposure time on target position # 8 12 seconds for MULTIACCUM read out
Science exposure, NIRC2 F1.87W	9.9	211 seconds chop 180 seconds exposure time on background # 8 12 seconds for MULTIACCUM read out 192 seconds chopping slew
<i>Orbit 4</i>		
Guide Star re-acquisition	6.0	Start of new orbit
Science exposure, NIRC2 F1.87W	3.4	12 seconds for instrument set-up 180 seconds exposure time on target position # 9 12 seconds for MULTIACCUM read out
Science exposure, NIRC2 F1.87W	6.7	211 seconds chop 180 seconds exposure time on background # 9 12 seconds for MULTIACCUM read out

The size of the chop is determined by the distance between the pointings; the time for the slew between the target and the background is always 211 (180 + 31) seconds, while that for the slew between the background and the target depends

on the position in the pattern. For instance, the time for the slew between the background #1 and the target position #2 is  $(180 - 19.2 + 31) = 192$  seconds, while that for the slew between background #2 and target position #3 is  $[\text{sort}(180^2 + 19.2^2) + 31] = 212$  seconds.

### Example 7: Observation of the Calibration Star P041-C

In Chapter 6 we have derived exposure times for the calibration star P041-C for the purpose of characterizing the medium band filters F222M and F237M and the two narrow band filters F215H and F216H in Camera 2 (see Example 4 in Chapter 6, page 87). For this source, high signal to noise ratios can be reached in 20 seconds for the medium band filters and in 150 seconds for the narrow band filters. We want to observe the star at different positions on the camera, both for (a) removing flat field response effects from the photometric calibration and (b) building background images for the two long wavelength medium band filters. The SPIRAL-DITH pattern is selected for this purpose: the first pointing will be at the center of Camera 2 and the camera field of view will be covered with 9 pointings in total; the dithering step will be 6 arcsecs. Since the source is point-like, background images will be obtained by stacking and filtering all the exposures (see Chapter 10).

The exposure times in the F222M and F237M filters are short enough that few cosmic ray events are expected to affect the images; therefore the ACCUM readout mode, with NREAD=1 is selected. For the exposures in the F215H and F216H filters, we choose the MULTIACCUM readout mode, in order to remove cosmic ray events.

The declination of the source is about 72 degrees so the visibility period during one orbit is 58 minutes. The orbit requirements are summarized in Table 9.8.

Table 9.8: Orbit Determination for Example 7

Action	Time (minutes)	Explanation
<i>Orbit 1</i>		
Initial Guide Star Acquisition	9.0	Needed at start of observation of new target
Science exposure, NIC2 F215H	2.9	12 seconds for instrument set-up 150 seconds exposure time on position # 1 12 seconds for MULTIACCUM read out
Science exposure, NIC2 F216H	2.9	12 seconds for filter change 150 seconds exposure time on position # 1 12 seconds for MULTIACCUM read out
Science exposure, NIC2 F222M	0.7	12 seconds for filter change 20 seconds exposure time on position # 1 6.705 seconds for ACCUMFAST read out
Science exposure, NIC2 F237M	0.7	12 seconds for filter change 20 seconds exposure time on position # 1 6.705 seconds for ACCUMFAST read out

Table 9.8: Orbit Determination for Example 7 (Continued)

Action	Time (minutes)	Explanation
Science exposure, MICE F237M	0.7	16 seconds dither 20 seconds exposure time on position # 2 6.705 seconds for ACCUMFAST read out
Science exposure, MICE F222M	0.7	12 seconds for filter change 20 seconds exposure time on position # 2 6.705 seconds for ACCUMFAST read out
Science exposure, MICE F216M	2.9	12 seconds for filter change 150 seconds exposure time on position # 2 12 seconds for MULTIACCUM read out
Science exposure, MICE F215M	2.9	12 seconds for filter change 150 seconds exposure time on position # 2 12 seconds for MULTIACCUM read out
Science exposure, MICE F215M	3.0	16 seconds dither 150 seconds exposure time on position # 3 12 seconds for MULTIACCUM read out
Science exposure, MICE F216M	2.9	12 seconds for filter change 150 seconds exposure time on position # 3 12 seconds for MULTIACCUM read out
Science exposure, MICE F222M	0.7	12 seconds for filter change 20 seconds exposure time on position # 3 6.705 seconds for ACCUMFAST read out
Science exposure, MICE F237M	0.7	12 seconds for filter change 20 seconds exposure time on position # 3 6.705 seconds for ACCUMFAST read out
Science exposure, MICE F237M	0.7	16 seconds dither 20 seconds exposure time on position # 4 6.705 seconds for ACCUMFAST read out
Science exposure, MICE F222M	0.7	12 seconds for filter change 20 seconds exposure time on position # 4 6.705 seconds for ACCUMFAST read out
Science exposure, MICE F216M	2.9	12 seconds for filter change 150 seconds exposure time on position # 4 12 seconds for MULTIACCUM read out
Science exposure, MICE F215M	2.9	12 seconds for filter change 150 seconds exposure time on position # 4 12 seconds for MULTIACCUM read out
Science exposure, MICE F215M	3.0	16 seconds dither 150 seconds exposure time on position # 5 12 seconds for MULTIACCUM read out
Science exposure, MICE F216M	2.9	12 seconds for filter change 150 seconds exposure time on position # 5 12 seconds for MULTIACCUM read out

Table 9.8: Orbit Determination for Example 7 (Continued)

Action	Time (minutes)	Explanation
Science exposure, M1C2 F222M	0.7	12 seconds for filter change 20 seconds exposure time on position # 5 6.705 seconds for ACCUMFAST read out
Science exposure, M1C2 F237M	0.7	12 seconds for filter change 20 seconds exposure time on position # 5 6.705 seconds for ACCUMFAST read out
Science exposure, M1C2 F237M	0.7	16 seconds dither 20 seconds exposure time on position # 6 6.705 seconds for ACCUMFAST read out
Science exposure, M1C2 F222M	0.7	12 seconds for filter change 20 seconds exposure time on position # 6 6.705 seconds for ACCUMFAST read out
Science exposure, M1C2 F216M	2.9	12 seconds for filter change 150 seconds exposure time on position # 6 12 seconds for MULTIACCUM read out
Science exposure, M1C2 F215M	2.9	12 seconds for filter change 150 seconds exposure time on position # 6 12 seconds for MULTIACCUM read out
Science exposure, M1C2 F215M	3.0	16 seconds dither 150 seconds exposure time on position # 7 12 seconds for MULTIACCUM read out
Science exposure, M1C2 F222M	0.7	12 seconds for filter change 20 seconds exposure time on position # 7 6.705 seconds for ACCUMFAST read out
Science exposure, M1C2 F187M	0.7	12 seconds for filter change 20 seconds exposure time on position # 7 6.705 seconds for ACCUMFAST read out
<i>Orbit 2</i>		
Guide Star re-acquisition	6.0	Start of new orbit
Science exposure, M1C2 F216M	2.9	12 seconds for instrument set-up 150 seconds exposure time on position # 7 12 seconds for MULTIACCUM read out
-	-	-
-	-	-
-	-	-
and so on, until the entire pattern is completed. The observation then requires less than two orbits.		

## CHAPTER 10

# Techniques for Background Measurement and Mosaicing

### In This Chapter...

Introduction /	139
Chopping and Dithering Strategies /	141
Chopping and Dithering Patterns /	143
Examples /	147
Orienting Patterns /	152
Phase II Proposal Instructions for Patterns /	152

In this chapter we deal with techniques for mapping areas larger than the size of the field of view of the NICMOS cameras, and the issue of removing the thermal background of the telescope. Special procedures have been created to enable you to perform both these operations.

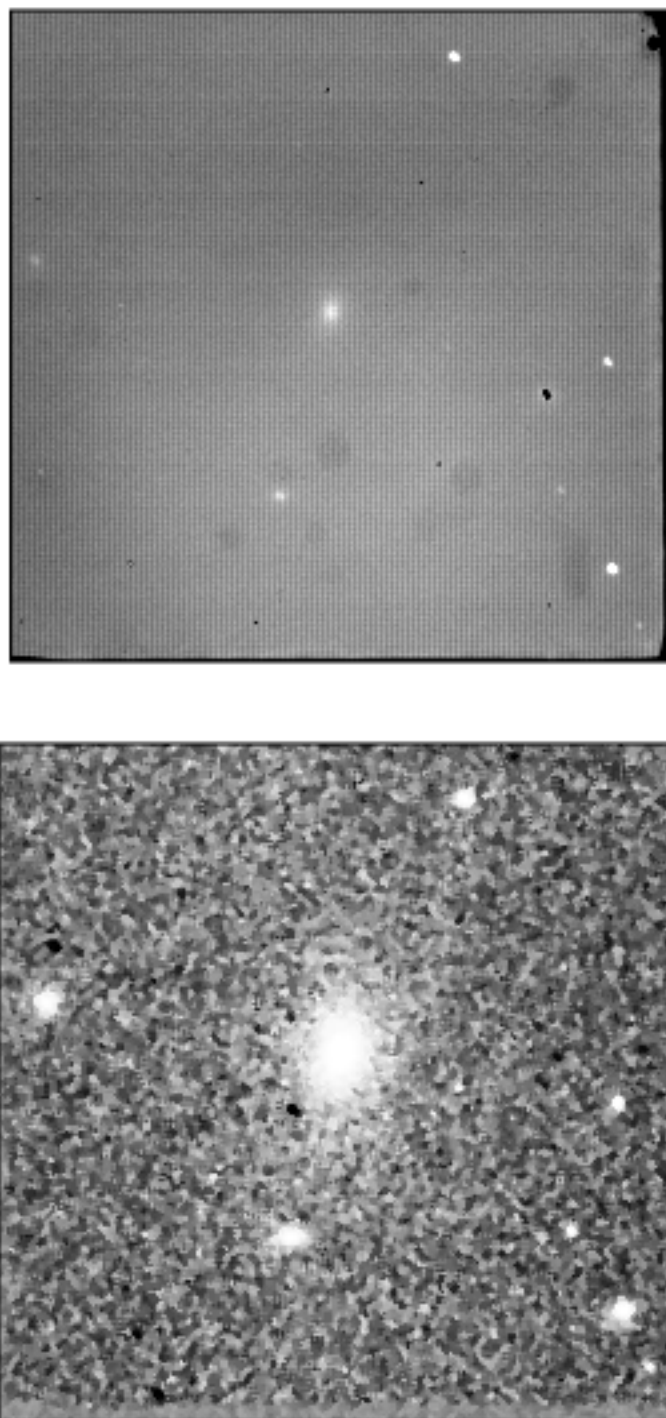
---

## Introduction

Beyond 1.6 microns the contribution of the thermal background to NICMOS science images may be sufficiently high that a proper removal is required to obtain useful data (see Chapter 3). The problem is worsened by the fact that the background is variable on a time scale dictated by the thermal variations of the telescope. Currently, we don't know if the background level will be stable enough that general purpose *background images* can be built, for instance, as part of the NICMOS calibrations. Therefore, we encourage observers who are interested in the wavelength region beyond 1.6 microns to adopt the standard ground-based technique: to alternate on-target exposures with background exposure. To give an idea of how important it is to remove the background contamination from infrared

images, we provide in Figure 10.1 below the example of a galaxy observed in the K band. The image on top is how the object looks after a complete data reduction, but before the background subtraction. The image at the bottom is the same object after the background has been subtracted.

Figure 10.1: K Band Image of a Galaxy, Before and After Background Subtraction



It is possible that on board HST the thermal background will be more stable than in typical ground based situations. As a consequence it might be possible that the object-background interleaving can be carried out with a slower duty cycle. One objective of the SMOV phase will be to determine the required rate.

Background images will be obtained by offsetting the telescope from the target to point to an “empty” region of the sky. The ability to routinely offset the telescope pointing will then be a fundamental operational requirement for NLCMOS. To make it easier to plan observations beyond 1.6 microns, a set of pre-defined observing *patterns* was built; these patterns will combine exposures taken at different telescope pointings into an *association*. A *pattern* is a set of images of the same astronomical target obtained at pointings offset from each other, for the purpose, for instance, of creating background images. The *associations* of exposures are created for the purpose of processing simultaneously all the images from a single pattern. In addition to background subtraction at long NLCMOS wavelengths, the *patterns* will be useful for creating *maps* of extended targets at any wavelength.

Two distinct type of telescope motion are defined:

- *Dither*: Individual motions are limited to no more than 40 arcsecs. These are intended to be used to accomplish sequences of overlapping exposures for the construction of mosaics. Such sequences will be assembled into a single final image by the calibration pipeline.
- *Chop*: Motions up to 1800 arcsecs are permitted. These are intended for the measurement of the background at one or more locations significantly removed from the target pointing. Each non-contiguous background pointing will be assembled into its own final image in addition to the target pointing by the calibration pipeline.

Telescope motions involve overheads for physically moving the telescope and, if necessary, for re-acquiring the guide stars. Therefore, significant time overheads may be incurred by observations which need background subtraction or propose to map extended regions of the sky. A careful estimate of the overheads associated with a specific observation or set of observations is necessary to evaluate the number of orbits required (see Chapter 9).

---

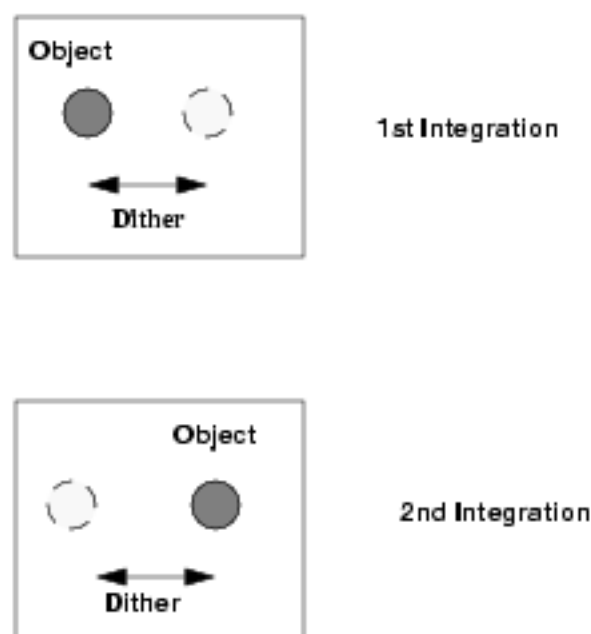
## Chopping and Dithering Strategies

The most efficient strategy for removing the background from a science exposure strongly depends on the nature of the target and of the science to be accomplished. In general two types of targets can be defined: compact and extended.

## Compact Objects

For compact objects, such as point sources, background subtraction can be achieved by moving the target across the camera field of view (see Figure 10.2). A dither pattern, which involves movements of a few arcsecs from one exposure to the next, can then be used. This is an efficient way to build background images, since the target is present in each exposure, and a background image can be created from the stacking and filtering of all exposures.

Figure 10.2: Dithering.

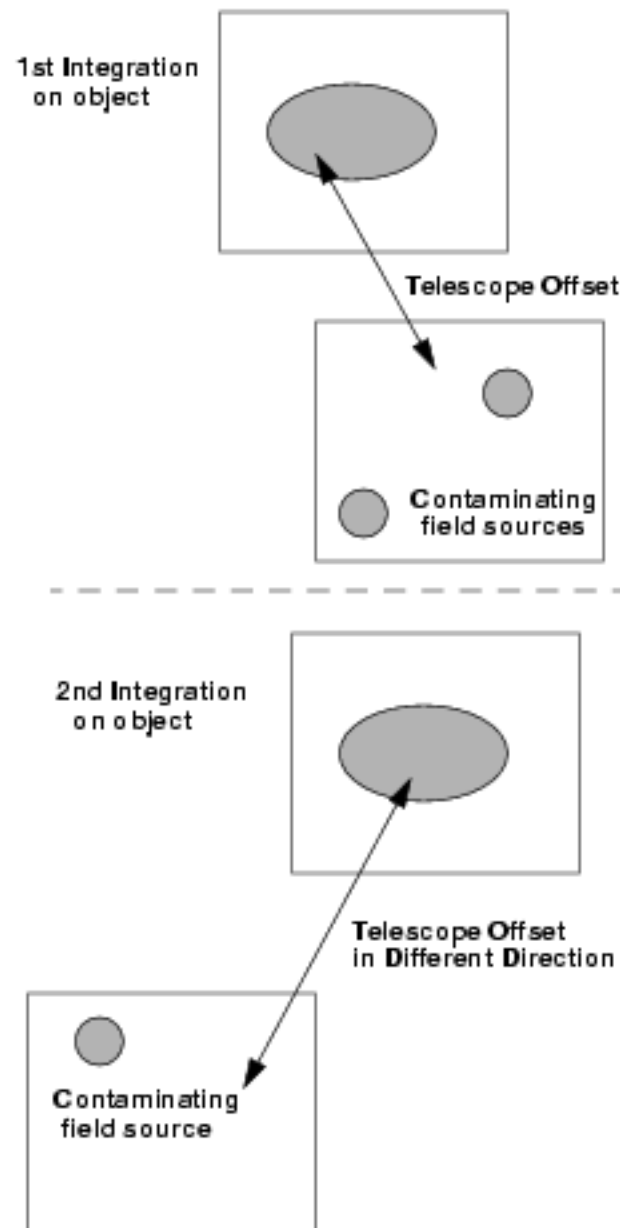


## Extended Objects

For an extended object which occupies a significant portion of the NICMOS field of view, the dithering technique does not apply to building background images. In this case, offsets to an adjacent field (chopping), chosen to be at least one camera field away in an arbitrary direction, are necessary. By offsetting in different directions a stacked and filtered sky can be created which removes the effect of contaminating objects in the offset fields (see Figure 10.3). As in the case of compact objects, these offsets might be quite small, but for large galaxies for example, they may need to be over considerable distances. The user will have the ability to specify the offset values and directions and their number in the Phase II instructions.



Figure 10.3: Chopping



## Chopping and Dithering Patterns

There will be a set of 11 pre-designed patterns available for NICMOS observations. They include: 4 dither patterns, 4 chop patterns, and 3 dither-chop patterns. For each of these, the observer will be able to specify, during the Phase II Proposal submission, the total number of positions desired (2 to 40), the dither size (0 to 40 arcsecs), the chop size (0 to 1800 arcsecs), and the orientation of the

pattern on the sky. The option `POSTARG` will be still available for offsetting the telescope and creating custom-design patterns, but there are a number of advantages in using the pre-designed patterns:

- They simplify the specification of complex observations in the Phase II proposal.
- All the observations pertaining to a pattern result in one association and are simultaneously calibrated and combined in the data calibration pipeline, including background calibration, cosmic ray removal, and flat field averaging. Observations obtained with `POSTARG` do not result in associations, and will have to be combined manually by the observer.
- They permit the observation of a mosaic with a fixed position angle without fixing spacecraft roll, which increases the number of opportunities to schedule the observations.

Multiple exposures may be obtained at each position by the use of the `NEXP` optional parameter. These may be useful for cosmic ray removal.

The 11 patterns are listed in Table 10.1, together with applicable parameters, such as the allowed values for the number of steps in the pattern (`Num Pos`), for the dither size and for the chop size. In addition, the figure number where the pattern is graphically shown is given in column 5 of Table 10.1. Offset sizes and number of steps in a pattern affect the amount of overhead time required to perform an observation (see Chapter 9). The effects of dithering or chopping on an astronomical image are shown in a set of examples in the next section.

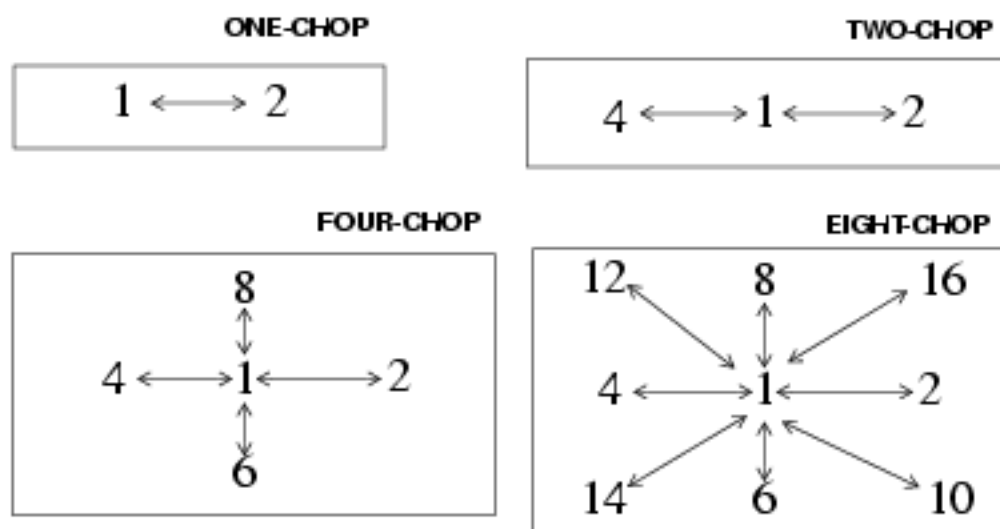
Table 10.1: NICMOS Pre-designed Observing Patterns and Parameters

Pattern Name	Num. Pos.	Dither Size	Chop Size	See Figure
<code>NONE</code> (default)	NA	NA	NA	
<code>SPIRAL-DITH</code>	2 - 40	0.0 - 40.0	NA	Fig. 10.4
<code>SQUARE-WAVE-DITH</code>	2 - 40	0.0 - 40.0	NA	Fig. 10.4
<code>XSTRIP-DITH</code>	2 - 40	0.0 - 40.0	NA	Fig. 10.4
<code>YSTRIP-DITH</code>	2 - 40	0.0 - 40.0	NA	Fig. 10.4
<code>ONE-CHOP</code>	2 - 40	NA	0.0 - 1800.0	Fig. 10.5
<code>TWO-CHOP</code>	2 - 40	NA	0.0 - 1800.0	Fig. 10.5
<code>FOUR-CHOP</code>	2 - 40	NA	0.0 - 1800.0	Fig. 10.5
<code>EIGHT-CHOP</code>	2 - 40	NA	0.0 - 1800.0	Fig. 10.5
<code>SPIRAL-DITH-CHOP</code>	2 - 40	0.0 - 40.0	0.0 - 1800.0	Fig. 10.6
<code>XSTRIP-DITH-CHOP</code>	2 - 40	0.0 - 40.0	0.0 - 1800.0	Fig. 10.6
<code>YSTRIP-DITH-CHOP</code>	2 - 40	0.0 - 40.0	0.0 - 1800.0	Fig. 10.6



target (position 1). The names of the chop patterns are: **ONE-CHOP**, **TWO-CHOP**, **FOUR-CHOP**, and **EIGHT-CHOP**. The **ONE-CHOP** pattern produces one image of the target and one image of the background. the **TWO-CHOP** pattern produces one image (with two exposures) of the target and two background images, with the background fields positioned on opposite sides of the target. The two other patterns increase the number of target-background pairs to four and eight, respectively. A large number of background images may be required if they contain a large number of contaminating sources or if the background is highly structured. The four chop patterns are shown in the figure below:

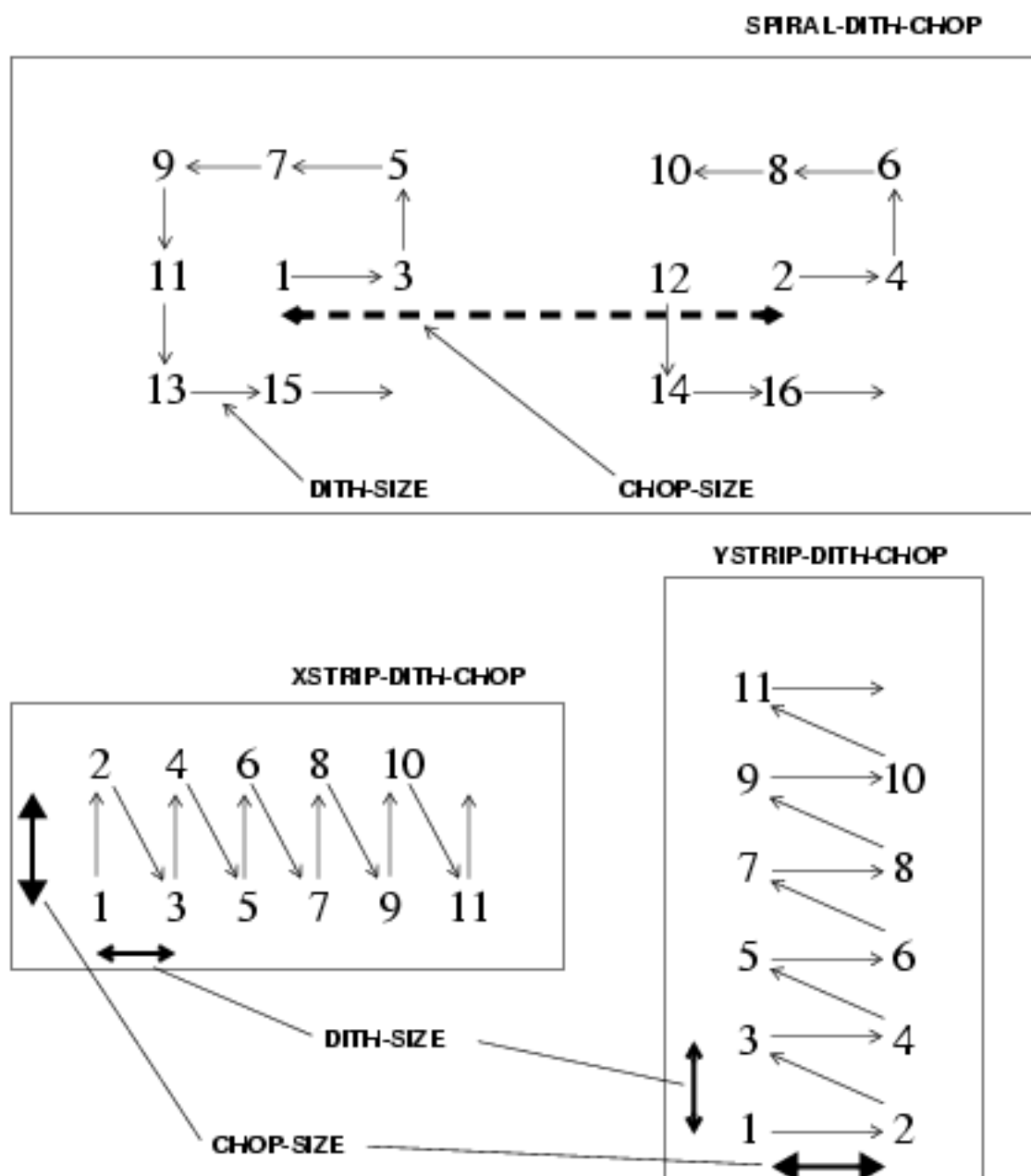
Figure 10.5: Chop Patterns



### Combined Patterns

The combined patterns permit dithering interleaved with chops to measure the background. They are recommended for simultaneous mapping and background subtraction during observations of extended targets, beyond 1.6 microns. Three combined patterns are implemented: **SPIRAL-DITH-CHOP**, **XSTRIP-DITH-CHOP**, and **YSTRIP-DITH-CHOP**. Their characteristics are analogous to the dither patterns **SPIRAL-DITH**, **XSTRIP-DITH**, and **YSTRIP-DITH**, respectively, with the addition that each dither step is coupled with a background image obtained by chopping. The three combined patterns are shown in Figure 10.6.

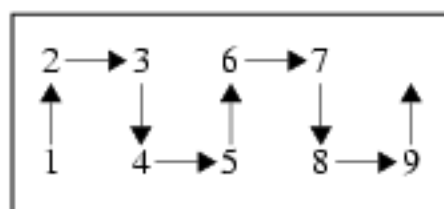
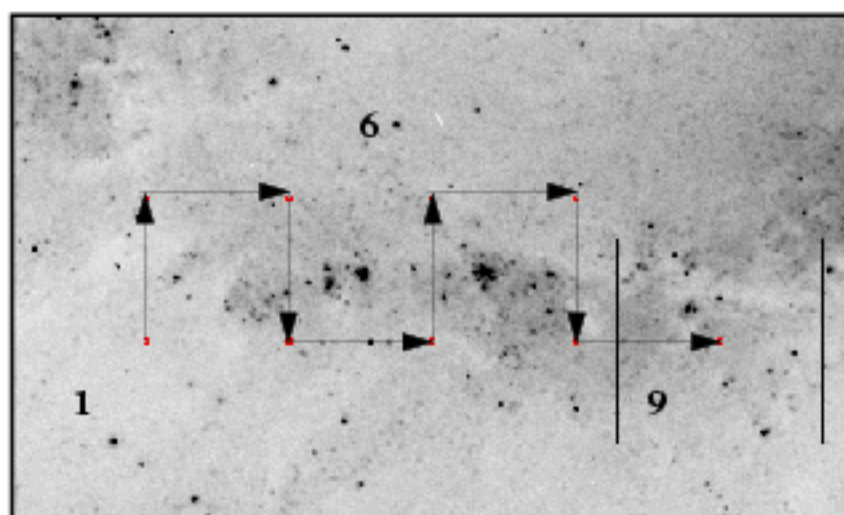
Figure 10.6: Combined Patterns



## Examples

The next few pages show a few selected examples of how the patterns work on astronomical observations.

Figure 10.7: Square Wave Dither



Images Taken:

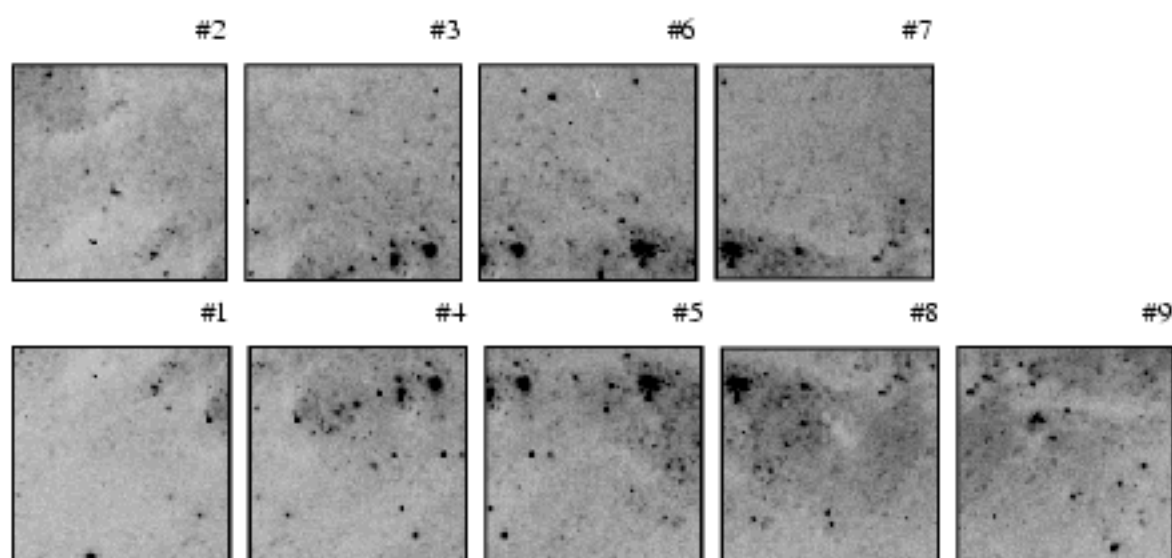
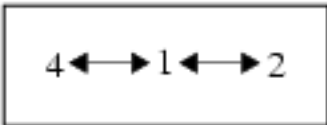
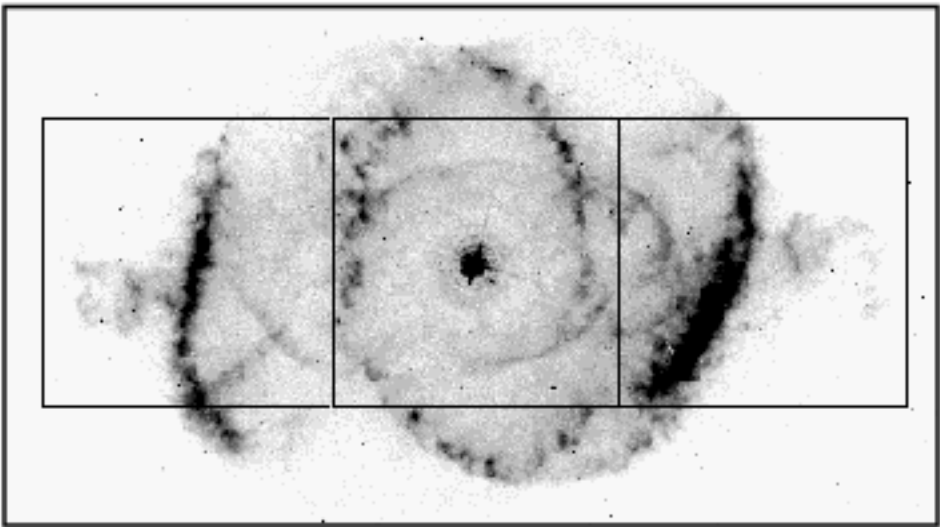


Figure 10.8: Two-Chop Pattern



Images Taken:

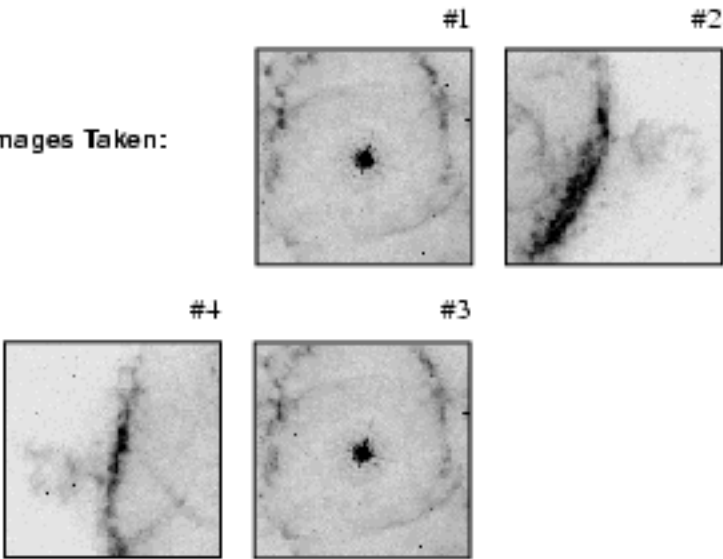
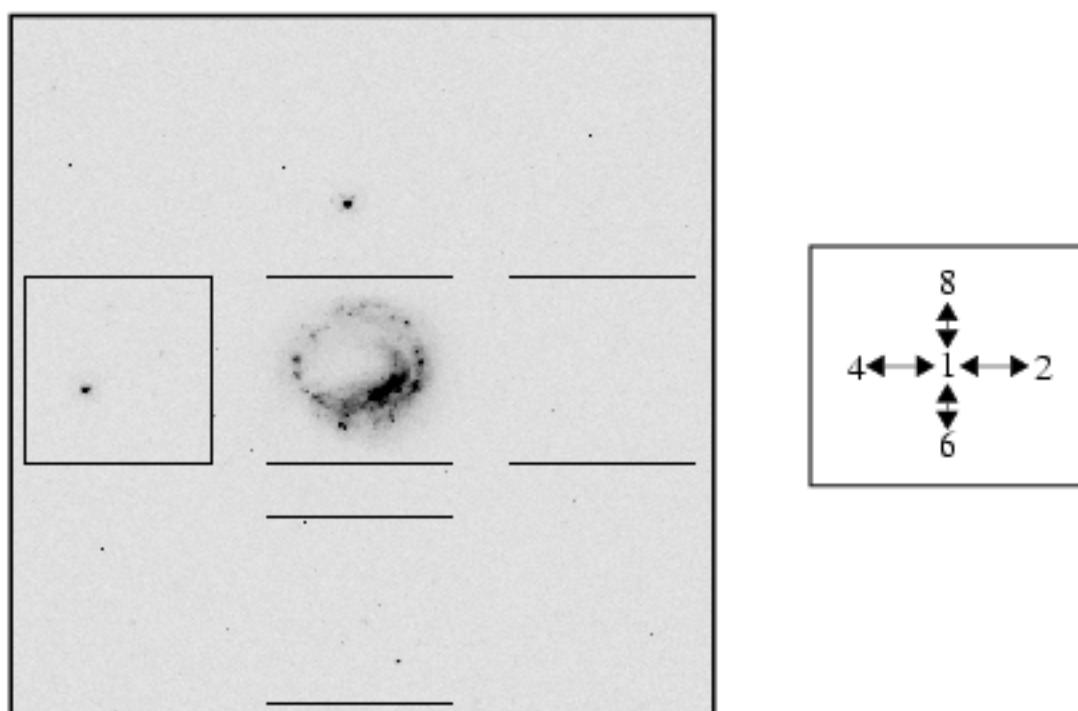


Figure 10.9: Four-Chop Pattern



Images Taken:

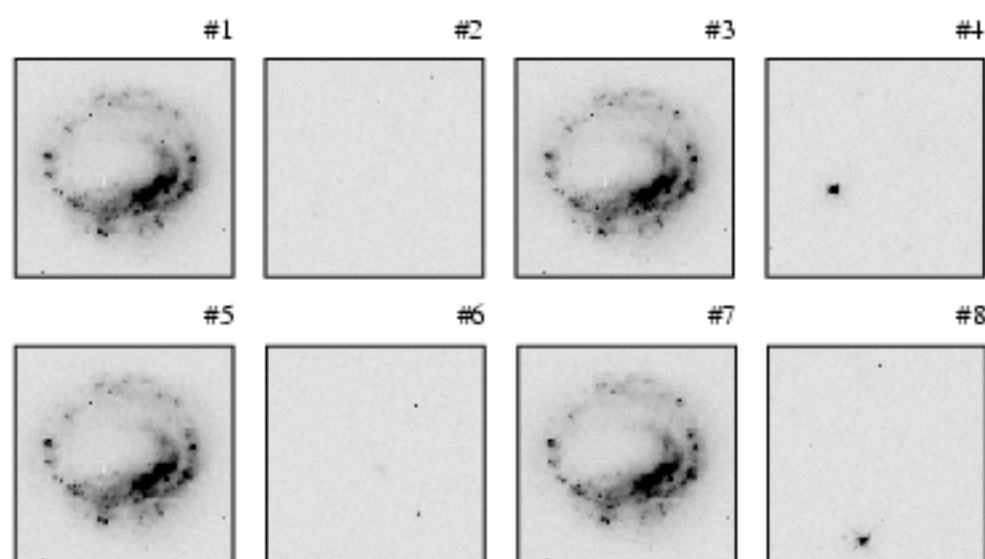
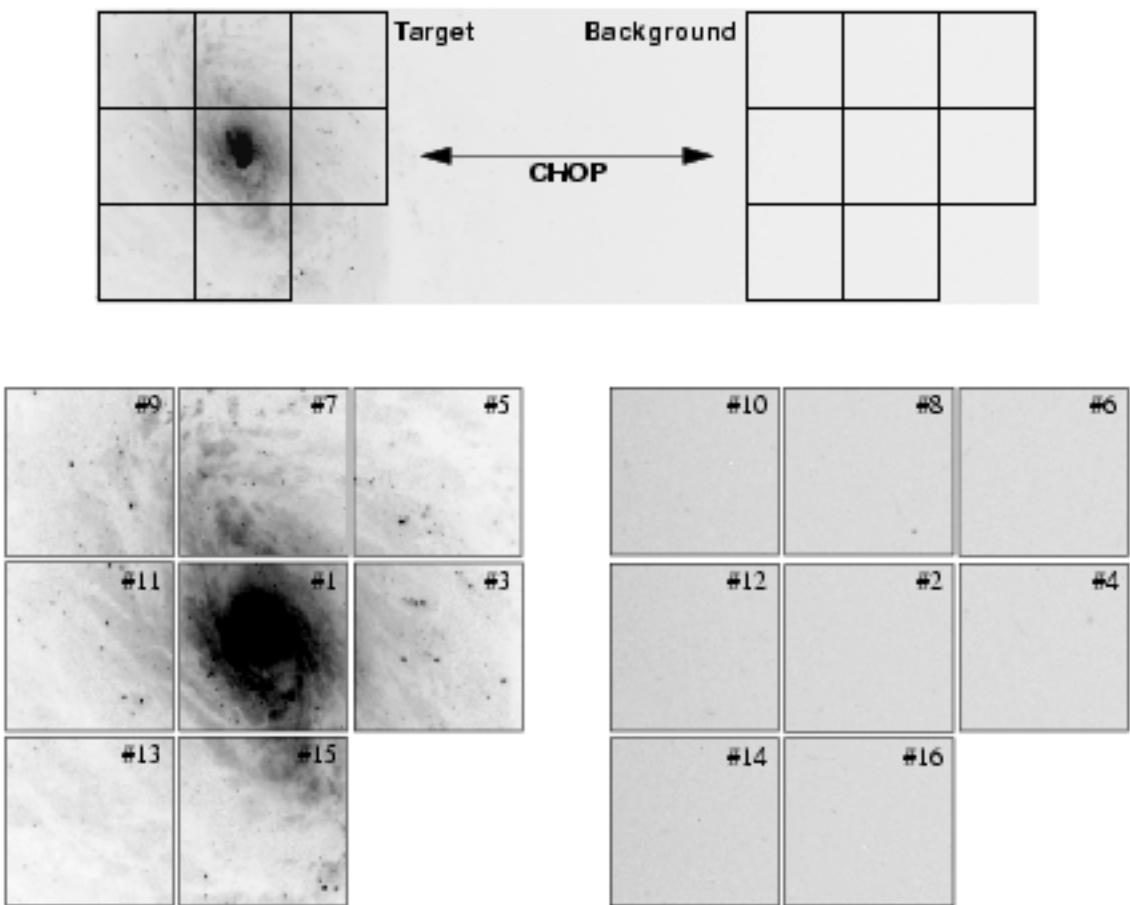




Figure 10.10: Spiral-Dith-Chop Pattern



Sequence of Frames



## Orienting Patterns

Observations will often require that patterns are executed with specific position angles (PA) on the sky. For instance an observer may need to map an elongated region with PA= $n$  degrees on the sky, using the `SQUARE-WAVE-DITH` pattern. Since the use of the `ORIENT` special requirement usually constrains the scheduling opportunities for a target (and may result in the unavailability of suitable guide stars), NLCMOS implements an optional parameter called `PATTERN-ORIENT` (see next section). With this parameter, the orientation of the pattern on the sky can be set independently of the orientation of the three NLCMOS detectors (and vice-versa). If a specific orientation of the detectors is also required, then the observatory level special requirement `ORIENT` must be set together with `PATTERN-ORIENT`.

The default value for `PATTERN-ORIENT` is `DETECTOR`, and the pattern motions are in the NLCMOS (x-y) focal plane orientation, i.e., rotated 225 degrees from the U3 axis. The orientation of the patterns on the sky is then determined by the orientation of the telescope with the `ORIENT` special requirement. Other values for the `PATTERN-ORIENT` parameter are given by the standard convention for PA, from 0.0 to 360.0, North through East. For example, the `XSTRIP-DITH` pattern with `PATTERN-ORIENT=0` will track from East to West on the sky (the +Y axis is pointing North), and with `PATTERN-ORIENT=45` from Southeast to Northwest. The `YSTRIP-DITH` pattern with `PATTERN-ORIENT=0` will track from North to South.

## Phase II Proposal Instructions for Patterns



We discuss the Phase II instructions for patterns in this section in order to illustrate the options available, however, this is *not* an exhaustive description and is *not* the appropriate reference to use when preparing a Phase II proposal. At that stage you should refer to the Institute's Phase II Proposal Instructions, which contain a complete and up-to-date guide.

This section is not crucial for preparing the Phase I proposal, but it may be relevant to know beforehand which parameters will be available, and what values these parameters can have. One, and only one, pattern may be defined on an individual exposure logsheet line. A pattern may only be specified on the *prime* NLCMOS camera. The motions between each exposure are carried out by expanding the pattern into a sequence of individual exposures separated by `POSTARG` operations.

The set of exposures resulting from a pattern is called an association. A number of optional parameters are implemented for associations, and are listed below.

## Parameters

- **PATTERN=NONE** (default) or **Pattern\_Name** (see Table 10.1).
- **NUM-POS = 2 to 40** (number of steps in dither or chop pattern to perform).
- **DITH-SIZE = 0.0 to 40.0** (size of *each* step in arcsecs).
- **CHOP-SIZE = 0.0 to 1800.0** (size of *each* step in arcsecs).
- **OFFSET-SAM** (default), (use SAMs; gyros for large moves with re-acquire); **SAM-NO-REACQ**, (use SAMs; do not attempt to re-acquire guide stars); **SAM-NO-GYRO**, (use SAMs; must use same or new guide stars).
- **PATTERN-ORIENT-DETECTOR** (default), (move in detector X-Y system) 0.0 - 360.0 degrees from PA=0 increasing to East (Note that this does *not* constrain telescope roll; use existing ORIENT requirement).

## Types of Motions

The **OFFSET** parameter defines which type of telescope motion will be performed during a pattern, in order to dither or chop. Telescope motions fall into three categories:

- Small angle motions (SAMs) where FGS Fine Lock guiding is maintained. Such SAMs are typically limited to < 2 arcmins from the point of the initial guide star acquisition. This is the practical limit of the radial extent of the pattern. Often it will be smaller due to guide star availability.
- SAMs without FGS guiding (i.e., **GYRO HOLD** pointing control). These are necessary for larger motions (> 2 arcmins). The telescope will drift at a rate of 1 to 2 milli-arcsecs per second of time (elapsed time—*not* exposure time).
- SAMs with **RE-ACQUISITIONS** at each return to the target position. This can be used to chop between a target and an offset background measurement pointing (which would be observed with **GYRO HOLD** pointing control).

The available options for **OFFSET** are:

- **SAM**, the default, will use guide stars whenever possible. If a motion, or the sequence of motions, moves the telescope sufficiently from the original position that guide stars are no longer available then exposures will be obtained using **GYRO HOLD**. If a subsequent motion returns the telescope to a point where the original guide stars become available then it will **RE-ACQUIRE** the guide stars. This incurs an overhead of ~3 minutes for each **RE-ACQUISITION**.
- **SAM-NO-REACQ** will use guide stars (FGS Fine Lock) until the *first* instance in the pattern when guide stars become unavailable. The remainder of the pattern will be executed using **GYRO HOLD** pointing control.

- SAM-110-GYRO will use guide stars for all exposures. If guide stars are not available, the observation cannot be scheduled.

## CHAPTER 11

# Imaging Reference Material

This chapter provides the sensitivity information for the imaging filters, ordered by camera and increasing central wavelength. See Chapter 4 for a detailed description of the the figures in this chapter. The corresponding information for the grism and polarizer elements is provided in the same format in Chapter 5.

# Camera 1, Filter F090M

Central wavelength( $\mu\text{m}$ )	Mean Wavelength( $\mu\text{m}$ )	Peak Wavelength ( $\mu\text{m}$ )	FWHM ( $\mu\text{m}$ )	Range ( $\mu\text{m}$ )	MaxTr %	Pixel Fraction
0.9003	0.8970	0.9175	0.1885	0.8 - 1.0	79.64	0.30

Figure 11.1: Camera 1, Filter F090M

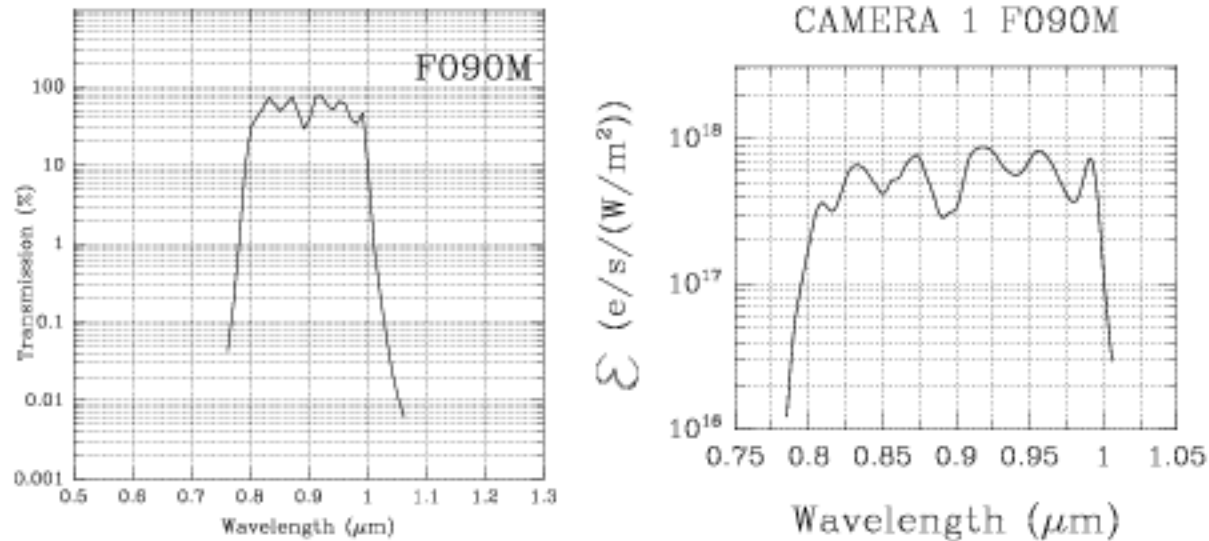
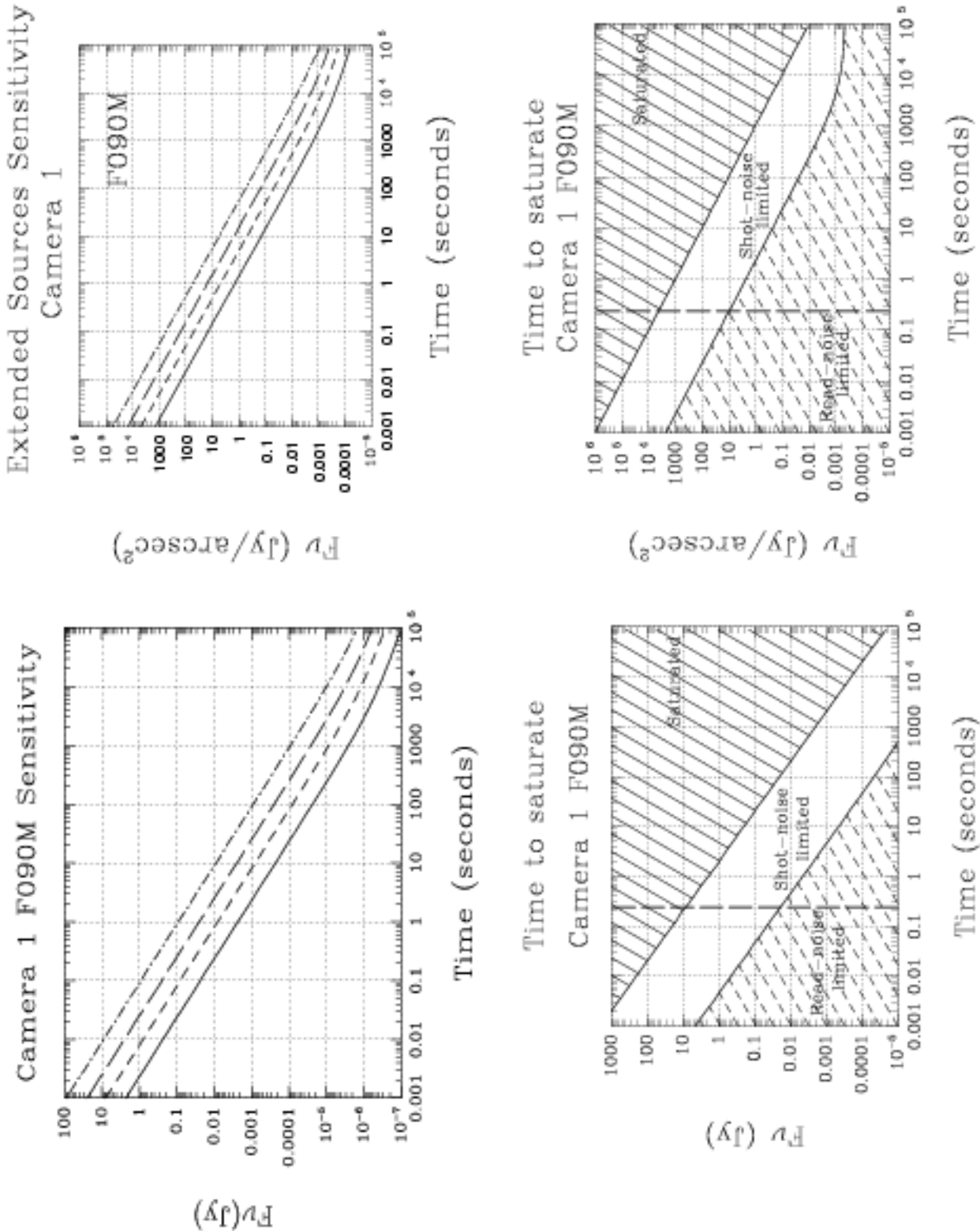


Figure 11.2: Sensitivity and Exclusion Curves, Camera 1, Filter F090M

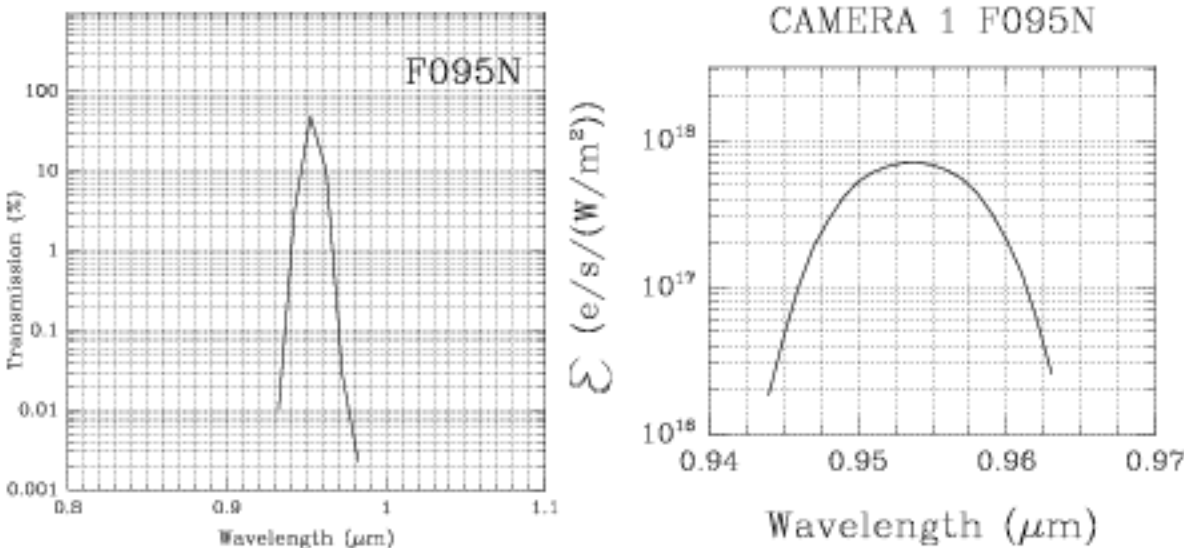


# Camera 1, Filter F095N

[S III] Line

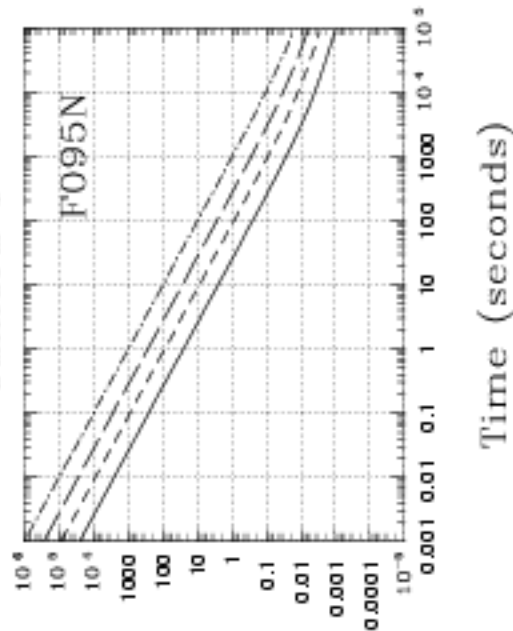
Central wavelength (μm)	Mean wavelength (μm)	Peak wavelength (μm)	FWHM (μm)	Range (μm)	MaxTr %	Pixel Fraction
0.9538	0.9536	0.9508	0.0088	1%	66.31	0.21

Figure 11.3: Camera 1, Filter F095M

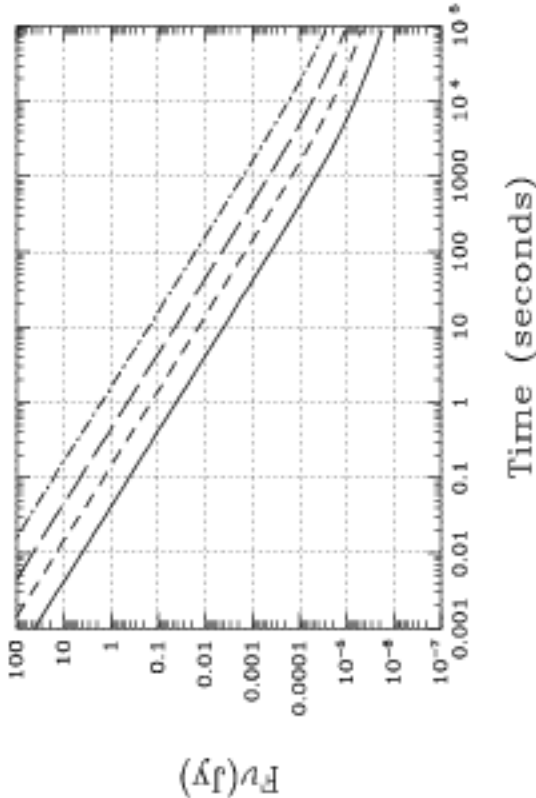




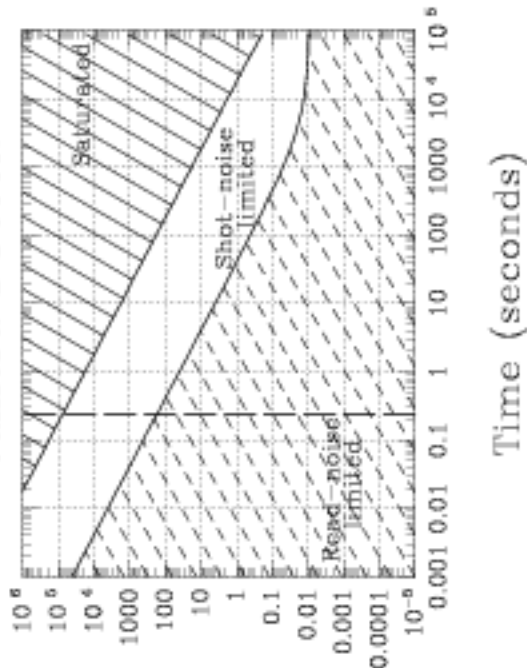
Extended Sources Sensitivity  
Camera 1



Camera 1 F095N Sensitivity



Time to saturate  
Camera 1 F095N



Time to saturate  
Camera 1 F095N

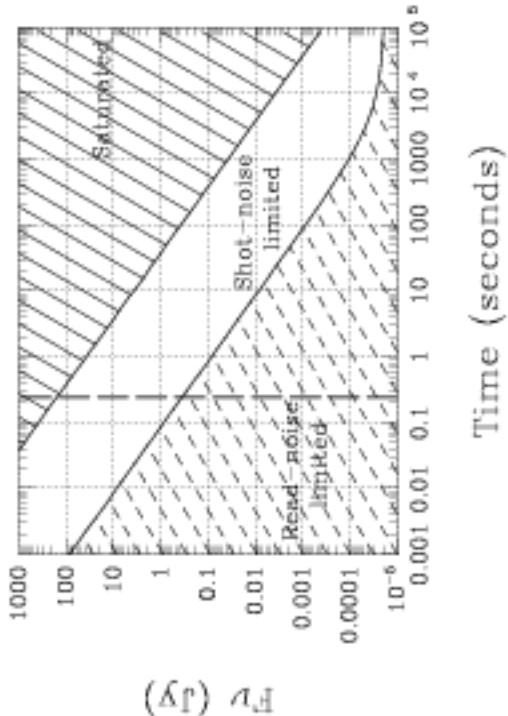


Figure 11.4: Sensitivity and Exclusion Curves, Camera 1, Filter F095N

# Camera 1, Filter F097N

## [SIII] Continuum

Central wavelength (μm)	Mean wavelength (μm)	Peak wavelength (μm)	FWHM (μm)	Range (μm)	MaxTr %	Pixel Fraction
0.9717	0.9715	0.9740	0.0094	1%	73.51	0.22

Figure 11.5: Camera 1, Filter F097N

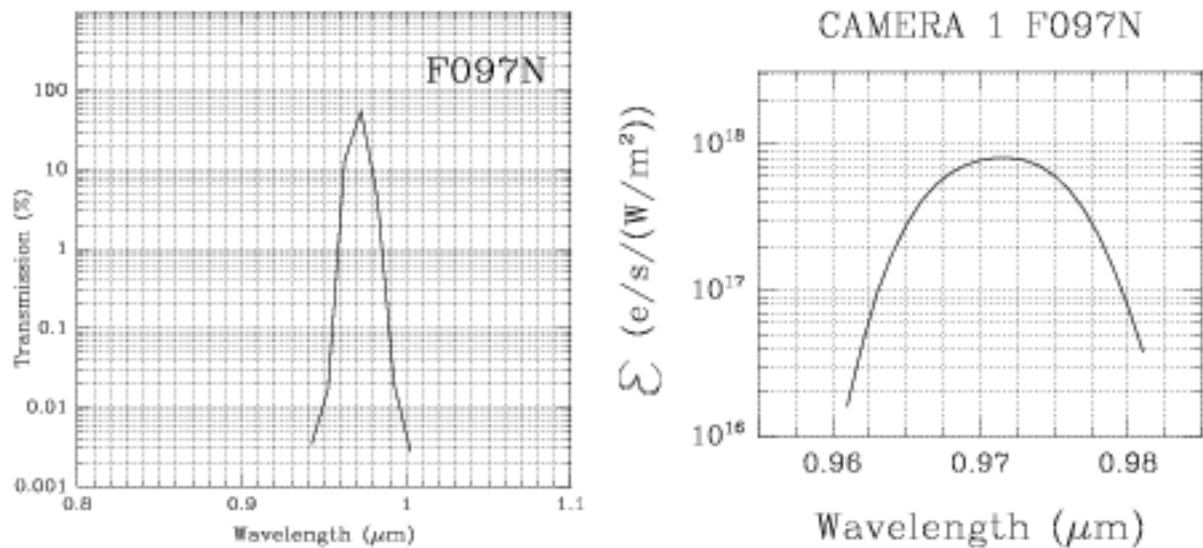
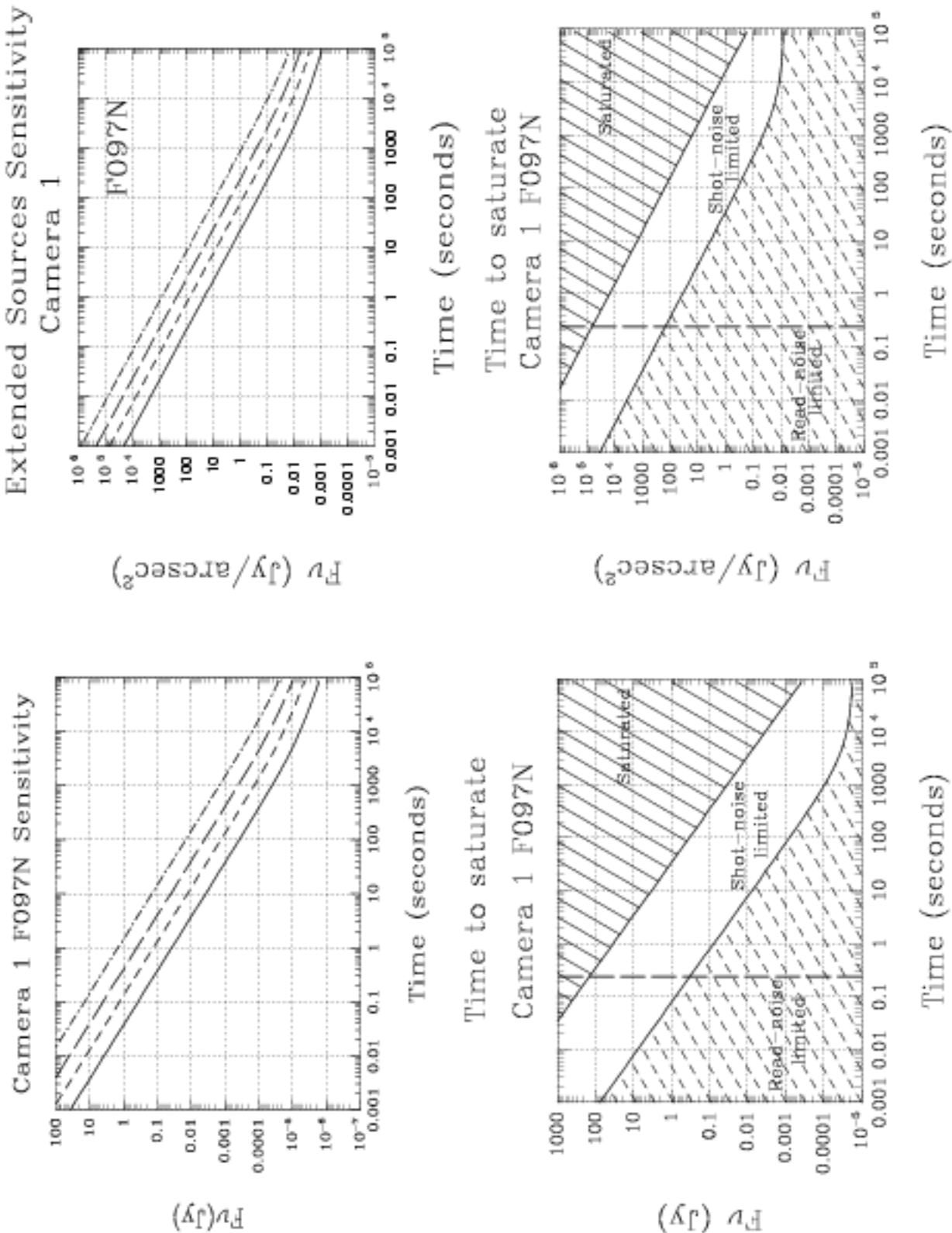


Figure 11.6: Sensitivity and Exclusion Curves, Camera 1, Filter F097N



## Camera 1, Filter F108N

### Hel Line

Filter F108N is also available in Camera 3.

Central wavelength ( $\mu\text{m}$ )	Mean wavelength ( $\mu\text{m}$ )	Peak wavelength ( $\mu\text{m}$ )	FWHM ( $\mu\text{m}$ )	Range ( $\mu\text{m}$ )	MaxTr %	Pixel Fraction
1.0817	1.0816	1.0790	0.0094	1%	81.94	0.21

Figure 11.7: Camera 1, Filter F108N

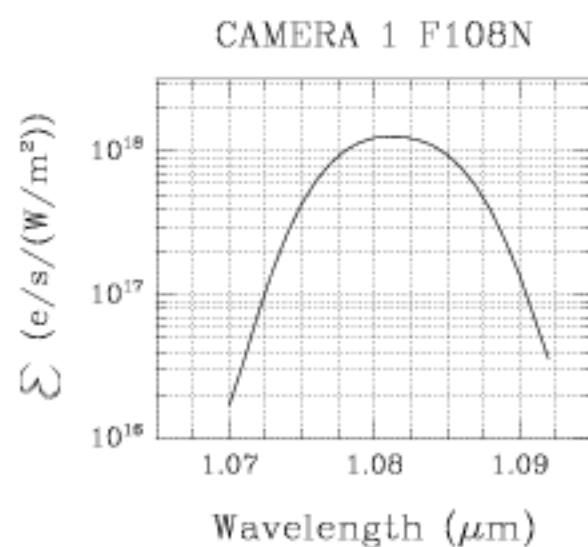
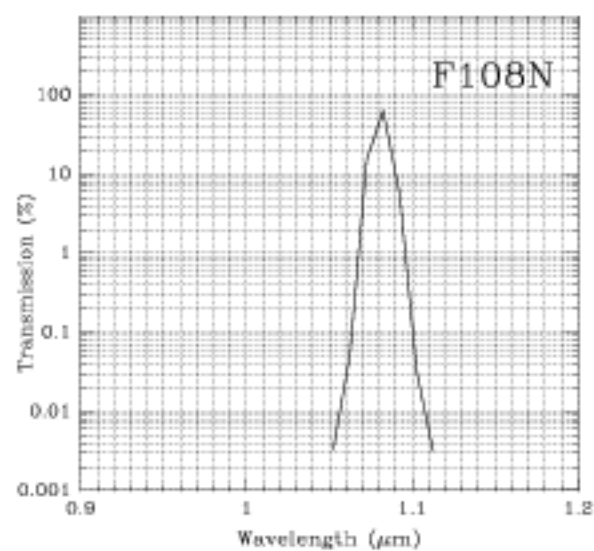
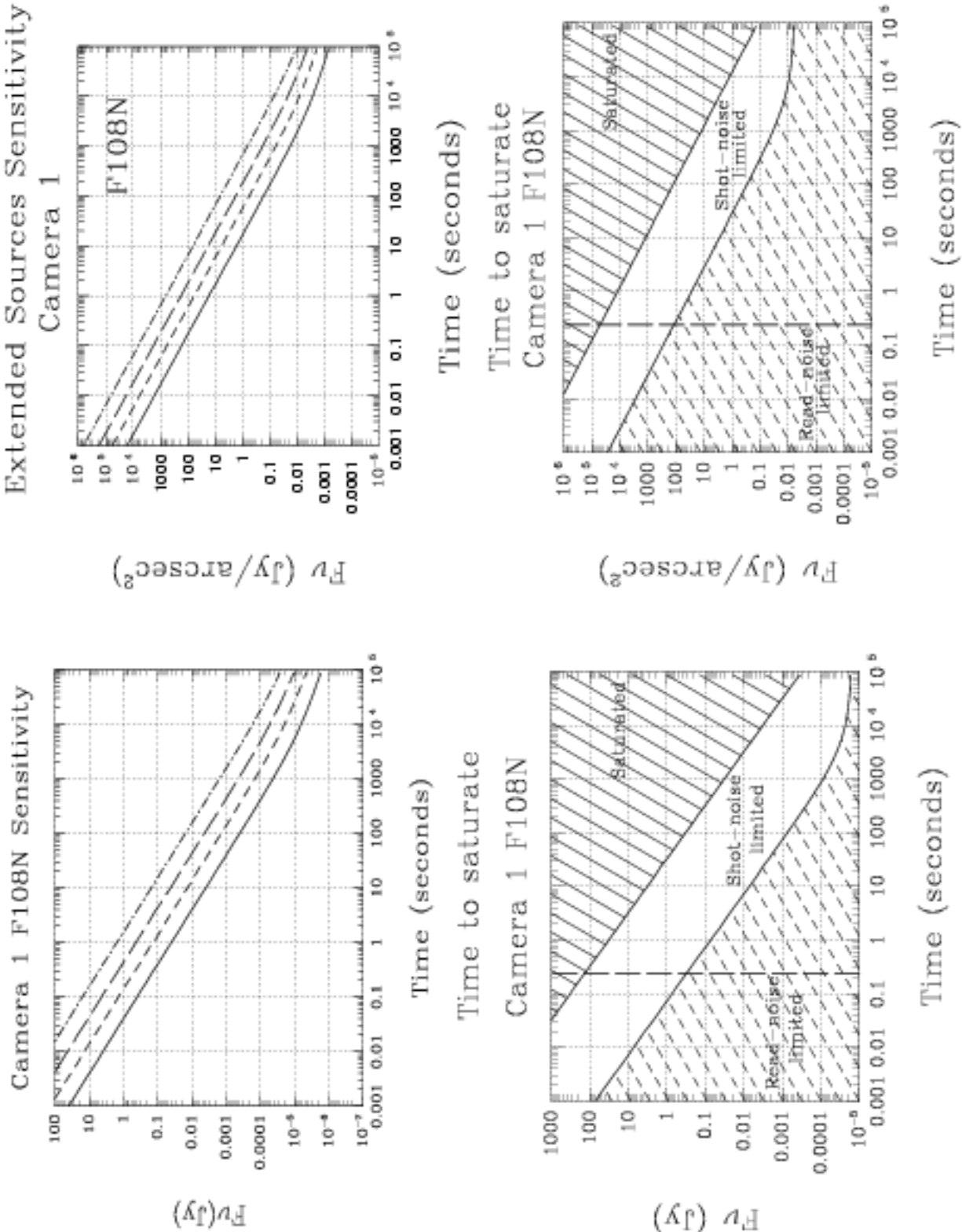


Figure 11.8: Sensitivity and Exclusion Curves, Camera 1, Filter F108N



# Camera 1, Filter F110M

Note: Camera 1 also has a broader F110W filter.

Central Wavelength (μm)	Mean Wavelength (μm)	Peak Wavelength (μm)	FWHM (μm)	Range (μm)	MaxTr %	Pixel Fraction
1.1013	1.1003	1.1295	0.1995	1.0-1.2	90.49	0.16

Figure 11.9: Camera 1, Filter F110M

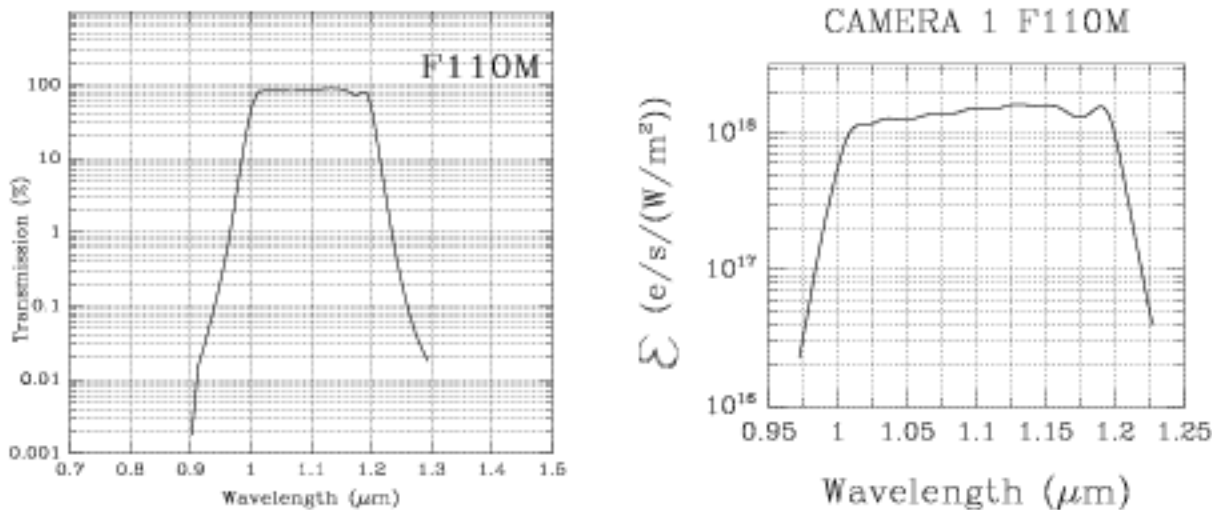
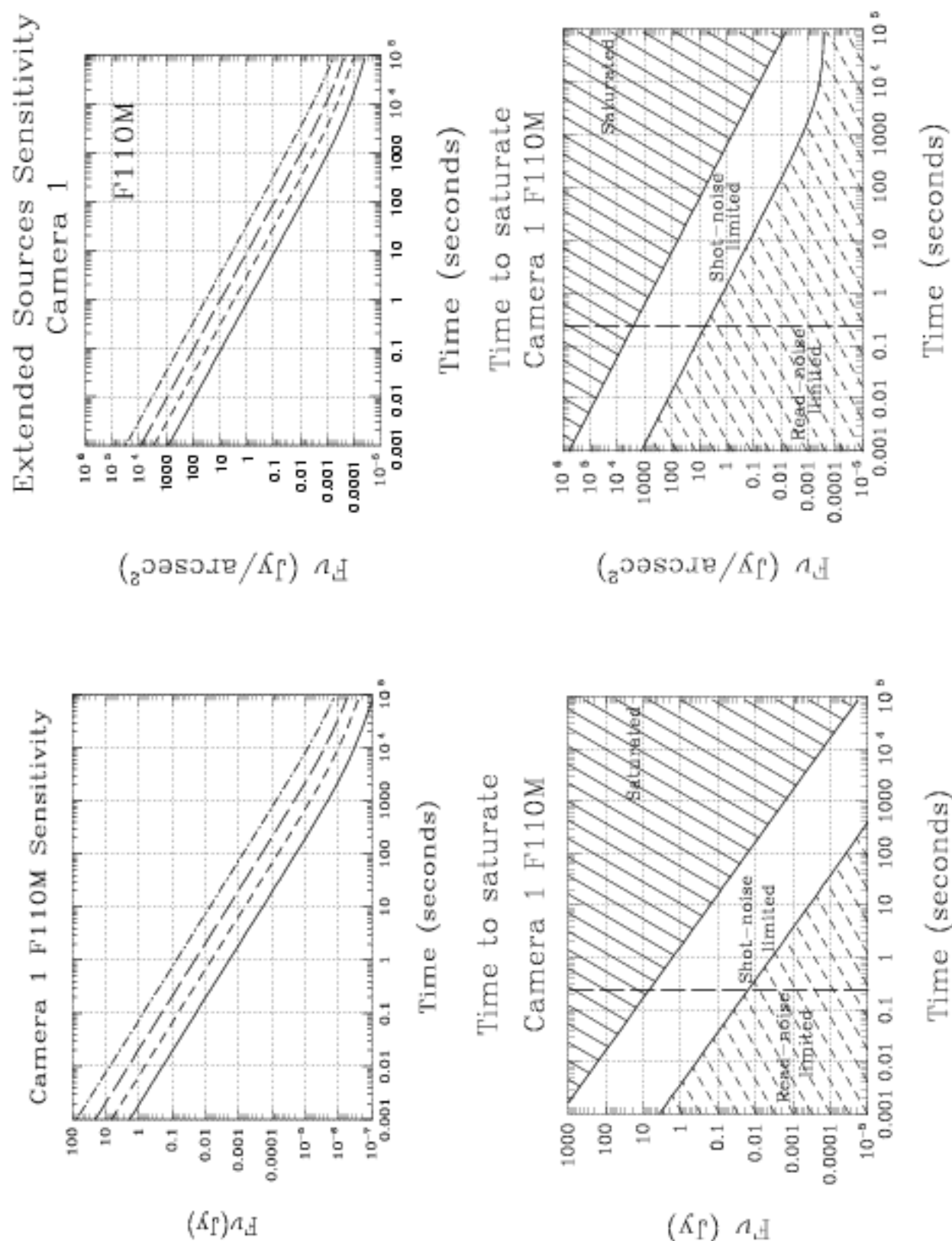


Figure 11.10: Sensitivity and Exclusion Curves for Camera 1, Filter F110M



# Camera 1, Filter F110W

This filter is also available on Cameras 2 and 3.

Central wavelength (μm)	Mean wavelength (μm)	Peak wavelength (μm)	FWHM (μm)	Range (μm)	MaxTr %	Pixel Fraction
1.0985	1.1022	1.2760	0.5920	0.8-1.35	95.11	0.160

Figure 11.11: Camera 1, Filter F110W

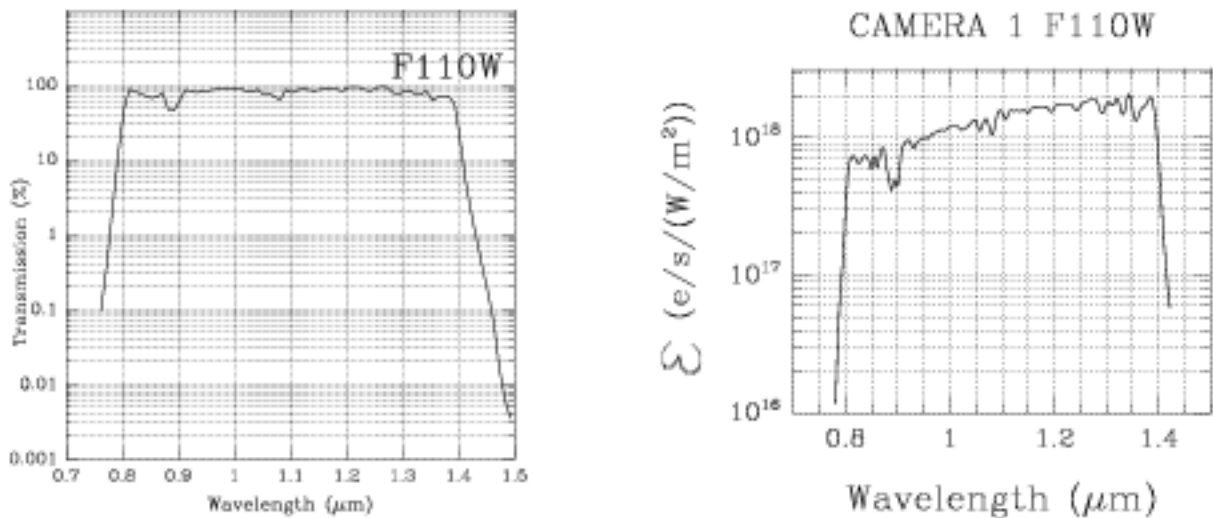
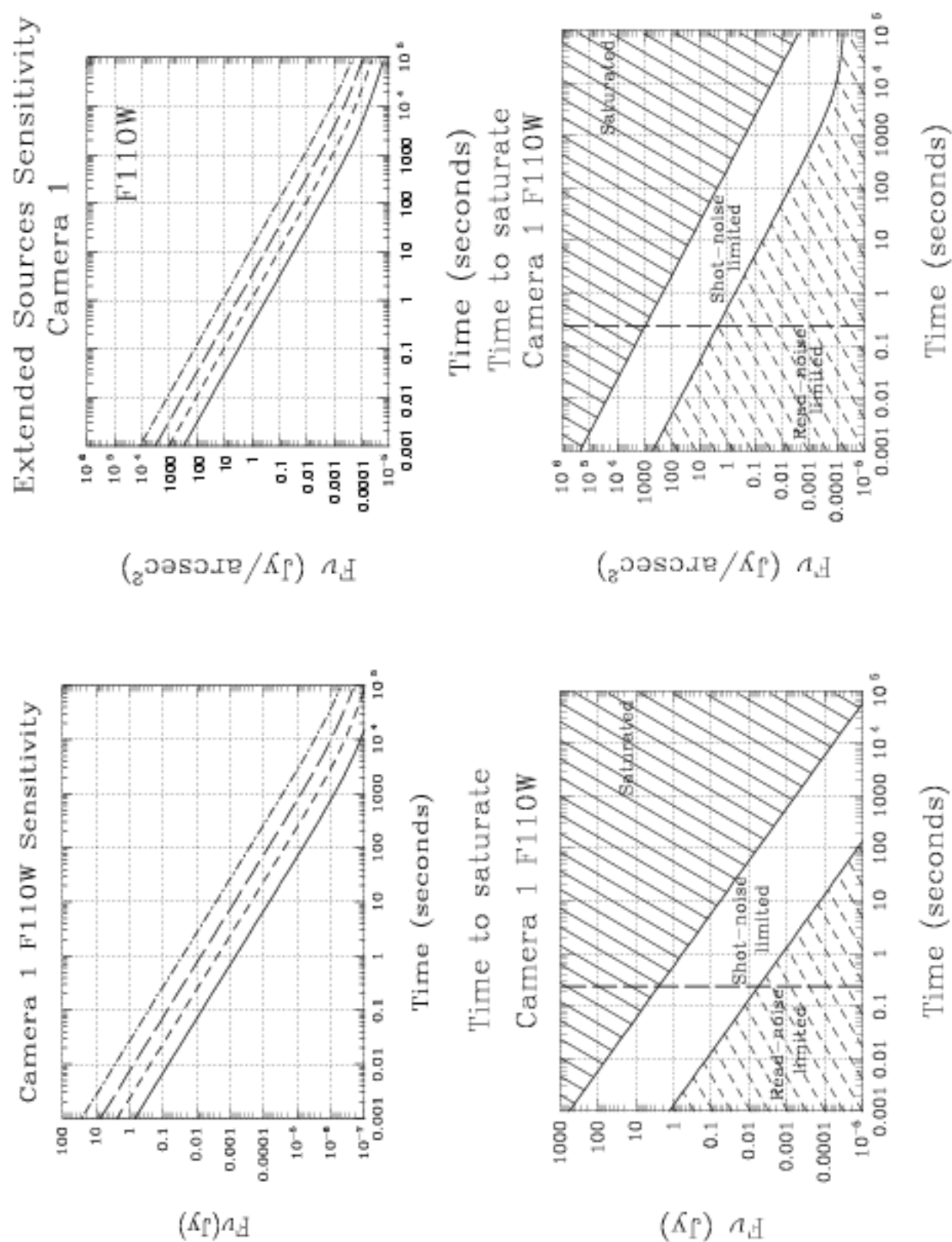




Figure 11.12: Sensitivity and Exclusion Curves for Camera 1, Filter F110W



# Camera 1, Filter F113N

## Hel Continuum

This filter is also available on Camera 3.

Central wavelength (μm)	Mean wavelength (μm)	Peak wavelength (μm)	FWHM (μm)	Range (μm)	MaxTr %	Pixel Fraction
1.1297	1.1298	1.1312	0.0110	1%	86.24	0.14

Figure 11.13: Camera 1, Filter F113N

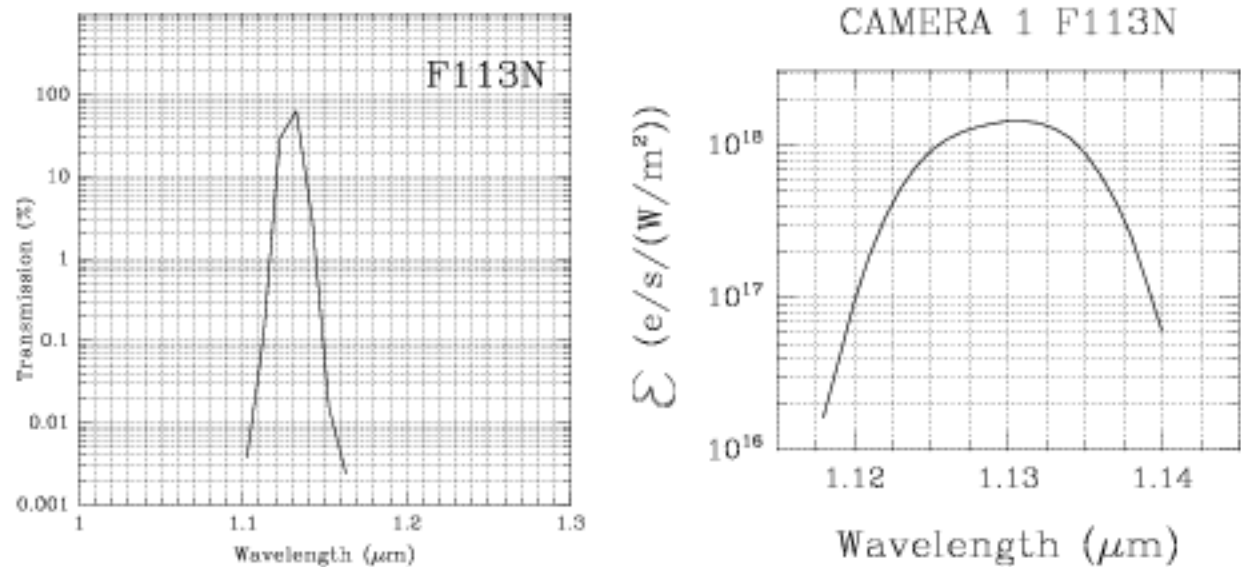
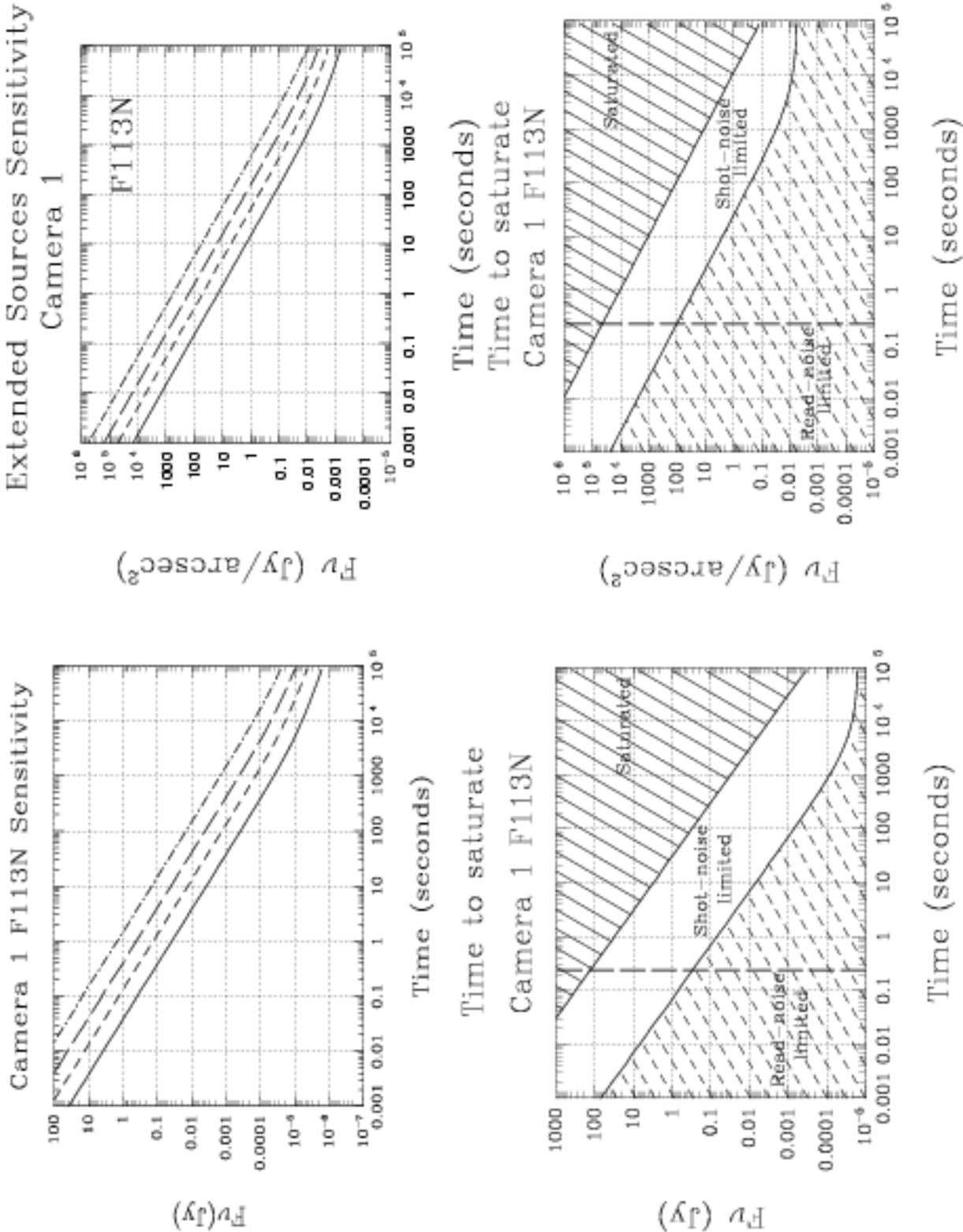


Figure 11.14: Sensitivity and Exclusion Curves for Camera 1, Filter F113N



# Camera 1, Filter F140W

Central wavelength (μm)	Mean wavelength (μm)	Peak wavelength (μm)	FWHM (μm)	Range (μm)	MaxTr %	Pixel Fraction
1.3973	1.3993	1.2240	0.7965	0.8-1.8	95.50	0.14

Figure 11.15: Camera 1, Filter F140W

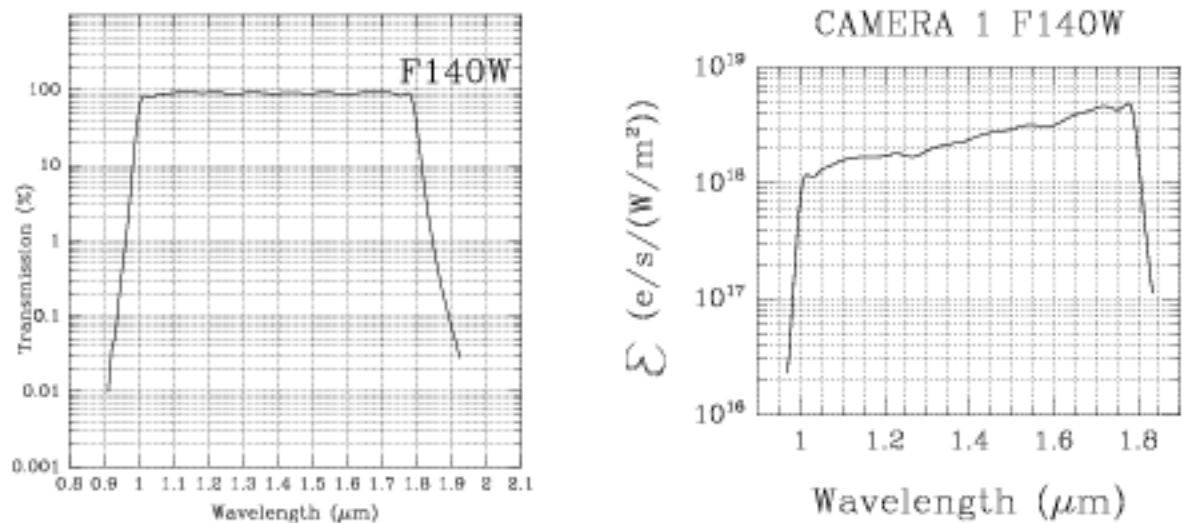
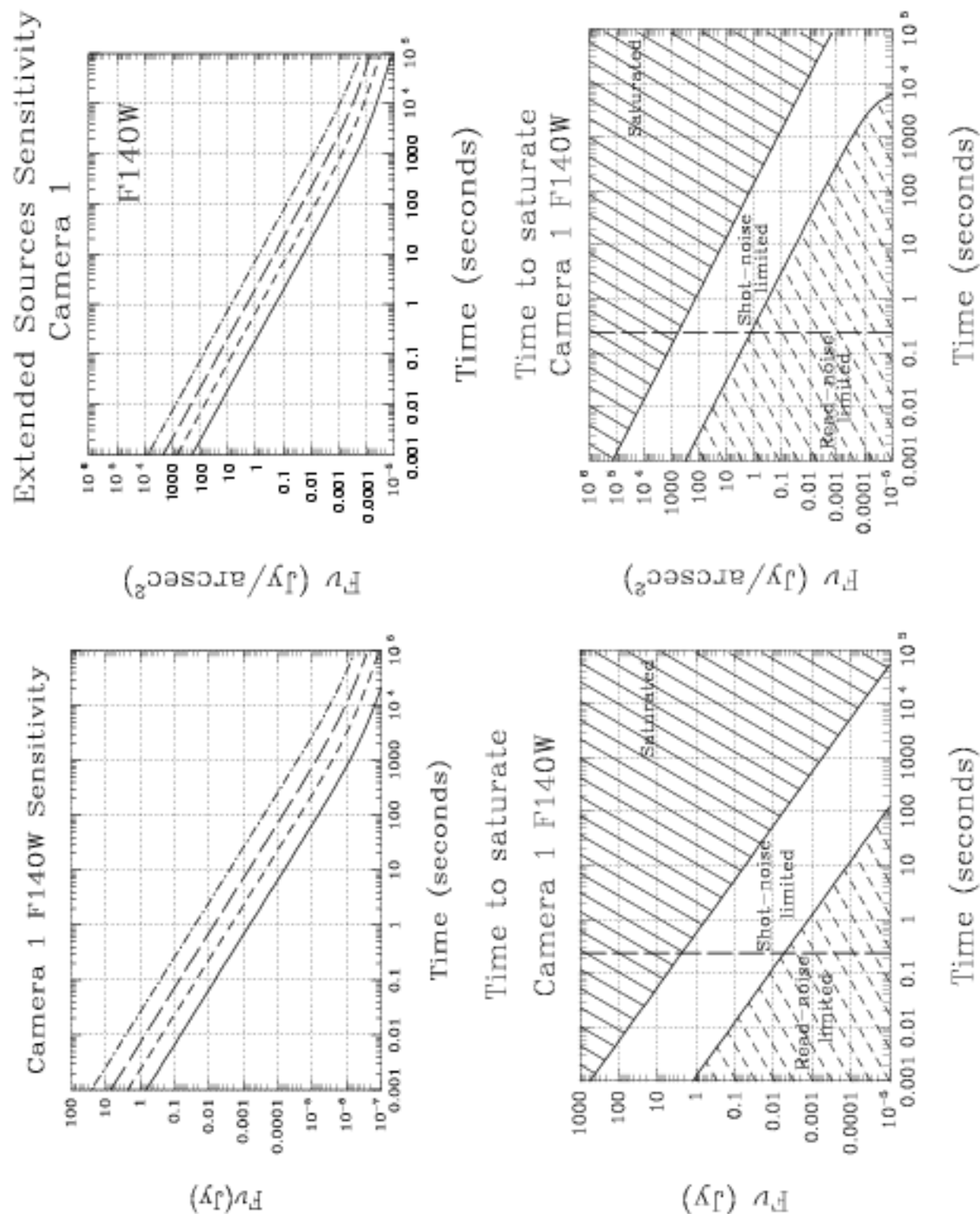


Figure 11.16: Sensitivity and Exclusion Curves for Camera 1, Filter F140W



# Camera 1, Filter F145M

## H<sub>2</sub>O Band

Central wavelength (μm)	Mean wavelength (μm)	Peak wavelength (μm)	FWHM (μm)	Range (μm)	MaxTr %	Pixel Fraction
1.4513	1.4524	1.5100	0.1965	1.35-1.55	94.03	0.07

Figure 11.17: Camera 1, Filter F145M

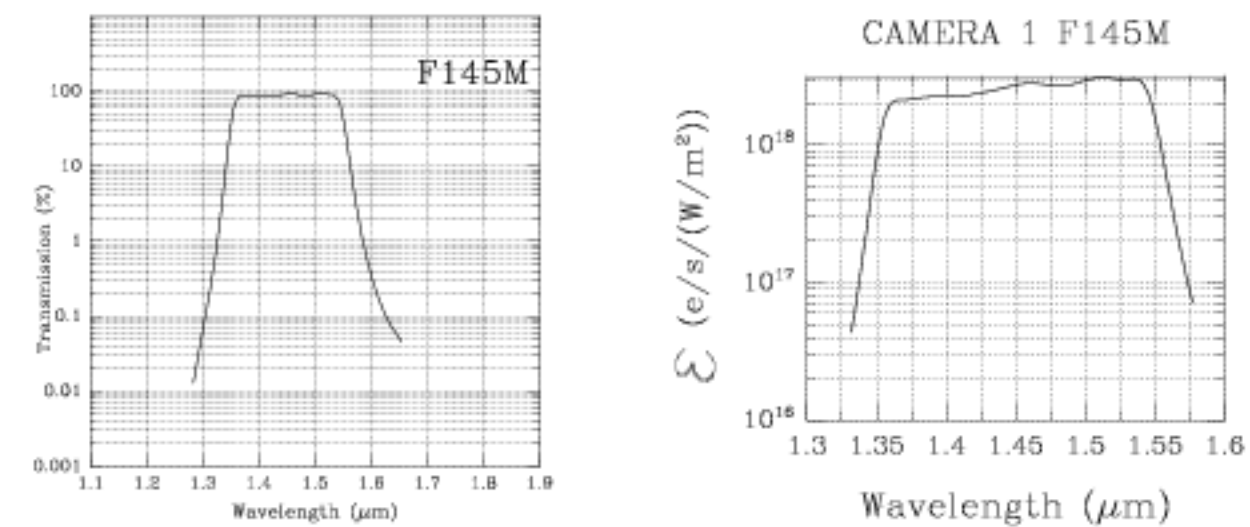
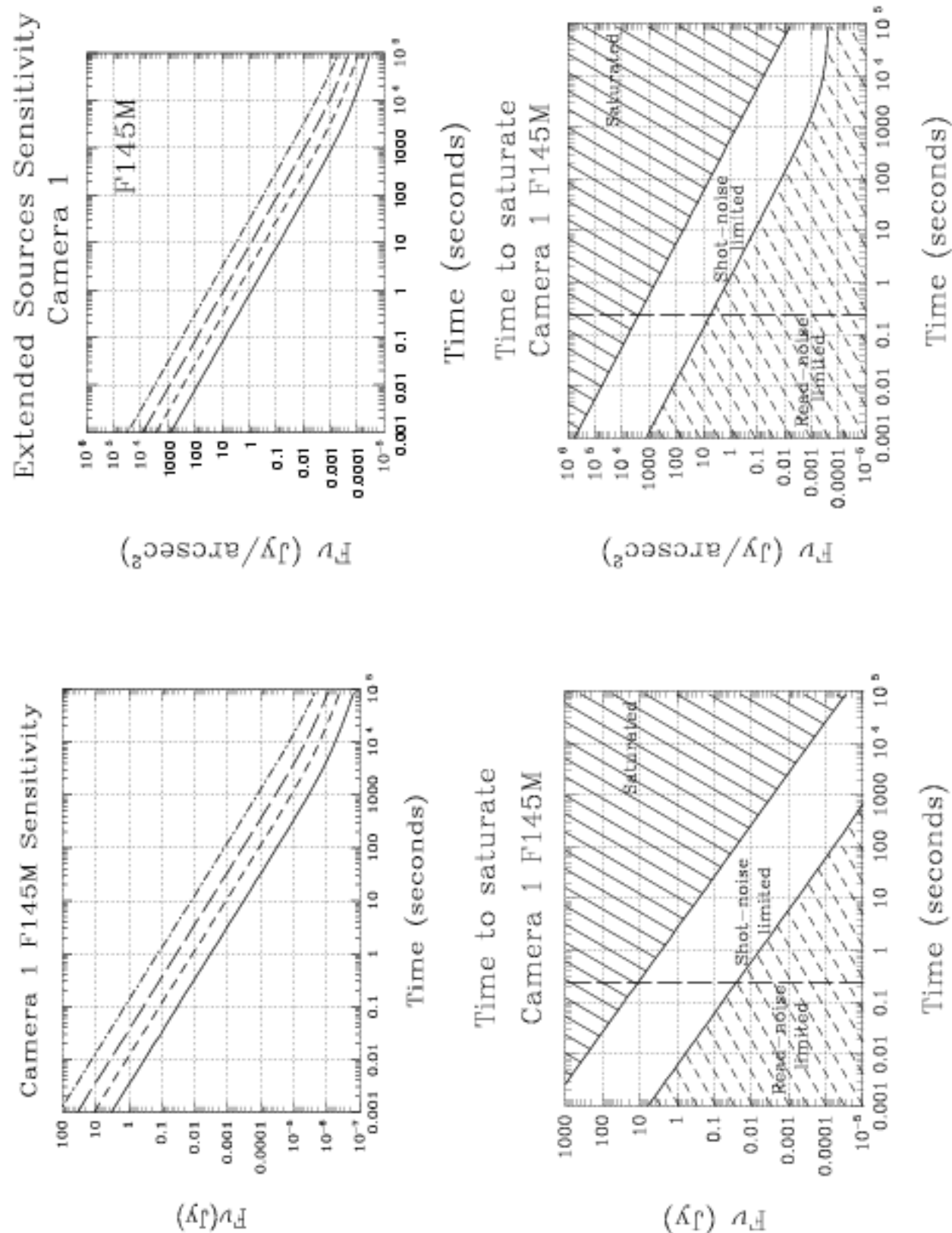


Figure 11.18: Sensitivity and Exclusion Curves, Camera 1, Filter F145M



# Camera 1, Filter F160W

Minimum background.  
This filter is also available on Cameras 2 and 3.

Central wavelength (μm)	Mean wavelength (μm)	Peak wavelength (μm)	FWHM (μm)	Range (μm)	MaxTr %	Pixel Fraction
1.5960	1.5947	1.5830	0.4000	1.35-1.75	96.37	0.070

Figure 11.19: Camera 1, Filter F160W

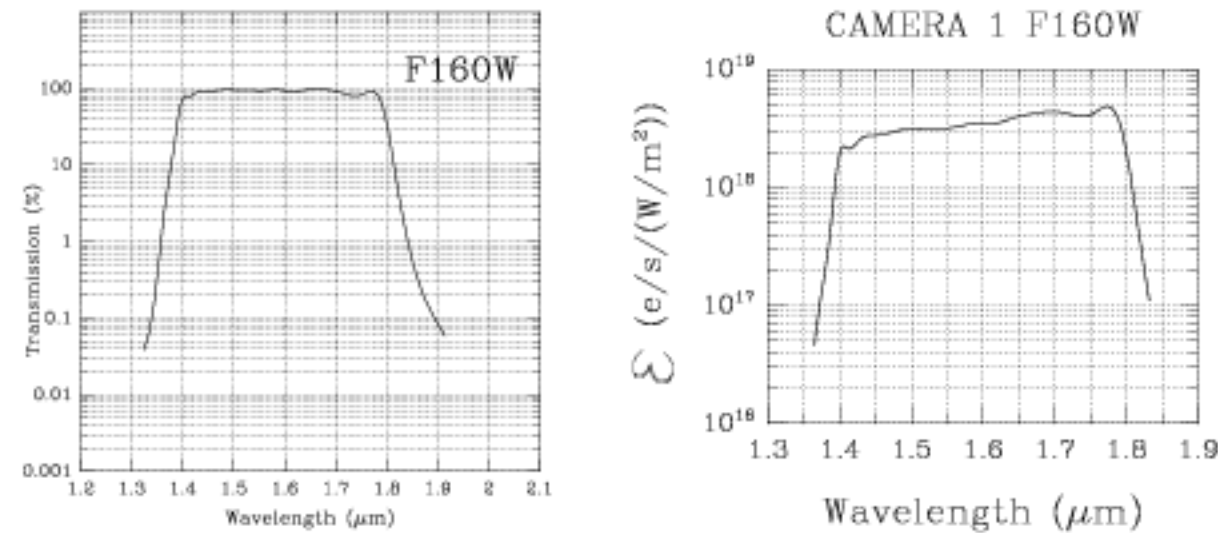
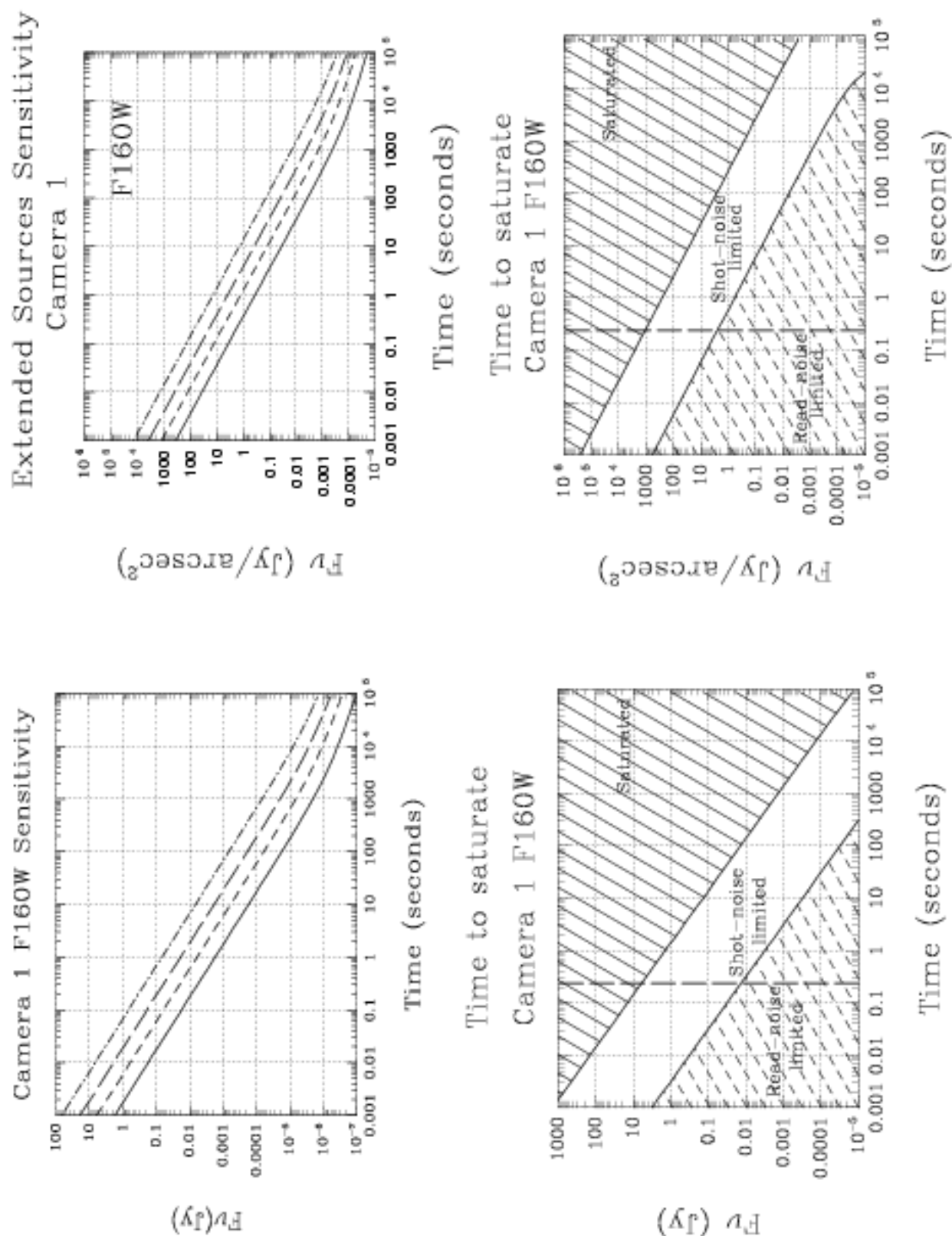




Figure 11.20: Sensitivity and Exclusion Curves for Camera 1, Filter F160W



# Camera 1, Filter F164N

## [FeII] Line

This filter is also available on Camera 3.

Central wavelength (μm)	Mean wavelength (μm)	Peak wavelength (μm)	FWHM (μm)	Range (μm)	MaxTr %	Pixel Fraction
1.6353	1.6354	1.6378	0.0166	1%	93.41	0.067

Figure 11.21: Camera 1, Filter F164N

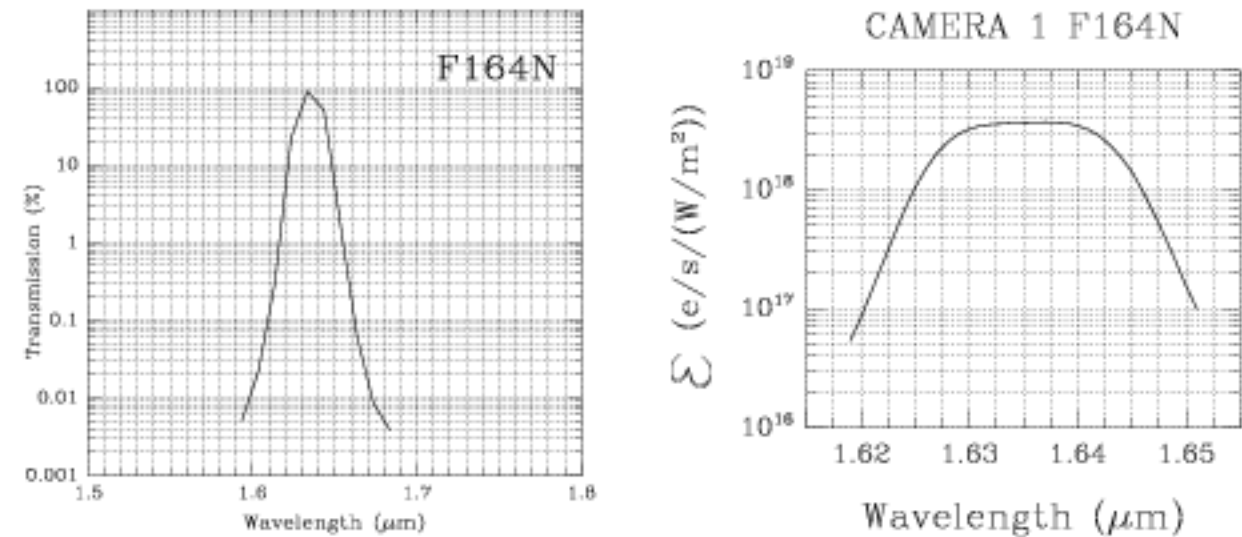
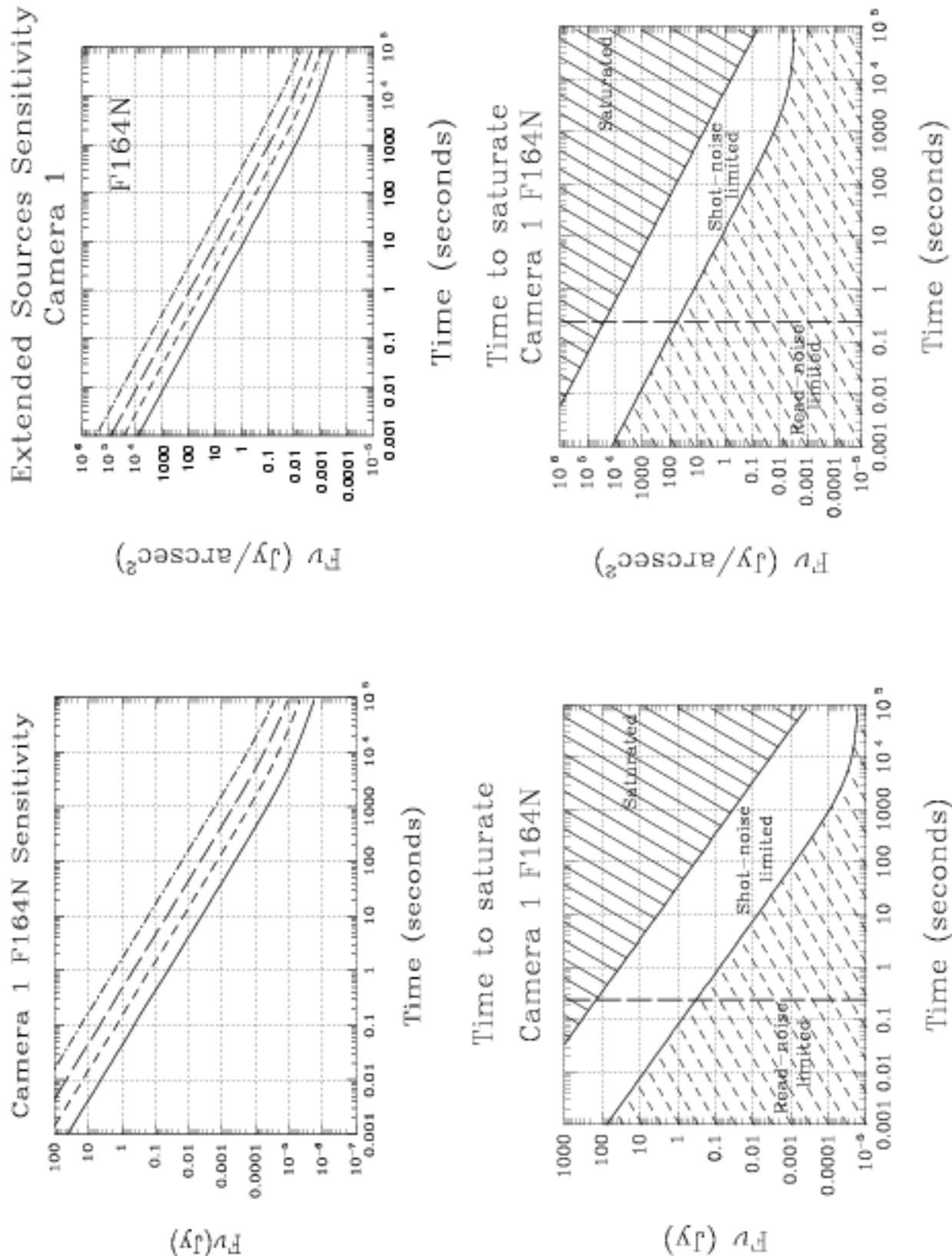


Figure 11.22: Sensitivity and Exclusion Curves for Camera 1, Filter F164N



# Camera 1, Filter F165M

## H<sub>2</sub>O Continuum

This filter is also available on Camera 2.

Central wavelength (μm)	Mean wavelength (μm)	Peak wavelength (μm)	FWHM (μm)	Range (μm)	MaxTr %	Pixel Fraction
1.6438	1.6446	1.5735	0.1985	1.55-1.75	94.78	0.081

Figure 11.23: Camera 1, F165M

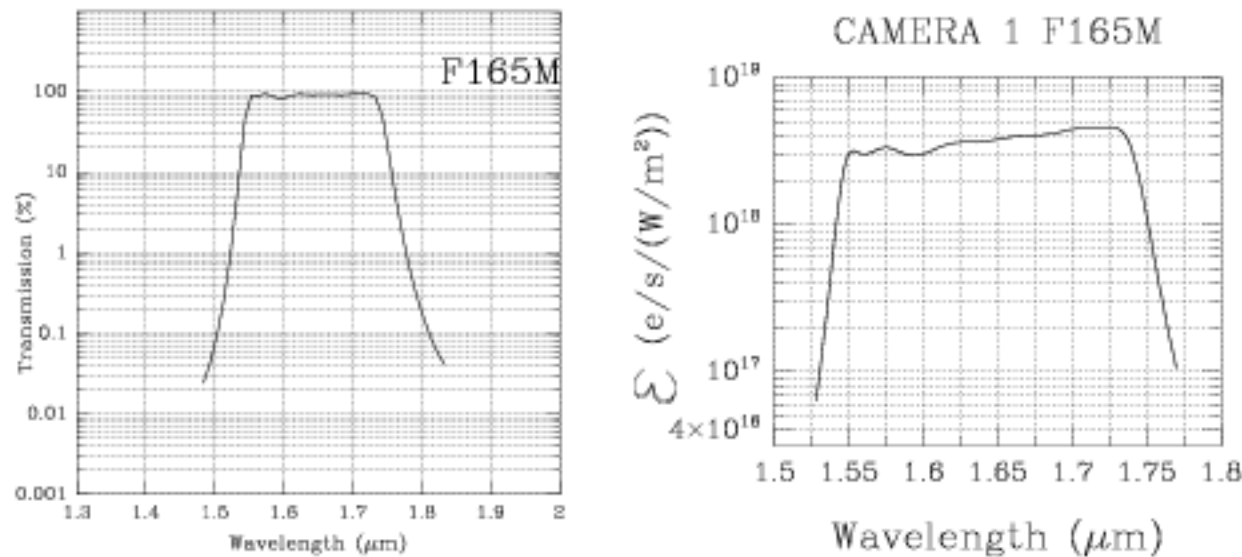
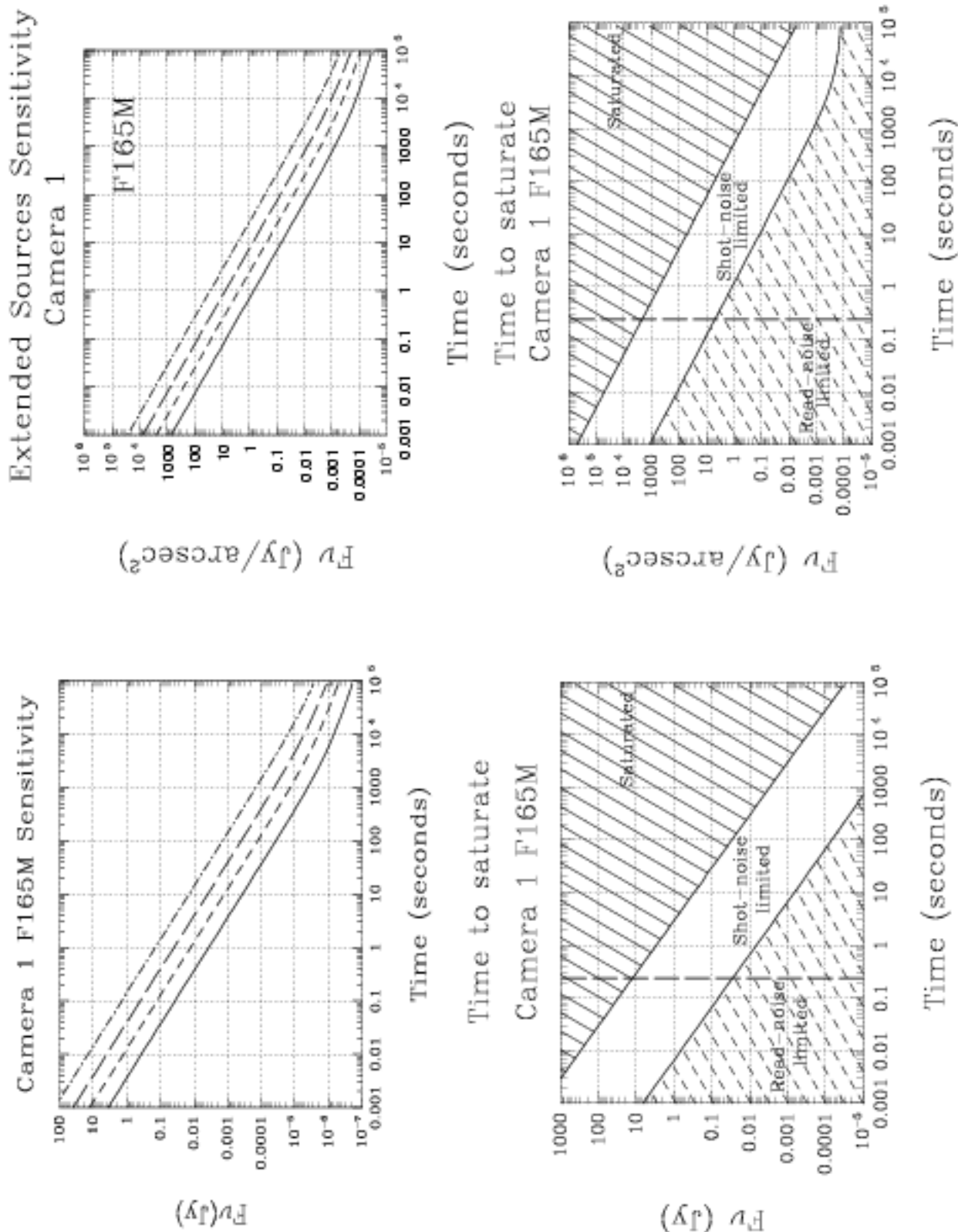


Figure 11.24: Sensitivity and Exclusion Curves for Camera 1, Filter F165M



# Camera 1, Filter F166N

## [FeII] Continuum

This filter is also available on Camera 3.

Central wavelength (μm)	Mean wavelength (μm)	Peak wavelength (μm)	FWHM (μm)	Range (μm)	MaxTr %	Pixel Fraction
1.6606	1.6606	1.6622	0.0168	1%	90.12	0.069

Figure 11.25: Camera 1, Filter F166N

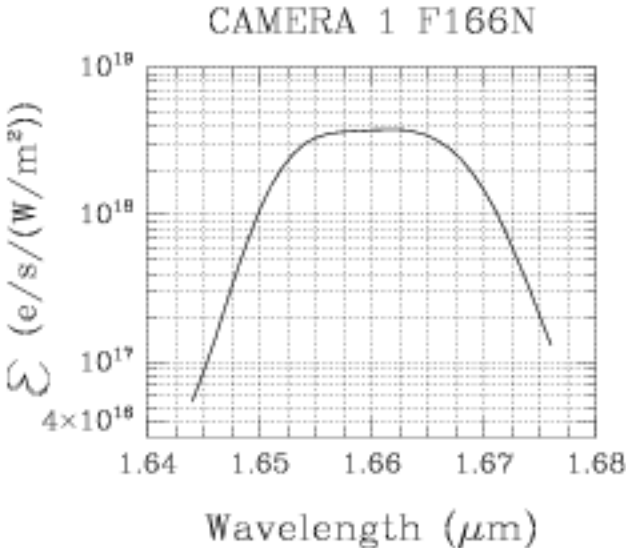
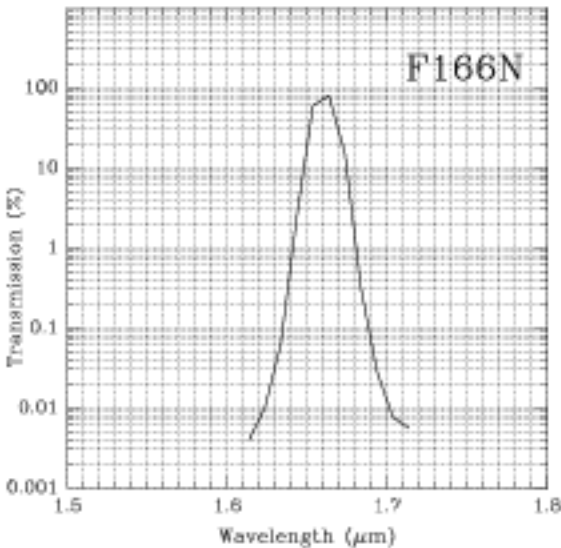
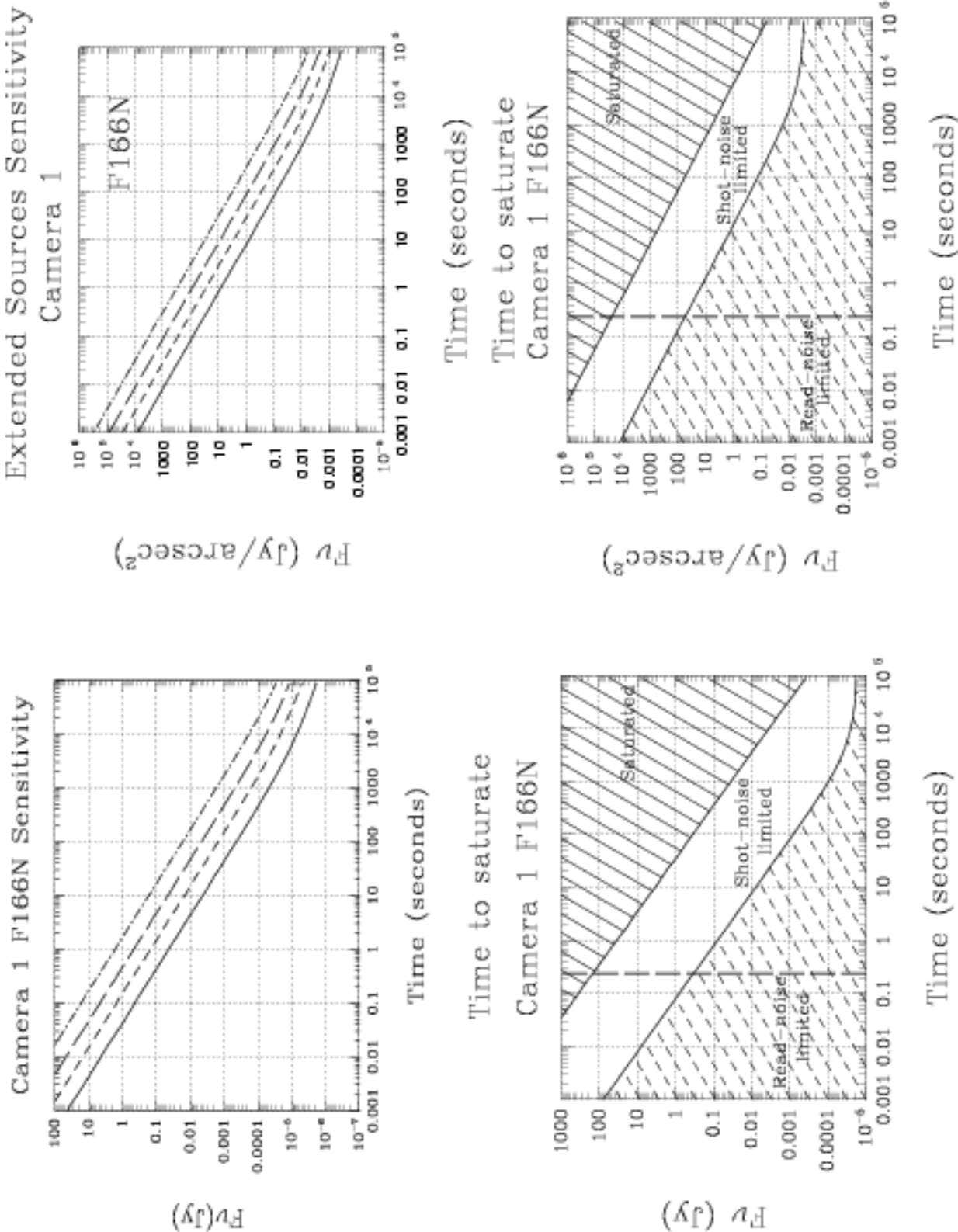


Figure 11.26: Sensitivity and Exclusion Curves for Camera 1, Filter F166N



# Camera 1, Filter F170M

This filter is also available on Camera 2.

Central wavelength (μm)	Mean wavelength (μm)	Peak wavelength (μm)	FWHM (μm)	Range (μm)	MaxTr %	Pixel Fraction
1.7025	1.7032	1.6330	0.2030	1.6-1.8	95.55	0.077

Figure 11.27: Camera 1, Filter F170M

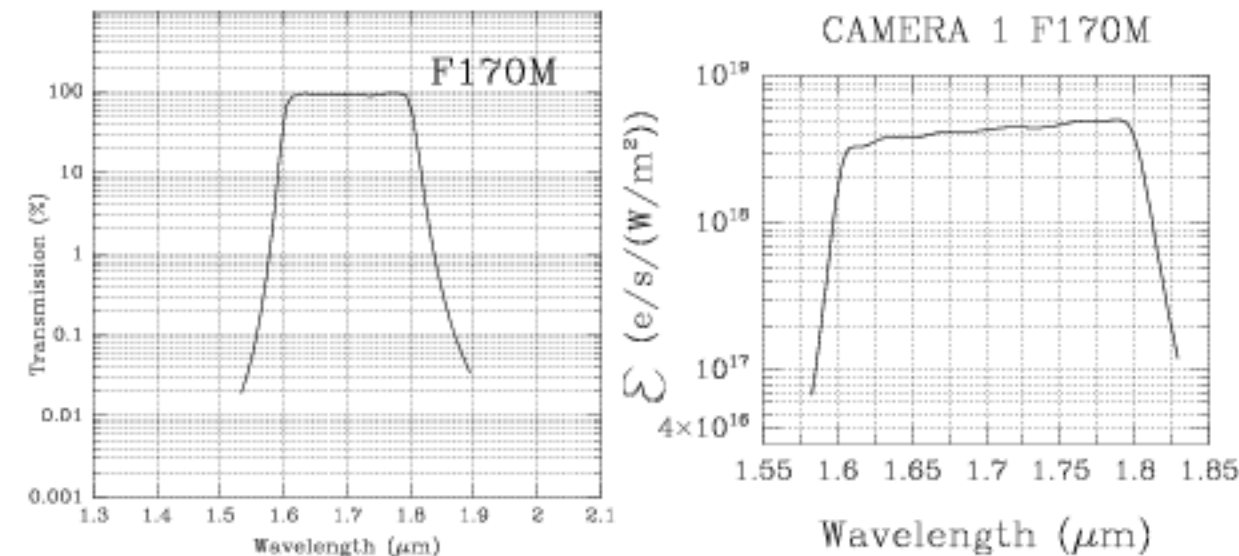
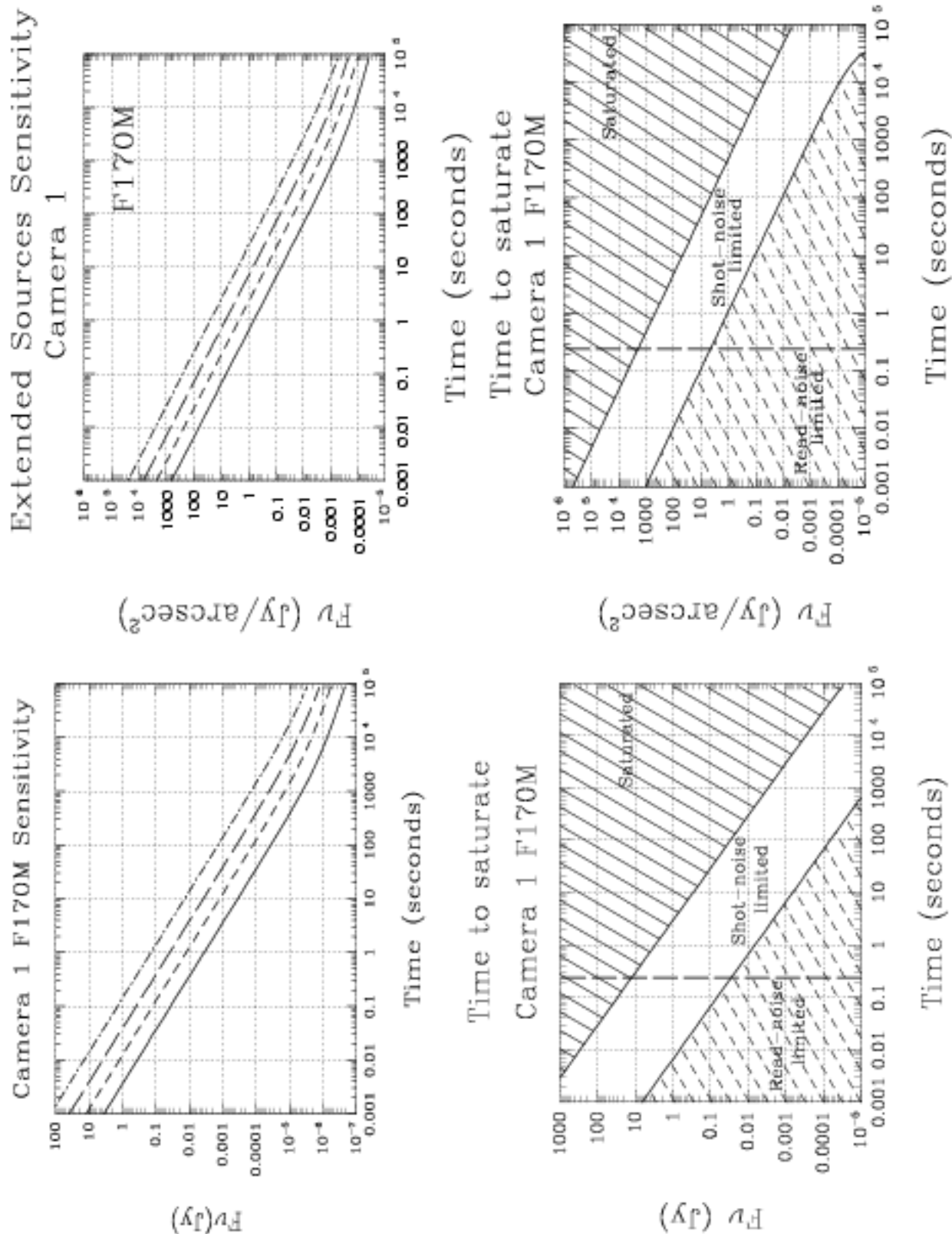




Figure 11.28: Sensitivity and Exclusion Curves for Camera 1, Filter F170M



# Camera 1, Filter F187N

## Paschen $\alpha$

This filter is also available on Camera 2 and 3.

Central wavelength ( $\mu\text{m}$ )	Mean wavelength ( $\mu\text{m}$ )	Peak wavelength ( $\mu\text{m}$ )	FWHM ( $\mu\text{m}$ )	Range ( $\mu\text{m}$ )	MaxTr %	Pixel Fraction
1.875	1.8748	1.8756	0.0188	1%	88.93	0.062

Figure 11.29: Camera 1, Filter F187N

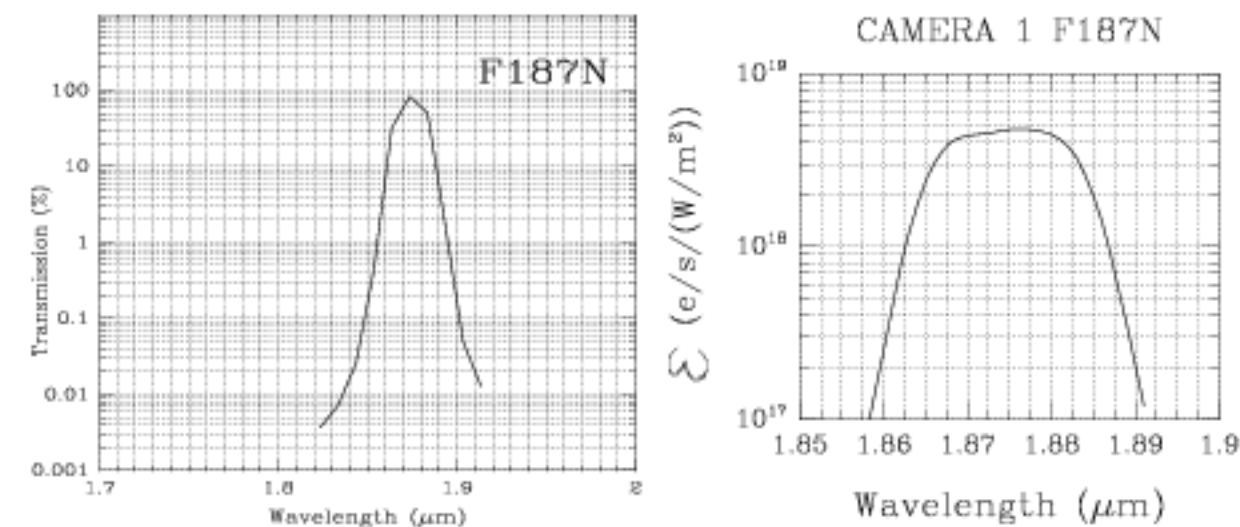
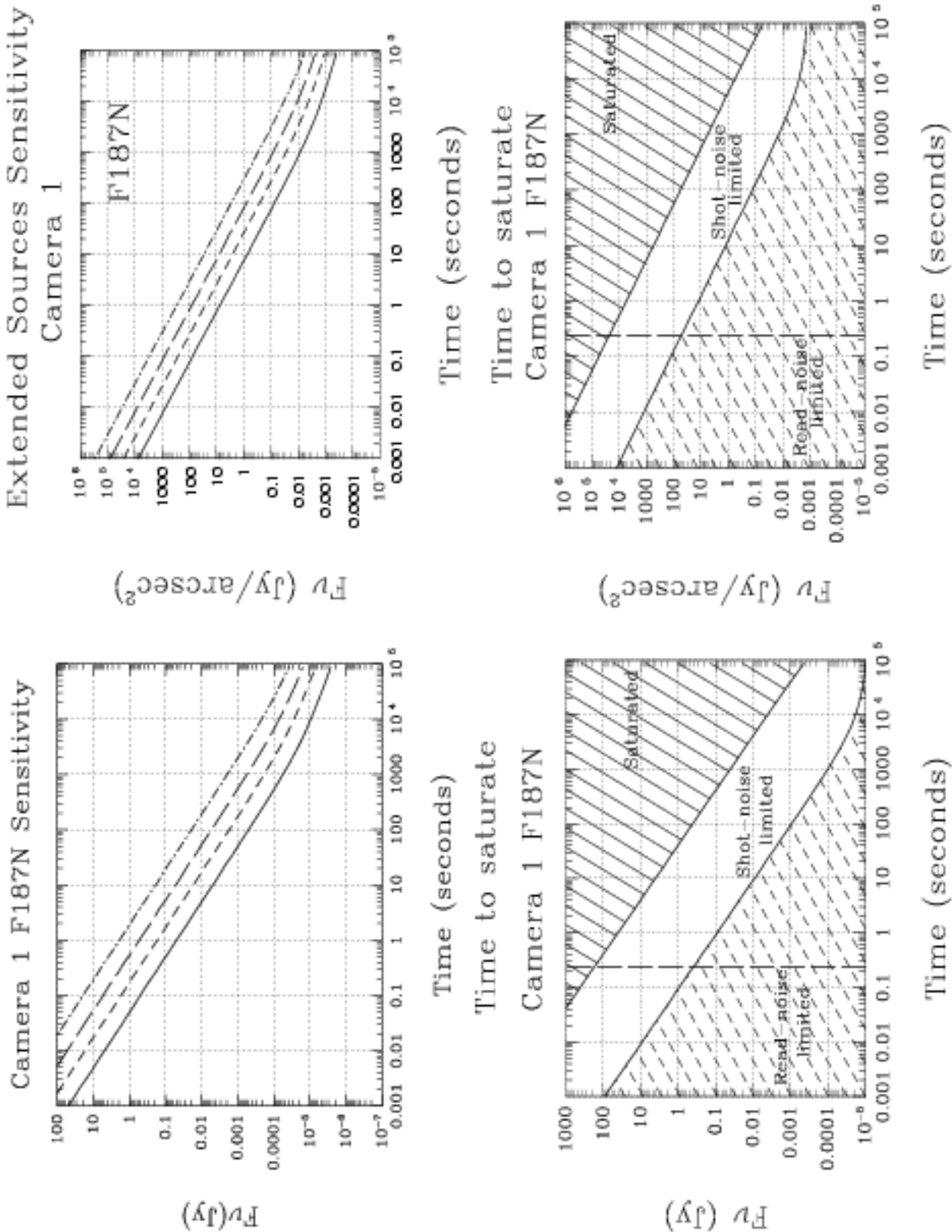


Figure 11.30: Sensitivity and Exclusion Curves for Camera 1, Filter F187N



# Camera 1, Filter F190N

## Paschen $\alpha$ continuum

This filter is also available on Cameras 2 and 3.

Central wavelength ( $\mu\text{m}$ )	Mean wavelength ( $\mu\text{m}$ )	Peak wavelength ( $\mu\text{m}$ )	FWHM ( $\mu\text{m}$ )	Range ( $\mu\text{m}$ )	MaxTr %	Pixel Fraction
1.8987	1.8986	1.8942	0.0174	1%	93.05	0.055

Figure 11.31: Camera 1, Filter F190N

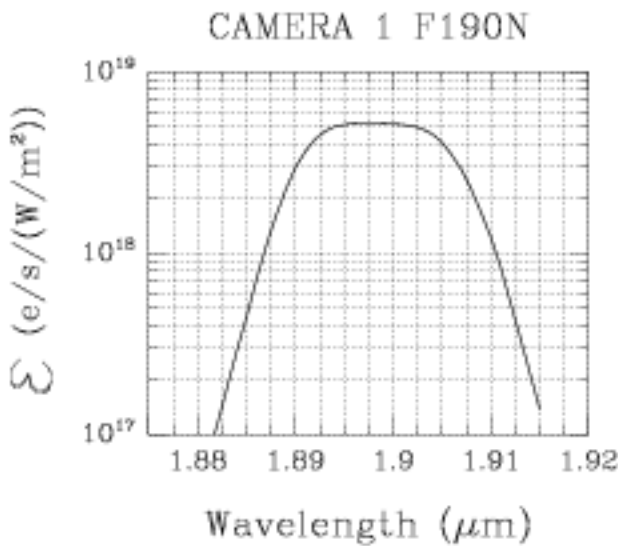
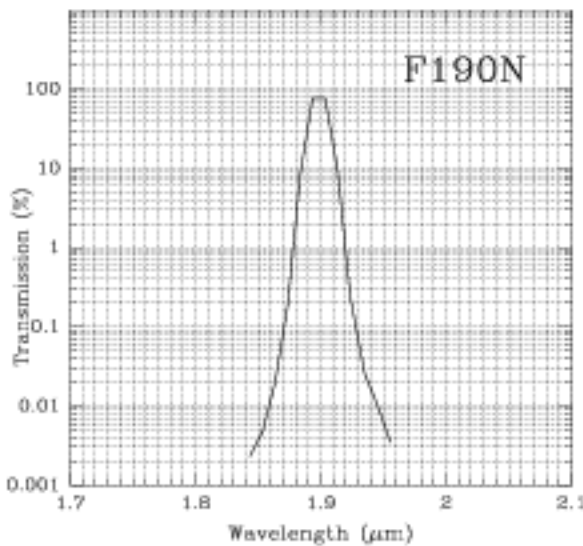
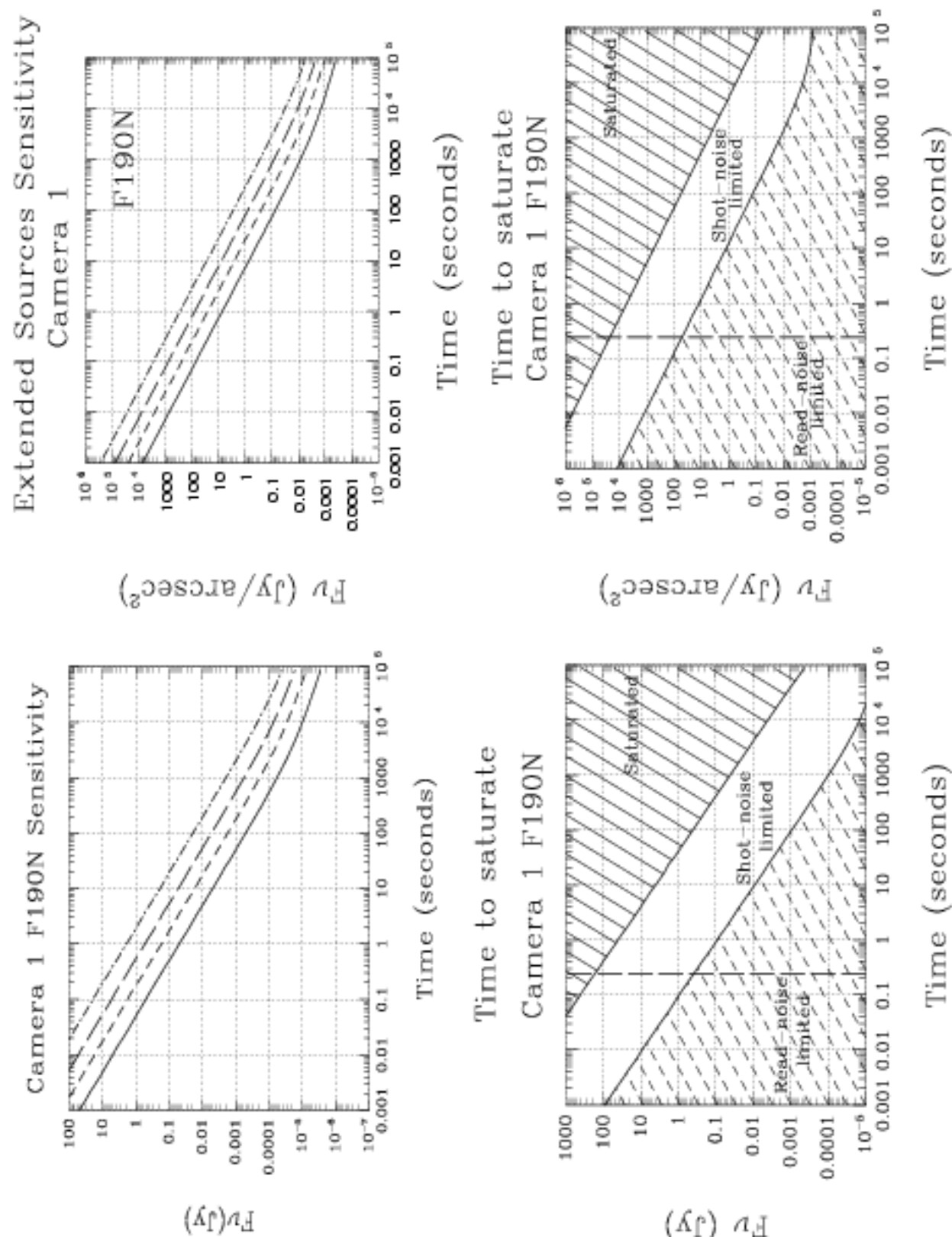


Figure 11.32: Sensitivity and Exclusion Curves for Camera 1, Filter F190N



# Camera 2, Filter F110W

This filter is also available on Cameras 1 and 3.

Central wavelength (μm)	Mean wavelength (μm)	Peak wavelength (μm)	FWHM (μm)	Range (μm)	MaxTr %	Pixel Fraction
1.0998	1.1035	1.2035	0.5915	0.8-1.4	94.90	0.34

Figure 11.33: Camera 2, Filter F110W

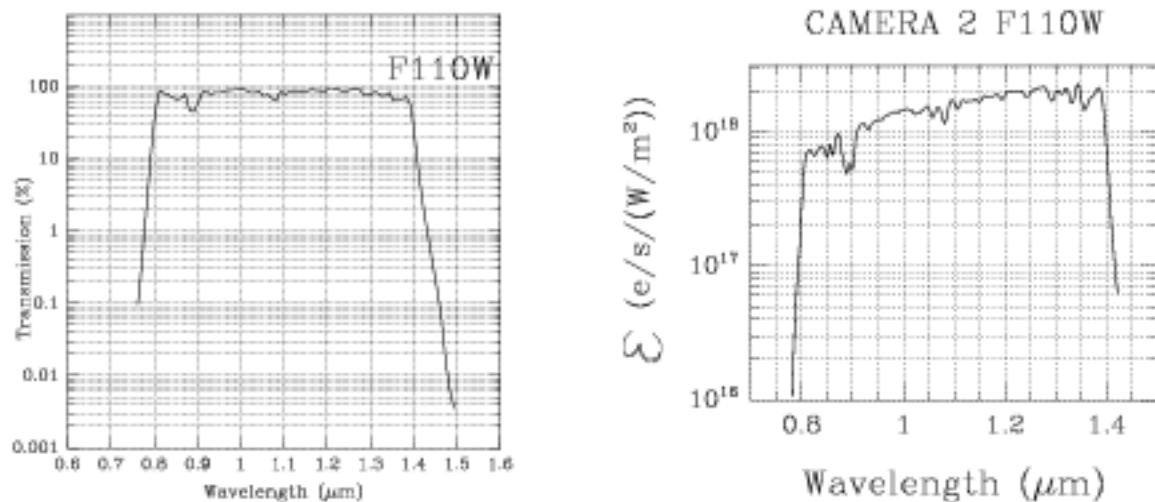
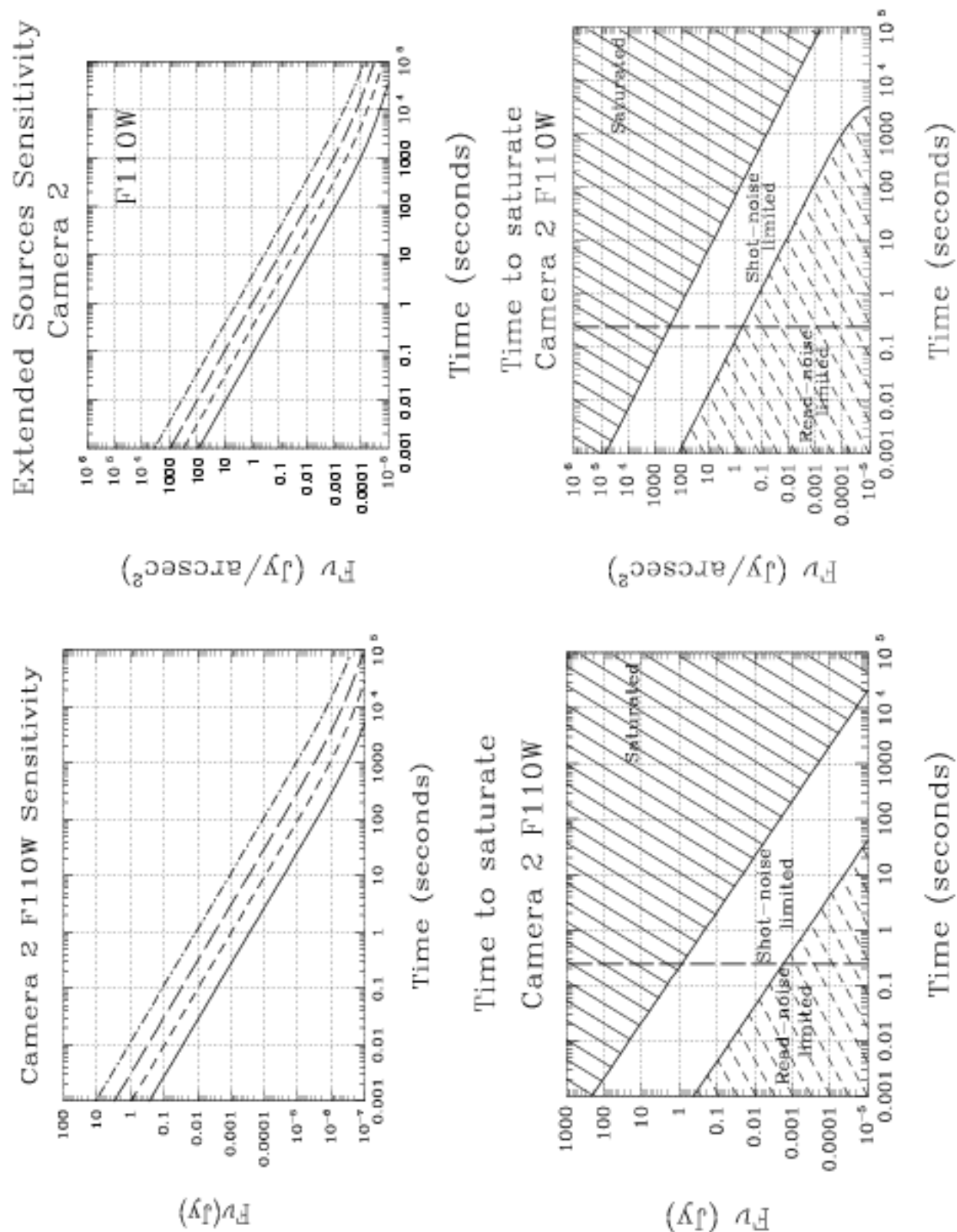


Figure 11.34: Sensitivity and Exclusion Curves for Camera 2, Filter F110W



# Camera 2, Filter F160W

## Minimum background

This filter is also available on Cameras 1 and 3.

Central wavelength (μm)	Mean wavelength (μm)	Peak wavelength (μm)	FWHM (μm)	Range (μm)	MaxTr %	Pixel Fraction
1.5940	1.5931	1.5820	0.4030	1.4-1.8	96.59	0.19

Figure 11.35: Camera 2, Filter F160W

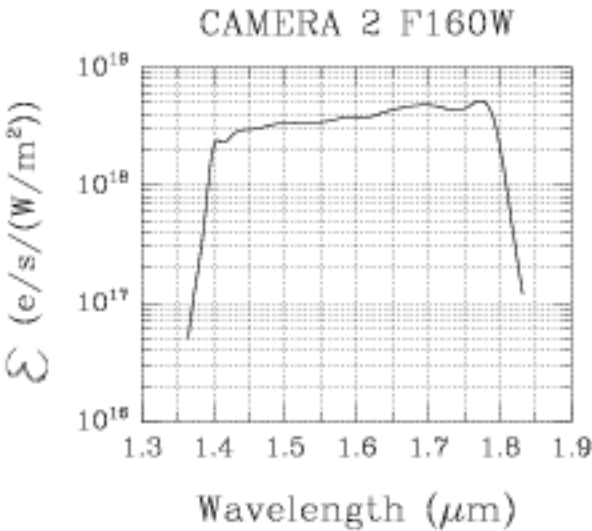
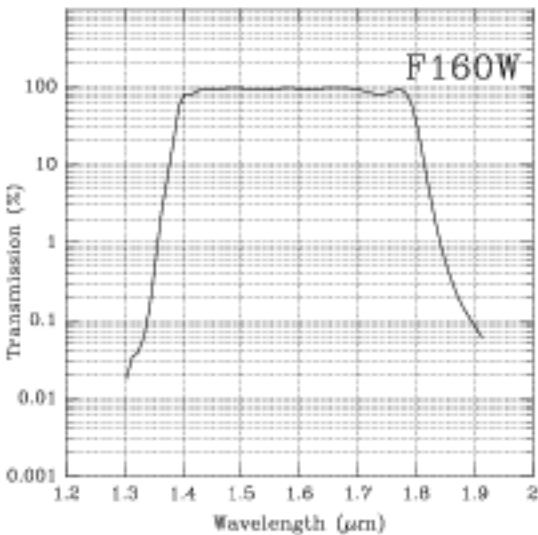
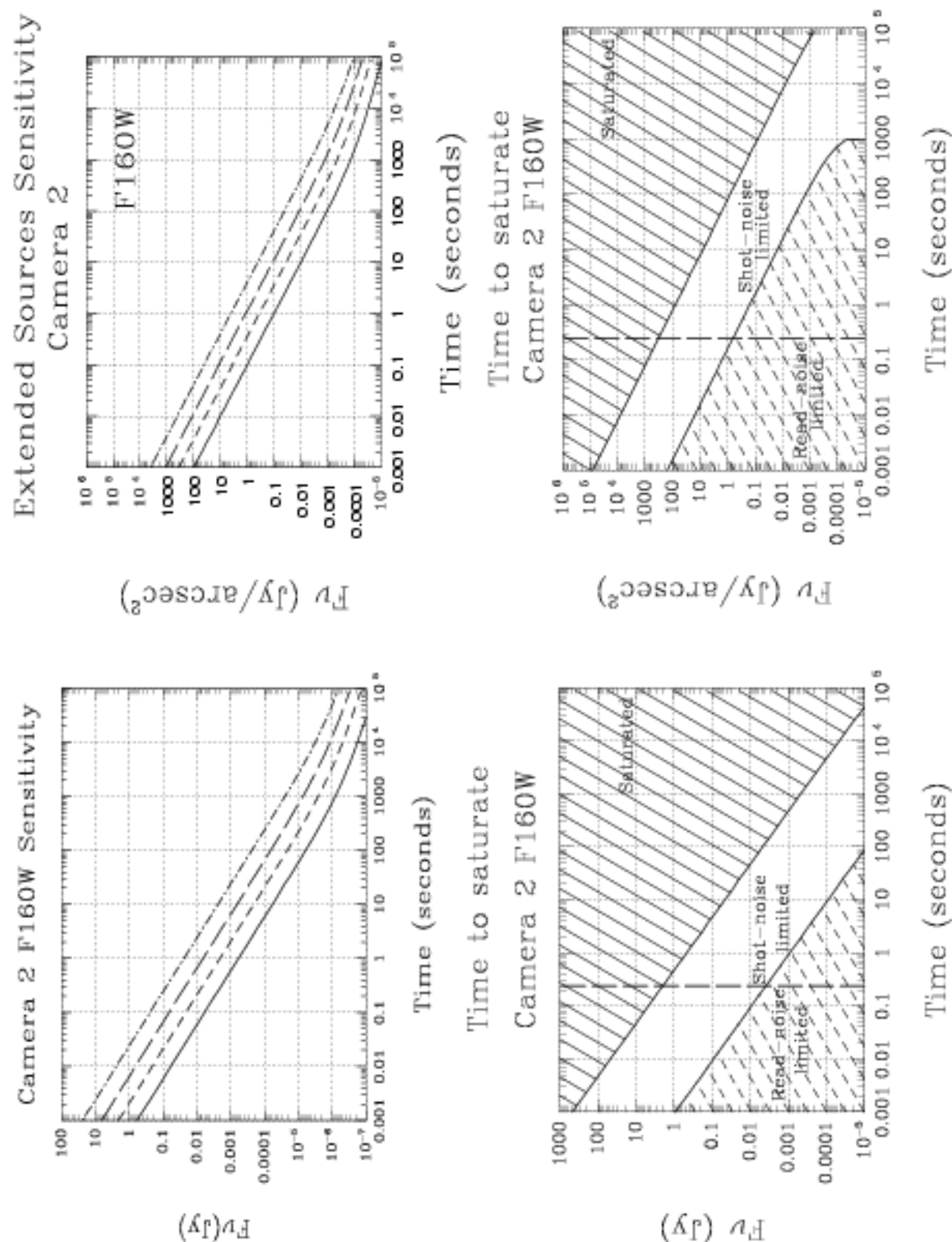




Figure 11.36: Sensitivity and Exclusion Curves for Camera 2, Filter F160W



# Camera 2, Filter F165M

## Planetary continuum

This filter is also available on Camera 1.

Central wavelength (μm)	Mean wavelength (μm)	Peak wavelength (μm)	FWHM (μm)	Range (μm)	MaxTr %	Pixel Fraction
1.6463	1.6473	1.5540	0.1985	1.55-1.75	95.36	0.19

Figure 11.37: Camera 2, Filter F165M

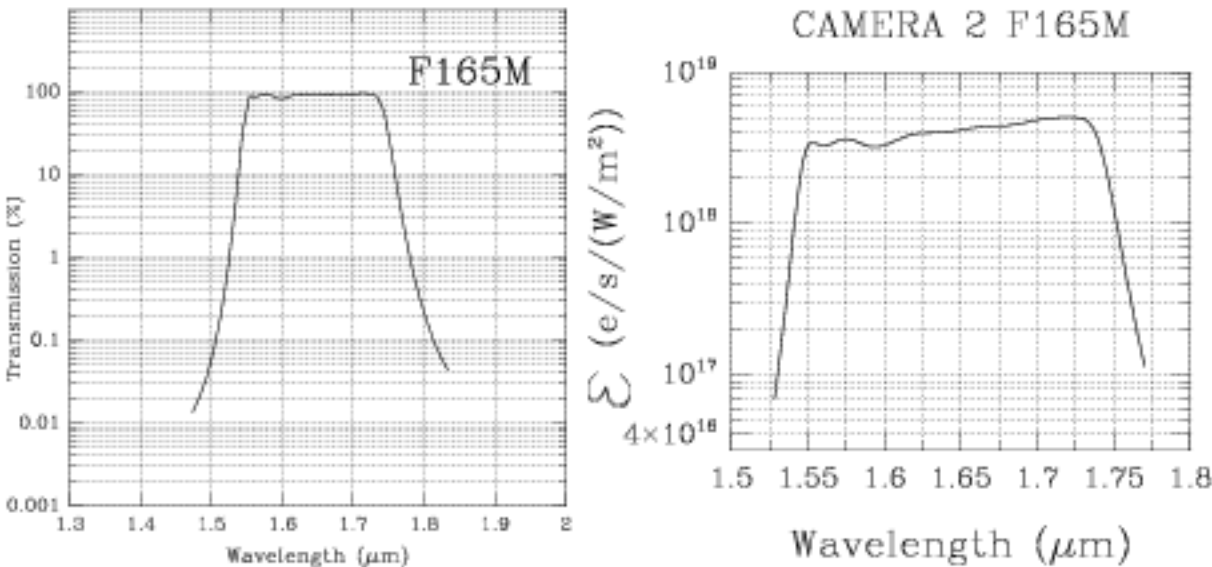
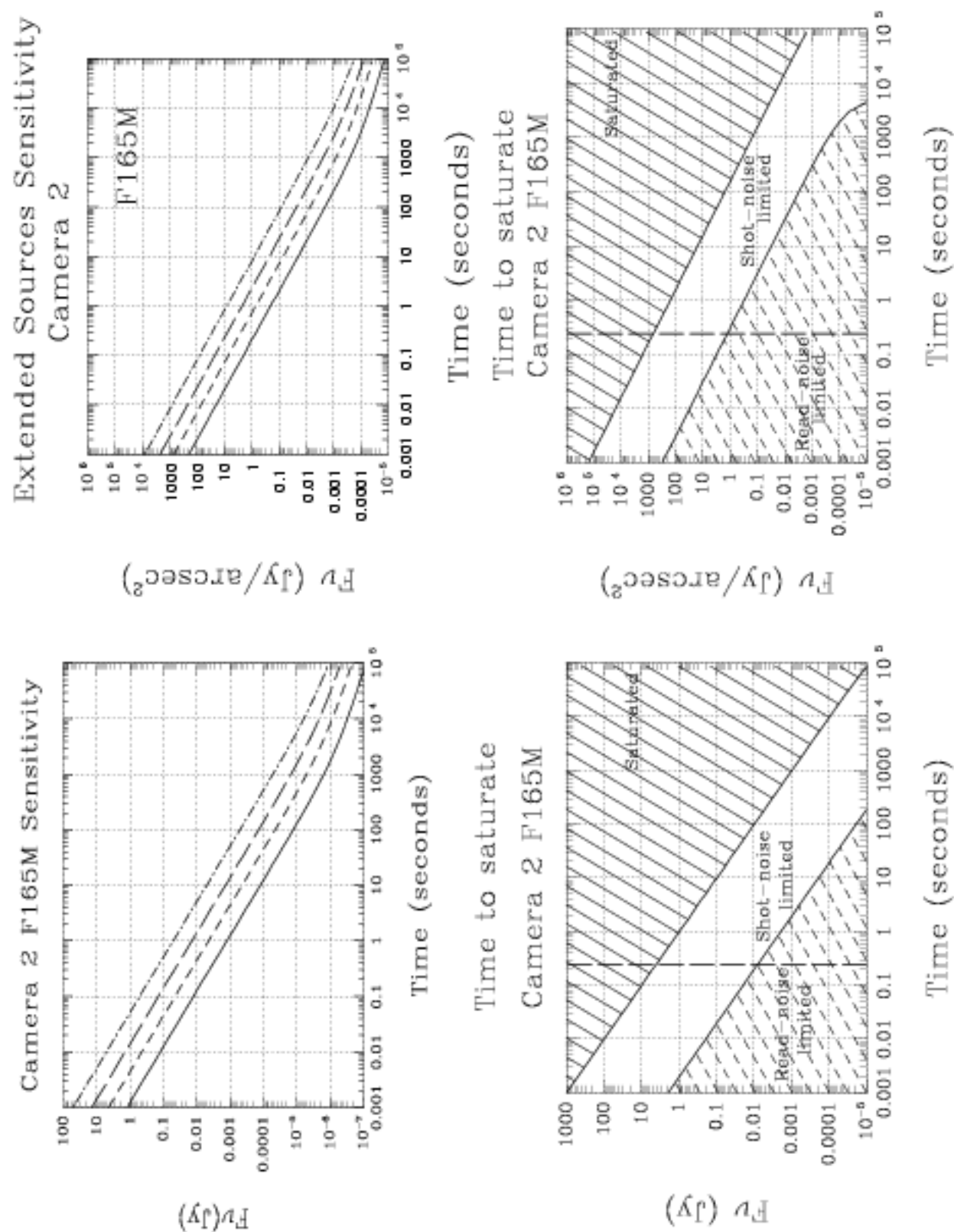


Figure 11.38: Sensitivity and Exclusion Curves for Camera 2, Filter F165M



## Camera 2, Filter F171M

### HCO<sub>2</sub> and C<sub>2</sub> continuum

Central wavelength (μm)	Mean wavelength (μm)	Peak wavelength (μm)	FWHM (μm)	Range (μm)	MaxTr %	Pixel Fraction
1.7206	1.7209	1.7224	0.0712	1.68-1.75	95.15	0.20

Figure 11.39: Camera 2, Filter F171M

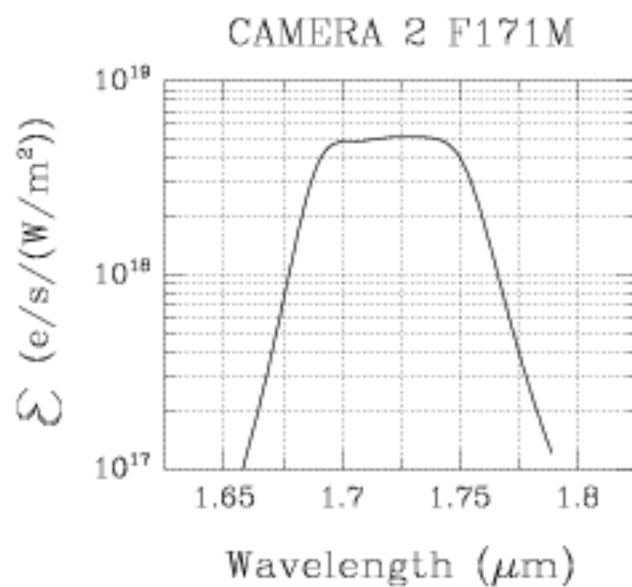
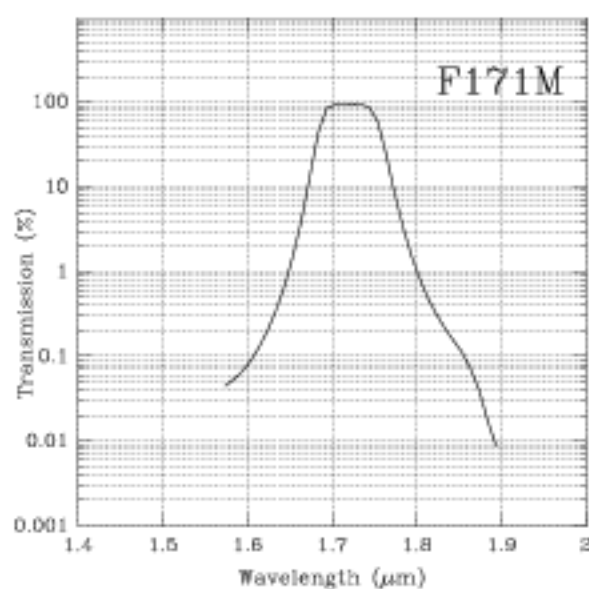
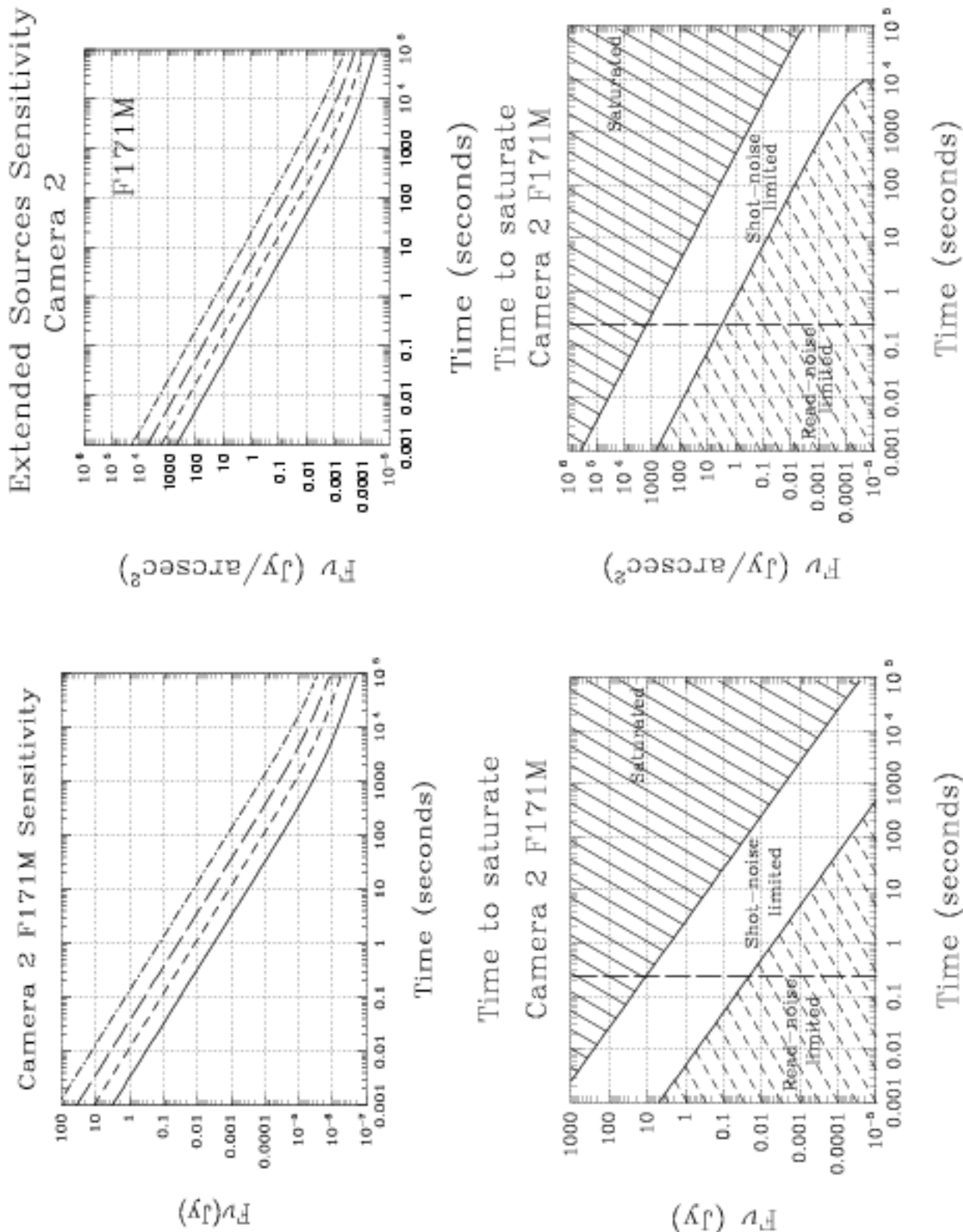


Figure 11.40: Sensitivity and Exclusion Curves for Camera 2, Filter F171M



## Camera 2, Filter F180M

**HCO<sub>2</sub> and C<sub>2</sub>**

*Thermal background important*

Central wavelength (μm)	Mean wavelength (μm)	Peak wavelength (μm)	FWHM (μm)	Range (μm)	MaxTr %	Pixel Fraction
1.7968	1.7971	1.8108	0.0684	1.765-1.835	93.40	0.11

Figure 11.41: Camera 2, Filter F180M

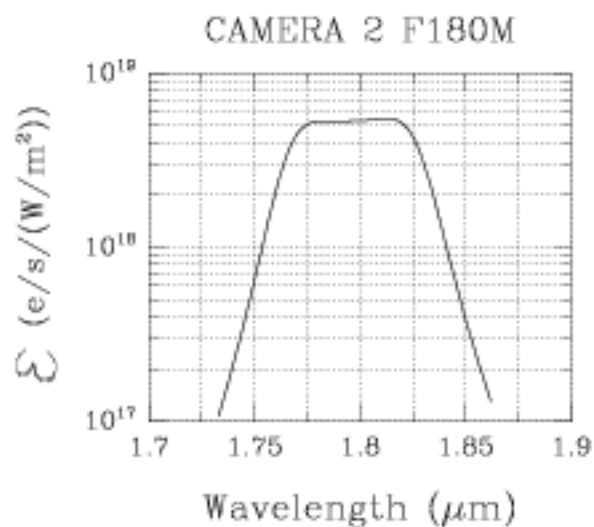
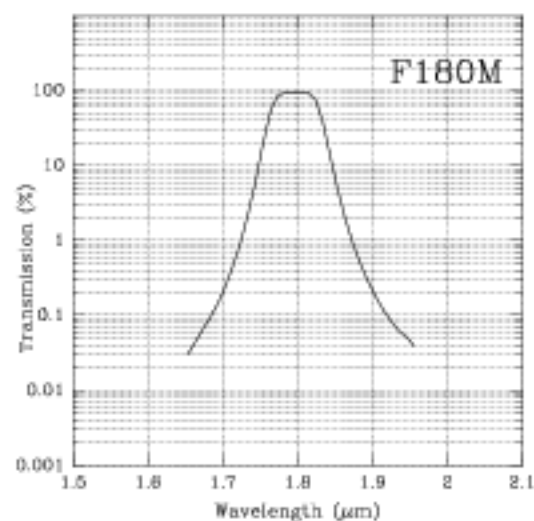
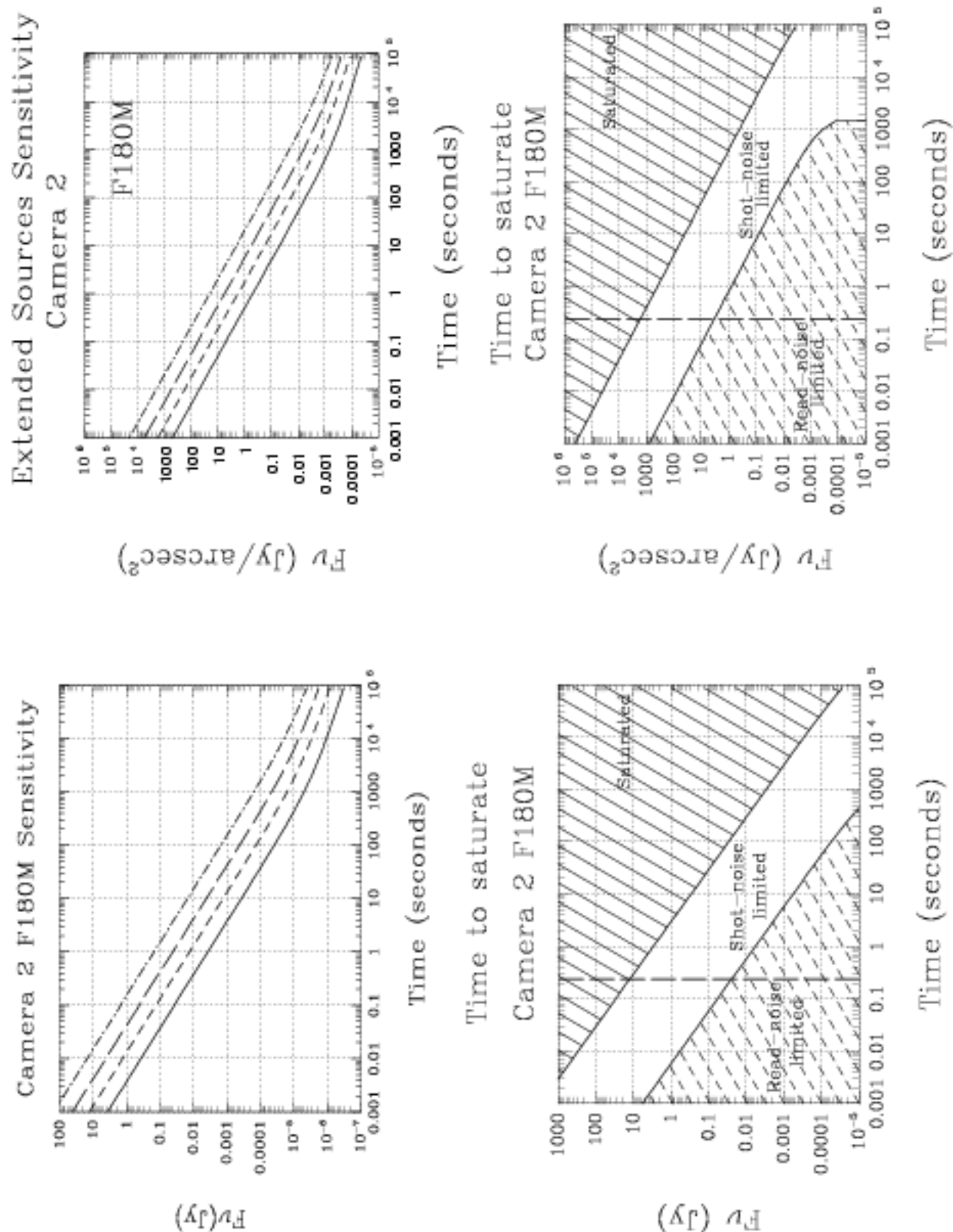


Figure 11.42: Sensitivity and Exclusion Curves for Camera 2, Filter F180M



# Camera 2, Filter F187N

**Paschen  $\alpha$**   
Also available on Cameras 1 and 3.

Central wavelength ( $\mu\text{m}$ )	Mean wavelength ( $\mu\text{m}$ )	Peak wavelength ( $\mu\text{m}$ )	FWHM ( $\mu\text{m}$ )	Range ( $\mu\text{m}$ )	MaxTr %	Pixel Fraction
1.8740	1.8738	1.8746	0.0192	1%	88.91	0.18

Figure 11.43: Camera 2, Filter F187N

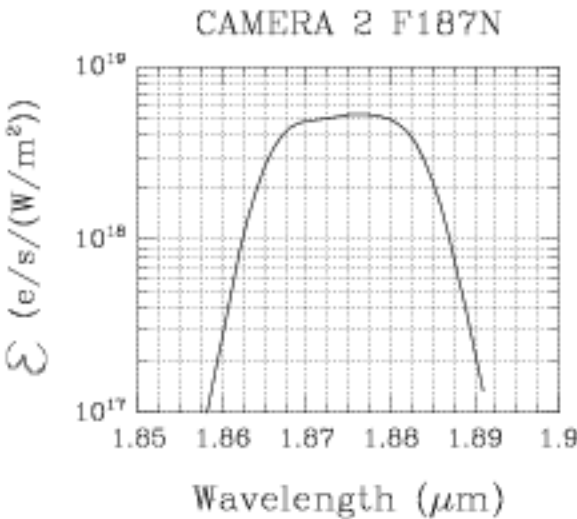
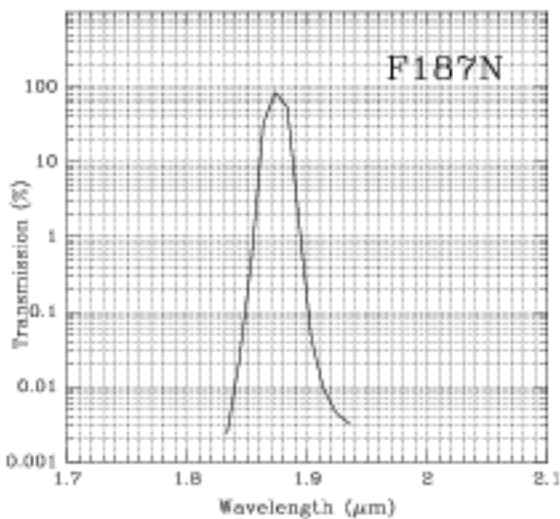
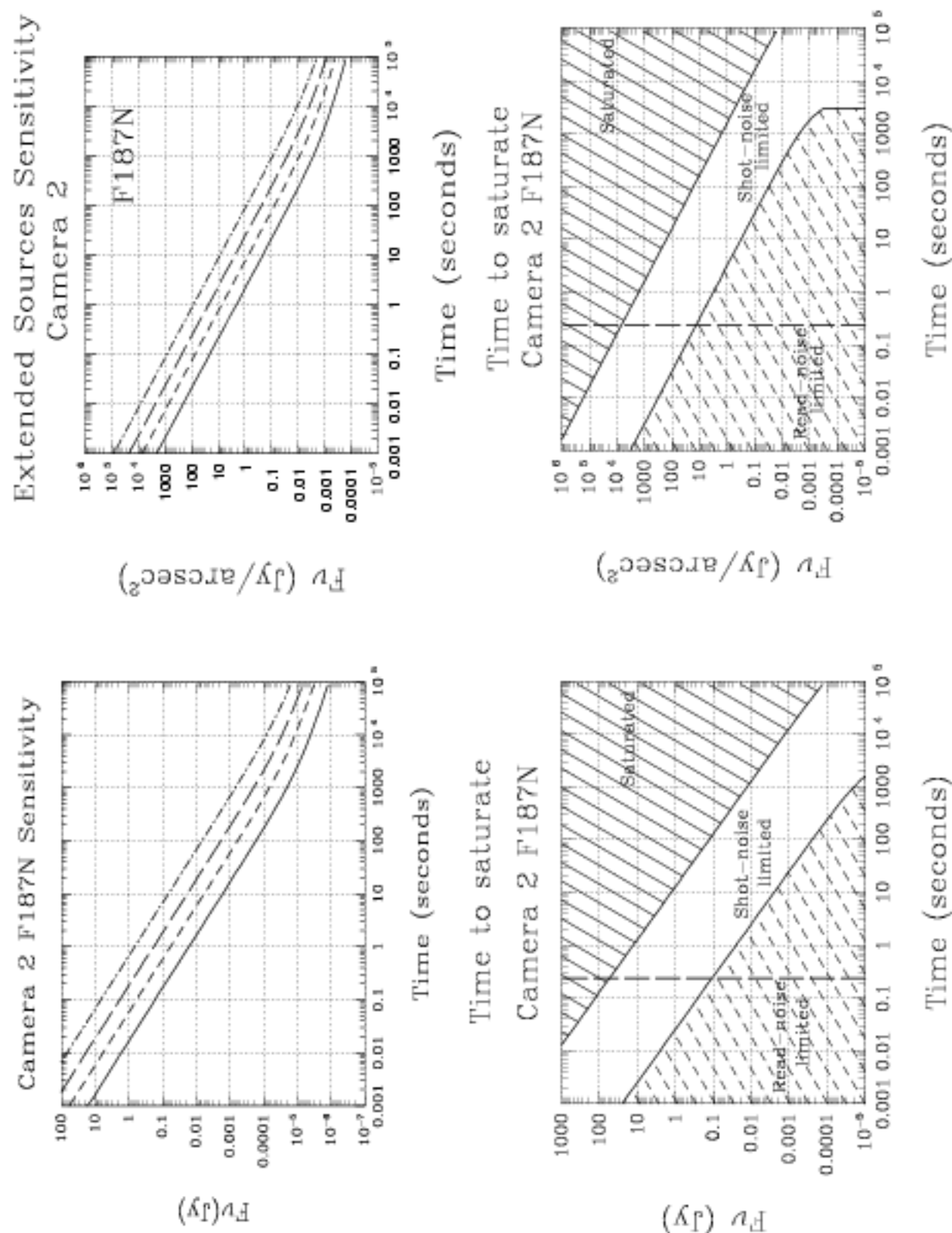




Figure 11.44: Sensitivity and Exclusion Curves for Camera 2, Filter F187N



## Camera 2, Filter F187W

*Thermal background important.*

Central wavelength ( $\mu\text{m}$ )	Mean wavelength ( $\mu\text{m}$ )	Peak wavelength ( $\mu\text{m}$ )	FWHM ( $\mu\text{m}$ )	Range ( $\mu\text{m}$ )	MaxTr %	Pixel Fraction
1.8722	1.8708	1.8930	0.2436	1.75-2.35	87.97	0.18

Figure 11.45: Camera 2, Filter F187W

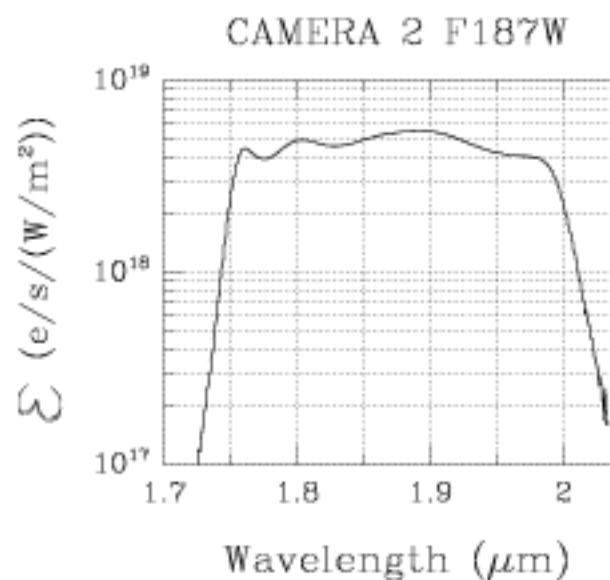
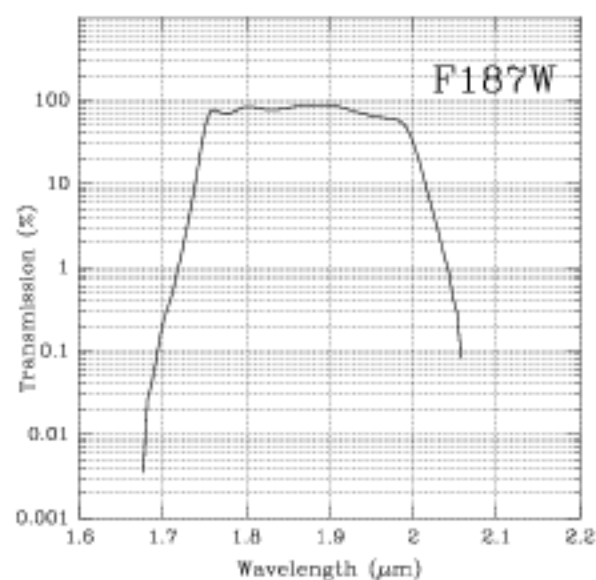
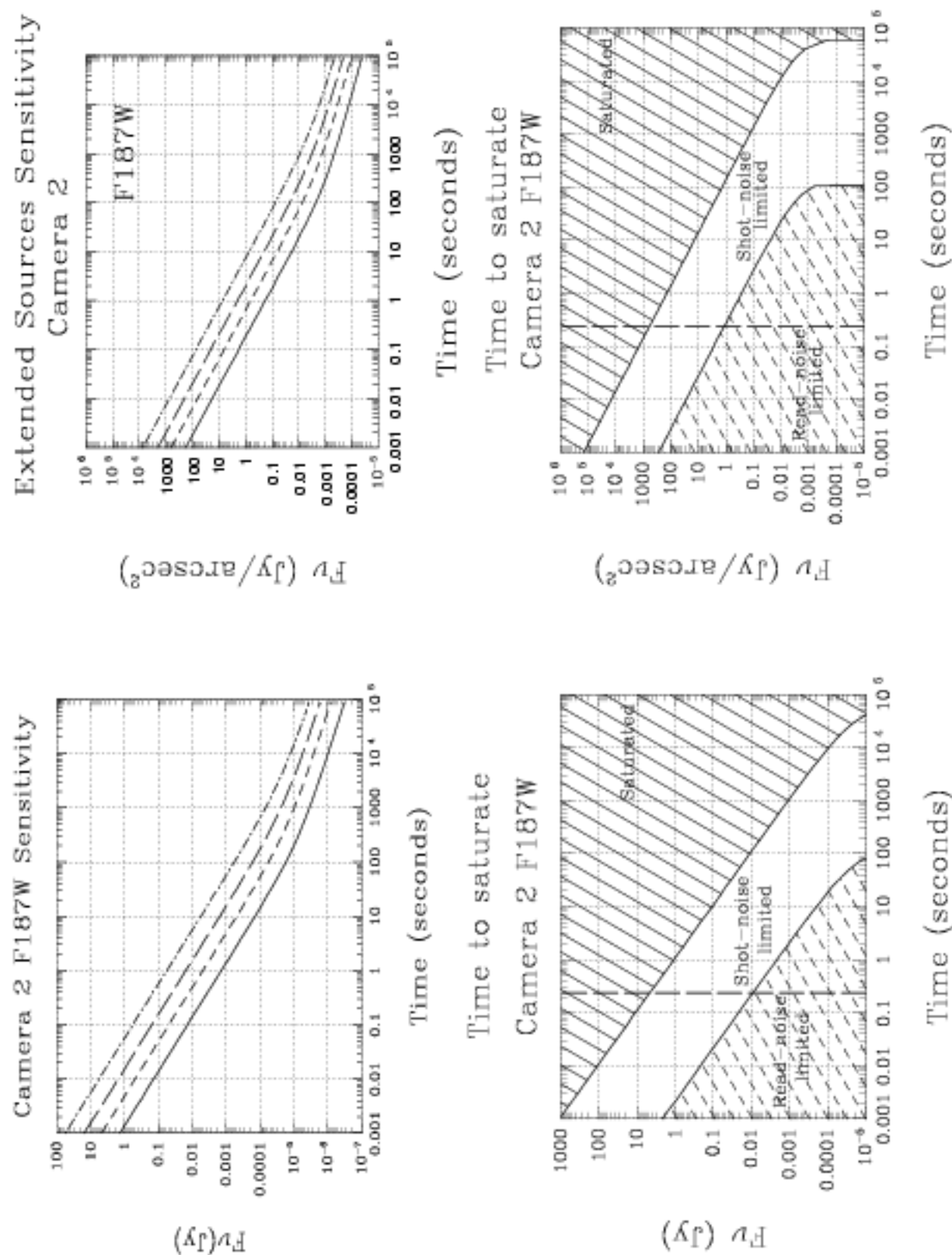


Figure 11.46: Sensitivity and Exclusion Curves for Camera 2, Filter F187W



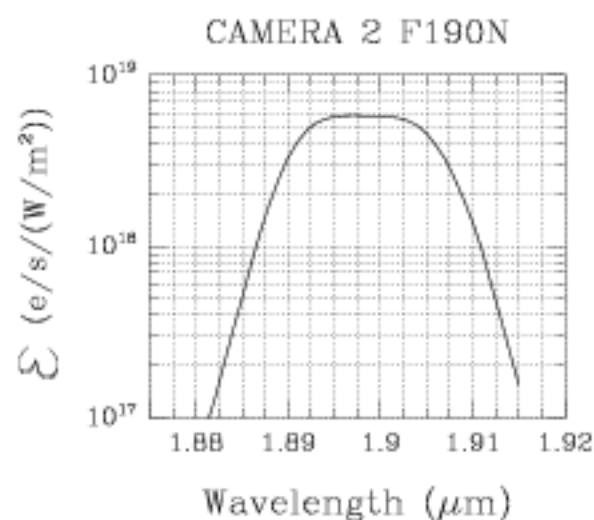
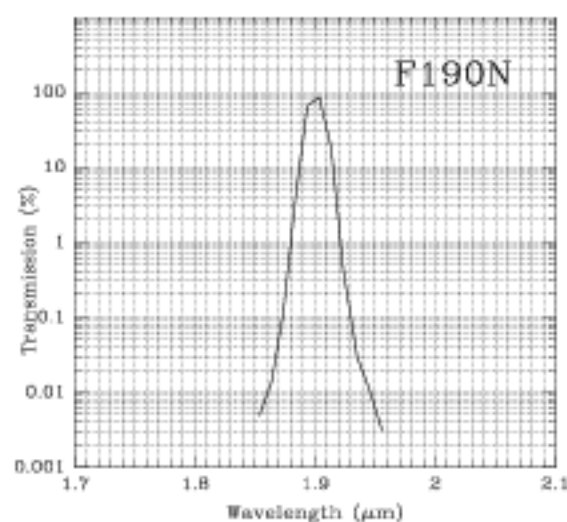
## Camera 2, Filter F190N

### Paschen $\alpha$ continuum

Also available on Cameras 1 and 3.

Central wavelength ( $\mu\text{m}$ )	Mean wavelength ( $\mu\text{m}$ )	Peak wavelength ( $\mu\text{m}$ )	FWHM ( $\mu\text{m}$ )	Range ( $\mu\text{m}$ )	MaxTr %	Pixel Fraction
1.9005	1.9003	1.9004	0.0174	1%	93.22	0.17

Figure 11.47: Camera 2, Filter F190N





## Camera 2, Filter F204M

### Methane band

*Thermal background important.*

Central wavelength ( $\mu\text{m}$ )	Mean wavelength ( $\mu\text{m}$ )	Peak wavelength ( $\mu\text{m}$ )	FWHM ( $\mu\text{m}$ )	Range ( $\mu\text{m}$ )	MaxTr %	Pixel Fraction
2.0313	2.0327	2.0342	0.105	1.99-2.09	91.77	0.17

Figure 11.49: Camera 2, Filter F204M

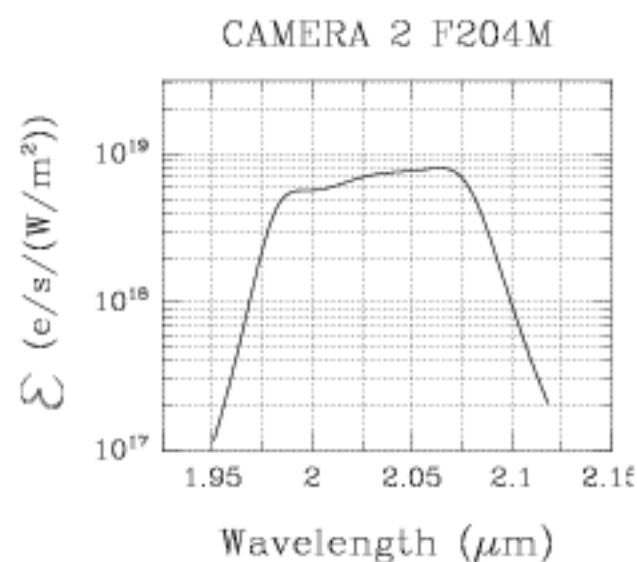
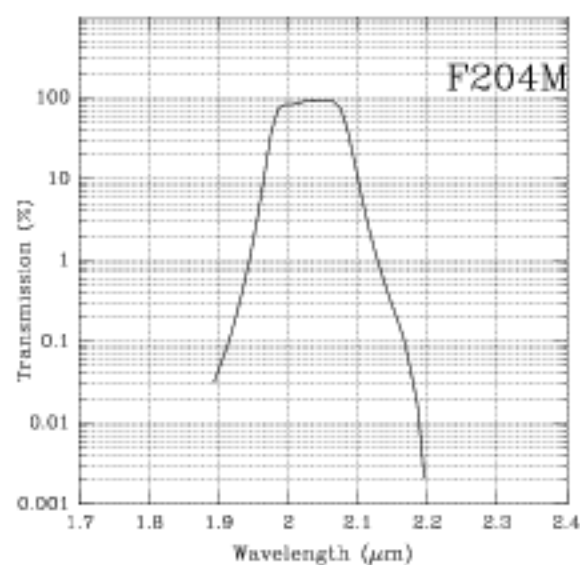
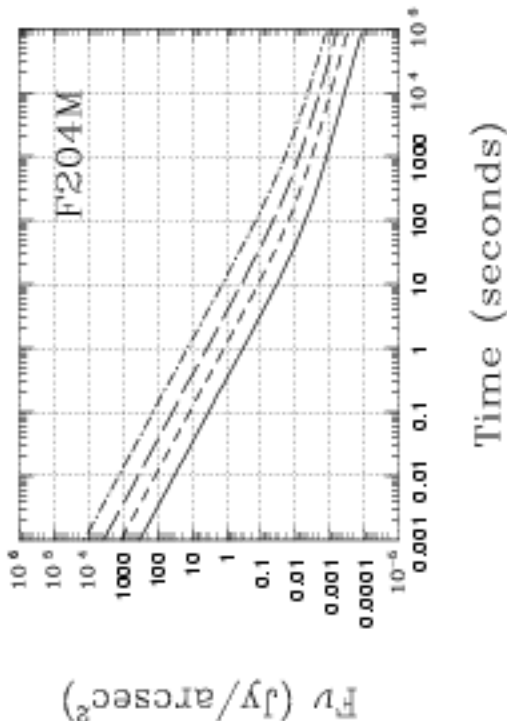
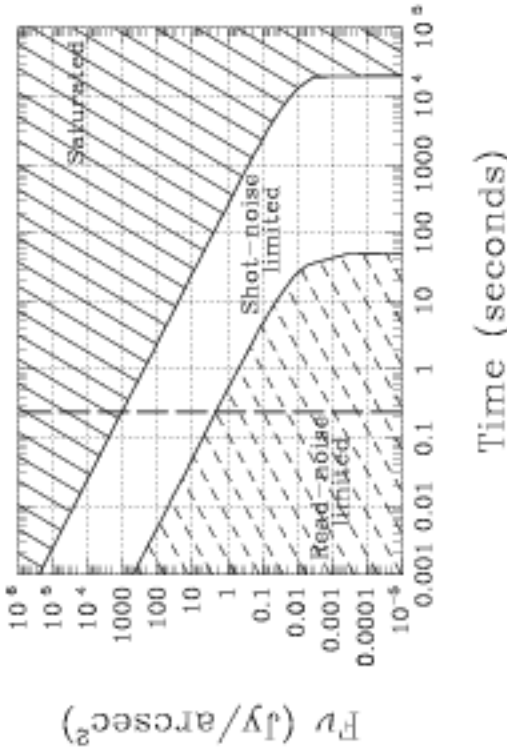


Figure 11.50: Sensitivity and Exclusion Curves for Camera 2, Filter F204M

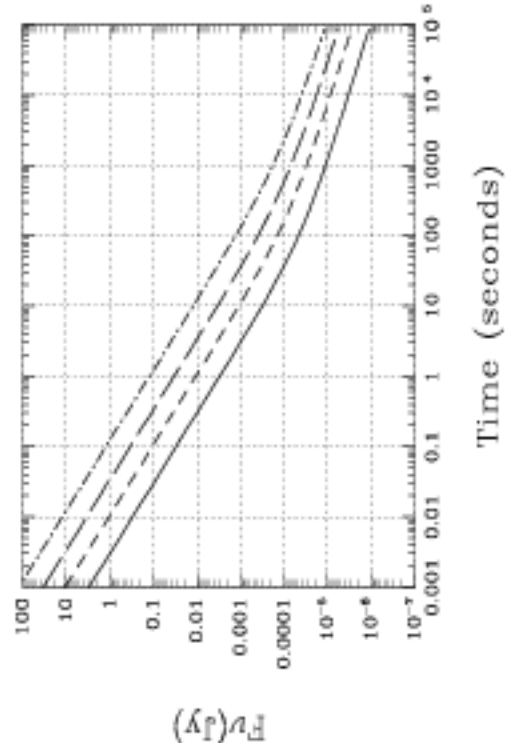
Extended Sources Sensitivity  
Camera 2



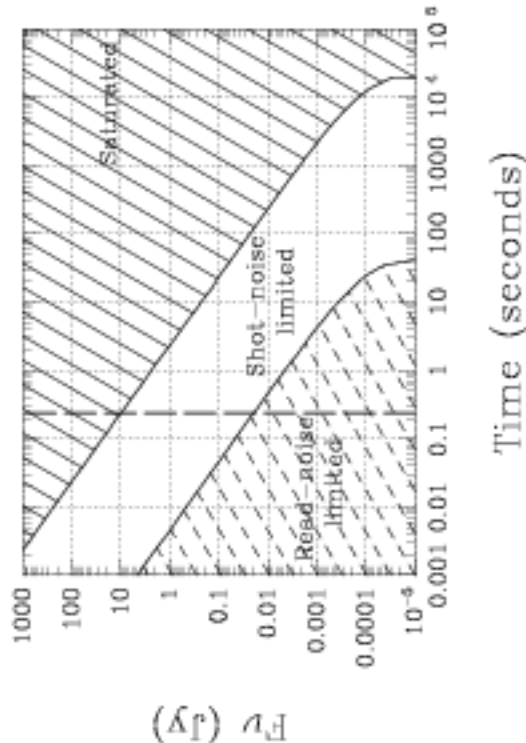
Time to saturate  
Camera 2 F204M



Camera 2 F204M Sensitivity



Time to saturate  
Camera 2 F204M



## Camera 2, Filter F205W

*Thermal background important.*

Central wavelength (μm)	Mean wavelength (μm)	Peak wavelength (μm)	FWHM (μm)	Range (μm)	MaxTr %	Pixel Fraction
2.0428	2.0406	1.9560	0.6125	1.75-2.0	98.14	0.18

Figure 11.51: Camera 2, Filter F205W

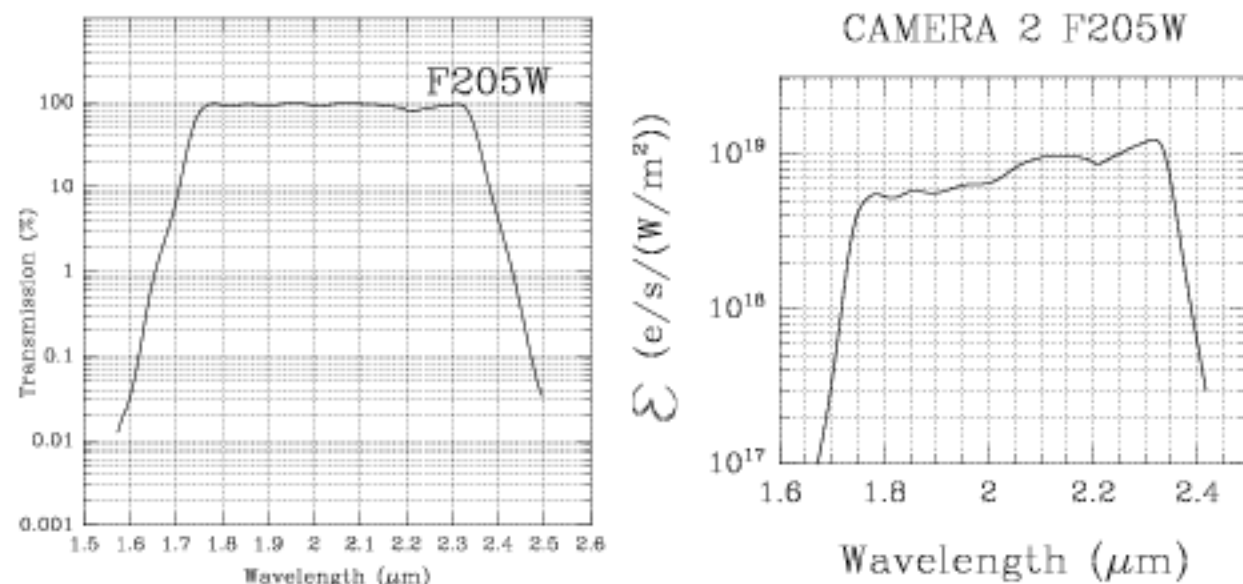
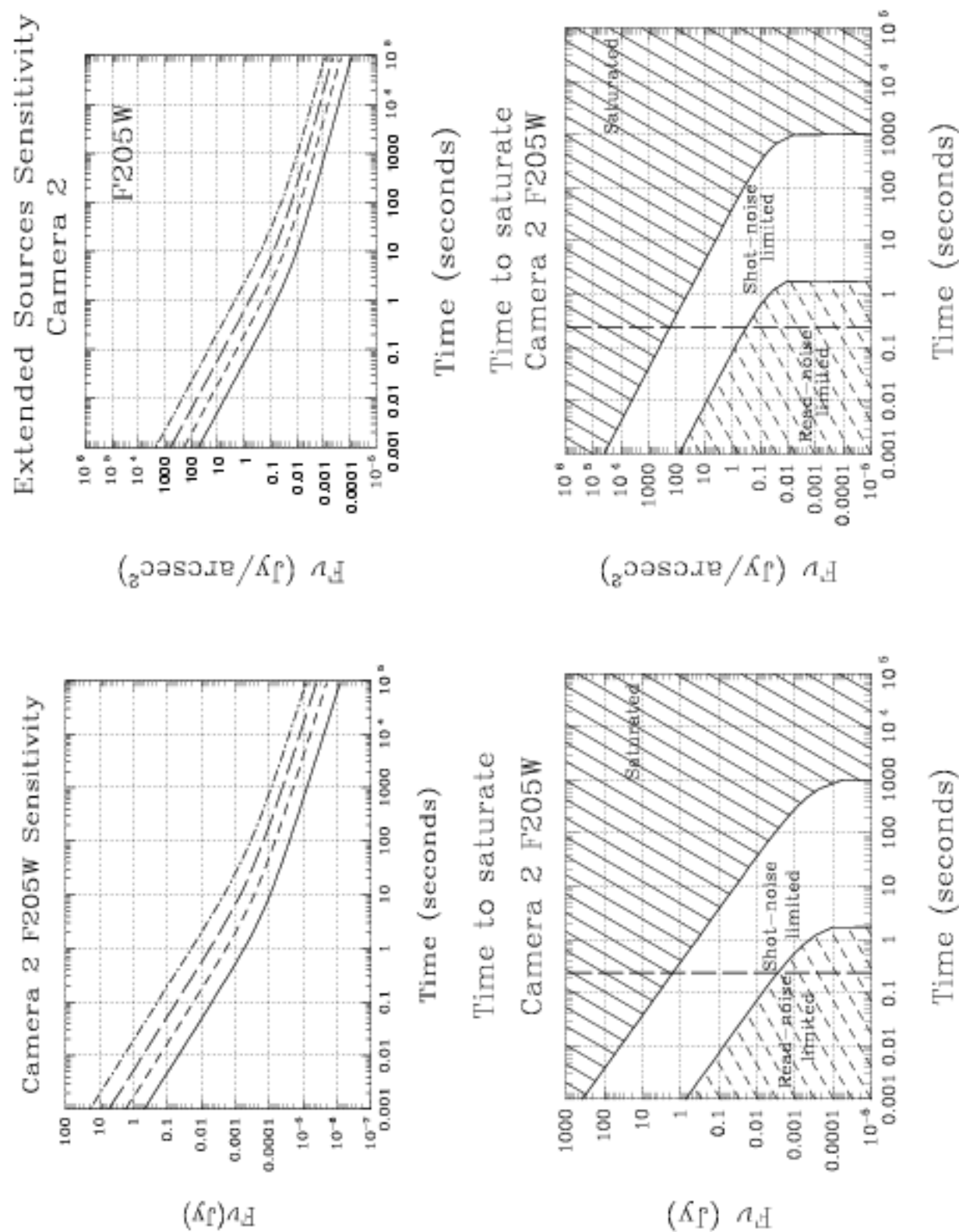




Figure 11.52: Sensitivity and Exclusion Curves for Camera 2, Filter F205W



## Camera 2, Filter F207M

*Thermal background important.*

Central wavelength ( $\mu\text{m}$ )	Mean wavelength ( $\mu\text{m}$ )	Peak wavelength ( $\mu\text{m}$ )	FWHM ( $\mu\text{m}$ )	Range ( $\mu\text{m}$ )	MaxTr %	Pixel Fraction
2.0827	2.0786	2.0252	0.1522	2.0-2.15	96.40	0.11

Figure 11.53: Camera 2, Filter F207M

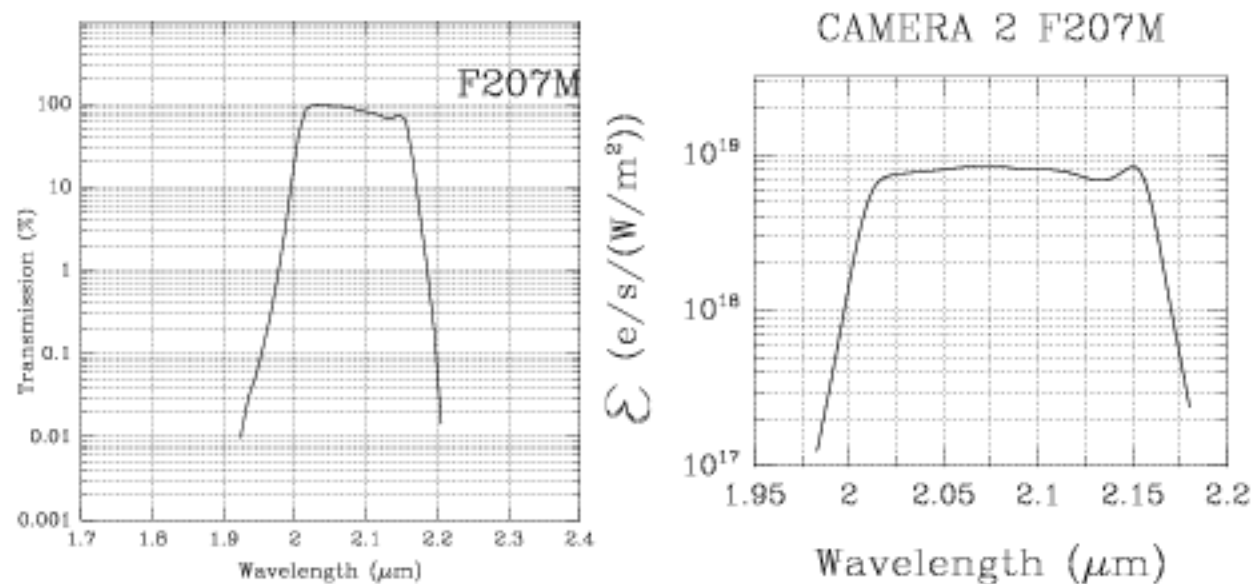
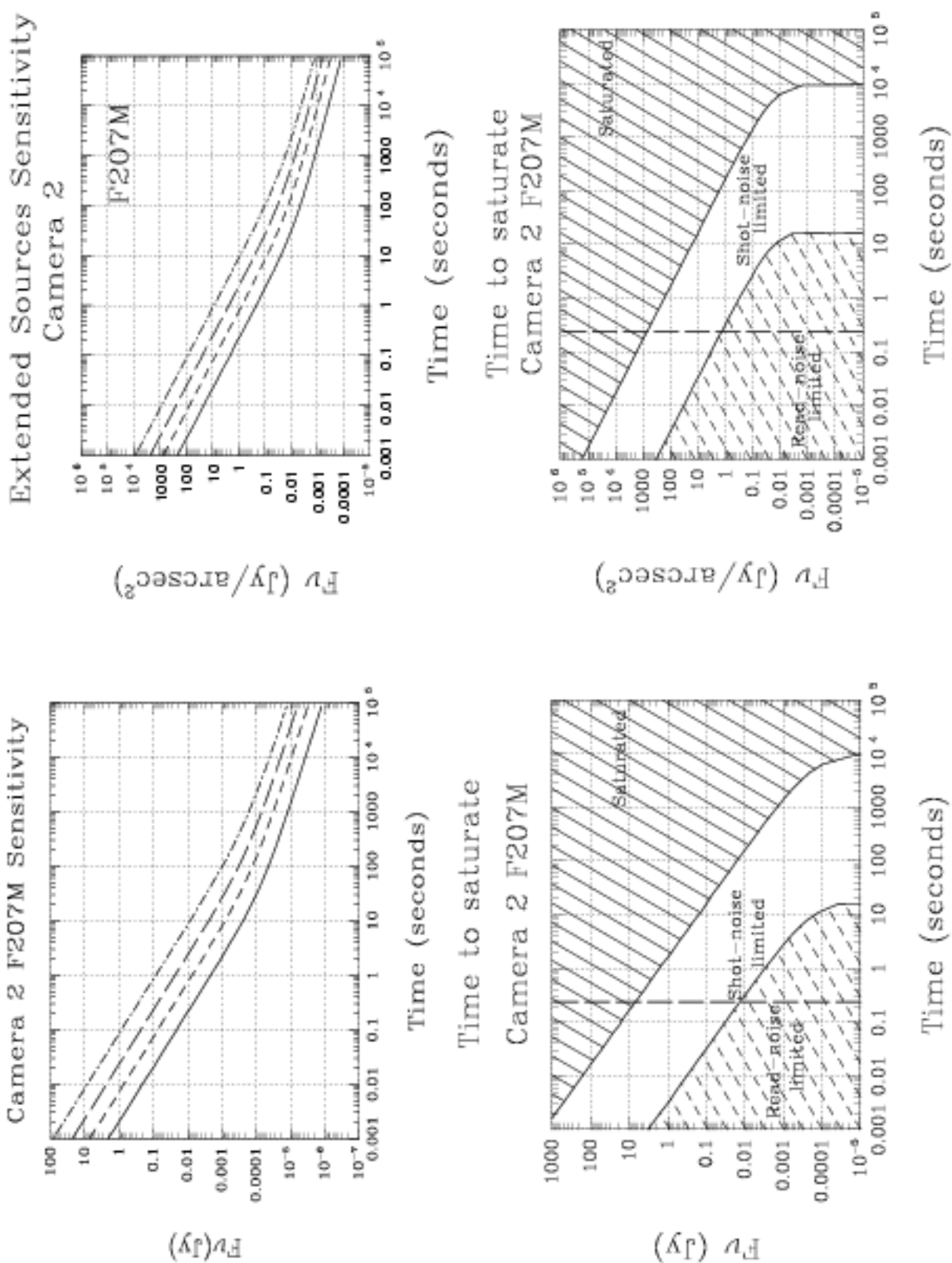


Figure 11.54: Sensitivity and Exclusion Curves for Camera 2, Filter F207M



## Camera 2, Filter F212N

**H<sub>2</sub> line**

Also available on Camera 3.

*Thermal background important.*

Central wavelength (μm)	Mean wavelength (μm)	Peak wavelength (μm)	FWHM (μm)	Range (μm)	MaxTr %	Pixel Fraction
2.1211	2.1213	2.1228	0.0206	1%	90.90	0.14

Figure 11.55: Camera 2, Filter F212N

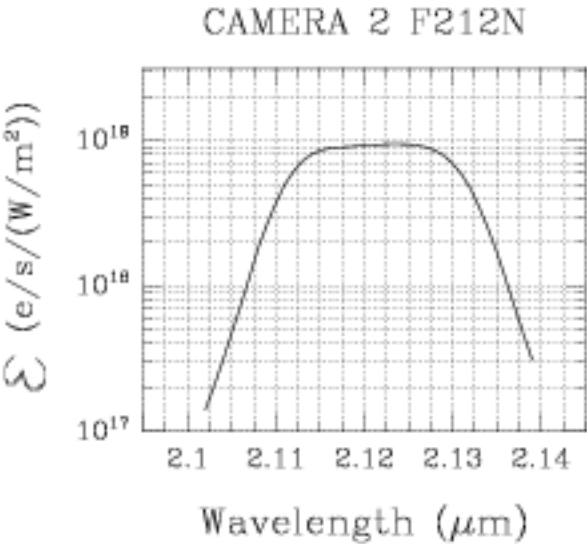
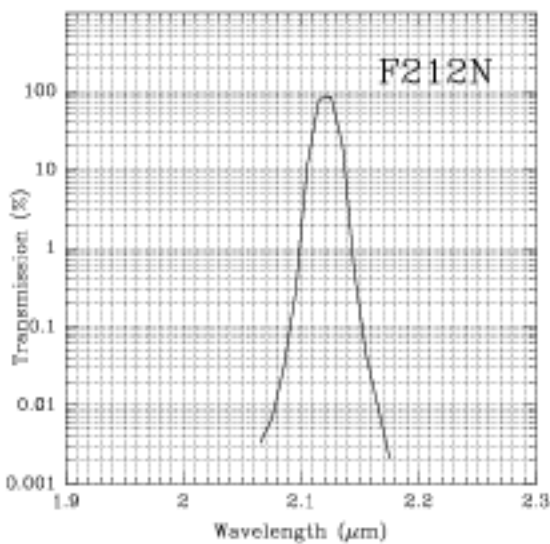
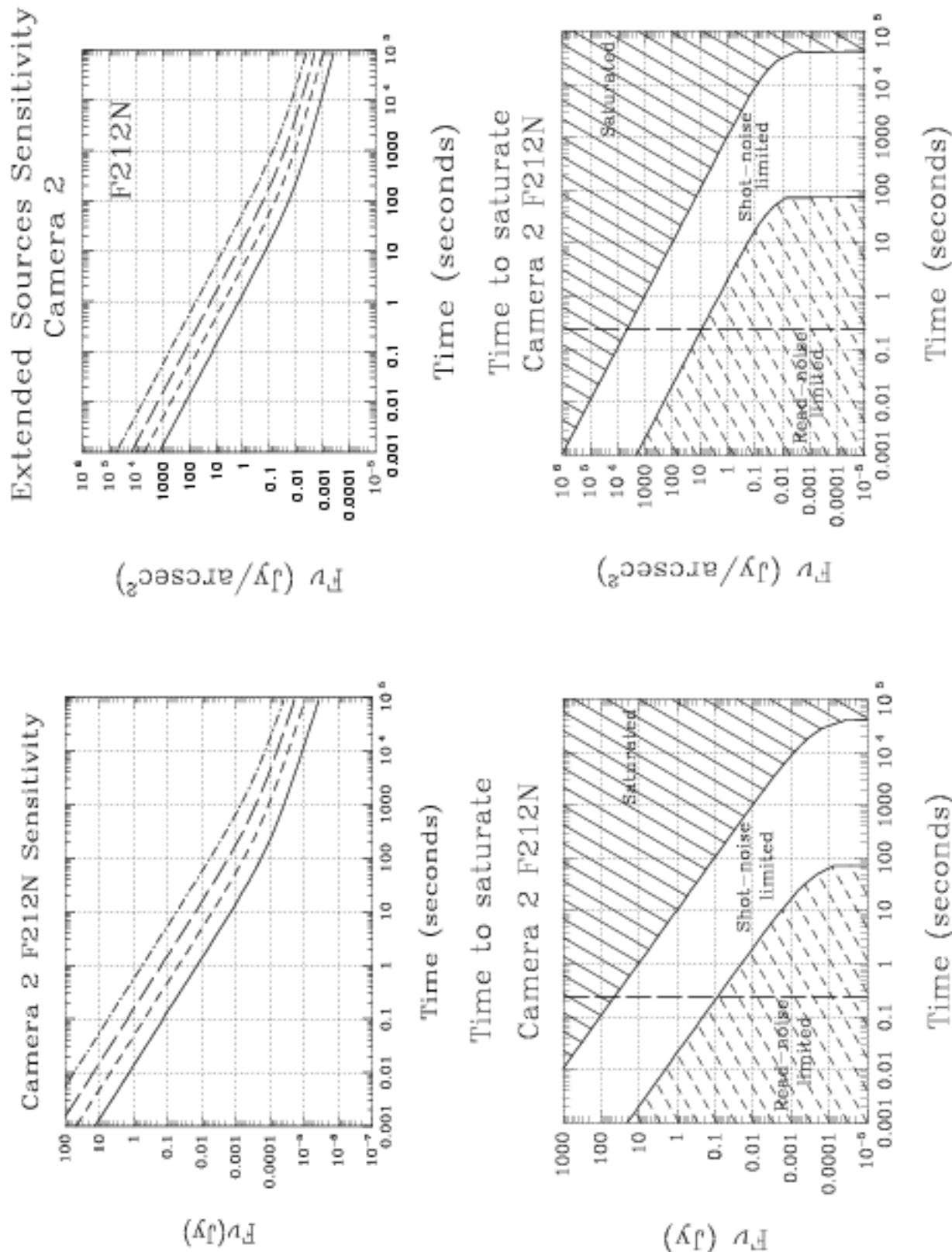


Figure 11.56: Sensitivity and Exclusion Curves for Camera 2, Filter F212N



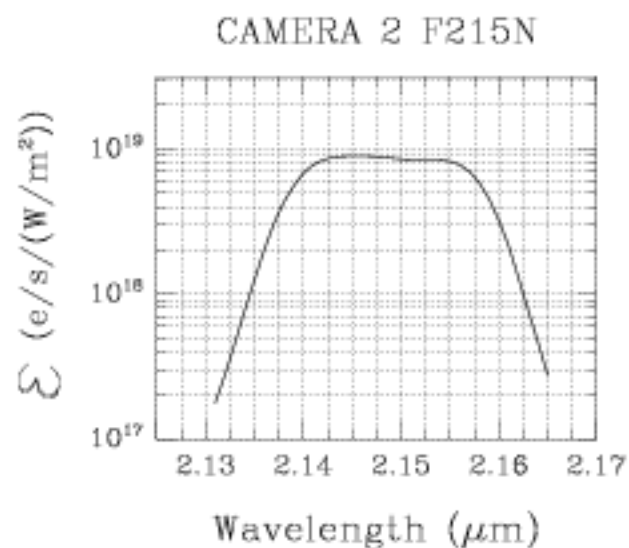
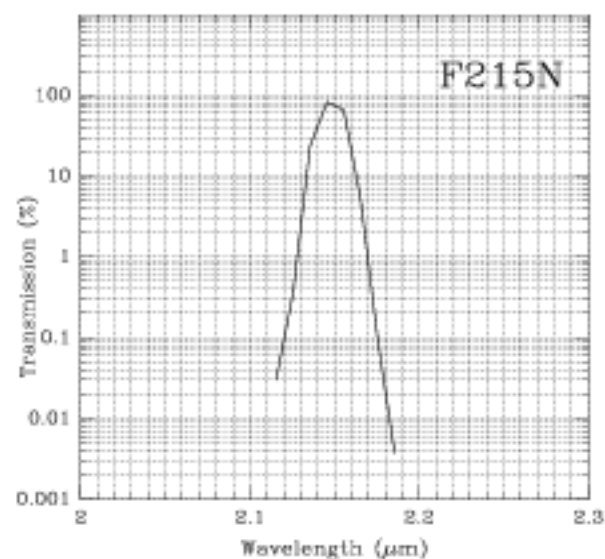
## Camera 2, Filter F215N

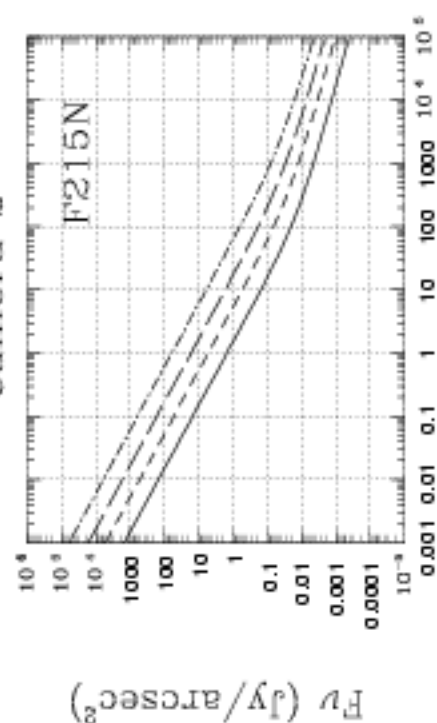
**H<sub>2</sub> + Brackett  $\gamma$  continuum**

*Thermal background important*

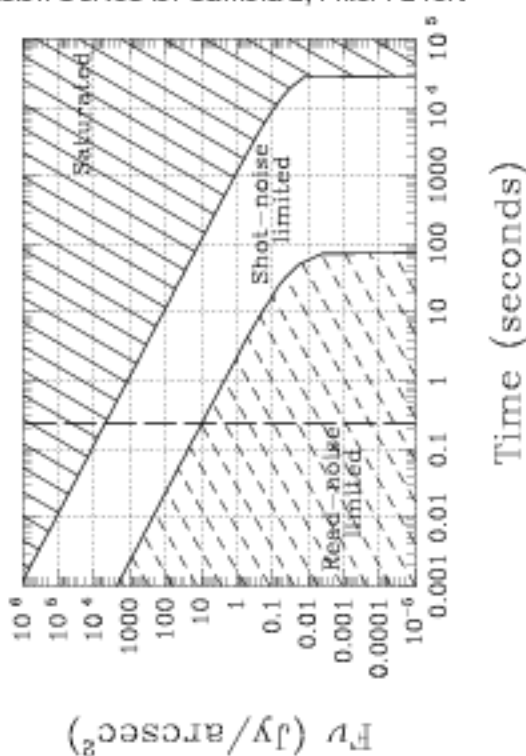
Central wavelength ( $\mu\text{m}$ )	Mean wavelength ( $\mu\text{m}$ )	Peak wavelength ( $\mu\text{m}$ )	FWHM ( $\mu\text{m}$ )	Range ( $\mu\text{m}$ )	MaxTr %	Pixel Fraction
2.1488	2.1487	2.1562	0.0200	1%	85.91	0.14

Figure 11.57: Camera 2, Filter F215N



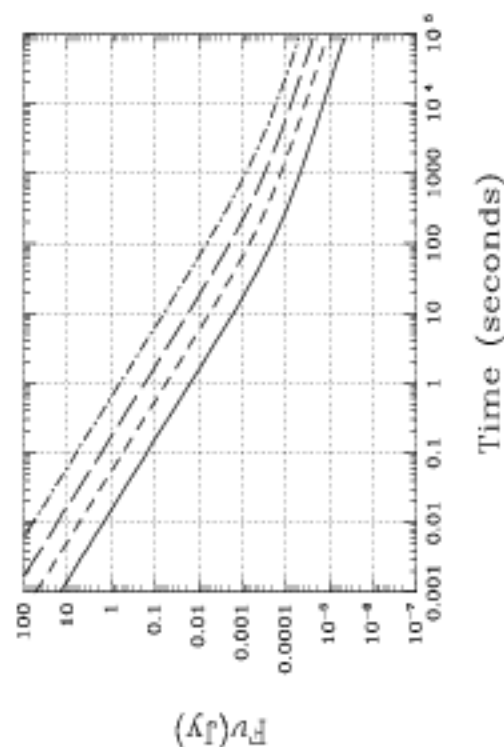
Extended Sources Sensitivity  
Camera 2

Time (seconds)

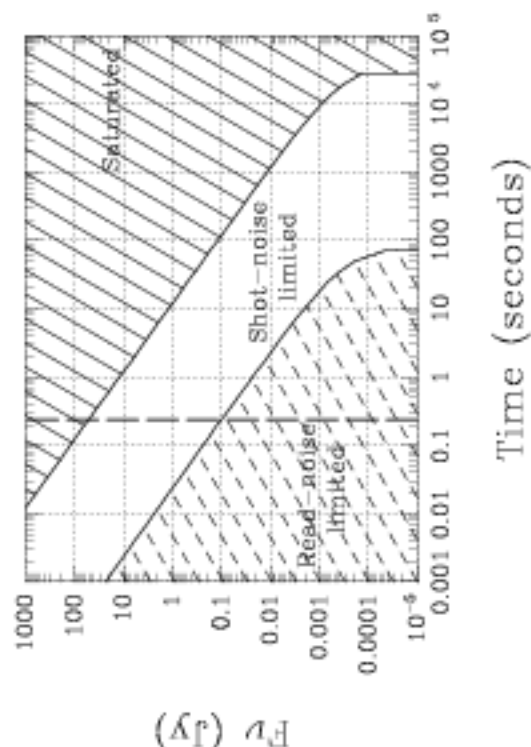
Time to saturate  
Camera 2 F215N

Time (seconds)

Camera 2 F215N Sensitivity



Time (seconds)

Time to saturate  
Camera 2 F215N

Time (seconds)

Figure 11.58: Sensitivity and Exclusion Curves for Camera 2, Filter F215N

## Camera 2, Filter F216N

### Brackett $\gamma$ line

*Thermal background important.*

Central wavelength ( $\mu\text{m}$ )	Mean wavelength ( $\mu\text{m}$ )	Peak wavelength ( $\mu\text{m}$ )	FWHM ( $\mu\text{m}$ )	Range ( $\mu\text{m}$ )	MaxTr %	Pixel Fraction
2.1642	2.1641	2.1668	0.0208	1%	90.07	0.14

Figure 11.59: Camera 2, Filter F216N

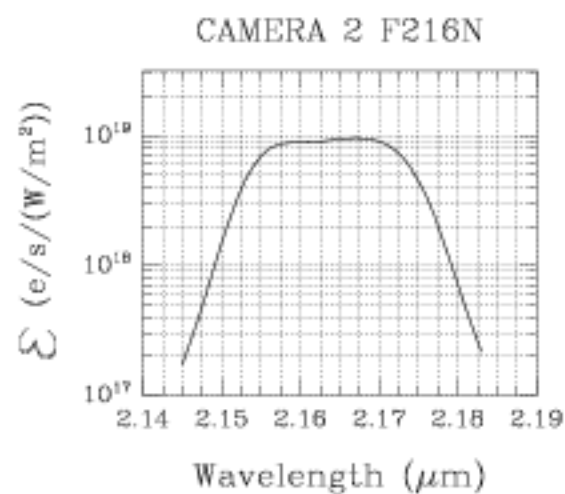
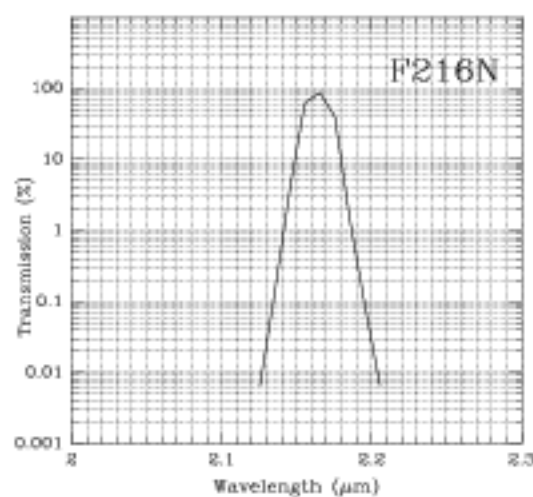
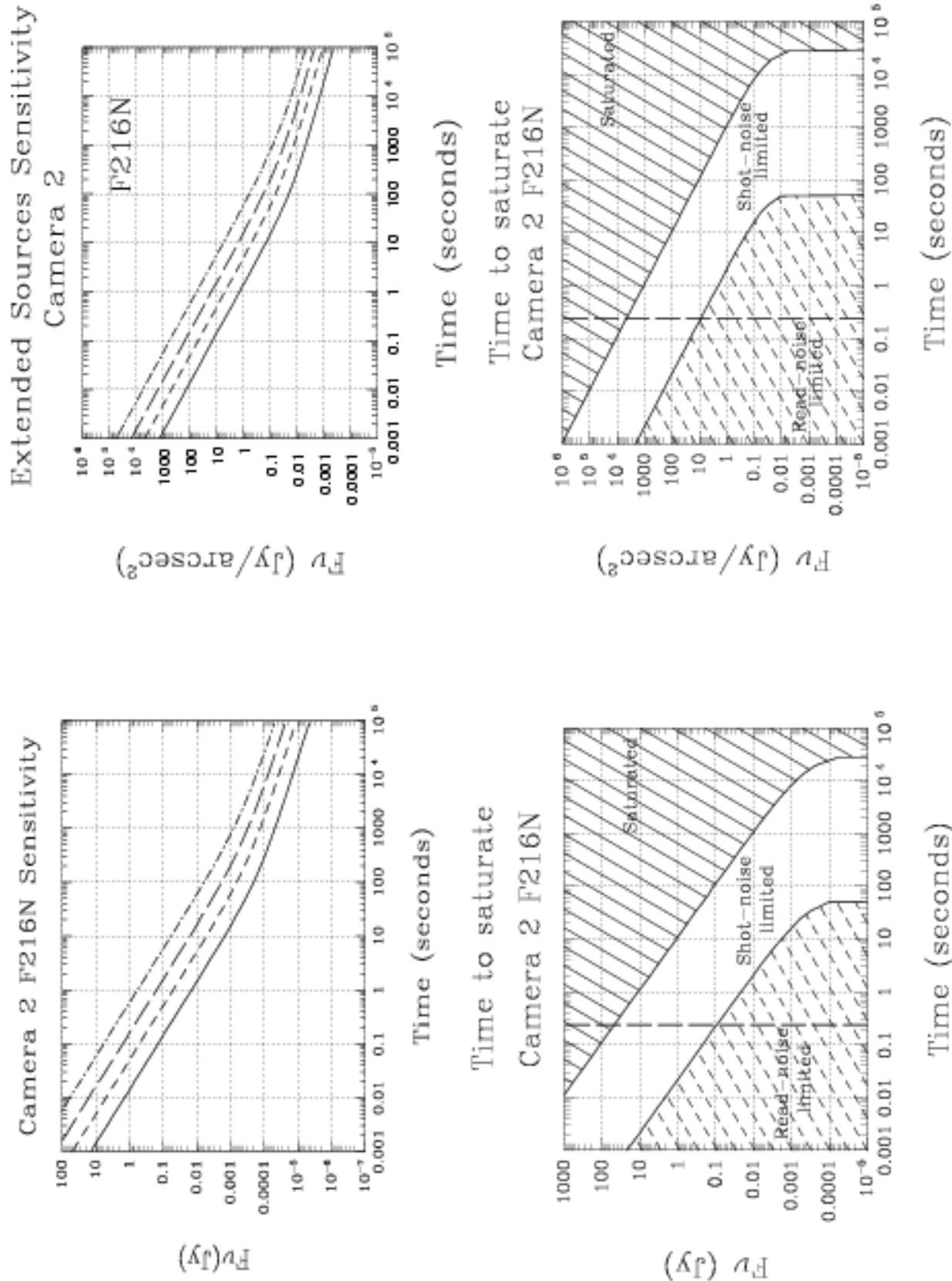




Figure 11.60: Sensitivity and Exclusion Curves for Camera 2, Filter F216N



## Camera 2, Filter F222M

### CO continuum

Also available on Camera 3.

*Thermal background important.*

Central wavelength ( $\mu\text{m}$ )	Mean wavelength ( $\mu\text{m}$ )	Peak wavelength ( $\mu\text{m}$ )	FWHM ( $\mu\text{m}$ )	Range ( $\mu\text{m}$ )	MaxTr %	Pixel Fraction
2.2160	2.2164	2.1804	0.1432	2.15-2.3	89.90	0.14

Figure 11.61: Camera 2, Filter F222M

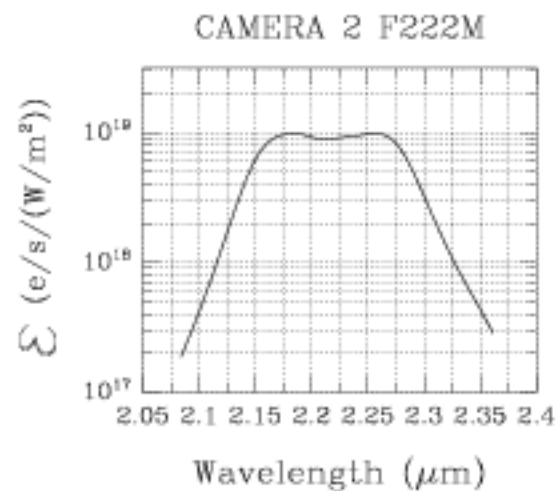
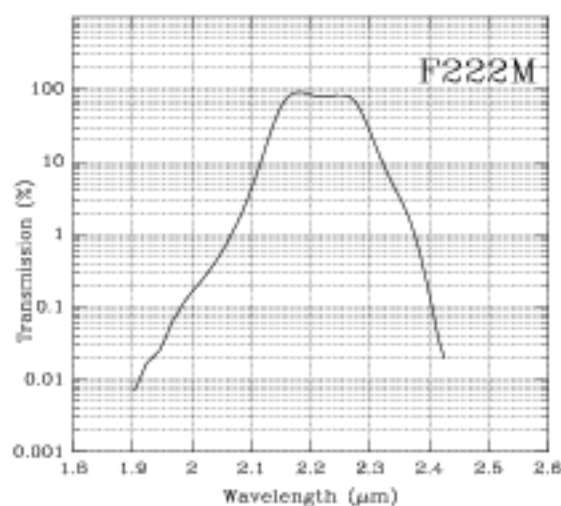
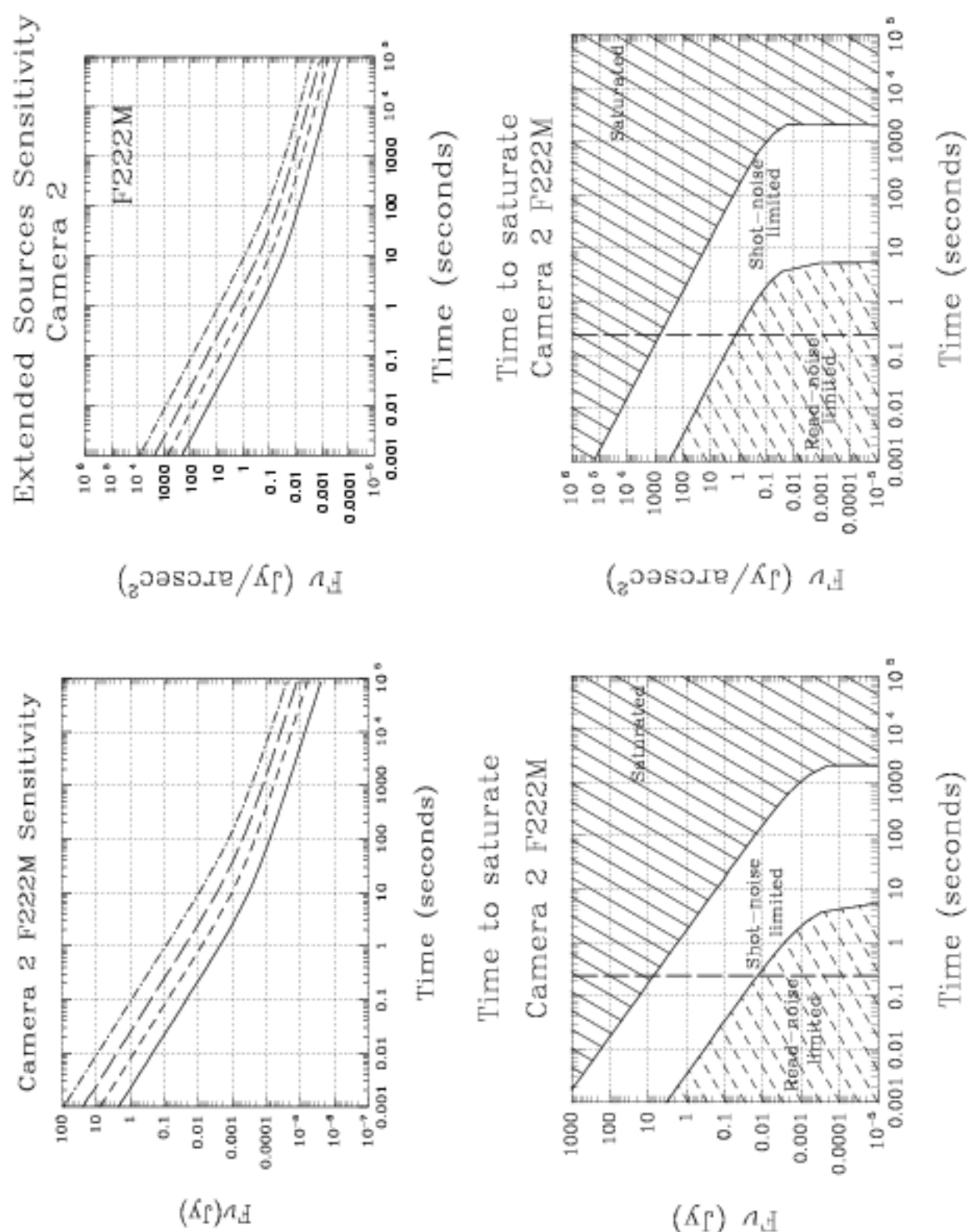


Figure 11.62: Sensitivity and Exclusion Curves for Camera 2, Filter F222M



## Camera 2, Filter F237M

**CO**

Also available on Camera 3 as F240M.

*Thermal background important.*

Central wavelength ( $\mu\text{m}$ )	Mean wavelength ( $\mu\text{m}$ )	Peak wavelength ( $\mu\text{m}$ )	FWHM ( $\mu\text{m}$ )	Range ( $\mu\text{m}$ )	MaxTr %	Pixel Fraction
2.3677	2.3694	2.3852	0.1546	2.3-2.45	92.38	0.12

Figure 11.63: Camera 2, Filter F237M

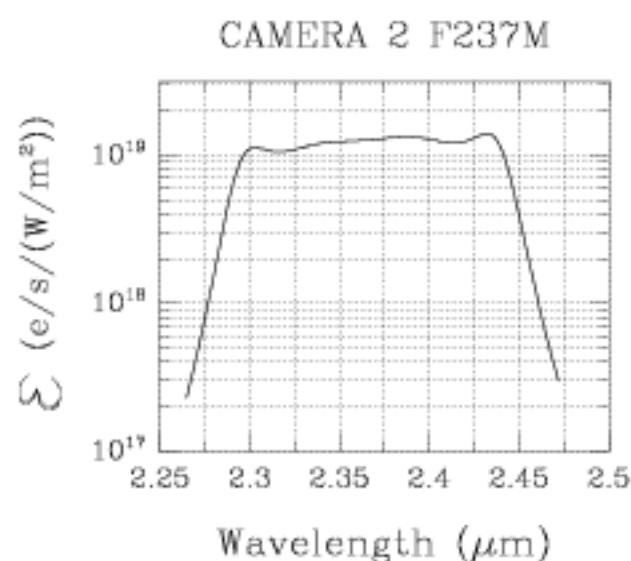
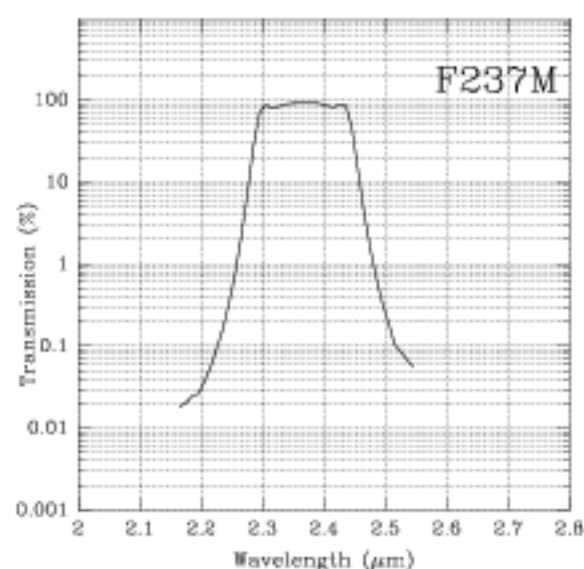
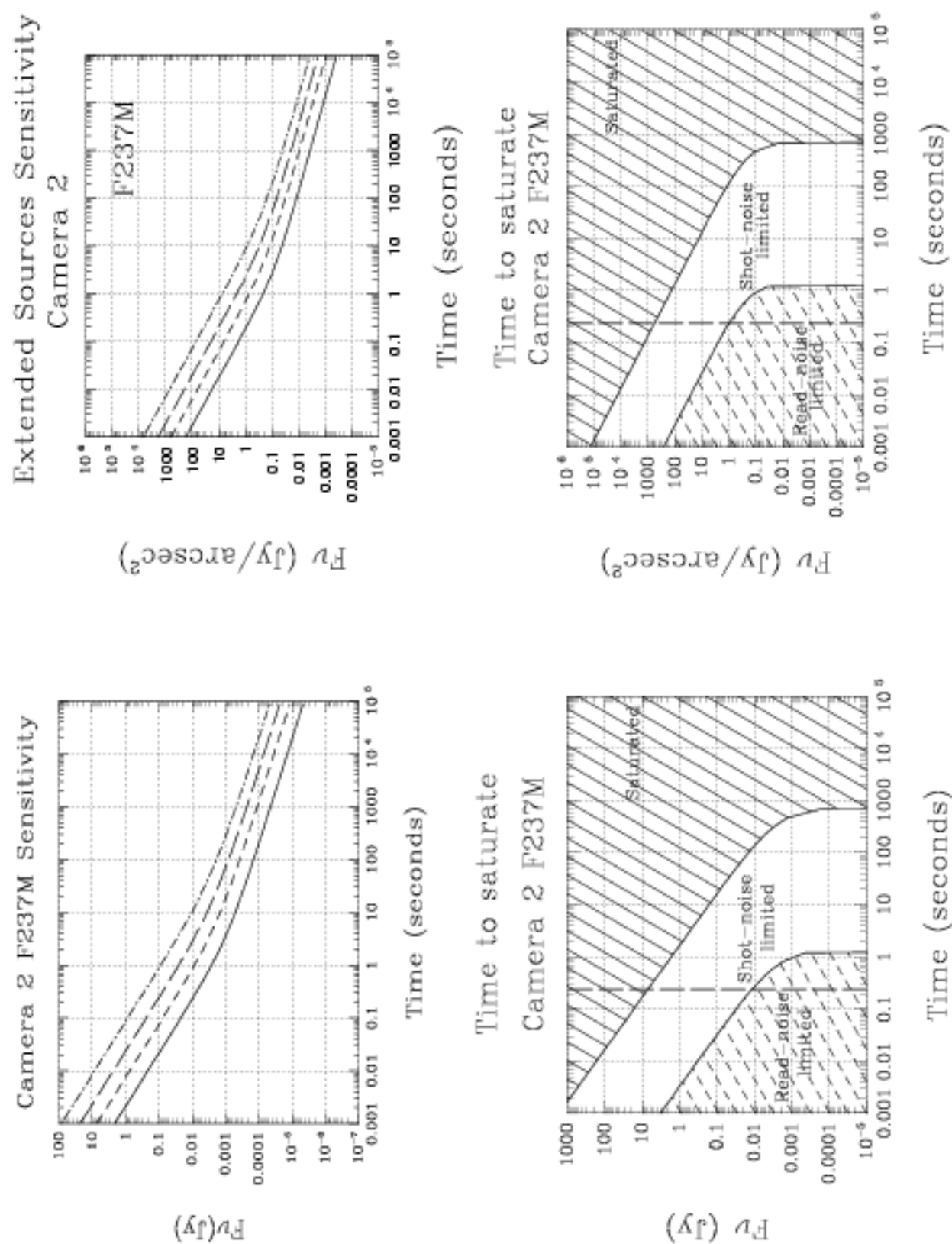


Figure 11.64: Sensitivity and Exclusion Curves for Camera 2, Filter F237M



# Camera 3, Filter F108N

**Hel line**  
Also available on Camera 1.

Central wavelength (μm)	Mean wavelength (μm)	Peak wavelength (μm)	FWHM (μm)	Range (μm)	MaxTr %	Pixel Fraction
1.0800	1.0799	1.0776	0.0096	1%	75.82	0.84

Figure 11.65: Camera 3, Filter F108N

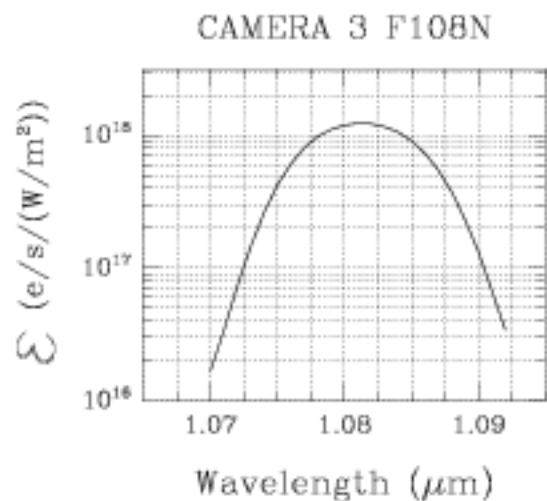
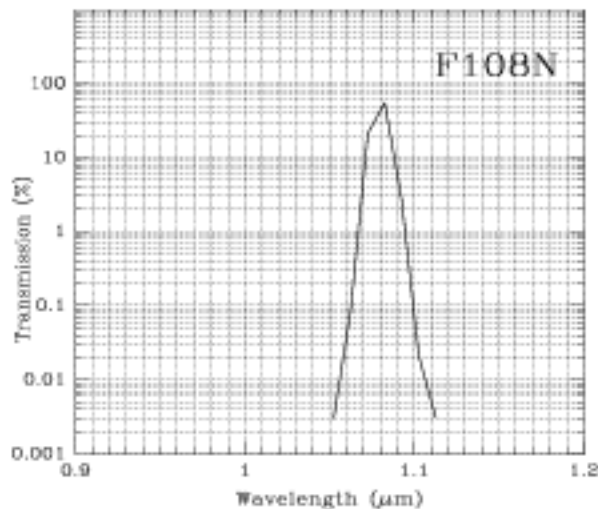
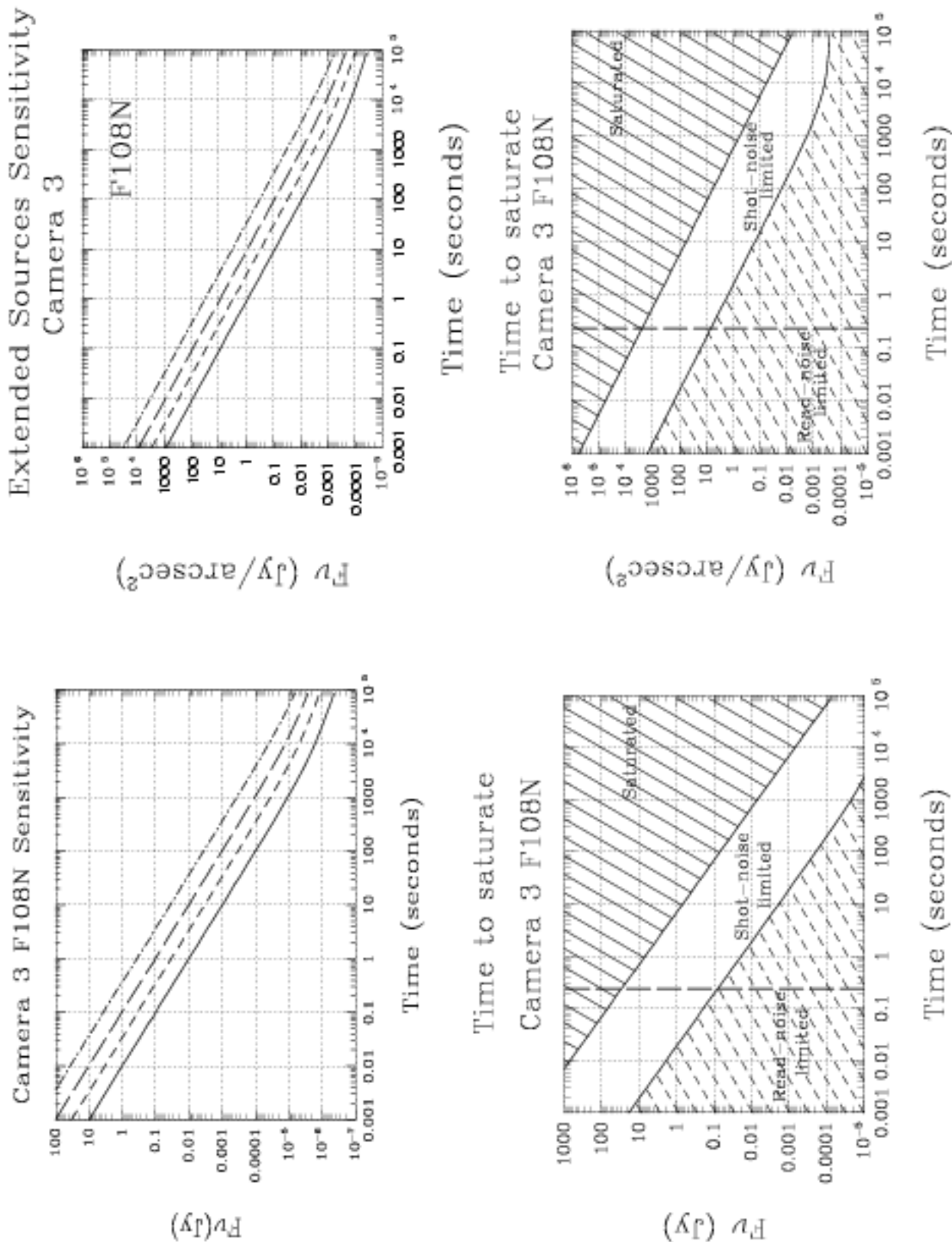


Figure 11.66: Sensitivity and Exclusion Curves for Camera 3, Filter F108N



# Camera 3, Filter F110W

Also available on Cameras 1 and 2.

Central wavelength (μm)	Mean wavelength (μm)	Peak wavelength (μm)	FWHM (μm)	Range (μm)	MaxTr %	Pixel fraction
1.0998	1.1035	1.2035	0.5915	0.8-1.4	94.90	0.66

Figure 11.67: Transmission Curve for F110W

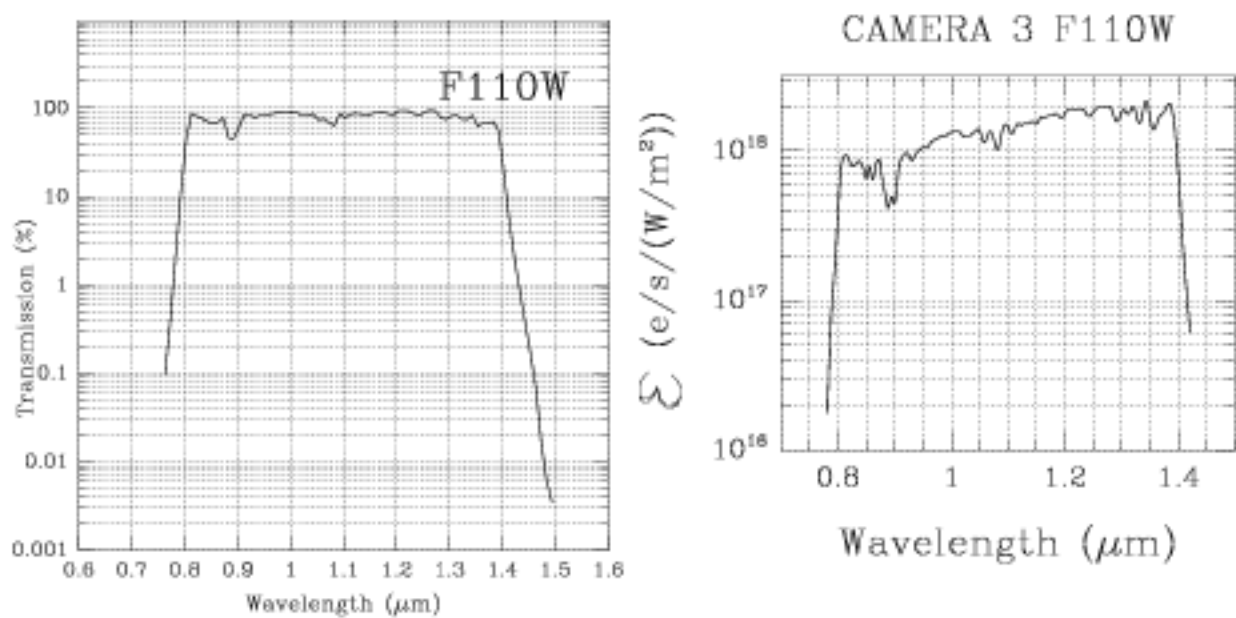
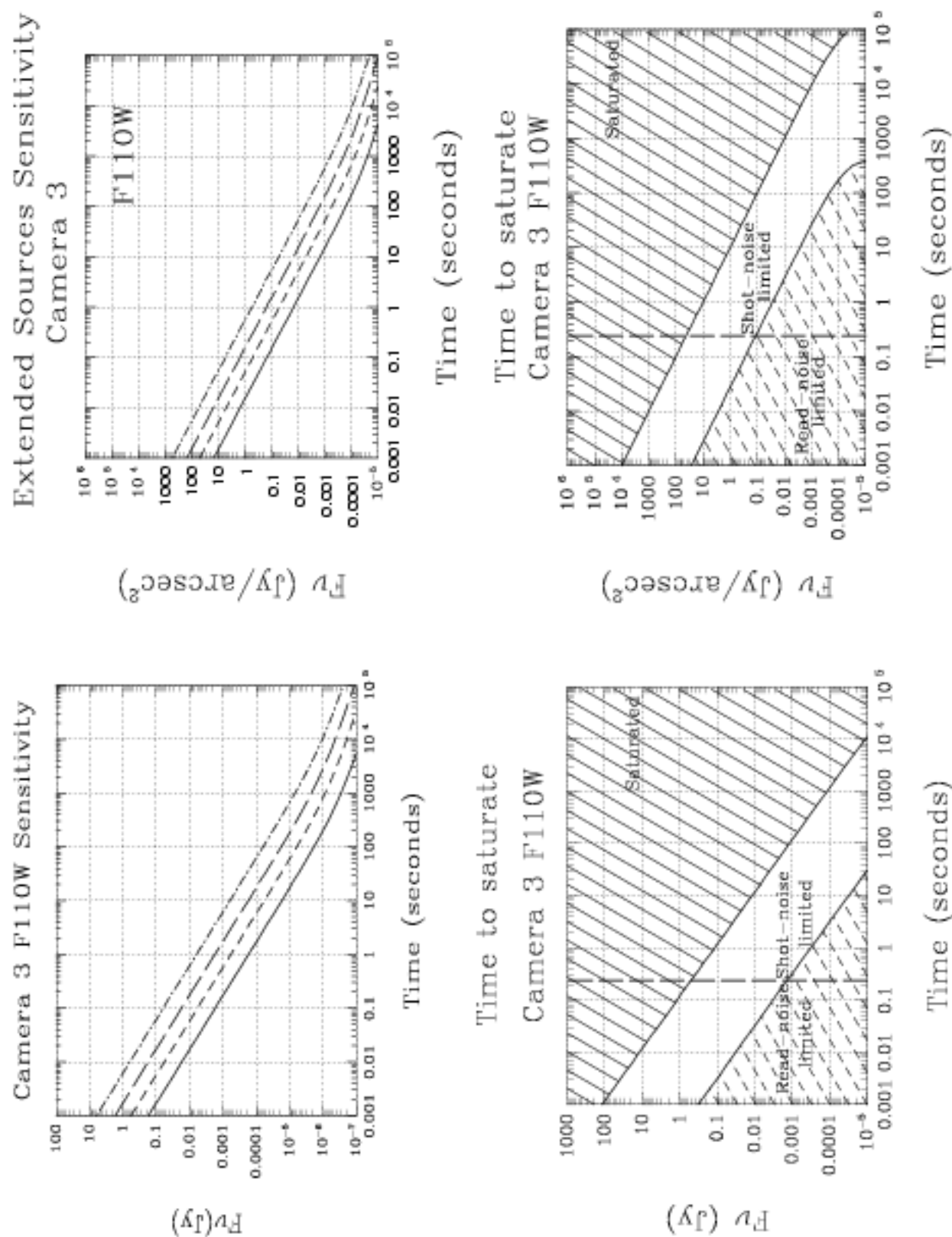




Figure 11.68: Sensitivity and Exclusion Curves for Camera 3, Filter F110W



# Camera 3, Filter F113N

**Hel continuum**  
Also available on Camera 1.

Central wavelength (μm)	Mean wavelength (μm)	Peak wavelength (μm)	FWHM (μm)	Range (μm)	MaxTr %	Pixel Fraction
1.1283	1.1283	1.1316	0.0110	1%	84.81	0.83

Figure 11.69: Camera 3, Filter F113N

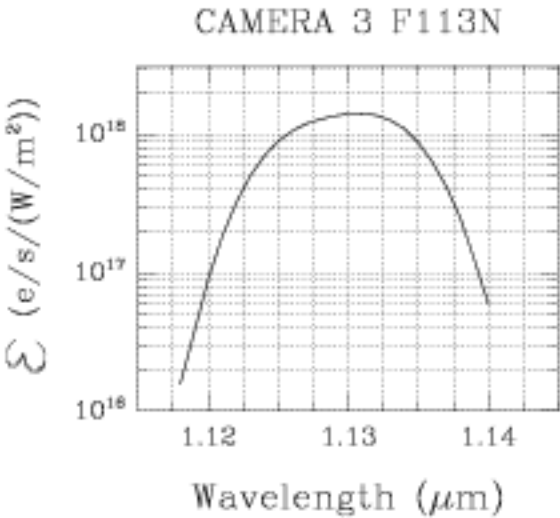
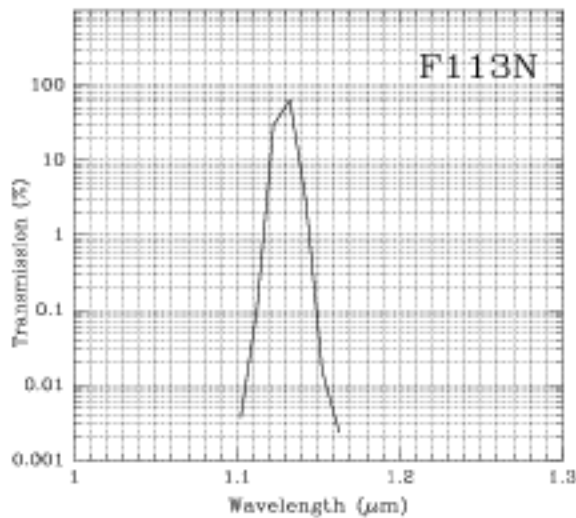
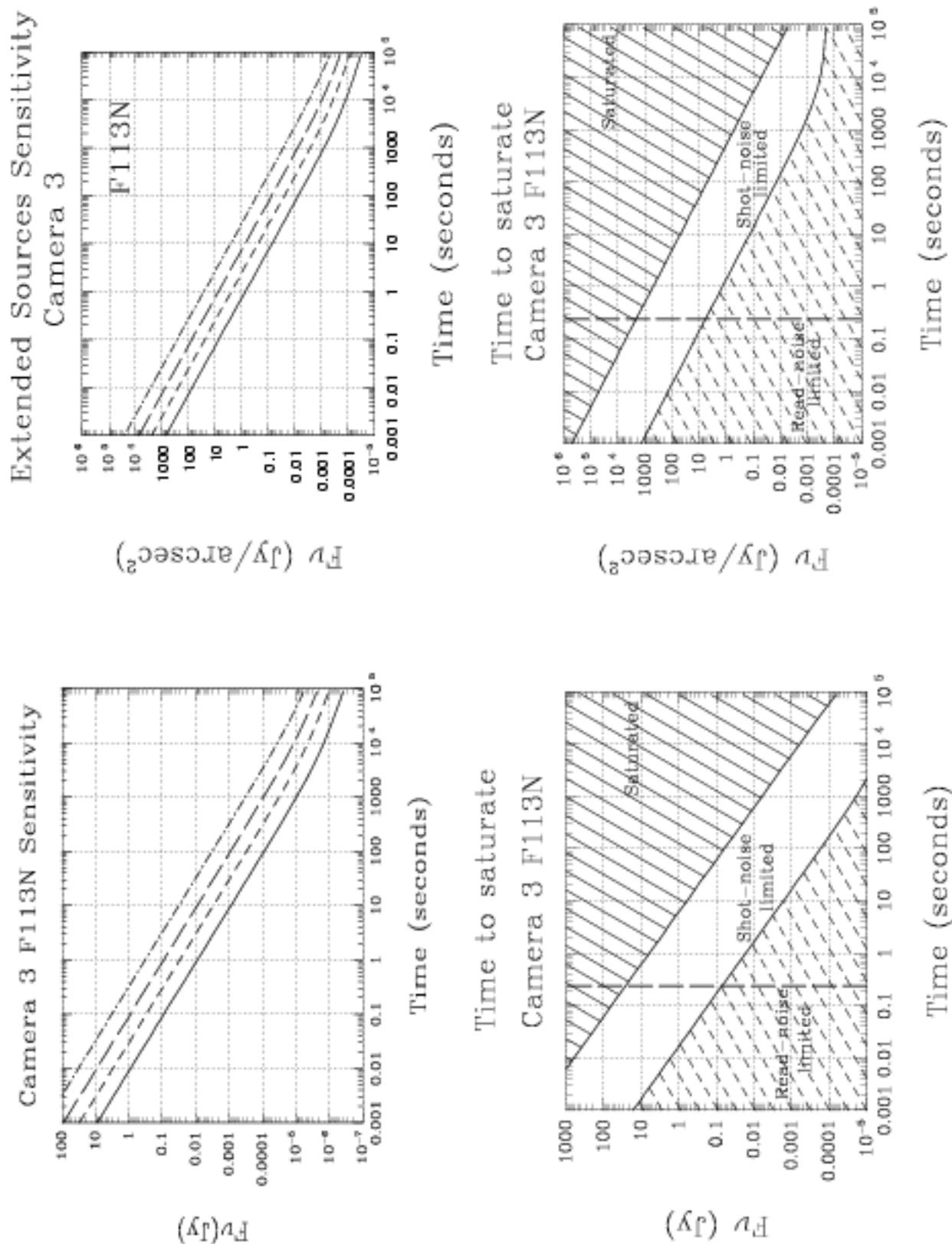


Figure 11.70: Sensitivity and Exclusion Curves for Camera 3, Filter F113N



## Camera 3, Filter F150W

### Grism B continuum

*Thermal background important.*

Central wavelength ( $\mu\text{m}$ )	Mean wavelength ( $\mu\text{m}$ )	Peak wavelength ( $\mu\text{m}$ )	FWHM ( $\mu\text{m}$ )	Range ( $\mu\text{m}$ )	MaxTr %	Pixel fraction
1.5035	1.5069	1.6355	0.8020	1.1-1.9	97.67	0.78

Figure 11.71: Camera 3, Filter F150W

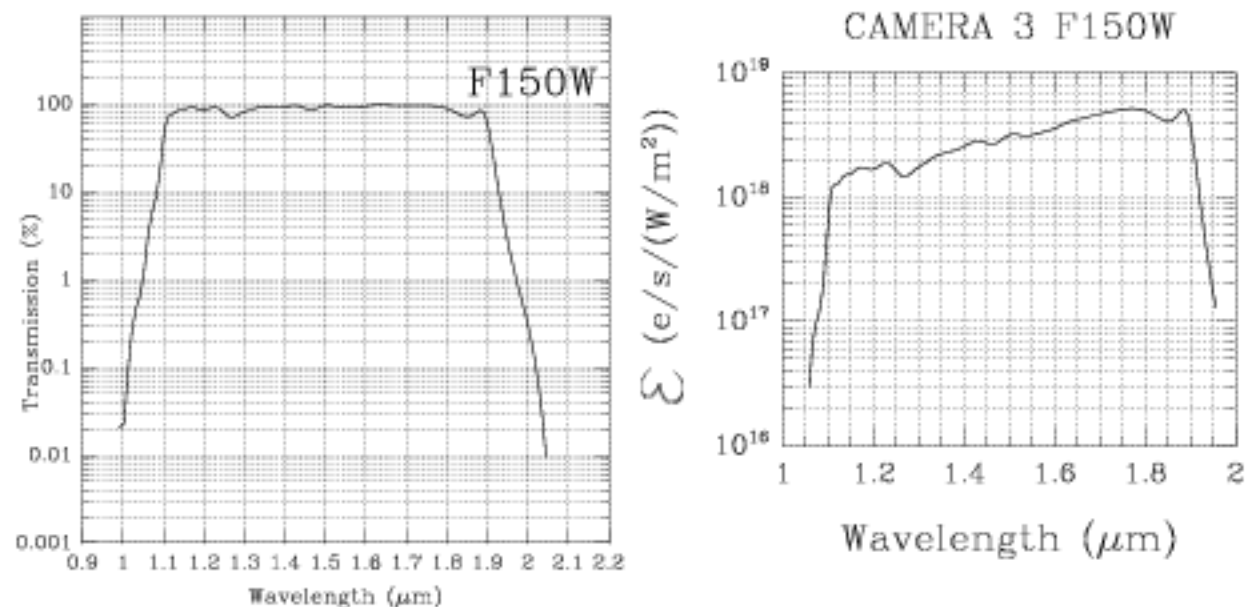
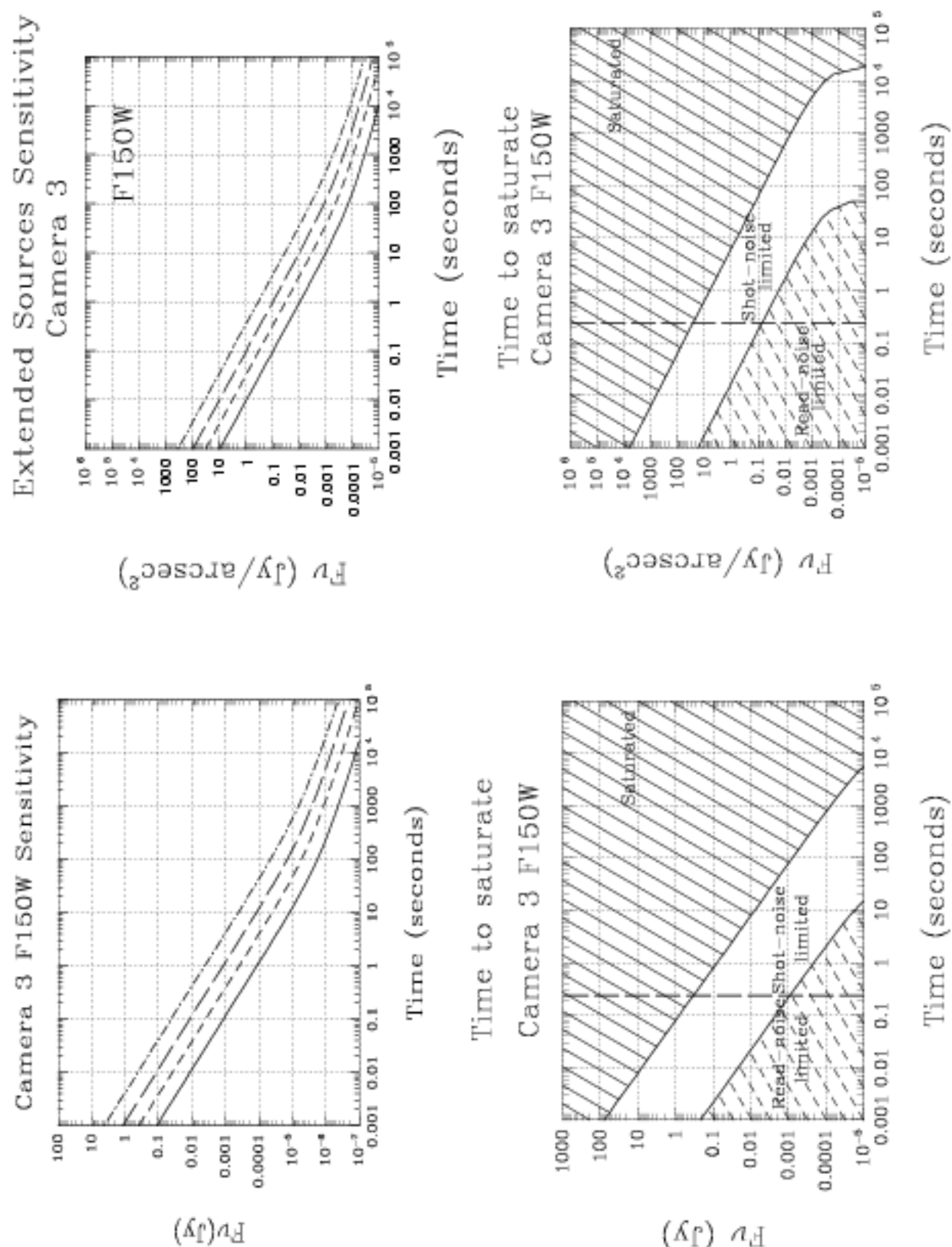


Figure 11.72: Sensitivity and Exclusion Curves for Camera 3, Filter F150W



## Camera 3, Filter F160W

### Minimum background

Also available on Cameras 1 and 2.

Central wavelength ( $\mu\text{m}$ )	Mean wavelength ( $\mu\text{m}$ )	Peak wavelength ( $\mu\text{m}$ )	FWHM ( $\mu\text{m}$ )	Range ( $\mu\text{m}$ )	MaxTr %	Pixel fraction
1.5940	1.5931	1.5820	0.4030	1.4-1.8	96.59	0.62

Figure 11.73: Camera 3, Filter F160W

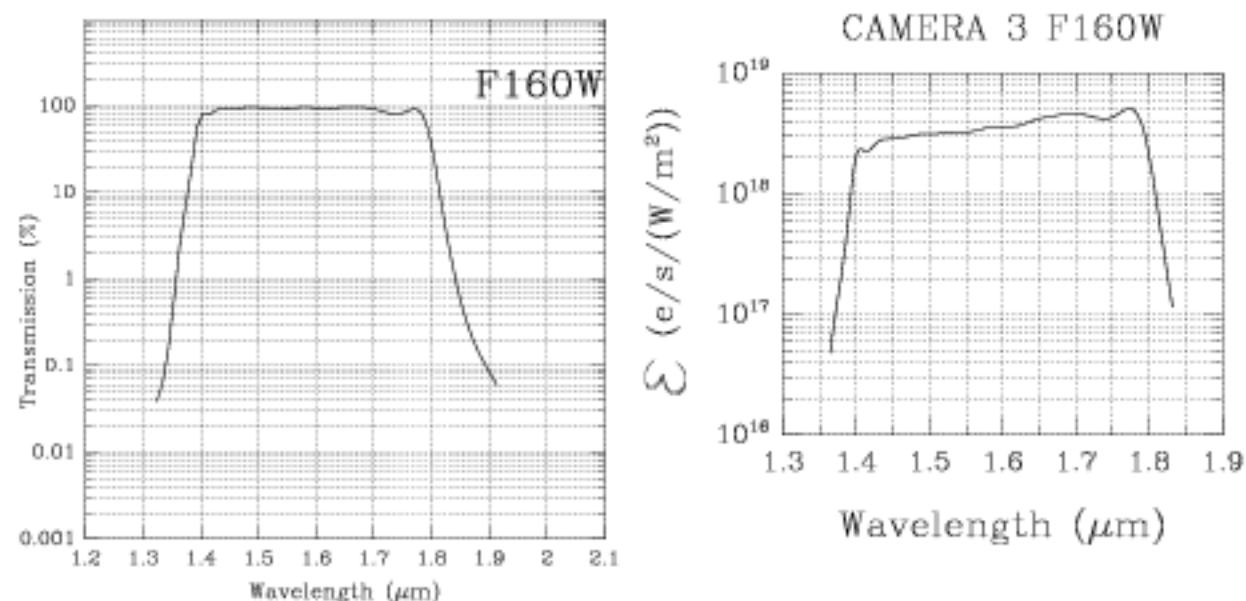
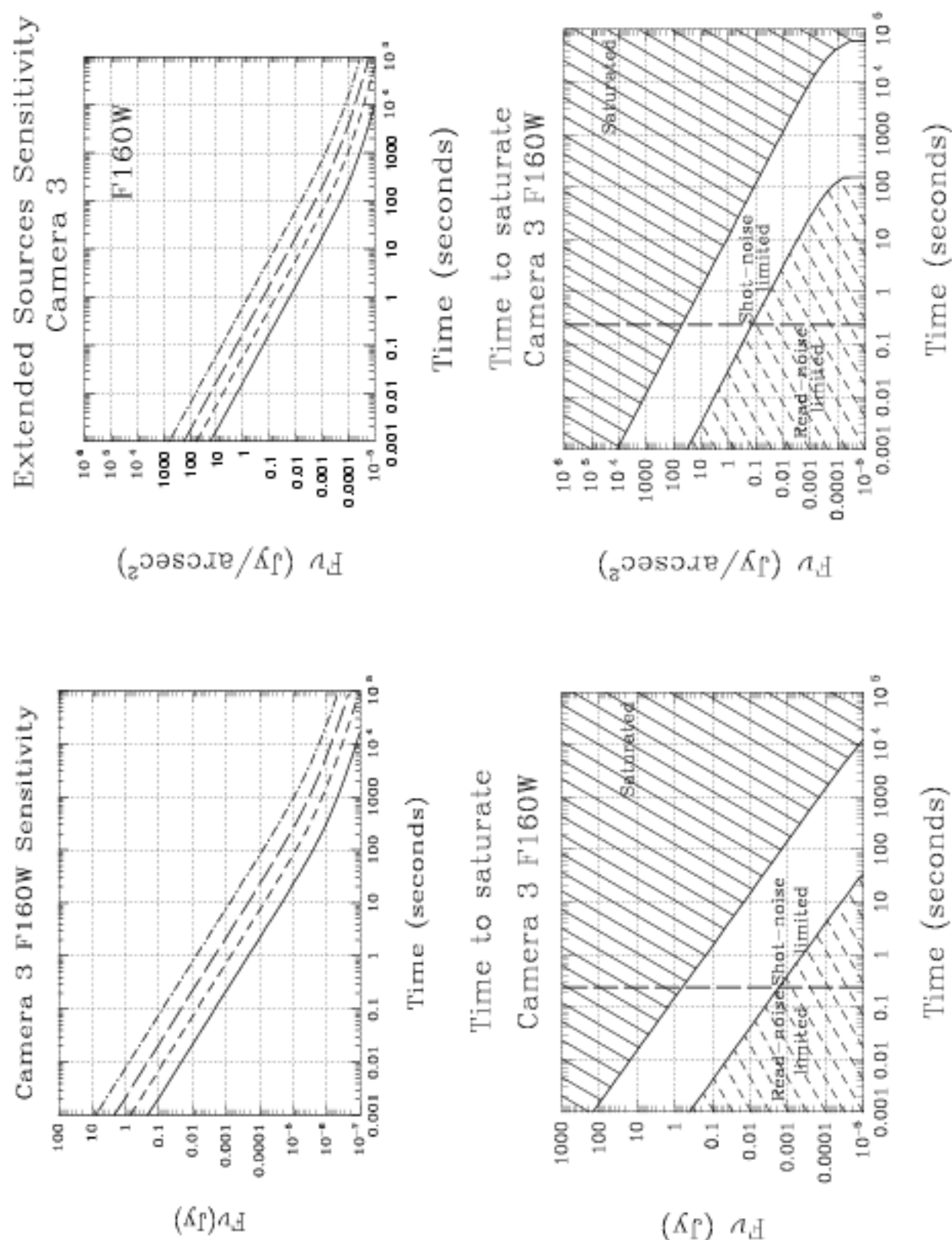


Figure 11.74: Sensitivity and Exclusion Curves for Camera 3, Filter F160W



# Camera 3, Filter F164N

**[FeII] line**  
Also available on Camera 1.

Central wavelength (μm)	Mean wavelength (μm)	Peak wavelength (μm)	FWHM (μm)	Range (μm)	MaxTr %	Pixel Fraction
1.646	1.6460	1.6476	0.0170	1%	86.27	0.76

Figure 11.75: Camera 3, Filter F164N

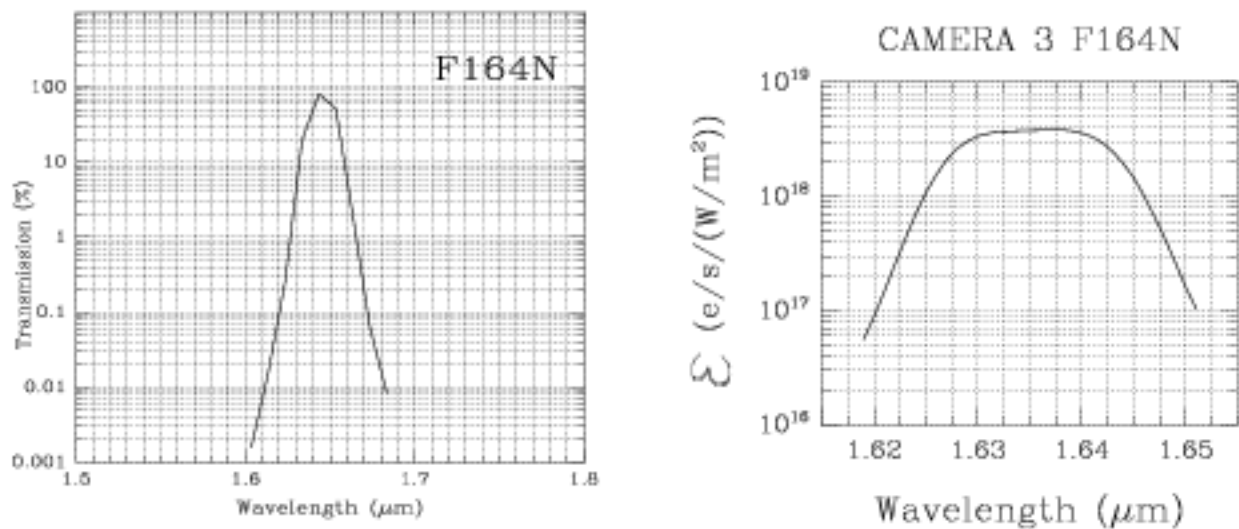
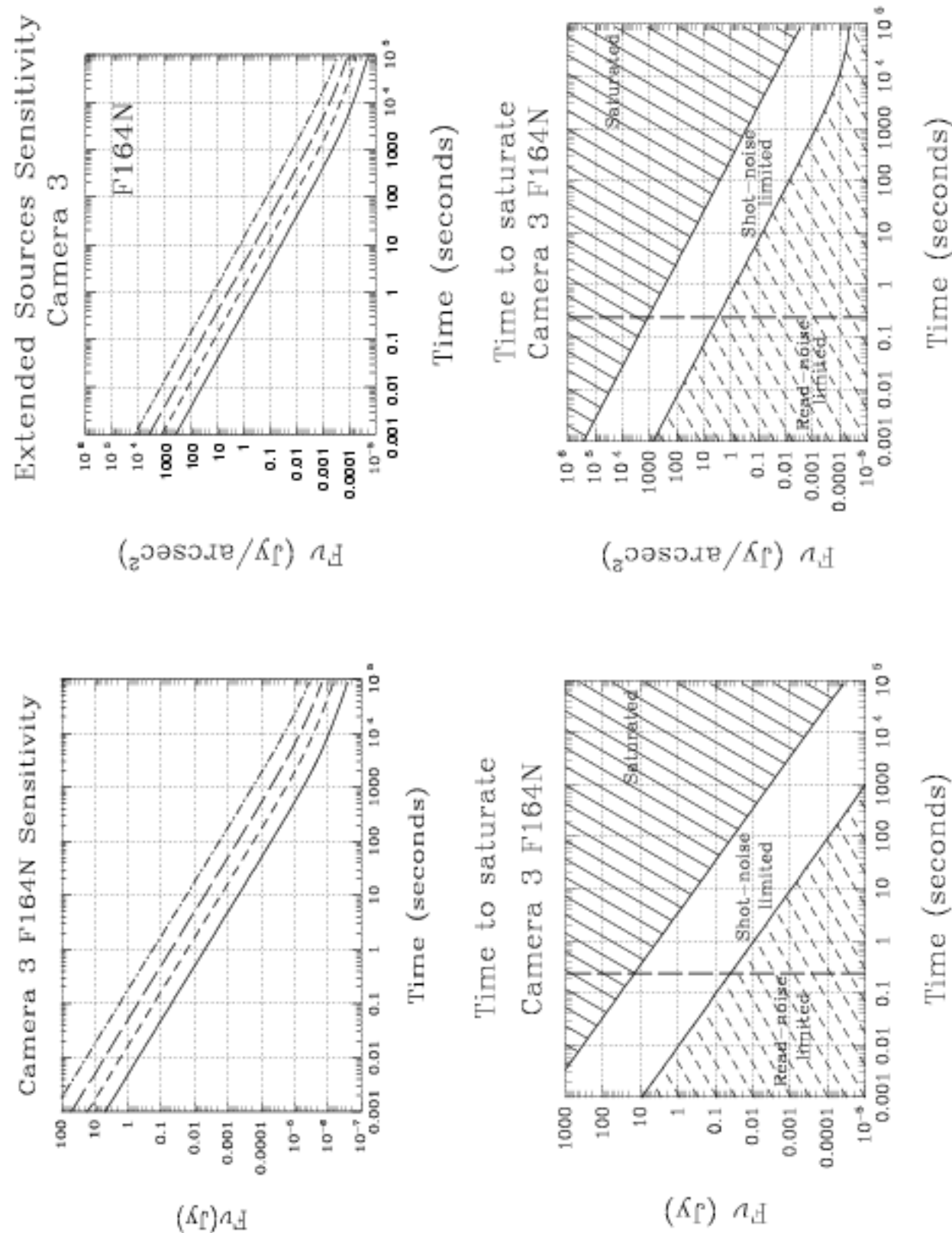




Figure 11.76: Sensitivity and Exclusion Curves for Camera 3, Filter F164N



## Camera 3, Filter F166N

### [FeII] continuum

Also available in Camera 1.

Central wavelength ( $\mu\text{m}$ )	Mean wavelength ( $\mu\text{m}$ )	Peak wavelength ( $\mu\text{m}$ )	FWHM ( $\mu\text{m}$ )	Range ( $\mu\text{m}$ )	MaxTr %	Pixel Fraction
1.6582	1.6582	1.6602	0.0164	1%	87.24	0.75

Figure 11.77: Camera 3, Filter F166N

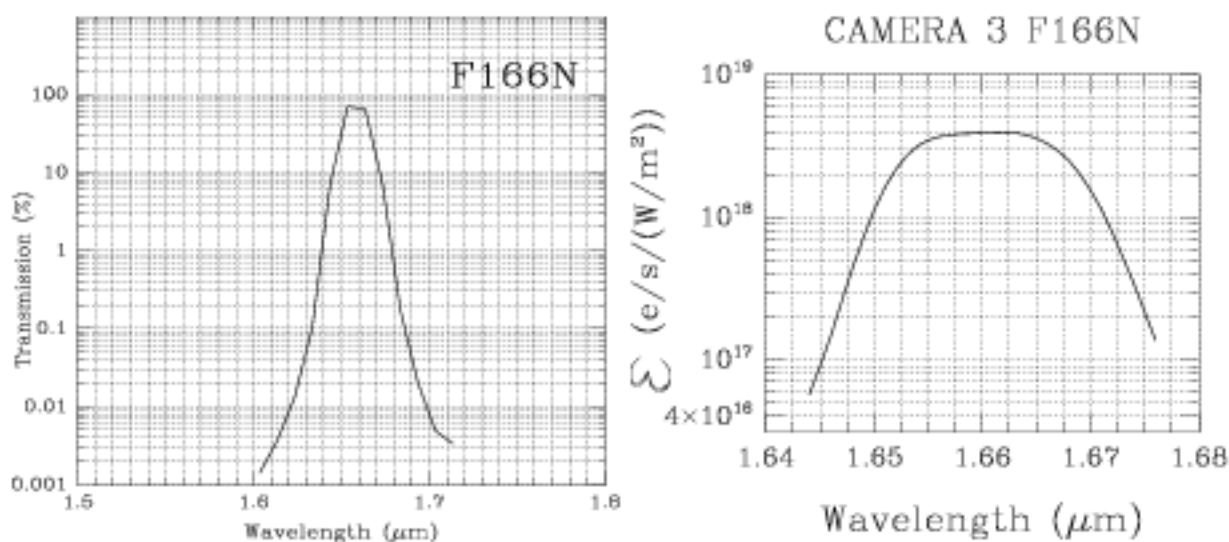
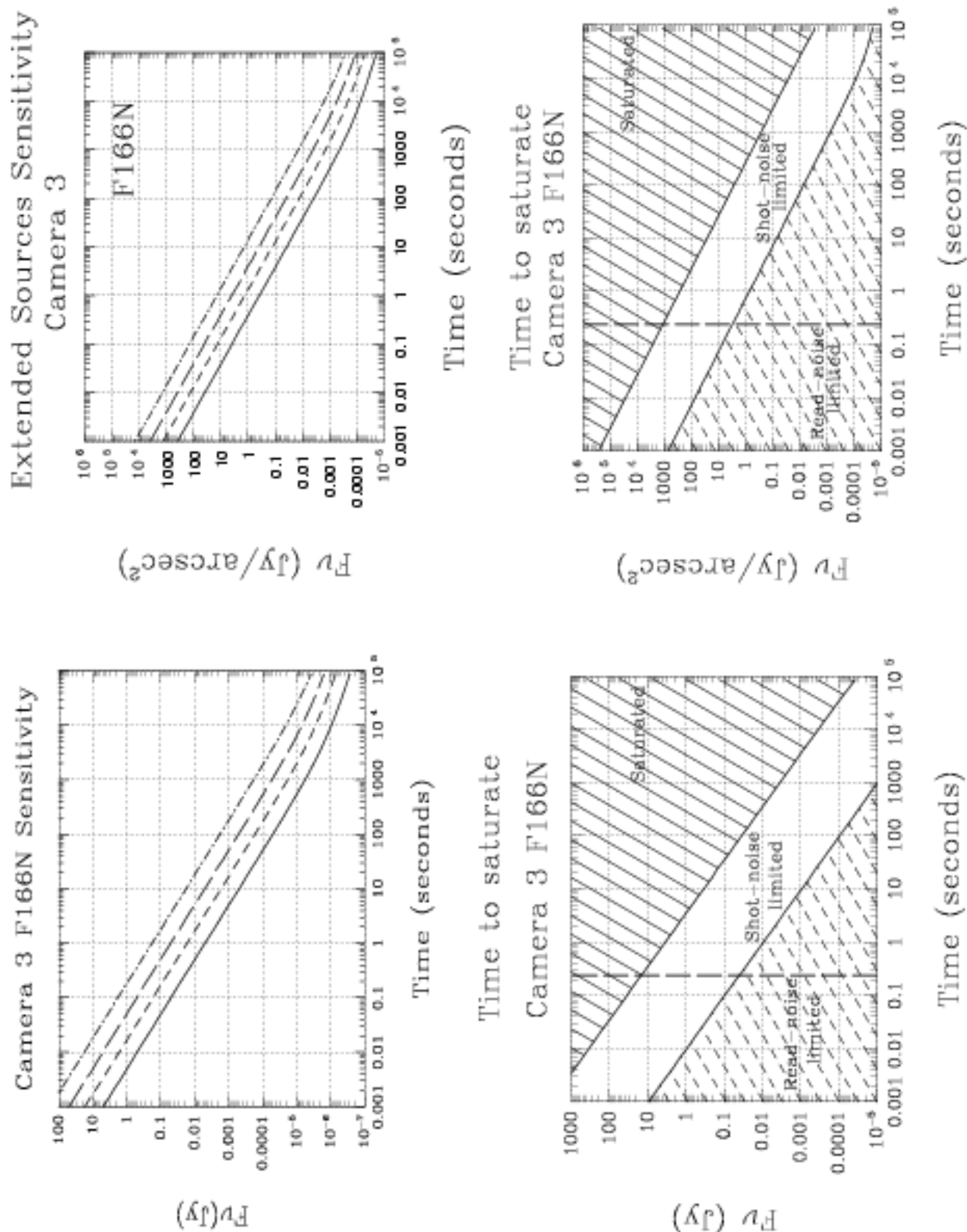


Figure 11.78: Sensitivity and Exclusion Curves for Camera 3, Filter F166N



# Camera 3, Filter F175W

Also available on Cameras 2 and 3.

*Thermal background important.*

Central wavelength (μm)	Mean wavelength (μm)	Peak wavelength (μm)	FWHM (μm)	Range (μm)	MaxTr %	Pixel fraction
1.7530	1.7508	1.9070	1.0940	1.3-2.3	96.58	0.71

Figure 11.79: Camera 3, Filter F175W

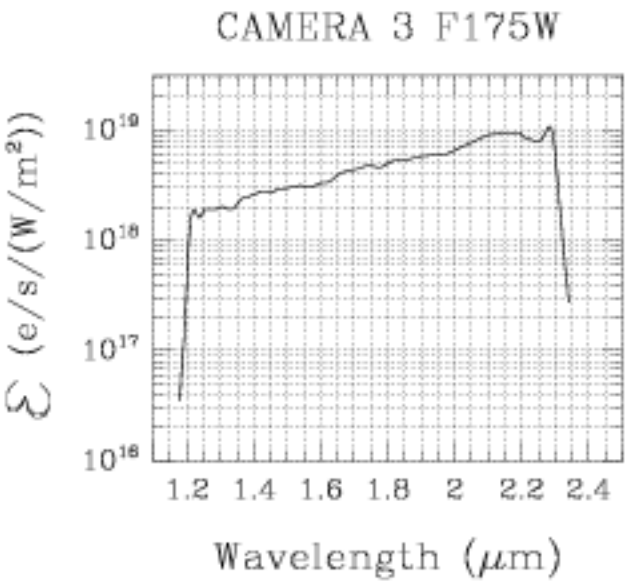
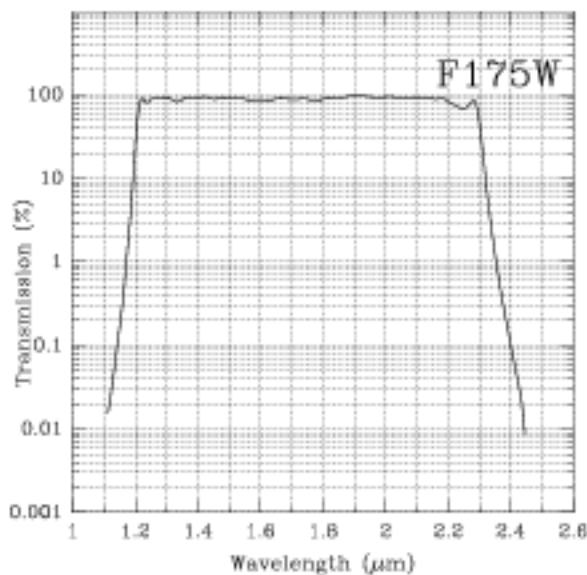
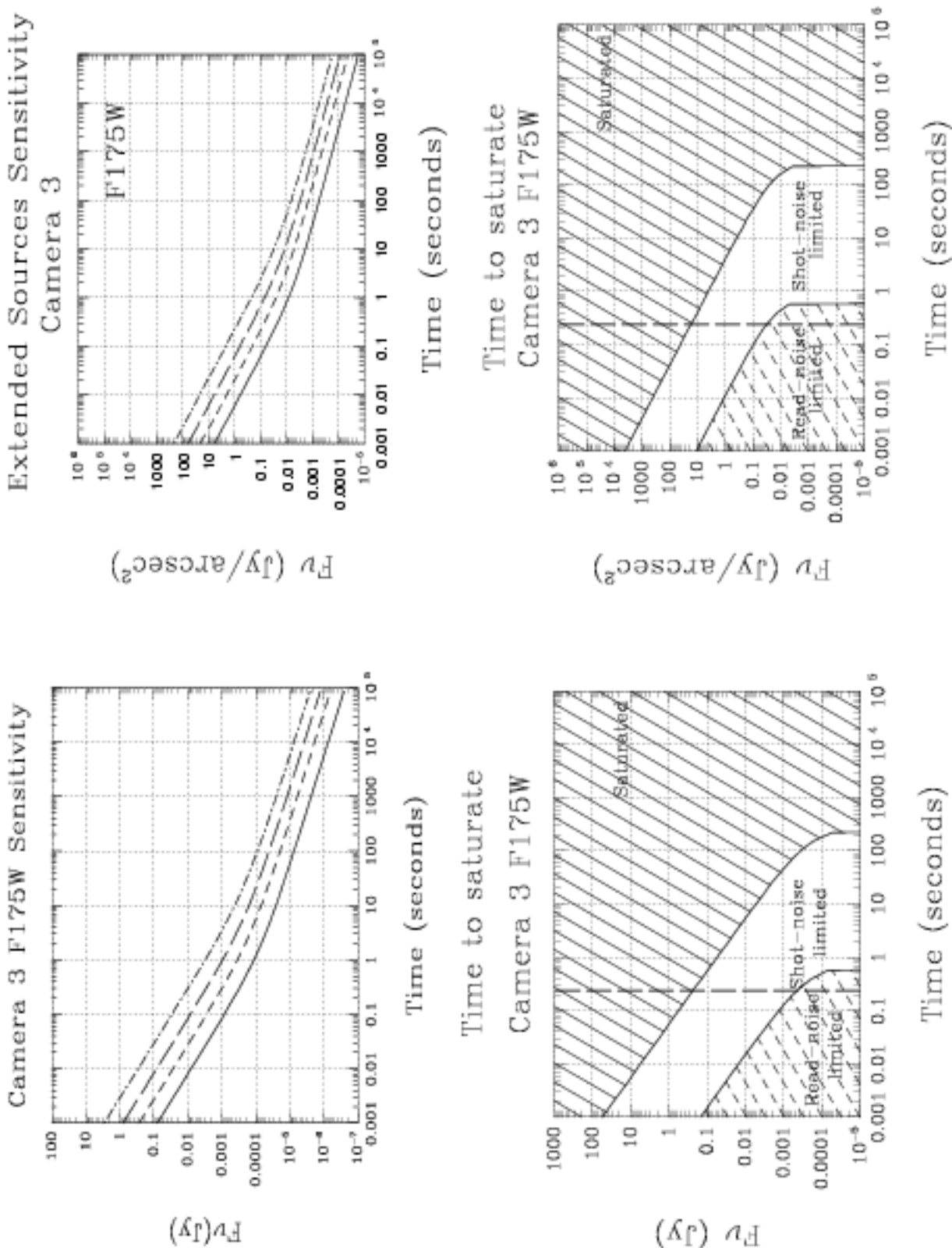


Figure 11.80: Sensitivity and Exclusion Curves for Camera 3, Filter F175W



# Camera 3, Filter F187N

**Paschen  $\alpha$  line**  
Also available on Cameras 1 and 2.

Central wavelength ( $\mu\text{m}$ )	Mean wavelength ( $\mu\text{m}$ )	Peak wavelength ( $\mu\text{m}$ )	FWHM ( $\mu\text{m}$ )	Range	MaxTr %	Pixel fraction
1.8740	1.8738	1.8746	0.0192	1%	88.91	0.71

Figure 11.81: Camera 3, Filter F187N

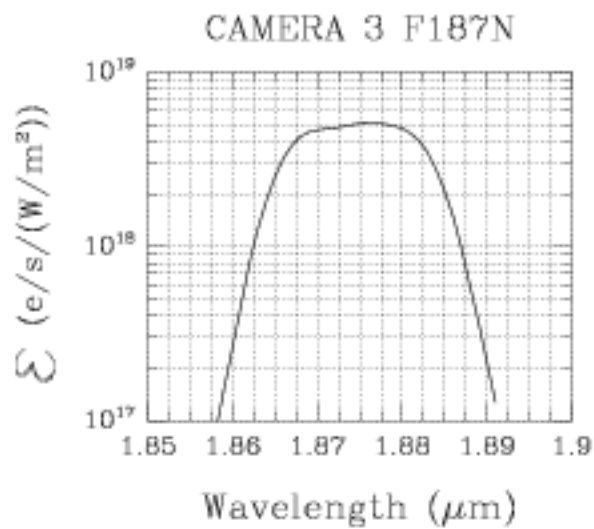
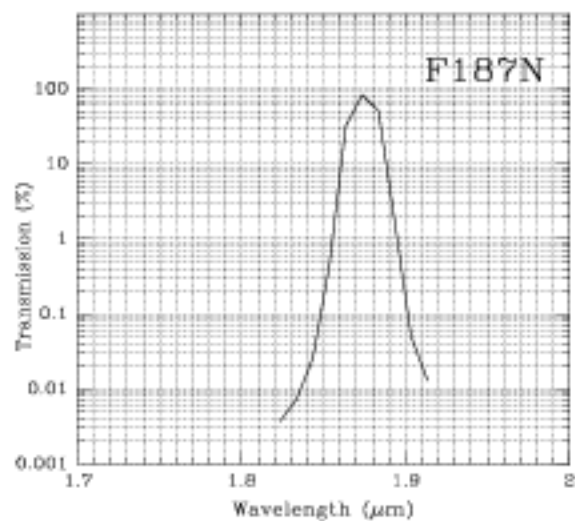
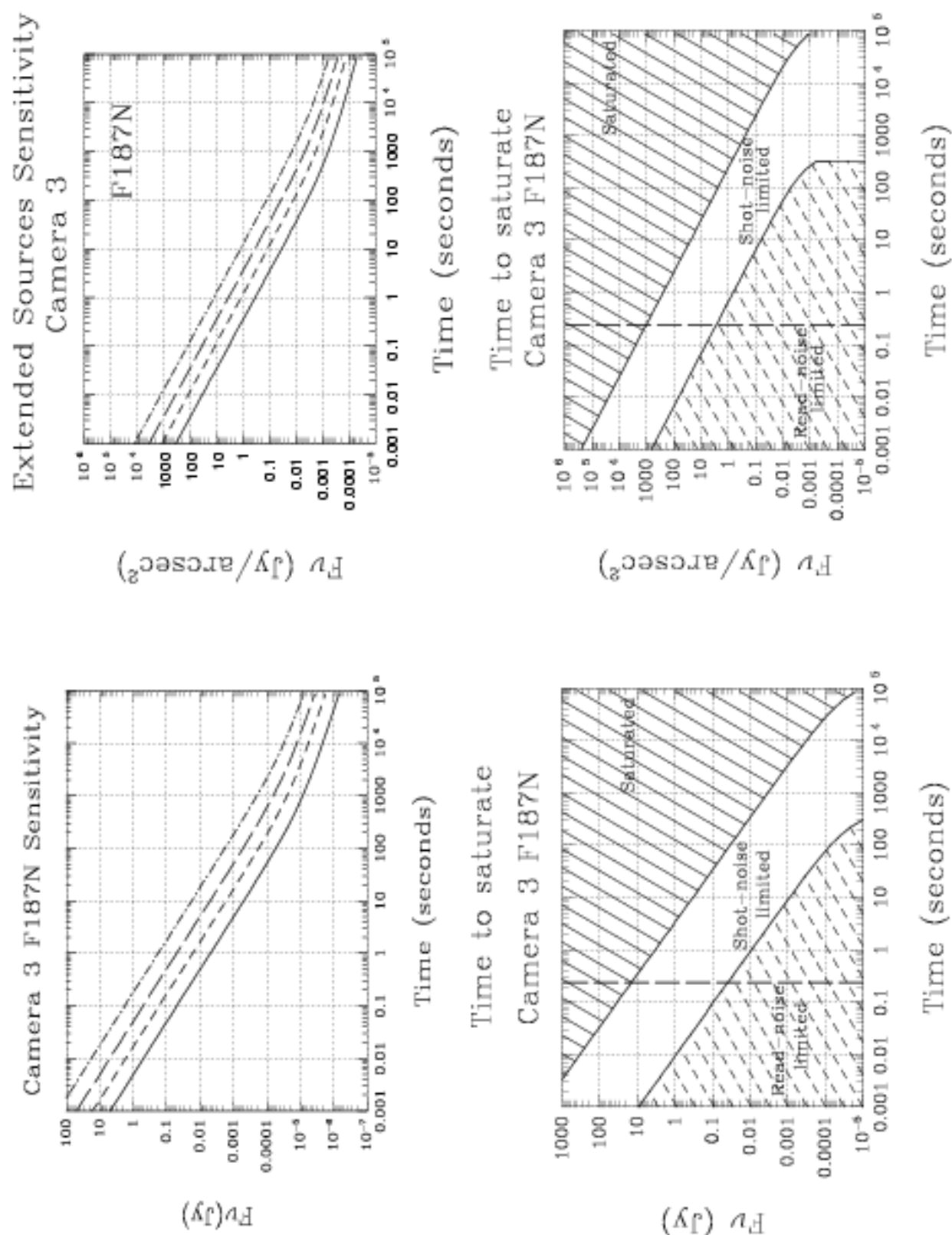


Figure 11.82: Sensitivity and Exclusion Curves for Camera 3, Filter F187N



# Camera 3, Filter F190N

**Paschen  $\alpha$  continuum**  
Also available on Cameras 1 and 2.

Central wavelength ( $\mu\text{m}$ )	Mean wavelength ( $\mu\text{m}$ )	Peak wavelength ( $\mu\text{m}$ )	FWHM ( $\mu\text{m}$ )	Range ( $\mu\text{m}$ )	MaxTr %	Pixel Fraction
1.9005	1.9003	1.9004	0.0174	1%	93.22	0.70

Figure 11.83: Camera 3, Filter F190N

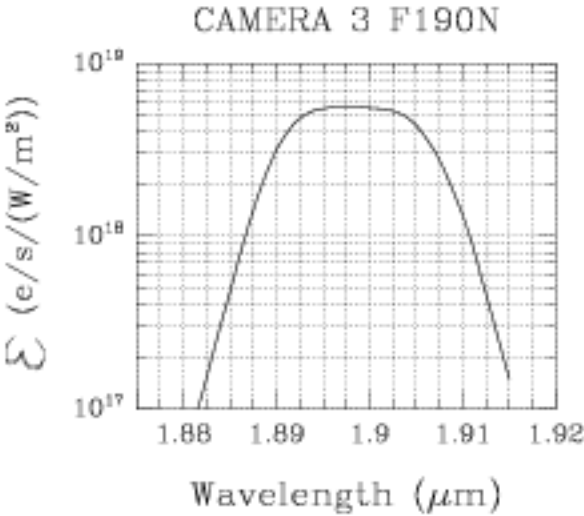
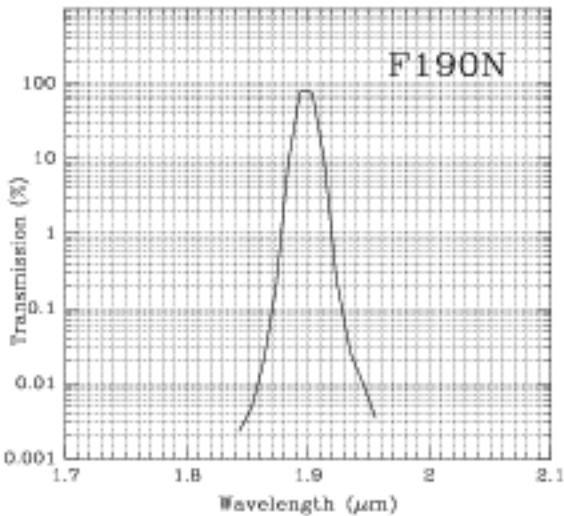
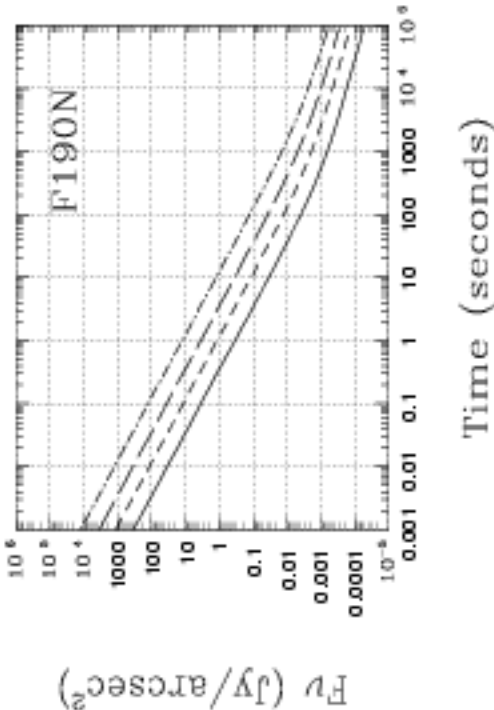


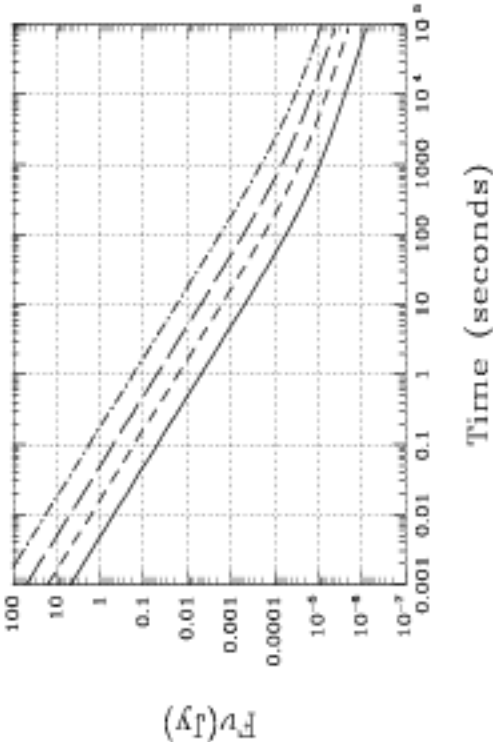


Figure 11.84: Sensitivity and Exclusion Curves for Camera 3, Filter F190N

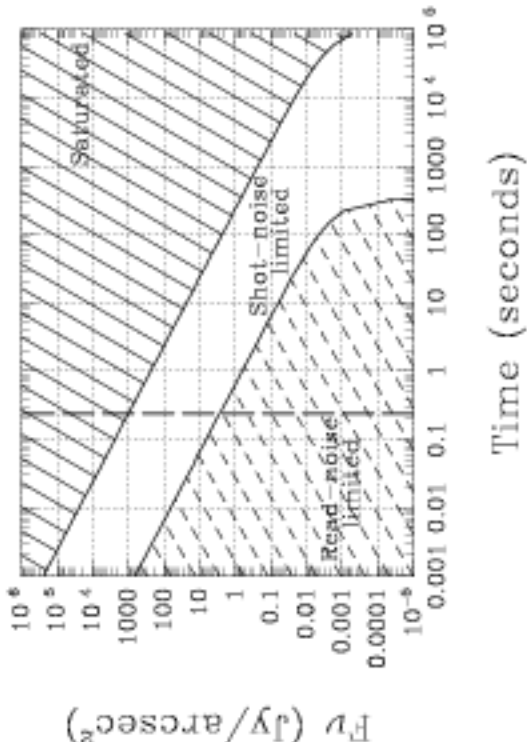
Extended Sources Sensitivity  
Camera 3



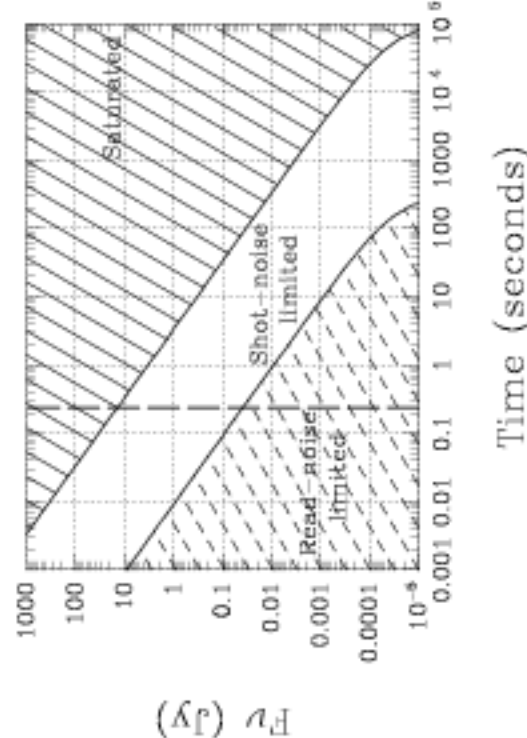
Camera 3 F190N Sensitivity



Time to saturate  
Camera 3 F190N



Time to saturate  
Camera 3 F190N



# Camera 3, Filter F196N

[SIV]  
*Thermal background important.*

Central wavelength (μm)	Mean wavelength (μm)	Peak wavelength (μm)	FWHM (μm)	Range	MaxTr %	Pixel fraction
1.9641	1.9639	1.9698	0.0186	1%	93.74	0.71

Figure 11.85: Camera 3, Filter F196N

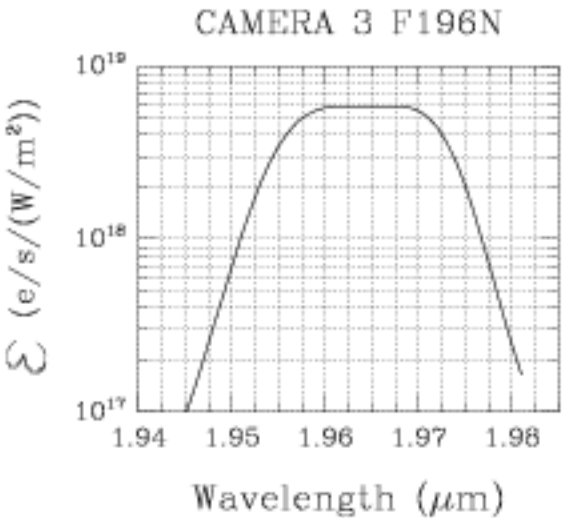
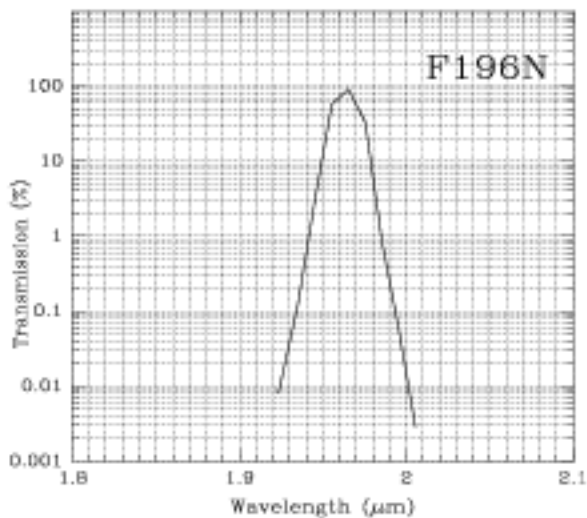
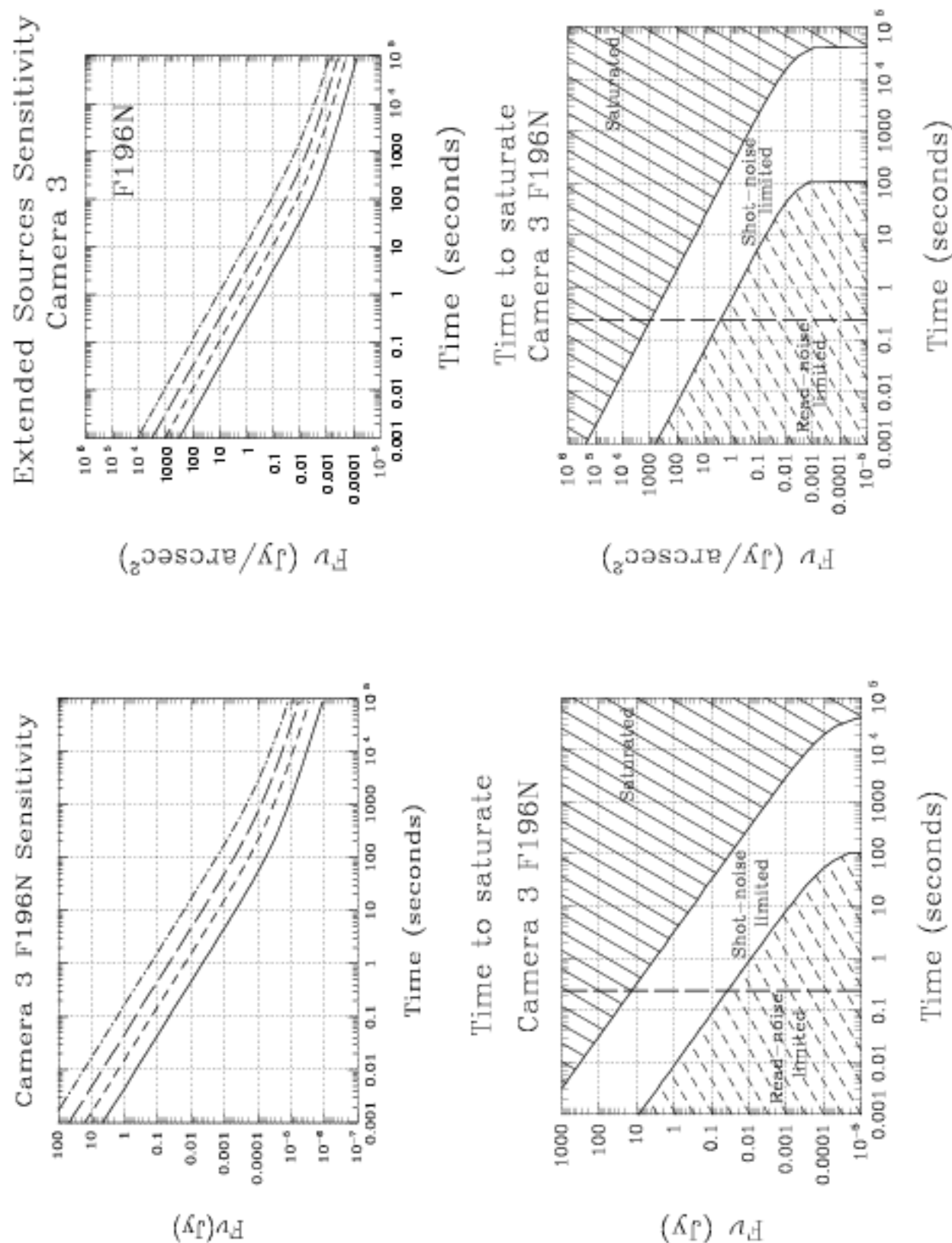


Figure 11.86: Sensitivity and Exclusion Curves for Camera 3, Filter F196N



## Camera 3, Filter F200N

### [SiVI] continuum

*Thermal background important.*

Central wavelength ( $\mu\text{m}$ )	Mean wavelength ( $\mu\text{m}$ )	Peak wavelength ( $\mu\text{m}$ )	FWHM ( $\mu\text{m}$ )	Range ( $\mu\text{m}$ )	MaxTr %	Pixel Fraction
1.9973	1.9974	1.9996	0.0206	1%	91.75	0.71

Figure 11.87: Camera 3, Filter F200N

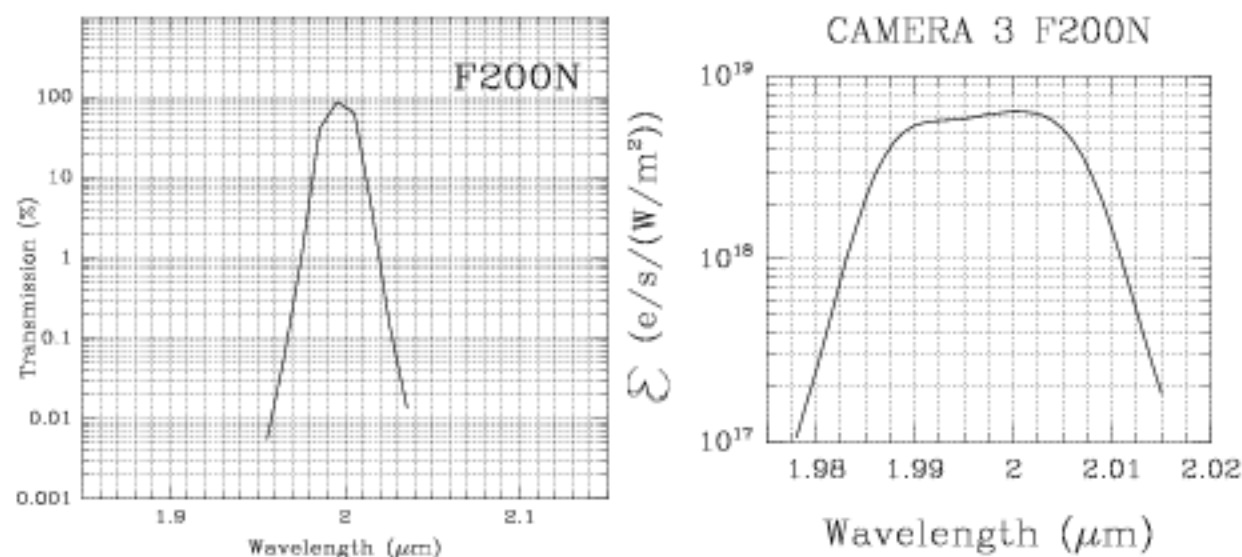
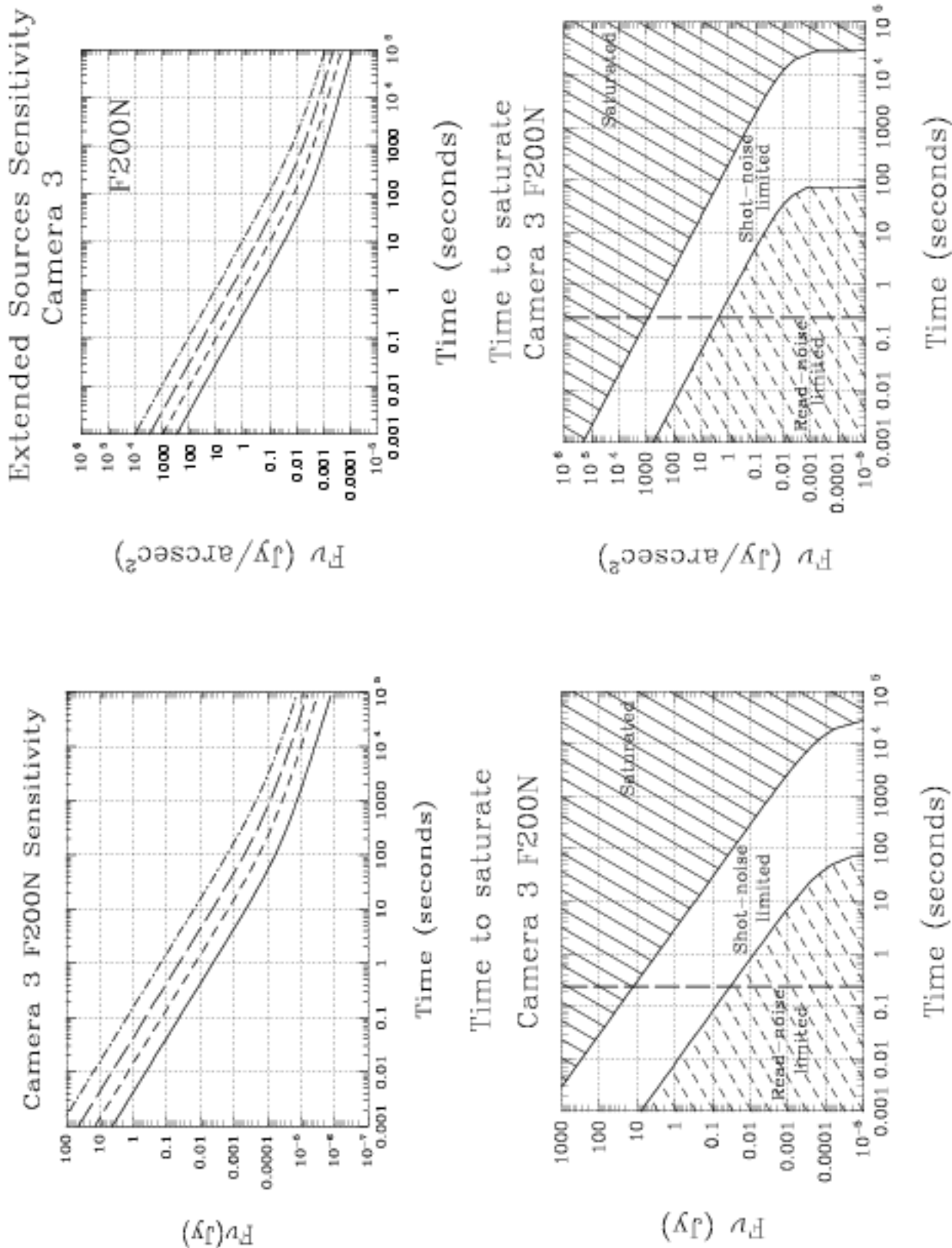


Figure 11.88: Sensitivity and Exclusion Curves for Camera 3, Filter F200N



## Camera 3, Filter F212N

### H<sub>2</sub> line

Also available in Camera 2.

*Thermal background important.*

Central wavelength ( $\mu\text{m}$ )	Mean wavelength ( $\mu\text{m}$ )	Peak wavelength ( $\mu\text{m}$ )	FWHM ( $\mu\text{m}$ )	Range	MaxTr %	Pixel fraction
2.1211	2.1213	2.1228	0.0206	1%	90.90	0.63

Figure 11.89: Camera 3, Filter F212N

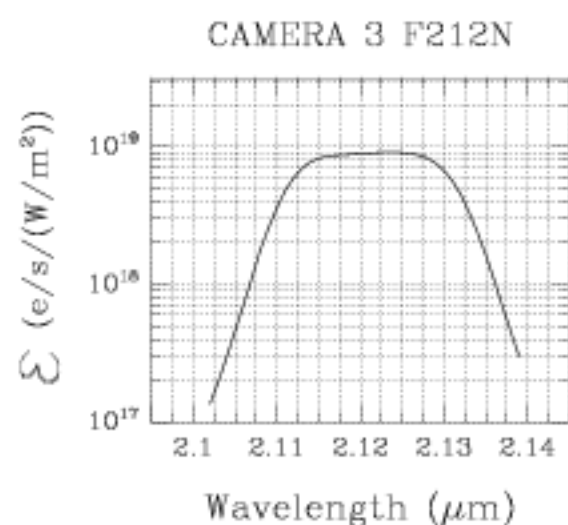
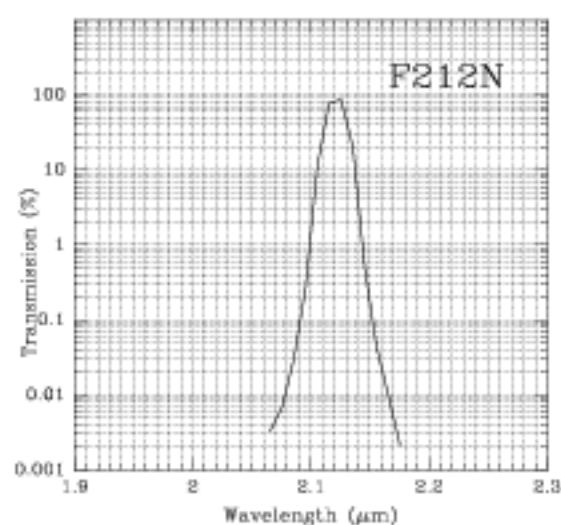
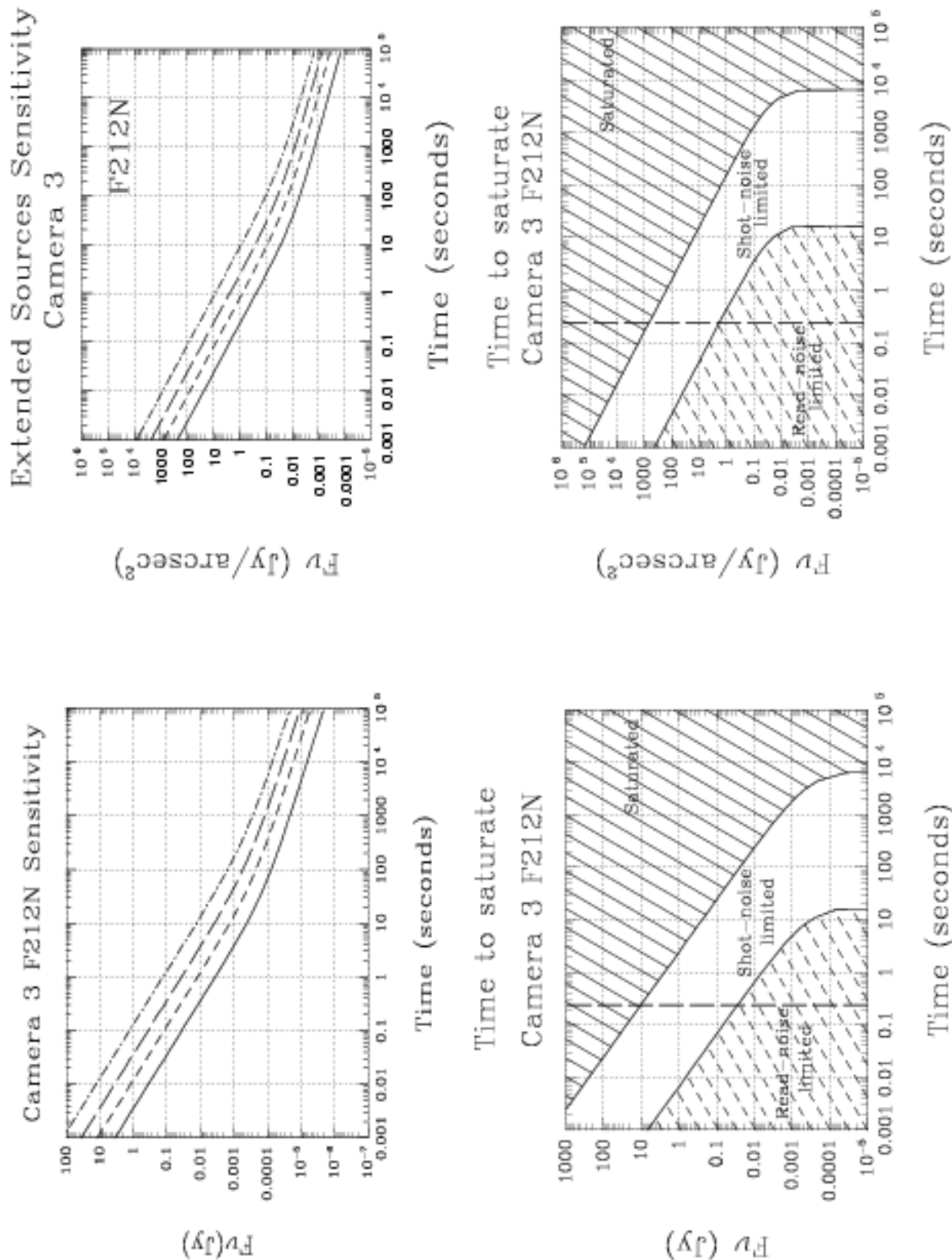


Figure 11.90: Sensitivity and Exclusion Curves for Camera 3, Filter F212N



## Camera 3, Filter F215N

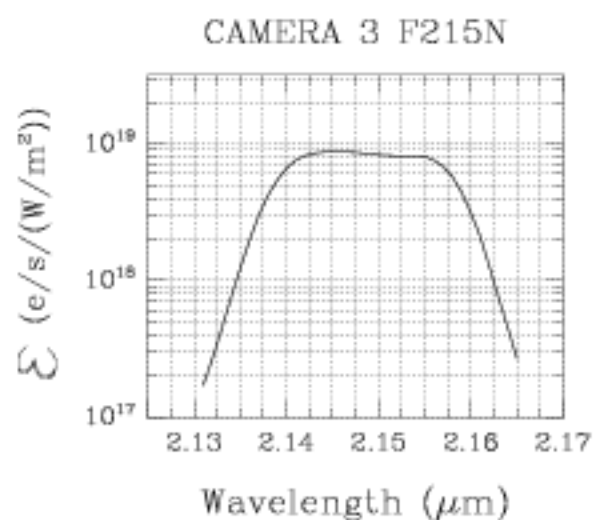
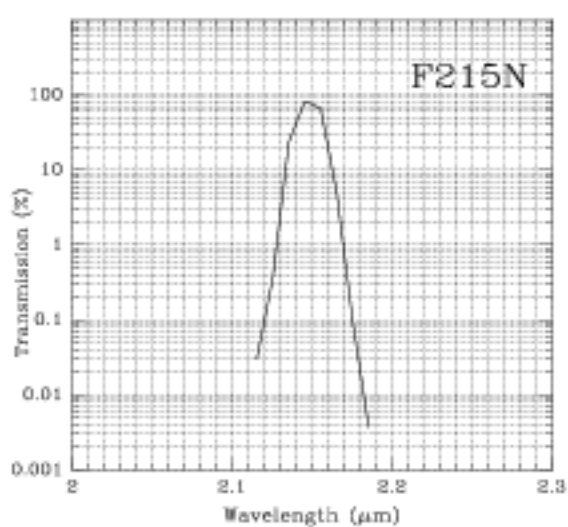
### H<sub>2</sub> continuum

Also available in Camera 2.

*Thermal background important.*

Central wavelength (μm)	Mean wavelength (μm)	Peak wavelength (μm)	FWHM (μm)	Range (μm)	MaxTr %	Pixel Fraction
2.1488	2.1487	2.1562	0.0200	1%	85.91	0.62

Figure 11.91: Camera 3, Filter F215N







## Camera 3, Filter F222M

### CO continuum

Also available on Camera 2.

*Thermal background important.*

Central wavelength (μm)	Mean wavelength (μm)	Peak wavelength (μm)	FWHM (μm)	Range (μm)	MaxTr %	Pixel Fraction
2.216	2.216	2.18	0.1432	2.15-2.3	89.9	0.55

Figure 11.93: Camera 3, Filter F222M

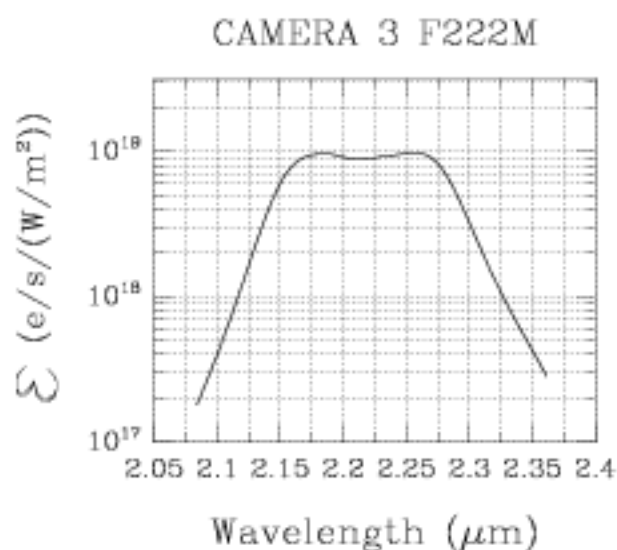
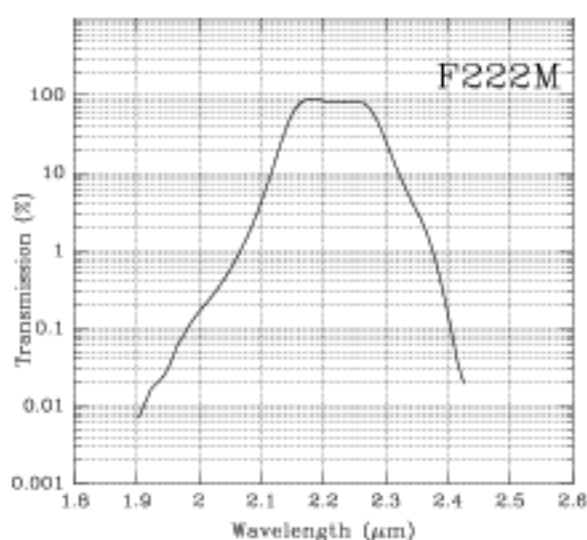
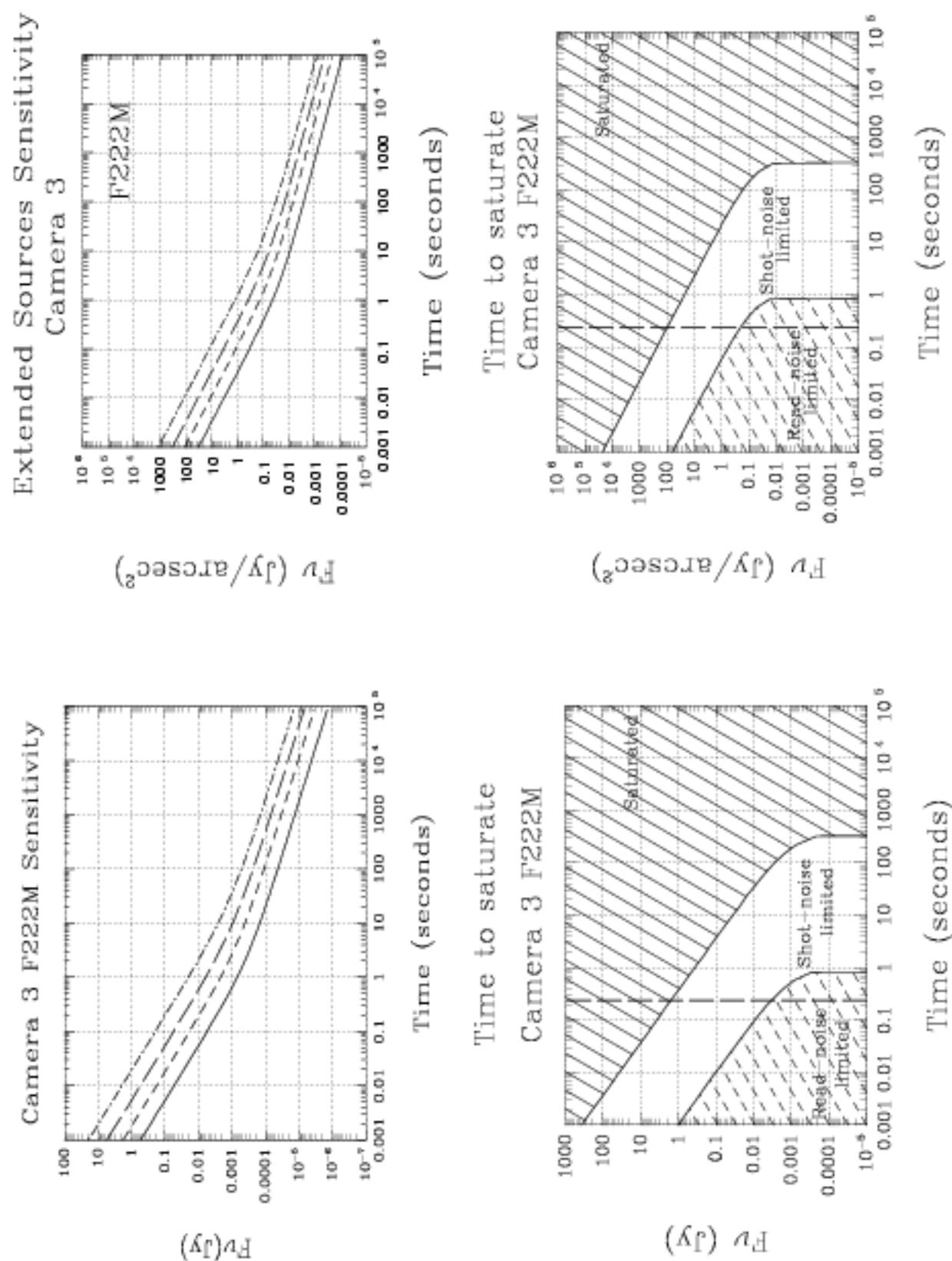


Figure 11.94: Sensitivity and Exclusion Curves for Camera 3, Filter F222M



## Camera 3, Filter F240M

### CO band

*Thermal background important.*

Central wavelength ( $\mu\text{m}$ )	Mean wavelength ( $\mu\text{m}$ )	Peak wavelength ( $\mu\text{m}$ )	FWHM ( $\mu\text{m}$ )	Range ( $\mu\text{m}$ )	MaxTr %	Pixel Fraction
2.3978	2.3977	2.3155	0.1975	2.3-2.5	92.43	0.49

Figure 11.95: Camera 3, Filter F240M

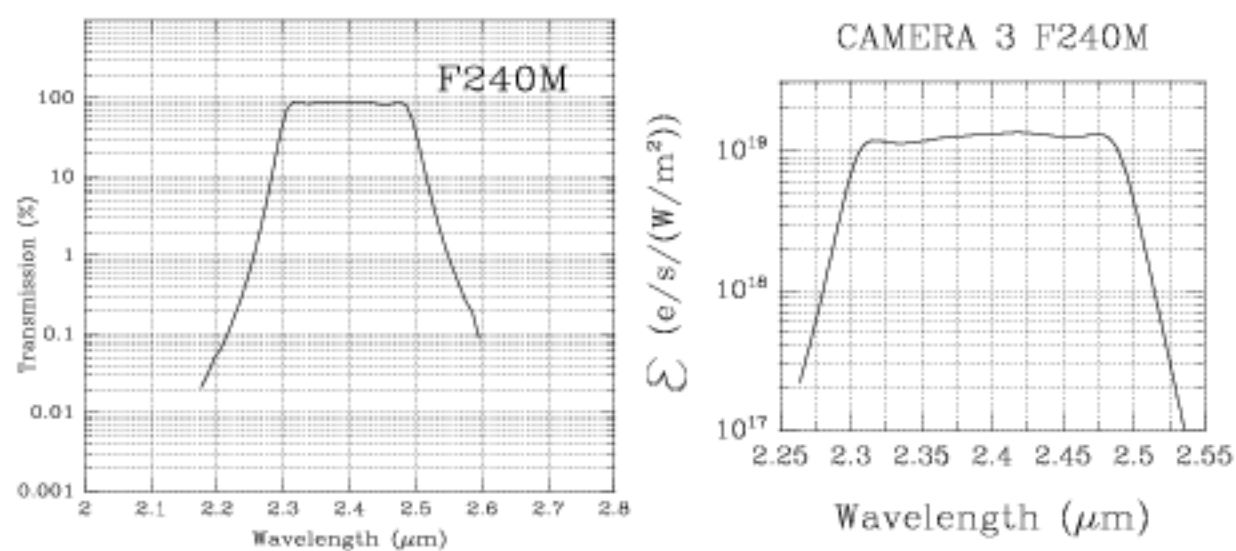
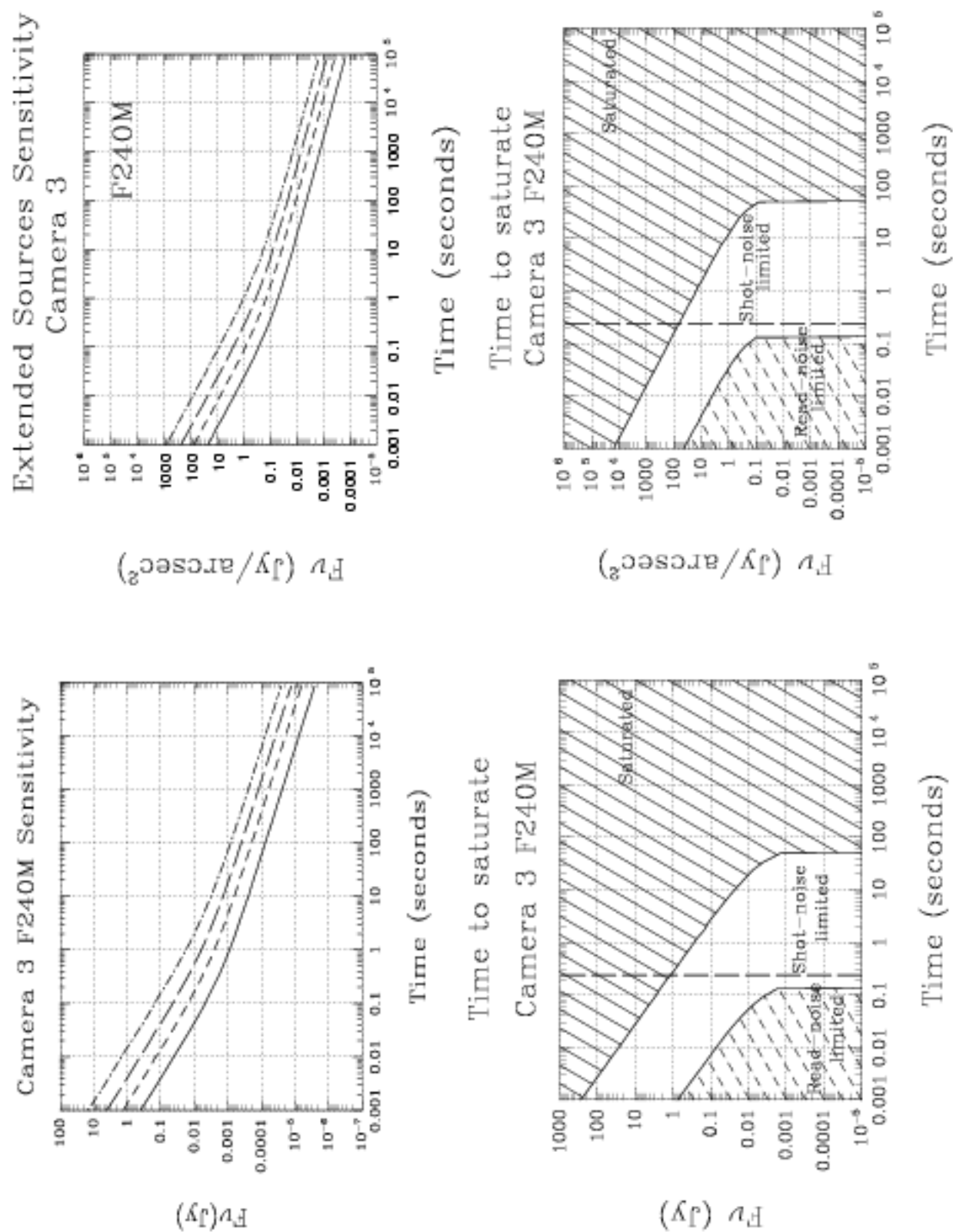


Figure 11.96: Sensitivity and Exclusion Curves for Camera 3, Filter F240M





## CHAPTER 12

# Flux Units and Line Lists

### In This Chapter...

Infrared Flux Units / 253
Formulae / 255
Look-up Tables and Software / 257
Examples / 264
Infrared Line Lists / 264

In this chapter we provide a variety of background material that may be useful when preparing proposals. This material includes a discussion of the flux and surface brightness units often used in the infrared, which may not be familiar to some users, plus a large compilation of spectral lines that may be encountered in the infrared, and which are either in the NLCMOS waveband or which are related to lines which are.

---

## Infrared Flux Units

In the infrared, as in the optical, the means of reporting source brightnesses and the units employed have varied considerably. In recent years, however, magnitude systems have been used less frequently, and the most popular unit for expressing brightnesses, both for point source fluxes and surface brightnesses, is steadily becoming the Jansky. We have adopted the Jansky as the standard flux unit for NLCMOS in our documentation and in observer-oriented software. Here we provide some simple formulae and tables to facilitate the conversion from other units into Jy.

## Background

Infrared astronomy really began in the 1960s, when the vast majority of astronomy was still carried out in the visual region. Flux measurements were routinely reported in the UBV magnitude system, and to attempt to integrate IR astronomy into this system, Johnson (*Ap.J.*, **134**, 69) defined the first IR magnitude system. This involved four new photometric bands, the J, K, L and M bands which were centered on wavelengths of 1.3, 2.2, 3.6 and 5.0 microns. These bands were defined not only by the filter bandpasses, but also by the wavebands of the ‘windows’ of high transmission through the atmosphere. In this system, all measurements were referred to the Sun, which was assumed to be a G2V star with an effective temperature of 5785K, and was taken to have a V-K color of roughly +2.2. From his own measurements in this system, Johnson determined Vega to have a K magnitude of +0.02 and K-L=+0.04.

Until the early 1980s IR astronomical observations were restricted to spectra or single channel photometry, and most photometry was reported in systems at least loosely based on Johnson’s system, though with the addition of a new band at 1.6 microns known as the H band and the development of two bands in place of the one formerly defined by Johnson as the L band, a new definition of the L band centered on 3.4 microns, and a rather narrower band known as L’ centered on 3.74 microns.

As the new science of infrared astronomy rapidly expanded its wavelength coverage, many new photometric bands were adopted, both for ground-based observations and for use by the many balloon- and rocket-borne observations and surveys. The differing constraints presented by these different environments for IR telescopes resulted in systems with disappointingly little commonality or overlap, and today the IR astronomer is left with a plethora of different systems to work with.

The IRAS survey results, which were published in 1986, presented observations made photometrically in four bands in the mid- and far-infrared, and mid-infrared spectra, and all were presented in units of Janskys, rather than defining yet another new magnitude system. Since then, IR data from many sites around the world have been increasingly commonly presented in Janskys (Jy), or in Jy/arcsec<sup>2</sup> in the case of surface brightness data (although IRAS maps are often presented in the rather grandiloquent units of MJy/steradian).

Ground-based mid-IR photometry is usually carried out using the N and Q photometric bands, which are themselves defined more by the atmospheric transmission than by any purely scientific regard. IRAS, freed of the constraints imposed by the atmosphere, adopted its own 12 micron and 25 micron bands, which were extremely broad and therefore offered high sensitivity. Similarly, NICMOS, being above the atmosphere, is not forced to adopt filter bandpasses (See Chapter 4) like those used at ground-based observatories, but instead has filters constrained purely by the anticipated scientific demands. Thus in practice NICMOS does not have filters matched to any of the standard ground-based photometric bands.



## Units for NICMOS

In order to facilitate proposal preparation by observers, STScI is making available a number of computer programs to assist with signal to noise ratio and integration time calculations. We have also presented a great deal of sensitivity information here in Chapters 11 and 5 of the *NICMOS Instrument Handbook*. Given the multitude of units and systems that have been used for IR photometry (magnitudes, Janskys,  $\text{Wm}^{-2}\mu\text{m}^{-1}$ ,  $\text{Wcm}^{-2}\mu\text{m}^{-1}$ , erg  $\text{sec}^{-1}\text{cm}^{-2}\mu\text{m}^{-1}$ ) and for surface brightness measurements (Janskys  $\text{arcsec}^{-2}$ , MJy  $\text{steradian}^{-1}$ , magnitudes  $\text{arcsec}^{-2}$ ), presenting these data to observers could become somewhat cumbersome. Additionally, given the lack of any *standard* IR filters (as explained above), in order to express brightnesses in magnitudes we would have to adopt our own NICMOS magnitude system, and observers would have to transform ground-based photometry into the NICMOS bands. We have therefore adopted a single standard set of flux units, Janskys for all photometry and spectroscopy, and Janskys  $\text{arcsec}^{-2}$  for all surface brightness measurements in all NICMOS documentation and observer-oriented software. The NICMOS calibration pipeline software will deliver results calibrated in Janskys  $\text{arcsec}^{-2}$ .

We are aware that some observers do not routinely use these units, and therefore below we give a set of simple formulae to use to convert between systems, and some conversion tables. In the future we will also make available, via the World Wide Web, software to perform conversions between different systems and units.

---

## Formulae

### Converting Between $F_{\nu}$ and $F_{\lambda}$

One Jansky (Jy) is defined as  $10^{-26}\text{Wm}^{-2}\text{Hz}^{-1}$ , so it is a unit of measurement of the spectral flux density,  $F_{\nu}$ .

For  $F_{\nu}$  in Jy, use the following formula:

$$F_{\lambda} = \beta F_{\nu} / \lambda^2,$$

where  $\lambda$  is the wavelength in microns ( $\mu\text{m}$ ), and  $\beta$  is a constant chosen from Table 12.1 and depending on the units of  $F_{\lambda}$ . (This is simply derived, using the fact that  $d\nu/d\lambda = c/\lambda^2$ .)

Table 12.1: Constants for Converting  $F_\lambda$  and  $F_V$ 

$F_\lambda$ measured in	$\beta$
$\text{Wm}^{-2}\mu\text{m}^{-1}$	$3 \times 10^{-12}$
$\text{Wcm}^{-2}\mu\text{m}^{-1}$	$3 \times 10^{-16}$
$\text{erg sec}^{-1} \text{cm}^{-2} \mu\text{m}^{-1}$	$3 \times 10^{-9}$
$\text{erg sec}^{-1} \text{cm}^{-2} \text{\AA}^{-1}$	$3 \times 10^{-13}$

Remember that  $1 \text{ W} = 10^7 \text{ erg sec}^{-1}$ , and  $1 \mu\text{m} = 10^4 \text{\AA}$ .

## Conversion Between Fluxes and Magnitudes

The spectral flux density  $F_V$  can be calculated from its magnitude as

$$F_V = 10^{-m/2.5} F_0$$

where  $m$  is the magnitude and  $F_0$  the zero-point flux for the given photometric band. We list the central wavelengths and zero-point fluxes for the more commonly encountered photometric bands below in Table 12.2. The CIT system was originally based on Beckwith et al (1976, Ap.J., **208**, 390); the UKIRT system is in fact based on the original CIT system, but with adjustments made largely owing to different filter bandpasses. It should be noted that for a given photometric band there will be small differences in the effective wavelength and zero-point flux from one observatory to another, and for astronomical objects with radically different colors, so these figures can only be treated as approximate.

**Table 12.2:** Effective Wavelengths and Zero-points for Photometric Bands

Band	$\lambda[\mu\text{m}]$	$F_0[\text{Jy}]$ (CIT)	$F_0[\text{Jy}]$ (UKIRT)
V	0.56	3540	3540
R	0.70	2870	-
I	0.90	2250	-
J	1.25	1670	1600
H	1.65	980	1030
K	2.2	630	657
L	3.4	280	290
L'	3.74	-	252
M	4.8	150	163
N	10.1	37	39.8
Q	20.0	10	10.4

### Conversion Between Surface Brightness Units

Surface brightnesses are generally measured in Janskys  $\text{arcsec}^{-2}$ , MJy  $\text{steradian}^{-1}$  or magnitudes  $\text{arcsec}^{-2}$ . If you have a surface brightness  $S_V$  in MJy  $\text{steradian}^{-1}$ , then you can use:

$$S_V[\text{Jy arcsec}^{-2}] = S_V[\text{MJy ster}^{-1}] \times 0.084616.$$

If you have  $S_V$  in magnitudes  $\text{arcsec}^{-2}$ , you can simply use the formula and zero-points as given in the previous section for point sources.

---

## Look-up Tables and Software

In this section we provide look-up tables to facilitate rapid, approximate conversion between the different systems mentioned in the preceding section.

For both integrated source fluxes and surface brightnesses, we provide tables of conversions between systems at the wavelengths of the four commonly used photometric bands which cover the NICMOS operating waveband of 0.8–2.5 microns. To carry out some of the conversions described here, some simple Fortran programs will soon be available on the NICMOS World Wide Web pages at STScI. We are adopting here the CIT system defined in Table 12.2.

By using Table 12.3 it is possible to estimate the CIT magnitude corresponding to any flux in Jy, by using the property that multiplying or dividing the flux by one hundred adds or subtracts five magnitudes.

Table 12.3:  $F_V$  to Magnitude Conversion

$F_V$ [Jy]	I	J	H	K
10.0	5.88	5.56	4.98	4.48
8.0	6.12	5.80	5.22	4.72
6.0	6.44	6.11	5.53	5.04
5.0	6.63	6.31	5.73	5.23
4.0	6.88	6.55	5.97	5.48
3.0	7.19	6.86	6.29	5.79
2.5	7.39	7.06	6.48	5.99
2.0	7.63	7.30	6.73	6.23
1.5	7.94	7.62	7.04	6.54
1.25	8.14	7.81	7.24	6.74
1.0	8.38	8.06	7.48	6.98
0.8	8.62	8.30	7.72	7.22
0.6	8.94	8.61	8.03	7.54
0.5	9.13	8.81	8.23	7.73
0.4	9.38	9.05	8.47	7.98
0.3	9.69	9.36	8.79	8.29
0.25	9.89	9.57	8.98	8.49
0.2	10.13	9.8	9.23	8.73
0.15	10.44	10.12	9.54	9.04
0.125	10.64	10.31	9.74	9.24
0.1	10.88	10.56	9.98	9.48

Table 12.4: I- Band Flux Conversion

$F_{\nu}$ [Jy]	$I$ [mag]	$F_{\lambda}$ [W m <sup>-2</sup> μm <sup>-1</sup> ]	$F_{\lambda}$ [W cm <sup>-2</sup> μm <sup>-1</sup> ]	$F_{\lambda}$ [erg s <sup>-1</sup> cm <sup>-2</sup> Å <sup>-1</sup> ]
2250	0.0	$8.32 \times 10^{-9}$	$8.32 \times 10^{-13}$	$8.32 \times 10^{-10}$
894	1.0	$3.312 \times 10^{-9}$	$3.312 \times 10^{-13}$	$3.312 \times 10^{-10}$
356	2.0	$1.319 \times 10^{-9}$	$1.319 \times 10^{-13}$	$1.319 \times 10^{-10}$
142	3.0	$5.25 \times 10^{-10}$	$5.25 \times 10^{-14}$	$5.25 \times 10^{-11}$
56.4	4.0	$2.09 \times 10^{-10}$	$2.09 \times 10^{-14}$	$2.09 \times 10^{-11}$
22.5	5.0	$8.32 \times 10^{-11}$	$8.32 \times 10^{-15}$	$8.32 \times 10^{-12}$
8.94	6.0	$3.312 \times 10^{-11}$	$3.312 \times 10^{-15}$	$3.312 \times 10^{-12}$
3.56	7.0	$1.319 \times 10^{-11}$	$1.319 \times 10^{-15}$	$1.319 \times 10^{-12}$
1.42	8.0	$5.25 \times 10^{-12}$	$5.25 \times 10^{-16}$	$5.25 \times 10^{-13}$
0.564	9.0	$2.09 \times 10^{-12}$	$2.09 \times 10^{-16}$	$2.09 \times 10^{-13}$
0.225	10.0	$8.32 \times 10^{-13}$	$8.32 \times 10^{-17}$	$8.32 \times 10^{-14}$
0.0894	11.0	$3.312 \times 10^{-13}$	$3.312 \times 10^{-17}$	$3.312 \times 10^{-14}$
0.0356	12.0	$1.319 \times 10^{-13}$	$1.319 \times 10^{-17}$	$1.319 \times 10^{-14}$
0.0142	13.0	$5.25 \times 10^{-14}$	$5.25 \times 10^{-18}$	$5.25 \times 10^{-15}$
0.00564	14.0	$2.09 \times 10^{-14}$	$2.09 \times 10^{-18}$	$2.09 \times 10^{-15}$
0.00225	15.0	$8.32 \times 10^{-15}$	$8.32 \times 10^{-19}$	$8.32 \times 10^{-16}$
$8.94 \times 10^{-4}$	16.0	$3.312 \times 10^{-15}$	$3.312 \times 10^{-19}$	$3.312 \times 10^{-16}$
$3.56 \times 10^{-4}$	17.0	$1.319 \times 10^{-15}$	$1.319 \times 10^{-19}$	$1.319 \times 10^{-16}$
$1.42 \times 10^{-4}$	18.0	$5.25 \times 10^{-16}$	$5.25 \times 10^{-20}$	$5.25 \times 10^{-17}$
$5.64 \times 10^{-5}$	19.0	$2.09 \times 10^{-16}$	$2.09 \times 10^{-20}$	$2.09 \times 10^{-17}$
$2.25 \times 10^{-5}$	20.0	$8.32 \times 10^{-17}$	$8.32 \times 10^{-21}$	$8.32 \times 10^{-18}$
$8.94 \times 10^{-6}$	21.0	$3.312 \times 10^{-17}$	$3.312 \times 10^{-21}$	$3.312 \times 10^{-18}$
$3.56 \times 10^{-6}$	22.0	$1.319 \times 10^{-17}$	$1.319 \times 10^{-21}$	$1.319 \times 10^{-18}$
$1.42 \times 10^{-6}$	23.0	$5.25 \times 10^{-18}$	$5.25 \times 10^{-22}$	$5.25 \times 10^{-19}$
$5.64 \times 10^{-7}$	24.0	$2.09 \times 10^{-18}$	$2.09 \times 10^{-22}$	$2.09 \times 10^{-19}$
$2.25 \times 10^{-7}$	25.0	$8.32 \times 10^{-19}$	$8.32 \times 10^{-23}$	$8.32 \times 10^{-20}$
$8.94 \times 10^{-8}$	26.0	$3.312 \times 10^{-19}$	$3.312 \times 10^{-23}$	$3.312 \times 10^{-20}$

Table 12.5: J-band Flux Conversion

$F_{\nu}$ [Jy]	J [mag]	$F_{\lambda}$ [Wm <sup>-2</sup> μm <sup>-1</sup> ]	$F_{\lambda}$ [Wcm <sup>-2</sup> μm <sup>-1</sup> ]	$F_{\lambda}$ [erg cm <sup>-2</sup> s <sup>-1</sup> Å <sup>-1</sup> ]
1670	0.0	3.21x10 <sup>-9</sup>	3.21x10 <sup>-13</sup>	3.21x10 <sup>-10</sup>
665	1.0	1.28x10 <sup>-9</sup>	1.28x10 <sup>-13</sup>	1.28x10 <sup>-10</sup>
265	2.0	5.08x10 <sup>-10</sup>	5.08x10 <sup>-14</sup>	5.08x10 <sup>-11</sup>
106	3.0	2.02x10 <sup>-10</sup>	2.02x10 <sup>-14</sup>	2.02x10 <sup>-11</sup>
42.0	4.0	8.06x10 <sup>-11</sup>	8.06x10 <sup>-15</sup>	8.06x10 <sup>-12</sup>
16.7	5.0	3.21x10 <sup>-11</sup>	3.21x10 <sup>-15</sup>	3.21x10 <sup>-12</sup>
6.65	6.0	1.28x10 <sup>-11</sup>	1.28x10 <sup>-15</sup>	1.28x10 <sup>-12</sup>
2.65	7.0	5.08x10 <sup>-12</sup>	5.08x10 <sup>-16</sup>	5.08x10 <sup>-13</sup>
1.06	8.0	2.02x10 <sup>-12</sup>	2.02x10 <sup>-16</sup>	2.02x10 <sup>-13</sup>
0.420	9.0	8.06x10 <sup>-13</sup>	8.06x10 <sup>-17</sup>	8.06x10 <sup>-14</sup>
0.167	10.0	3.21x10 <sup>-13</sup>	3.21x10 <sup>-17</sup>	3.21x10 <sup>-14</sup>
0.0665	11.0	1.28x10 <sup>-13</sup>	1.28x10 <sup>-17</sup>	1.28x10 <sup>-14</sup>
0.0265	12.0	5.08x10 <sup>-14</sup>	5.08x10 <sup>-18</sup>	5.08x10 <sup>-15</sup>
0.0106	13.0	2.02x10 <sup>-14</sup>	2.02x10 <sup>-18</sup>	2.02x10 <sup>-15</sup>
0.00420	14.0	8.06x10 <sup>-15</sup>	8.06x10 <sup>-19</sup>	8.06x10 <sup>-16</sup>
0.00167	15.0	3.21x10 <sup>-15</sup>	3.21x10 <sup>-19</sup>	3.21x10 <sup>-16</sup>
6.65x10 <sup>-4</sup>	16.0	1.28x10 <sup>-15</sup>	1.28x10 <sup>-19</sup>	1.28x10 <sup>-16</sup>
2.65x10 <sup>-4</sup>	17.0	5.08x10 <sup>-16</sup>	5.08x10 <sup>-20</sup>	5.08x10 <sup>-17</sup>
1.06x10 <sup>-4</sup>	18.0	2.02x10 <sup>-16</sup>	2.02x10 <sup>-20</sup>	2.02x10 <sup>-17</sup>
4.20x10 <sup>-5</sup>	19.0	8.06x10 <sup>-17</sup>	8.06x10 <sup>-21</sup>	8.06x10 <sup>-18</sup>
1.67x10 <sup>-5</sup>	20.0	3.21x10 <sup>-17</sup>	3.21x10 <sup>-21</sup>	3.21x10 <sup>-18</sup>
6.65x10 <sup>-6</sup>	21.0	1.28x10 <sup>-17</sup>	1.28x10 <sup>-21</sup>	1.28x10 <sup>-18</sup>
2.65x10 <sup>-6</sup>	22.0	5.08x10 <sup>-18</sup>	5.08x10 <sup>-22</sup>	5.08x10 <sup>-19</sup>
1.06x10 <sup>-6</sup>	23.0	2.02x10 <sup>-18</sup>	2.02x10 <sup>-22</sup>	2.02x10 <sup>-19</sup>
4.20x10 <sup>-7</sup>	24.0	8.06x10 <sup>-19</sup>	8.06x10 <sup>-23</sup>	8.06x10 <sup>-20</sup>
1.67x10 <sup>-7</sup>	25.0	3.21x10 <sup>-19</sup>	3.21x10 <sup>-23</sup>	3.21x10 <sup>-20</sup>
6.65x10 <sup>-8</sup>	26.0	1.28x10 <sup>-19</sup>	1.28x10 <sup>-23</sup>	1.28x10 <sup>-20</sup>

Table 12.6: H-band Flux Conversion

$F_Y$ [Jy]	H [mag]	$F_\lambda$ [Wm <sup>-2</sup> μm <sup>-1</sup> ]	$F_\lambda$ [Wcm <sup>-2</sup> μm <sup>-1</sup> ]	$F_\lambda$ [erg s <sup>-1</sup> cm <sup>-2</sup> Å <sup>-1</sup> ]
980	0.0	$1.08 \times 10^{-9}$	$1.08 \times 10^{-13}$	$1.08 \times 10^{-10}$
390	1.0	$4.3 \times 10^{-10}$	$4.3 \times 10^{-14}$	$4.3 \times 10^{-11}$
155	2.0	$1.712 \times 10^{-10}$	$1.712 \times 10^{-14}$	$1.712 \times 10^{-11}$
618	3.0	$6.814 \times 10^{-11}$	$6.814 \times 10^{-15}$	$6.814 \times 10^{-12}$
246	4.0	$2.713 \times 10^{-11}$	$2.713 \times 10^{-15}$	$2.713 \times 10^{-12}$
98	5.0	$1.08 \times 10^{-11}$	$1.08 \times 10^{-15}$	$1.08 \times 10^{-12}$
39	6.0	$4.3 \times 10^{-12}$	$4.3 \times 10^{-16}$	$4.3 \times 10^{-13}$
155	7.0	$1.712 \times 10^{-12}$	$1.712 \times 10^{-16}$	$1.712 \times 10^{-13}$
0.618	8.0	$6.814 \times 10^{-13}$	$6.814 \times 10^{-17}$	$6.814 \times 10^{-14}$
0.246	9.0	$2.713 \times 10^{-13}$	$2.713 \times 10^{-17}$	$2.713 \times 10^{-14}$
0.098	10.0	$1.08 \times 10^{-13}$	$1.08 \times 10^{-17}$	$1.08 \times 10^{-14}$
0.039	11.0	$4.3 \times 10^{-14}$	$4.3 \times 10^{-18}$	$4.3 \times 10^{-15}$
0.0155	12.0	$1.712 \times 10^{-14}$	$1.712 \times 10^{-18}$	$1.712 \times 10^{-15}$
0.00618	13.0	$6.814 \times 10^{-15}$	$6.814 \times 10^{-19}$	$6.814 \times 10^{-16}$
0.00246	14.0	$2.713 \times 10^{-15}$	$2.713 \times 10^{-19}$	$2.713 \times 10^{-16}$
$9.8 \times 10^{-4}$	15.0	$1.08 \times 10^{-15}$	$1.08 \times 10^{-19}$	$1.08 \times 10^{-16}$
$3.9 \times 10^{-4}$	16.0	$4.3 \times 10^{-16}$	$4.3 \times 10^{-20}$	$4.3 \times 10^{-17}$
$1.55 \times 10^{-4}$	17.0	$1.712 \times 10^{-16}$	$1.712 \times 10^{-20}$	$1.712 \times 10^{-17}$
$6.18 \times 10^{-5}$	18.0	$6.814 \times 10^{-17}$	$6.814 \times 10^{-21}$	$6.814 \times 10^{-18}$
$2.46 \times 10^{-5}$	19.0	$2.713 \times 10^{-17}$	$2.713 \times 10^{-21}$	$2.713 \times 10^{-18}$
$9.8 \times 10^{-6}$	20.0	$1.08 \times 10^{-17}$	$1.08 \times 10^{-21}$	$1.08 \times 10^{-18}$
$3.9 \times 10^{-6}$	21.0	$4.3 \times 10^{-18}$	$4.3 \times 10^{-22}$	$4.3 \times 10^{-19}$
$1.55 \times 10^{-6}$	22.0	$1.712 \times 10^{-18}$	$1.712 \times 10^{-22}$	$1.712 \times 10^{-19}$
$6.18 \times 10^{-7}$	23.0	$6.814 \times 10^{-19}$	$6.814 \times 10^{-23}$	$6.814 \times 10^{-20}$
$2.46 \times 10^{-7}$	24.0	$2.713 \times 10^{-19}$	$2.713 \times 10^{-23}$	$2.713 \times 10^{-20}$
$9.8 \times 10^{-8}$	25.0	$1.08 \times 10^{-19}$	$1.08 \times 10^{-23}$	$1.08 \times 10^{-20}$
$3.9 \times 10^{-8}$	26.0	$4.3 \times 10^{-20}$	$4.3 \times 10^{-24}$	$4.3 \times 10^{-21}$

Table 12.7: K-band Flux Conversion

$F_V$ [ $\mu\text{y}$ ]	K [mag]	$F_\lambda$ [ $\text{Wm}^{-2}\mu\text{m}^{-1}$ ]	$F_\lambda$ [ $\text{Wcm}^{-2}\mu\text{m}^{-1}$ ]	$F_\lambda$ [ $\text{erg s}^{-1}\text{cm}^{-2}\text{\AA}^{-1}$ ]
620	0.0	$3.84 \times 10^{-10}$	$3.84 \times 10^{-14}$	$3.84 \times 10^{-11}$
24.7	1.0	$1.53 \times 10^{-10}$	$1.53 \times 10^{-14}$	$1.53 \times 10^{-11}$
9.83	2.0	$6.09 \times 10^{-11}$	$6.09 \times 10^{-15}$	$6.09 \times 10^{-12}$
3.91	3.0	$2.43 \times 10^{-11}$	$2.43 \times 10^{-15}$	$2.43 \times 10^{-12}$
1.56	4.0	$9.66 \times 10^{-12}$	$9.66 \times 10^{-16}$	$9.66 \times 10^{-13}$
0.620	5.0	$3.84 \times 10^{-12}$	$3.84 \times 10^{-16}$	$3.84 \times 10^{-13}$
0.247	6.0	$1.53 \times 10^{-12}$	$1.53 \times 10^{-16}$	$1.53 \times 10^{-13}$
0.0983	7.0	$6.09 \times 10^{-13}$	$6.09 \times 10^{-17}$	$6.09 \times 10^{-14}$
0.0391	8.0	$2.43 \times 10^{-13}$	$2.43 \times 10^{-17}$	$2.43 \times 10^{-14}$
0.0156	9.0	$9.66 \times 10^{-14}$	$9.66 \times 10^{-18}$	$9.66 \times 10^{-15}$
0.00620	10.0	$3.84 \times 10^{-14}$	$3.84 \times 10^{-18}$	$3.84 \times 10^{-15}$
0.00247	11.0	$1.53 \times 10^{-14}$	$1.53 \times 10^{-18}$	$1.53 \times 10^{-15}$
0.000983	12.0	$6.09 \times 10^{-15}$	$6.09 \times 10^{-19}$	$6.09 \times 10^{-16}$
0.000391	13.0	$2.43 \times 10^{-15}$	$2.43 \times 10^{-19}$	$2.43 \times 10^{-16}$
0.000156	14.0	$9.66 \times 10^{-16}$	$9.66 \times 10^{-20}$	$9.66 \times 10^{-17}$
$6.20 \times 10^{-4}$	15.0	$3.84 \times 10^{-16}$	$3.84 \times 10^{-20}$	$3.84 \times 10^{-17}$
$2.47 \times 10^{-4}$	16.0	$1.53 \times 10^{-16}$	$1.53 \times 10^{-20}$	$1.53 \times 10^{-17}$
$9.83 \times 10^{-5}$	17.0	$6.09 \times 10^{-17}$	$6.09 \times 10^{-21}$	$6.09 \times 10^{-18}$
$3.91 \times 10^{-5}$	18.0	$2.43 \times 10^{-17}$	$2.43 \times 10^{-21}$	$2.43 \times 10^{-18}$
$1.56 \times 10^{-5}$	19.0	$9.66 \times 10^{-18}$	$9.66 \times 10^{-22}$	$9.66 \times 10^{-19}$
$6.20 \times 10^{-6}$	20.0	$3.84 \times 10^{-18}$	$3.84 \times 10^{-22}$	$3.84 \times 10^{-19}$
$2.47 \times 10^{-6}$	21.0	$1.53 \times 10^{-18}$	$1.53 \times 10^{-22}$	$1.53 \times 10^{-19}$
$9.83 \times 10^{-7}$	22.0	$6.09 \times 10^{-19}$	$6.09 \times 10^{-23}$	$6.09 \times 10^{-20}$
$3.91 \times 10^{-7}$	23.0	$2.43 \times 10^{-19}$	$2.43 \times 10^{-23}$	$2.43 \times 10^{-20}$
$1.56 \times 10^{-7}$	24.0	$9.66 \times 10^{-20}$	$9.66 \times 10^{-24}$	$9.66 \times 10^{-21}$
$6.20 \times 10^{-8}$	25.0	$3.84 \times 10^{-20}$	$3.84 \times 10^{-24}$	$3.84 \times 10^{-21}$
$2.47 \times 10^{-8}$	26.0	$1.53 \times 10^{-20}$	$1.53 \times 10^{-24}$	$1.53 \times 10^{-21}$



Table 12.8: Surface Brightness Conversion

mag arcsec <sup>-2</sup>	I-Band		J-Band		H-Band		K-Band	
	Jy arcsec <sup>-2</sup>	MJy steradian <sup>-1</sup>	Jy arcsec <sup>-2</sup>	MJy steradian <sup>-1</sup>	Jy arcsec <sup>-2</sup>	MJy steradian <sup>-1</sup>	Jy arcsec <sup>-2</sup>	MJy steradian <sup>-1</sup>
0.0	22.50	2.66x10 <sup>-4</sup>	16.70	1.97x10 <sup>-4</sup>	980	1.16x10 <sup>-4</sup>	620	7320
1.0	894	1.06x10 <sup>-4</sup>	66.5	7860	390	4610	247	2930
2.0	356	4210	26.5	3130	155	1830	98.3	1160
3.0	142	1680	106	1250	61.8	730	39.1	462
4.0	56.4	667	42.0	496	24.6	291	15.6	184
5.0	22.5	266	16.7	197	9.8	116	6.20	732
6.0	8.94	106	6.65	78.6	3.9	46.1	2.47	29.3
7.0	3.56	42.1	2.65	31.3	1.55	18.3	0.983	11.6
8.0	1.42	16.8	1.06	12.5	0.618	7.3	0.391	4.62
9.0	0.564	6.67	0.420	4.96	0.246	2.91	0.156	1.84
10.0	0.225	2.66	0.167	1.97	0.098	1.16	0.0620	0.732
11.0	0.0894	1.06	0.0665	0.786	0.039	0.461	0.0247	0.293
12.0	0.0356	0.421	0.0265	0.313	0.0155	0.183	0.00983	0.116
13.0	0.0142	0.168	0.0106	0.125	0.00618	0.073	0.00391	0.0462
14.0	0.00564	0.0667	0.00420	0.0496	0.00246	0.0291	0.00156	0.0184
15.0	0.00225	0.0266	0.00167	0.0197	9.8x10 <sup>-4</sup>	0.0116	6.20x10 <sup>-4</sup>	0.00732
16.0	8.94x10 <sup>-4</sup>	0.0106	6.65x10 <sup>-4</sup>	0.00786	3.9x10 <sup>-4</sup>	0.00461	2.47x10 <sup>-4</sup>	0.00293
17.0	3.56x10 <sup>-4</sup>	0.00421	2.65x10 <sup>-4</sup>	0.00313	1.55x10 <sup>-4</sup>	0.00183	9.83x10 <sup>-5</sup>	0.00116
18.0	1.42x10 <sup>-4</sup>	0.00168	1.06x10 <sup>-4</sup>	0.00125	6.18x10 <sup>-5</sup>	7.3x10 <sup>-5</sup>	3.91x10 <sup>-5</sup>	4.62x10 <sup>-4</sup>
19.0	5.64x10 <sup>-5</sup>	6.67x10 <sup>-4</sup>	4.20x10 <sup>-5</sup>	4.96x10 <sup>-4</sup>	2.46x10 <sup>-5</sup>	2.91x10 <sup>-4</sup>	1.56x10 <sup>-5</sup>	1.84x10 <sup>-4</sup>
20.0	2.25x10 <sup>-5</sup>	2.66x10 <sup>-4</sup>	1.67x10 <sup>-5</sup>	1.97x10 <sup>-4</sup>	9.8x10 <sup>-6</sup>	1.16x10 <sup>-4</sup>	6.20x10 <sup>-6</sup>	7.32x10 <sup>-5</sup>
21.0	8.94x10 <sup>-6</sup>	1.06x10 <sup>-4</sup>	6.65x10 <sup>-6</sup>	7.86x10 <sup>-5</sup>	3.9x10 <sup>-6</sup>	4.61x10 <sup>-5</sup>	2.47x10 <sup>-6</sup>	2.93x10 <sup>-5</sup>
22.0	3.56x10 <sup>-6</sup>	4.21x10 <sup>-5</sup>	2.65x10 <sup>-6</sup>	3.13x10 <sup>-5</sup>	1.55x10 <sup>-6</sup>	1.83x10 <sup>-5</sup>	9.83x10 <sup>-7</sup>	1.16x10 <sup>-5</sup>
23.0	1.42x10 <sup>-6</sup>	1.68x10 <sup>-5</sup>	1.06x10 <sup>-6</sup>	1.25x10 <sup>-5</sup>	6.18x10 <sup>-7</sup>	7.3x10 <sup>-6</sup>	3.91x10 <sup>-7</sup>	4.62x10 <sup>-6</sup>
24.0	5.64x10 <sup>-7</sup>	6.67x10 <sup>-6</sup>	4.20x10 <sup>-7</sup>	4.96x10 <sup>-6</sup>	2.46x10 <sup>-7</sup>	2.91x10 <sup>-6</sup>	1.56x10 <sup>-7</sup>	1.84x10 <sup>-6</sup>
25.0	2.25x10 <sup>-7</sup>	2.66x10 <sup>-6</sup>	1.67x10 <sup>-7</sup>	1.97x10 <sup>-6</sup>	9.8x10 <sup>-8</sup>	1.16x10 <sup>-6</sup>	6.20x10 <sup>-8</sup>	7.32x10 <sup>-7</sup>
26.0	8.94x10 <sup>-8</sup>	1.06x10 <sup>-6</sup>	6.65x10 <sup>-8</sup>	7.86x10 <sup>-7</sup>	3.9x10 <sup>-8</sup>	4.61x10 <sup>-7</sup>	2.47x10 <sup>-8</sup>	2.93x10 <sup>-7</sup>

## Examples

1. Given a source with a flux of  $0.9 \text{ mJy}$  at  $1350 \text{ \AA}$ , convert this flux to  $\text{erg s}^{-1} \text{cm}^{-2} \text{\AA}^{-1}$ . From section 3, Table 12.1, we see that the conversion constant  $\beta$  is  $3 \times 10^{-13}$  and the wavelength is  $1350 \text{ \AA} = 0.135 \mu\text{m}$ . Thus:

$$F_{\lambda} = 3 \times 10^{-13} \times 9 \times 10^{-4} / 0.135^2 = 1.48 \times 10^{-14} \text{ erg s}^{-1} \text{cm}^{-2} \text{\AA}^{-1}$$

2. Given a V magnitude of 15.6, and knowledge that  $V-K=2.5$  in the UKIRT system, estimate the flux in Jy at K. Since  $V-K=2.5$  we know that  $K=13.1$ . From Table 12.2, the zero-point flux in the UKIRT system for K is  $657 \text{ Jy}$ . Thus the  $2.2 \mu\text{m}$  flux is:

$$F_V = 10^{-13.1/2.5} \times 657 = 3.8 \times 10^{-3} \text{ Jy}$$

3. Given a surface brightness of  $21.1$  magnitudes  $\text{arcsec}^{-2}$  at J, convert this into  $\text{Jy arcsec}^{-2}$  and into  $\text{MJy steradian}^{-1}$ . Taking the zero-point for the J band from Table 12.2, we determine that the surface brightness is:

$$10^{-21.1/2.5} \times 1670 = 6.06 \times 10^{-6} \text{ Jy arcsec}^{-2}, \text{ or } 6.06 \times 10^{-6} / 0.084616 = 7.17 \times 10^{-5} \text{ MJy ster}^{-1}$$

4. Given a flux at  $0.9 \mu\text{m}$  of  $2.3 \times 10^{-7} \text{ Jy}$ , estimate the I magnitude.  $2.3 \times 10^{-7} \text{ Jy}$  is less than  $2.3 \times 10^{-1} \text{ Jy}$  by three powers of a hundred, or 15 magnitudes. From Table 12.3 we see that  $0.25 \text{ Jy}$  is equivalent to an I-band magnitude of 9.89. Thus  $2.3 \times 10^{-7}$  is roughly 15 magnitudes fainter than this, or of order  $I=24.9$ .

## Infrared Line Lists

We present here lists of some of the more important atomic and molecular lines in the infrared. It is by no means exhaustive.

Table 12.9: Recombination Lines of Atomic Hydrogen: Paschen Series<sup>a</sup>

Transition ( $N_u - N_l$ )	Vacuum Wavelength (microns)	Vacuum Frequency ( $\text{cm}^{-1}$ )	$I/I(\text{H}\beta)$ $T_e = N_e = 10^4$
4-3	1.8756	5531.55	0.332
5-3	1.2822	7799.33	0.162
6-3	1.0941	9139.8	0.0901
7-3	1.0052	9948.1	

a. Intensities from Hummel & Storey, MNRAS 224, 801.

Table 12.10: Recombination Lines of Atomic Hydrogen: Brackett Series

Transition ( $N_U - N_L$ )	Vacuum Wavelength (microns)	Frequency ( $\text{cm}^{-1}$ )	$I/I(\text{H}\beta)$ $T_e = 10^4$
5-4	4.5225	2467.765	0.0777
6-4	2.6259	3808.25	
7-4	2.1661	4616.61	0.0275
8-4	1.9451	5141.14	0.0181
9-4	1.8181	5500.8	0.0126
10-4	1.7367	5758.1	0.00909
11-4	1.6811	5948.45	0.00679
12-4	1.6412	6093.22	0.00521
13-4	1.6114	6205.9	0.00409
14-4	1.5885	6295.3	0.00327
15-4	1.5705	6367.4	0.00266
16-4	1.5561	6426.4	0.00220
17-4	1.5443	6475.3	0.00184
18-4	1.5346	6516.3	0.00156
19-4	1.5265	6551.0	0.00133
20-4	1.5196	6580.7	0.00116
series limit	1.459	6855.	

Table 12.11: HeI and HeII Lines

ID	Transition	$\lambda$ ( $\mu\text{m}$ )
HeI	7F-3D, 3Fo-3D	1.0031
HeI	7F-3D, 1Fo-1D	1.0034
HeII	14-6	1.0049
HeII	5-4	1.0133
HeI	6D-3P, 3dD-3Po	1.0314
HeII	13-6	1.0422
HeI	6S-3P, 3S-3Po	1.0668
HeI	2P-2S, 3Po-3S, GU=3	1.0832
HeI	2P-2S, 3Po-3P, GU=1	1.0832
HeI	2P-2S, 3Po-3S, GU=5	1.0833

Table 12.11: Hel and Hell Lines

ID	Transition	$\lambda$ ( $\mu$ m)
Hel	2P-2S,3Po-3S,GU=9	1.0833
Hel	6P-3D,1Po-1d	1.0905
Hel	6F-3D,3Fo-3D	1.0916
Hel	6F-3D,1Fo-1D	1.0920
Hell	12-6	1.0938
Hel	6P-3D,3Po-3D	1.0997
Hel	5P-3S,1Po-1S	1.1016
Hel	6D-3P,1D-1Po	1.1048
Hell	7LIMIT	1.1164
Hel	6S-3P,1S-1Po	1.1229
Hell	7-5	1.1628
Hell	11-6	1.1677
Hel	5D-3P,3D-3Po	1.1972
Hell	21-7	1.2256
Hell	22-7	1.2418
Hel	4P-3S,3Po-3S	1.2531
Hell	20-7	1.2719
Hel	5P-3D,1Po-1D	1.2759
Hel	5F-3D,3Fo-3D	1.2789
Hell	10-6	1.2817
Hel	5S-3P,3S-3Po	1.2850
Hell	19-7	1.2914
Hel	5D-3P,1D-1Po	1.2971
Hel	5F-3D,1Fo-1D	1.2976
Hel	5P-3D,3Po-3D	1.2988
Hell	18-7	1.3150
Hel	5S-3P,1S-1Po	1.3415
Hell	17-7	1.3442
Hell	15-7	1.4273
Hell	8LIMIT	1.4578
Hell	9-6	1.4765

Table 12.11: HeI and HeII Lines

ID	Transition	$\lambda$ ( $\mu\text{m}$ )
HeII	14-7	1.4882
HeI	4P-3S, 1Po-1S	1.5088
HeII	13-7	1.5719
HeII	25-8	1.6241
HeII	24-8	1.6400
HeII	23-8	1.6584
HeII	22-8	1.6799
HeII	12-7	1.6926
HeI	4D-3P, 3D-3Po	1.7007
HeII	21-8	1.7053
HeII	20-8	1.7355
HeII	19-8	1.7717
HeII	18-8	1.8167
HeII	9LIMIT	1.8450
HeI	4P-3D, 1Po-1D	1.8561
HeII	6-5	1.8639
HeI	4F-3D, 3Fo-3D	1.8691
HeI	4F-3D, 1Fo-1d	1.8702
HeII	17-8	1.8725
HeII	8-6	1.8753
HeII	11-7	1.8770
HeI	8S-4P, 3S-3Po	1.9068
HeI	4D-3P, 1D-1Po	1.9094
HeI	4P-3D, 3Po-3D	1.9548
HeII	15-8	2.0379
HeI	6P-4S, 3Po-3S	2.0430
HeI	2P-2S, 1Po-1S	2.0587
HeI	4S-3P, 3S-3Po	2.1126
HeI	3pP-4sS	2.1132
HeI	4S-3P, 1S-1Po	2.1138
HeII	25-9	2.1195

Table 12.11: Hel and Hell Lines

ID	Transition	$\lambda$ ( $\mu$ m)
HeII	24-9	2.1469
HeI	75-4P,3S-3Po	2.1500
HeI	7F-4D,3Fo-3D	2.1614
HeI	4dD-7fF	2.1617
HeI	7F-4D,1Fo-1D	2.1623
HeII	14-8	2.1653
HeI	4-7	2.166
HeII	23-9	2.1786
HeI	7D-4P,1D-1Po	2.1847
HeII	10-7	2.1891
HeII	22-9	2.2155
HeI	75-4P,1S-1Po	2.2290
HeII	21-9	2.2601
HeII	10LIMIT	2.2778
HeI	6P-4S,1Po-1S	2.3069
HeII	20-9	2.314
HeII	13-8	2.348
HeII	19-9	2.3788
HeII	18-9	2.4606
HeI	6D-4P,3D-3Po	2.4734

Table 12.12: CO Vibration-rotation Band-heads<sup>a</sup>

	<sup>12</sup> C <sup>16</sup> O Vacuum Wavelength (microns)	Frequency (cm <sup>-1</sup> )	<sup>13</sup> C <sup>16</sup> O Vacuum Wavelength (microns)	Frequency (cm <sup>-1</sup> )
2-0	2.2935	4360.1	2.3448	4264.7
3-1	2.3227	4305.4	2.3739	4212.4
4-2	2.3535	4250.8	2.4037	4160.3
5-3	2.3829	4196.5	2.4341	4108.3
6-4	2.4142	4142.2	2.4652	4056.4
7-5	2.4461	4088.2	2.4971	4004.7

Table 12.12: CO Vibration-rotation Band-heads<sup>a</sup> (Continued)

	<sup>12</sup> C <sup>16</sup> O Vacuum Wavelength (microns)	Frequency (cm <sup>-1</sup> )	<sup>13</sup> C <sup>16</sup> O Vacuum Wavelength (microns)	Frequency (cm <sup>-1</sup> )
8-6	2.4787	4034.3		
9-7	2.5122	3980.5		
3-0	1.5582	6417.8		
4-1	1.5780	6337.2		
5-2	1.5982	6257.2		
6-3	1.6187	6177.7		
7-4	1.6397	6098.8		
8-5	1.6610	6020.5		

a. All of the  $\Delta v = 2$  bandheads occur near  $J=50$ .

Table 12.13: Important H<sub>2</sub> Lines<sup>a</sup>

Line Name		Wavel ( $\mu\text{m}$ )	Freq (cm <sup>-1</sup> )	$g(J)$	Upper (K)	A (10e <sup>-7</sup> s)	LTE I(line)/I(1-0S(1))			
							1000K	2000K	3000K	4000K
1-0	S(0)	2.2235	4497.41	5	6471	2.53	0.27	0.21	0.19	0.19
1-0	S(1)	2.1218	4712.91	21	6956	3.47	1.00	1.00	1.00	1.00
1-0	S(2)	2.0338	4917.01	9	7584	3.98	0.27	0.37	0.42	0.44
1-0	S(3)	1.9576	5108.40	33	8365	4.21	0.51	1.02	1.29	1.45
1-0	S(4)	1.8920	5282.52	13	9286	4.19	0.082	0.26	0.39	0.47
1-0	S(5)	1.8358	5447.25	45	10341	3.96	0.096	0.52	0.91	1.21
1-0	S(6)	1.7880	5592.9	17	11522	3.54	0.010	0.10	0.21	0.31
1-0	S(7)	1.7480	5720.8	57	12817	2.98	0.008	0.15	0.40	0.65
1-0	S(8)	1.7147	5831.9	21	14221	2.34	0.001	0.022	0.074	0.14
1-0	S(9)	1.6877	5925.1	69	15722	1.68	0.025	0.11	0.22	
1-0	S(10)	1.6665	6000.0	25	17311	1.05	0.003	0.015	0.034	
1-0	S(11)	1.6504	6059.0	81	18979	0.53	0.002	0.014	0.037	
1-0	Q(1)	2.4066	4155.25	9	6149	4.29	1.05	0.70	0.61	0.57
1-0	Q(2)	2.4134	4143.47	5	6471	3.03	0.30	0.23	0.22	0.21
1-0	Q(3)	2.4237	4125.87	21	6956	2.78	0.70	0.70	0.70	0.70
1-0	Q(4)	2.4375	412.57	9	7586	2.65	0.15	0.21	0.23	0.24

Table 12.13: Important H<sub>2</sub> Lines<sup>a</sup> (Continued)

Line Name		Wavel ( $\mu\text{m}$ )	Freq ( $\text{cm}^{-1}$ )	$g(J)$	Eupper (K)	A ( $10\text{e}^{-7}\text{s}$ )	LTE $I(\text{line})/I(1-0S(1))$			
							1000K	2000K	3000K	4000K
1-0	Q(5)	2.4548	4073.72	33	8365	2.55	0.24	0.49	0.62	0.70
1-0	Q(6)	2.4756	4039.5	13	9286	2.45	0.036	0.12	0.17	0.21
1-0	Q(7)	2.5001	3999.9	45	10341	2.34	0.042	0.11	0.40	0.53
3-2	S(0)	2.5014	3997.73	5	17387	3.88	0.001	0.007	0.016	
3-2	S(1)	2.3864	4190.33	21	17818	5.14	0.006	0.035	0.087	
3-2	S(2)	2.2870	4372.49	9	18386	5.63	0.002	0.014	0.037	
3-2	S(3)	2.2014	4542.57	33	19086	5.63	0.006	0.043	0.12	
3-2	S(4)	2.1280	4699.32	13	19912	5.22	0.001	0.012	0.036	
3-2	S(5)	2.0656	4841.3	45	20856	4.50	0.003	0.023	0.088	
3-2	S(6)	2.0130	4967.7	17	21911	3.57	0.006	0.021		
3-2	S(7)	1.9692	5078.1	57	23069	2.54	0.001	0.010	0.038	
4-3	S(3)	2.3446	4265.4	21						
4-3	S(4)	2.2668	4411.5	9						
4-3	S(5)	2.201	4543.5	33						
5-4	S(5)	2.3555	4245.4	45						
5-4	S(7)	2.2510	4442.5	57						
2-0	S(0)	1.2383	8075.3	5	12095	1.27	0.001	0.012	0.028	0.043
2-0	S(1)	1.1622	8604.2	21	12550	1.90	0.004	0.061	0.15	0.23
2-0	S(2)	1.1382	8785.5	9	13150	2.38	0.001	0.025	0.070	0.12
2-0	S(3)	1.1175	8948.6	33	13890	2.77	0.002	0.074	0.24	0.43
2-0	S(4)	1.0998	9092.4	13	14764	3.07	0.021	0.078	0.15	
2-0	S(5)	1.0851	9215.5	45	15763	3.28	0.001	0.048	0.21	0.44
2-0	Q(1)	1.2383	8075.3	9	11789	1.94	0.003	0.037	0.082	0.12
2-0	Q(2)	1.2419	8051.9	5	12095	1.38	0.001	0.012	0.029	0.045
2-0	Q(3)	1.2473	8017.2	21	12550	1.29	0.002	0.039	0.098	0.24
2-0	Q(4)	1.2545	7971.1	9	13150	1.27	0.001	0.012	0.033	0.056
2-0	Q(5)	1.2636	7913.3	33	13890	1.23	0.001	0.024	0.093	0.17
2-0	Q(2)	1.2932	7732.6	1	11635	3.47	0.001	0.008	0.016	0.024
2-0	Q(3)	1.3354	7488.3	9	11789	1.61	0.003	0.028	0.063	0.094
2-0	Q(4)	1.3817	7237.5	5	12095	1.03	0.001	0.008	0.020	0.030



Table 12.13: Important H<sub>2</sub> Lines<sup>a</sup> (Continued)

Line Name		Wavel ( $\mu\text{m}$ )	Freq ( $\text{cm}^{-1}$ )	g(J)	Eupper (K)	A ( $10\text{e}^{-7}\text{s}$ )	LTE I(line)/I(1-0S(1))			
							1000K	2000K	3000K	4000K
2-0	O(5)	1.4322	6982.5	21	12550	0.698	0.001	0.018	0.046	0.074

a. Energy levels calculated using Dabrowski & Herzberg, Can J Phys 62, 1639 (1984). Einstein coefficients from Turner et al. ApJ Suppl 35, 281 (1977).



# Calibration Pipeline

### In This Chapter...

Overview and New Features / 275

NICMOS Pipeline / 278

NICMOS Data Products / 282

This chapter describes the pipeline calibration system developed at STScI. This system provides observers with NICMOS data after various instrumental signatures are removed, conversions to flux units are performed, and patterns of exposures are combined. Several enhancements to the HST ground system have been made to support NICMOS, including the concept of associations of datasets and an improved file format for data storage and distribution. A detailed description of the analysis of HST data in general and NICMOS data in particular will be found in the next release of the *HST Data Handbook*.

---

## Overview and New Features

All data taken with NICMOS are automatically processed and calibrated by a suite of software programs known as the *pipeline*. The purpose of pipeline processing is to provide data products to observers and the HST Data Archive in a form suitable for most scientific analyses. Pipeline processing is also applied to engineering data, calibration data, and calibration software.

The basic sequence of steps in the STScI pipeline system (also known as OPUS) is:

1. Assemble data received from HST into datasets.
2. Perform a standard level of calibration of the science data.
3. Store both the uncalibrated and calibrated datasets in the Archive and populate the Archive database catalog to support StarView queries.

The pipeline must also handle exceptions (e.g., incomplete data) and perform a general data evaluation and quality control step. Final delivery of data to

observers is accomplished by the data distribution mechanisms of the Archive system.

The calibration step has several goals:

- Remove the known instrumental signatures (e.g., flat field and dark current).
- Correct linear and physical units (e.g., gain and flux calibration).
- Flag degraded or suspect data values and provide estimates of the statistical uncertainties of each pixel.

While a calibration pipeline may not be able to provide the optimal calibration for a specific observation (which may, in fact, not become available until some time after the data were obtained and calibrated), the goal is to provide data calibrated to a level suitable for initial evaluation and analysis for all users. Further, observers frequently require a detailed understanding of the calibrations applied to their data and the ability to repeat, often with improved calibration products, the calibration process at their home institution. To support this last goal, the calibration software is available within the STSDAS system and the calibration reference files (e.g., flat fields) are available from the HST Archive via StarView.

## Associations

To improve the utility of the pipeline processing for the second generation science instruments—NICMOS and STIS—several significant changes have been made to the structure of the calibration pipeline. The largest of these changes has been to enable the combination of multiple observations during the calibration process. This permits the pipeline to both generate a combined product and to use calibrations obtained contemporaneously with the science observations. This capability is designed to support the cosmic ray event removal, mosaicking, and background subtraction for NICMOS observations. As discussed in Chapter 10, mechanisms exist for compactly requesting such observations in the Phase II proposal.

### Concept

The basic element in the HST ground system has historically been the *exposure*. The first generation HST science instruments are commanded to generate single exposures, which result from a recognizably distinct sequence of commands to the instrument. This creates a flow of data which is assembled into a single *dataset*. Each dataset is given a unique 9 character identifier (an *IPPPSSOOT* in STScI terminology) and is processed by the pipeline, calibrated, and archived separately from all other datasets.

An illustrative (partial) counter example to this procedure is the WFPC2 *CRSPLIT* proposal instruction. This results in two WFPC2 exposures from a single line on the exposure logsheet (the way in which observers specify commands for HST). However, the HST ground system treats a *CRSPLIT* as two distinct exposures which are commanded, processed, calibrated, and archived

separately. The pipeline does not combine these two images (datasets) to create the single image without cosmic ray events *which was the observer's original intention*. Presently, the observers (and any future archival researchers) are left to perform this task on their own.

The second generation instruments present many instances in which the combination of data from two or more exposures is necessary to create a scientifically useful data product. Both NICMOS and STIS will need to combine exposures to remove cosmic rays and to improve flat fielding (by dithering or *stepping*). For NICMOS, the HST thermal background is expected to have significant temporal variations. Multiple exposures (dithered for small targets and offset onto blank sky—chopped—for larger targets) will be necessary to measure and remove this background. While this has been standard practice for ground based infrared observations and is the basis of essentially all existing infrared data reduction schemes, it is a new paradigm for the HST ground system.

### Usage

Associations exist to simplify the use of HST data by observers. This starts from the proposal phase, continues with a more complete calibration process than would be possible without associations, carries into the archiving and retrieval of associated data, and includes the use of HST data by observers within the STSDAS system.

An association is a set of one or more exposures along with an association table and, optionally, one or more products. We define the following terms:

- An *exposure* is the atomic unit of HST data.
- A *dataset* is a collection of files having a common rootname (first 9 characters).
- A *product* is a dataset derived from one or more exposures.

The first generation instruments all have a one-to-one correspondence between exposures and datasets. They do not have products. NICMOS and STIS use the association structure as a meta-dataset. Further, they use the information in multiple exposures during the calibration process to create products.

From a high level, an association is a means of identifying a set of exposures as belonging together and being, in some sense, dependent upon one another. The association concept permits these exposures to be calibrated, archived, retrieved, and reprocessed (within OPUS or STSDAS) as a set rather than as individual objects. In one sense, this is a book-keeping operation which is being transferred from the observer to the HST data pipeline and archive.

Associations are defined by optional parameters on a single exposure logsheet line. That is, there is a one-to-one correspondence between proposal logsheet lines and associations (although it is possible to have exposures which are not in associations).

Observers may obtain one or more exposures at each of one or more positions on the sky using the NICMOS proposal grammar. Typically usage will be:

- To obtain a sequence of slightly offset exposures (dithering) to improve the flat fielding, avoid bad pixels and cosmic rays, and, for sufficiently compact targets, to remove the background illumination.
- Mapping of targets larger than the NICMOS detector's field of view.
- To obtain a sequence of observations in which the telescope is chopped between the target and one or more offset regions of (hopefully blank) sky.

A set of pre-defined patterns are provided in the proposal instructions for these types of observations or a combination of both types. The Institute ground system will expand the observer's single line request into multiple exposures each with its own identifying name (LPPSSOOT) and populate the necessary database relations to describe this association for the OPUS system.

## Re-engineering

For the second generation science instruments several other modifications to the pipeline system have been made. The format of the data products from the pipeline has been changed from the GELS (Generic Edited Information Set) files used previously to FITS (Flexible Image Transport System) files with image extensions. The IRAF/STSDAS system has been modified to operate directly on these files. Each NICMOS image is expressed as a set of five image extensions representing the image, its variance, a bit encoded data quality map, the number of valid samples at each pixel, and the integration time at each pixel. This structure is used at all stages of the calibration process which permits the re-execution of selected elements of the pipeline without starting from the initial point. Third, the calibration code itself is now written in the C programming language (rather than IRAF's SPP language). An interface between the data files and a set of NICMOS specific data structures (called HSTIO) has also been written. These changes should greatly simplify the modification of the pipeline code by users and the development of new NICMOS specific data processing tasks.

---

## NICMOS Pipeline

The NICMOS calibration task is divided into two stages: **calnica**, which is used for every individual exposure, and **calnicb**, which is used after **calnica** on those exposures which comprise an association.

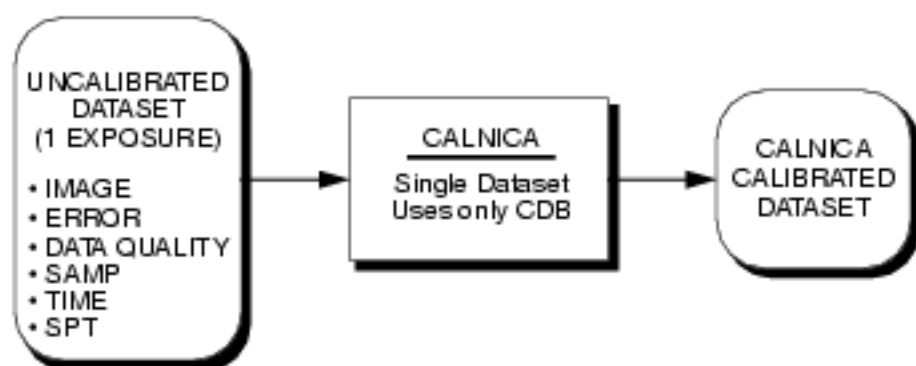
### Static Calibrations—calnica

The first calibration stage, **calnica**, (Figure 13.1) performs those calibrations which can be done to a single exposure using the configuration information from its telemetry and the Calibration Data Base. The calibrations used in this stage are obtained from the Calibration Data Base. Such calibrations are derived from the calibration program (see Chapter 15) and typically change on time scales of

months. This is analogous to the WFPC2 calibration process (*calwp2*). **Calnica** performs the following steps:

- Flag known bad pixels in the data quality array.
- Calculate a noise model for each pixel.
- Subtract the bias level.
- Correct for non-linearity.
- Scale (when necessary) and subtract the dark image.
- Flat field to bring each pixel to a common gain.
- Convert the image data to count rate units.
- Calculate various image statistics (e.g., median).
- Store the photometric calibration in image header keywords.
- Correct for cosmic ray events and pixel saturation (in *MULTIACCUM* data).
- Calculate estimates of the background.
- Analyze the internal engineering telemetry for potential problems with the observation.

Figure 13.1: Conceptual calnica Pipeline

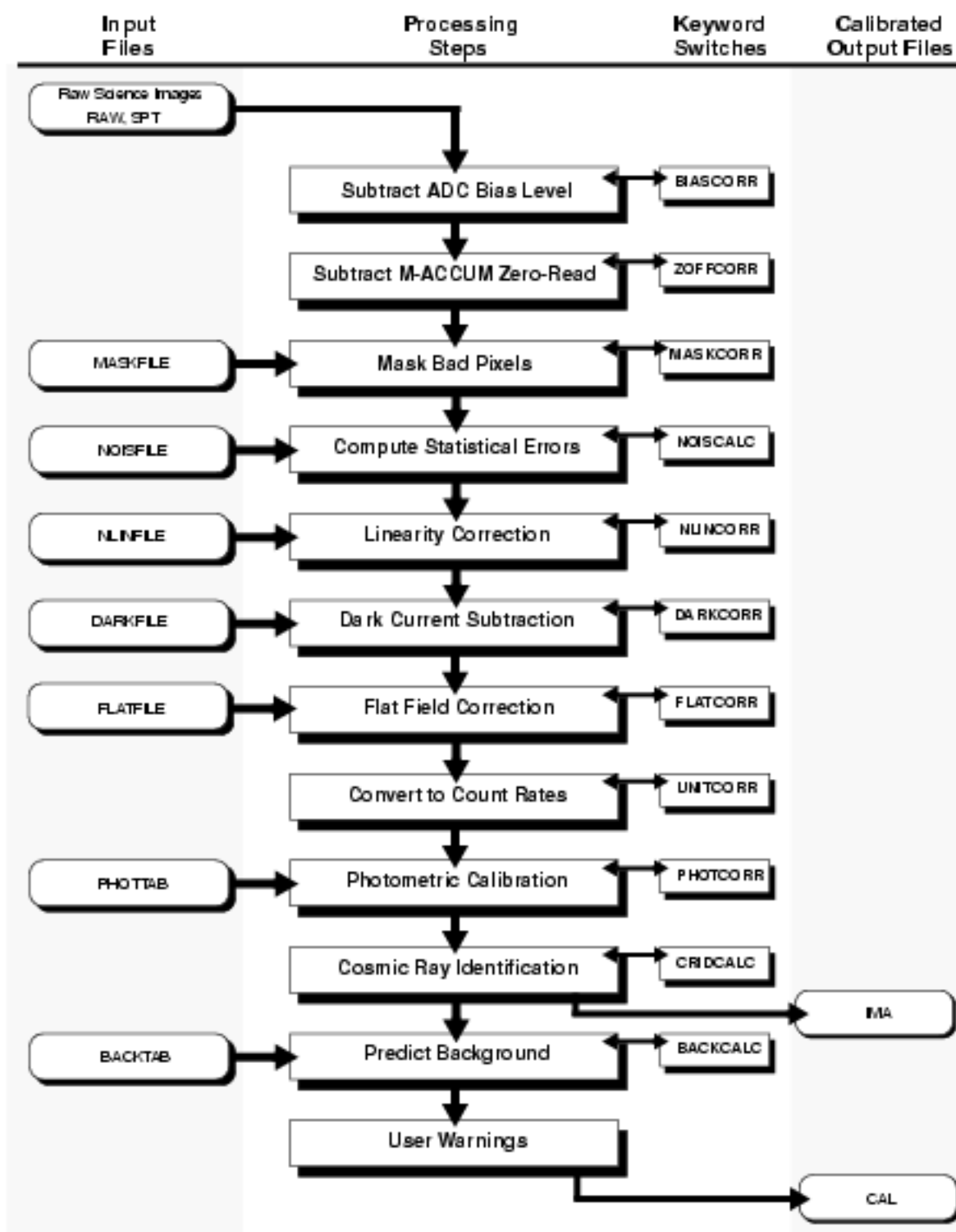


Observers will be given both the uncalibrated (*raw*) data and the processed data for each exposure. For *MULTIACCUM* observations, partially calibrated data for each readout will be generated (which excludes the cosmic ray and saturation corrections) in addition to a final single image.

To recalibrate NICMOS data, you will need the **calnica** software (soon to be included in the STSDAS distribution) and the necessary calibration reference files (available from the HST Data Archive using StarView).

The data processing flow chart for normal imaging and spectroscopic images is shown in Figure 13.2.

Figure 13.2: Calibration Steps of the calnica Pipeline



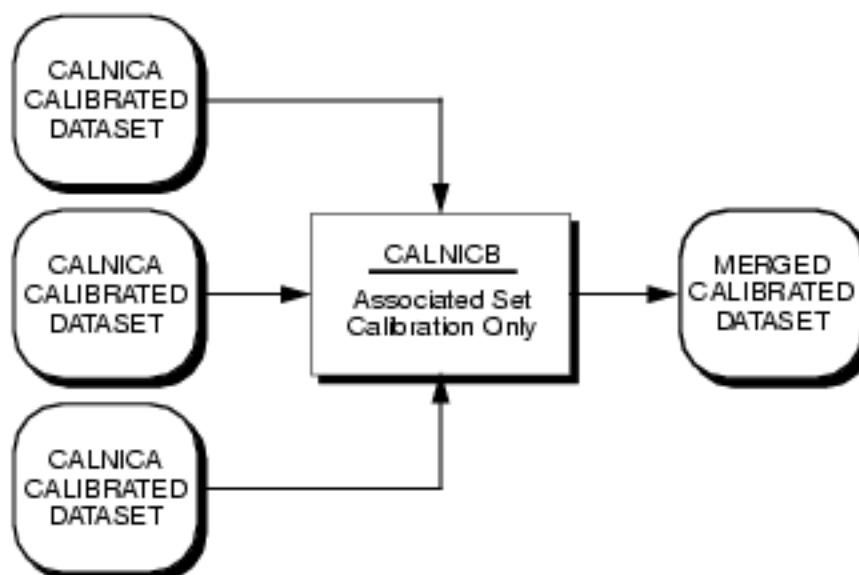


## Contemporaneous Observations—calnicb

While previously it has been possible to execute multiple exposures from a single proposal logsheet line (e.g., *WFPC2*, *CR-SPLIT*, and *NEXP=n* constructs), this capability has been significantly expanded to support new requirements of the second generation science instruments. Typical examples include the removal of cosmic rays, the construction of a mosaic image, and the subtraction of the sky background from a sequence of on-target and off-target observations. These observations are distinguished by the fact that their calibration and processing depends upon other observations obtained *at the same time*.

The **calnicb** part of the pipeline carries out the calibration and merging of associated data frames, each of which has first been processed by **calnica**. In the case shown in Figure 13.3, the associated set has 3 individual datasets that are combined into one merged and calibrated dataset.

Figure 13.3: Conceptual calnicb Pipeline



We refer to these sets of exposures as *associated sets*. The **calnicb** task operates on an entire associated set and produces one or more products from that set (Figure 13.3). While the **calnicb** capabilities that are expected at the start of Cycle 7 are still being defined, it is intended that the combination of multiple exposures without telescope motion, i.e., *NEXP=n* (to remove cosmic rays and to improve signal to noise and dynamic range), the creation of mosaics (for which the telescope remained in Fine Guidance mode), and the scalar subtraction of the sky background from offset images (chopping) will be supported. In the latter case, each region of the sky (i.e., the target and one or more offset background regions) is saved in the Archive as a separate entity to permit the HST Data Archive to correctly report which positions on the sky have been observed.

## NICMOS Data Products

### Standard NICMOS Dataset Structure

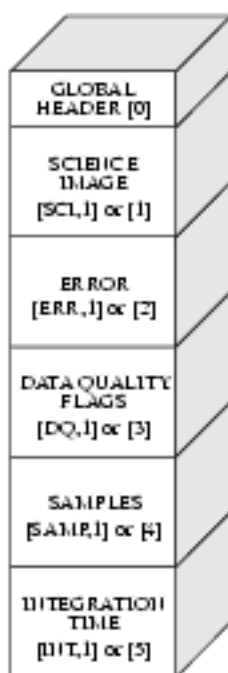
NICMOS data are represented by five arrays for each readout. These arrays contain the:

- Science image.
- Error array.
- Quality flags array.
- Samples array.
- Integration time array.

Each downlinked readout is always represented by these five arrays (Figure 13.4). Multiple readouts in the same dataset (e.g., MULTIACCUM data) are represented by repeated sets of these five arrays (Figure 13.5). It is expected that compact FITS representations will be available to store arrays in which all elements have the same value.

In the basic NICMOS data format, shown in Figure 13.4, each readout is represented by 5 arrays, each as a separate extension in the FITS container file. Any of the five arrays may be accessed by specifying its extension number: for example to access the data quality flags, specify the 3rd extension.

Figure 13.4: Data Format for ACCUM, RAMP, BRIGHTOBJ and ACQ Modes



### Science Image

The science image contains the information recorded by the NICMOS camera. The data may be represented as counts (i.e. data numbers) or as count rates (i.e. data numbers per second). Generally the latter is desirable since it is easier to interpret in mosaiced datasets and corresponds closely to flux.

### Error Array

The error array contains an estimate of the statistics error at each pixel. It is expressed as a real number of standard deviations. This is a calculated quantity based on a model of the instrument and its environment.

### Quality Flags Array

The quality flags array provides 16 independent flags for each pixel. Each flag has a true (set) or false (unset) state and is encoded as a bit in a 16 bit (short integer) word. Users are advised that this word should *not* be interpreted as an integer.

### Samples Array

The samples array is used for one of two purposes:

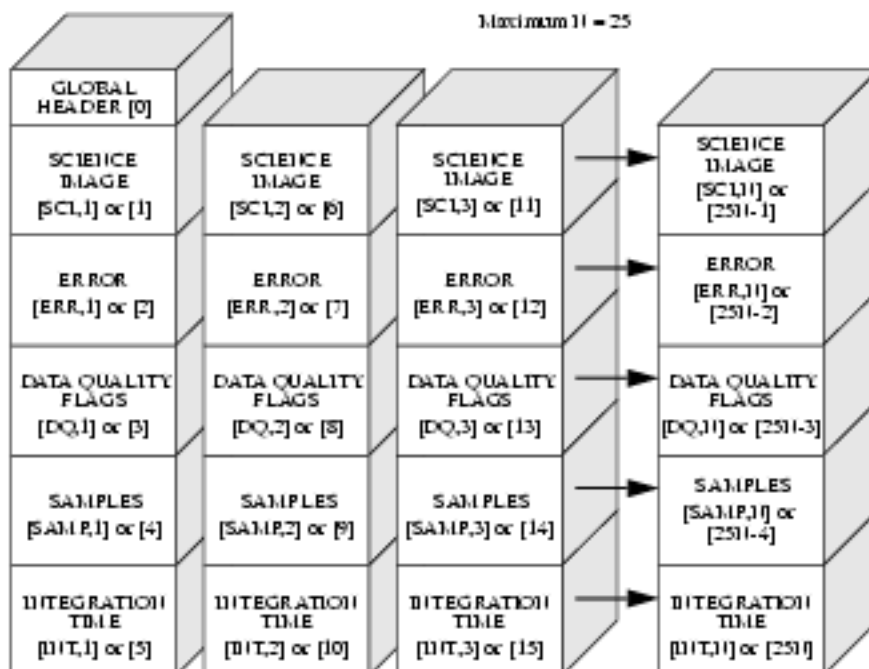
- For data where multiple samples of the array were obtained during the integration, the samples array denotes the number of samples for each pixel in the corresponding science image.
- When multiple integrations are combined to produce a single image, the samples array will contain the number of samples retained at each pixel. Note that this implies that the original number of samples information is not propagated forward into combined images.

### Integration Time Array

The integration time array contains the total integration time at each pixel. While initially a simple parameter in some observing modes, combining datasets into composite mosaics and using the information obtained by multiple non-destructive readouts during an integration requires us to keep track of the actual exposure time for each pixel. This array is useful for simple conversions between counts and count rates.

The MULTIACCUM mode (Figure 13.5) produces multiple images. The file structure for such a dataset consists of a lattice of the 5 image arrays which are created for each readout, as shown in Figure 13.5.

Figure 13.5: MULTIACCUM Data Format



## IRAF Access

### Backwards Compatibility

This data structure will be implemented so that the *default* array is the most meaningful science image array. For example, if you request IRAF to display a dataset, the first science image array would be displayed. Access to the other arrays within a dataset will be via element numbers (1–5; mod 5 for datasets containing multiple readouts) or via a standardized naming convention (see Figure 13.4 and Figure 13.5). It is a critical requirement that existing IRAF tasks be able to access any array in a NICMOS dataset.

### FITS File Format

The physical format of NICMOS datasets will be FITS with image extensions. Data will both be delivered to observers and used within IRAF and STSDAS in this format. A modified version of the IRAF kernel has been developed at STScI to support this data format directly. This permits the use of NICMOS data without conversion (i.e., the *strfits* task is not necessary). This will be distributed with the STSDAS system before Cycle 7.

# Expected Calibration Accuracies

**In This Chapter...**

Expected Accuracies / 285

This chapter describes the expected accuracies which should be reached in the calibration of NICMOS during Cycle 7.

---

## Expected Accuracies

### Remarks

In Table 14.1 we list a provisional summary of our calibration goals for Cycle 7. These goals will be achieved through the analysis of data obtained this summer during the ground testing and on-orbit during the Orbital Verification phase and Cycle 7. Observers may, and should, plan on NICMOS achieving these levels of performance. While higher levels of performance may indeed be possible (and even achieved) in Cycle 7, observers should not depend upon NICMOS being calibrated better than defined here. Science programs which require superior calibrations should request and justify additional observing time to reach the necessary calibration accuracy.

An update to these estimates will be provided in mid-August 1996 following analysis of the data obtained during the ground testing (SLTV) of NICMOS. Likewise, a revised set of calibration accuracy goals will be published in the early summer of 1997 for the Cycle 8 observing opportunity after on-orbit experience has been obtained.

## Areas of Significant Uncertainty

While the performance of NLCMOS can to a large extent be predicted from ground based testing, two significant uncertainties must wait for on-orbit measurements. First, the HST optics will be a source of thermal radiation which will contribute to the background. This will arise both from direct radiation from the  $\text{MgF}_2$  overcoated optics in the OTA and from radiation from baffles which has been scattered into the beam by dust and imperfections on the OTA mirror surfaces. Both of these sources are known to be fairly warm (15 to 17 C) and, while the OTA primary mirror has a fairly long thermal time constant, are subject to significant variations. This thermal radiation will affect only observations at fairly long wavelengths ( $>1.6$  microns).

Second, the effect of the charged particle environment on NLCMOS data is still uncertain. While extensive ground testing has demonstrated that degradation of the detectors is very unlikely over their planned lifetimes, electrons deposited by particle events are likely to be present in NLCMOS images. This will be similar to WFPC2 cosmic ray events, although their numbers, energy deposited, and sizes are still unknown.

Both of these topics will be studied early in the on-orbit SMOV test program.

## Provisional Cycle 7 Calibration Goals

Table 14.1: Summary of Cycle 7 Calibration Goals

Attribute	Accuracy	Limiting Factor/Notes
Detector dark current and shading	5% selected exposure times 10% overall	A subset of the available exposure times will have a direct dark calibration while all others will require interpolation.
Flat fields	1% broad band 2-3% narrow band	Color dependence may limit flats in some cases. The low spatial frequency may only be reliable to $\leq 3\%$ .
Photometry	10–15% absolute 5% relative	Photometric systems Intrapixel effects Filter leaks on red sources
Photometric stability over 1 year	1%	
PSF and focus	Maintained within 20% of best focus Strehl ratio.	Breathing and OTA desorption are approximately equal effects.
Co-nomographic PSF	0.18 arcsec positioning	Ability to control on target internal astrometry
Polarization	$\sim 1\%$ relative intensity <sup>a</sup>	
GRISM wavelength calibration	0.1 $\mu\text{m}$	Limited by centroiding of target for wavelength zero point determination.
GRISM photometric calibration	20–30% absolute and relative	Expected accuracy over central 80% of spectral range. Grism C flat field may not achieve this performance.
Astrometry	0.25% plate scale 0.1 <sup>0</sup> rotation	Limited by sampling of stellar images.
Telescope backgrounds	TBD Thermal background  TBD Stray light	Stability to be measured on orbit. Amplitude range and thermal variability to be measured on orbit. Artifacts and diffuse stray light to be measured on orbit.

a. The NICMOS fore-optics contain a number of reflections which are likely to introduce some instrumental polarization. The exact level of polarization induced is not yet known, but is most probably about 0.5–2%, and should be stable. Because the NICMOS detectors have high dynamic range, are not count rate limited, and the polarimeter forms the Stokes parameters using images through analyzers on the same locations on the detector, high intrinsic precision in polarimetry measurements should be possible, to an accuracy of 0.1–0.2%. Only flat fielding effects caused by image wander will potentially degrade this performance, and the as yet unknown quality of the analyzers. In principle then, a very accurate measurement of any instrumental polarization should be possible which will allow it to be subtracted from the science data. Given sufficient accuracy in the original data, we expect to be able to work down to polarization levels at least as low as the instrumental polarization.





## CHAPTER 15

# Calibration Plans

### In This Chapter...

Introduction / 289
Thermal Vacuum Test / 290
Servicing Mission Observatory Verification / 290
Cycle 7 Calibration Program / 290
Photometric Calibration / 293
References / 296

This Chapter describes the current state of the plans for the calibration of NICMOS during SLTV, SMOV and Cycle 7.

---

## Introduction

The calibrations available during Cycle 7 will be based on three distinct calibration activities. First, NICMOS will be extensively tested on the ground. These tests include a limited amount of calibration, particularly during the System Level Thermal Vacuum (SLTV) testing. Second, there will be a period following the installation of NICMOS into HST for testing and initial calibration. This activity is known as the Servicing Mission Observatory Verification (SMOV or SMOV2). Finally, the routine Cycle 7 calibration program will be performed.

It is important to distinguish between the various goals of these calibration activities. SLTV is intended to demonstrate the proper functioning of the Scientific Instrument (SI) and to obtain, if possible, an initial calibration of a subset of its capabilities. SMOV is intended to demonstrate that the instrument is functioning as expected, based on the SLTV experience, to characterize those parameters not measurable during SLTV (e.g., the thermal background generated by the HST optics), and to begin the calibration of NICMOS. In many cases the complete calibration will be conducted during Cycle 7 and SMOV will be used to demonstrate that the planned calibration is in fact feasible. This approach is designed to enable the acquisition of science observations at the earliest possible date, even if the best possible calibrations do not become available until some

time later. This contributes to the efficiency with which HST can be operated and maximizes the total number of NICMOS observations over its cryogen limited lifetime.

---

## Thermal Vacuum Test

The NICMOS System Level Thermal Vacuum test program (SLTV) will be conducted at Ball Aerospace during June 1996. The primary purpose of this activity is the validation of the operation of the assembled instrument in an environment nearly identical to HST's. This includes testing the thermal performance of the instrument, demonstrating proper operation of all commandable operating modes, exercising all mechanisms, and testing safing procedures. It also includes characterization of the detector performance (e.g., read noise and dark current). Of particular importance to the overall calibration program, flat fields using the flight optics and detectors will be obtained in each filter.

Enough calibrations should be obtained from SLTV to initially populate the Calibration Data Base at STScI. These calibrations are available to users (via the HST Data Archive) and are used by STScI in the routine data processing calibration pipeline. Clearly, some of these calibrations will require updating from on-orbit observations before they are of much scientific utility (e.g., the photometric zero points). However, others (e.g., linearity corrections) will probably be satisfactory.

---

## Servicing Mission Observatory Verification

The current SMOV plan for NICMOS consists of 22 activities as listed in Table 15.1. Some of these (e.g., 1 through 6) test specific components of the instruments while others characterize its performance within the HST environment (e.g., 7, 8, 17, and 22). Activities 12 and 13 align the NICMOS fore-optics; activities 9, 10, 11, and 21 enable the use of the coronagraph in Camera 2; activities 15 and 20 characterize the detectors; and activities 18 and 19 establish the initial photometric calibration.

---

## Cycle 7 Calibration Program

At the time this handbook was written, the Cycle 7 calibration programs had not yet been defined in detail. Therefore, this section should be regarded as a general statement of purpose but it is reasonable to expect the specifics to evolve. In particular, the calibration program is driven in large part by proposal demand. The initial version of the calibration program will be based on the GTO observing

Table 15.1: Planned NICMOS SMOV Activities

Activity	Title	Demonstrates or Calibrates
1	NICMOS to Hold Mode	Basic operation of computer and HST interfaces.
2	NICMOS Internal Parallel Test	Demonstrate absence of interference due to parallel operation of camera and filter wheels.
3	NICMOS Memory Load and Dump Test	Test memory and code in internal computer.
4	NICMOS Field Offset Mechanism Test	Test and characterize operation and optical performance of the Field Offset Mirror.
5	NICMOS Filter Wheel Mechanisms Test	Verify operation and correct location of each position on each filter wheel.
6	NICMOS SAA Contour Test	Characterize effects of radiation on NICMOS electronics and detector performance; determine optimal SAA limits.
7	NICMOS Dewar Heaters Setpoint Adjustment	Establish optimal external dewar temperature.
8	NICMOS Transfer Function Test	Set optimal detector DC offset voltages.
9	NICMOS Target Acquisition Test	Demonstrate Mode 2 (autonomous) acquisitions.
10	NICMOS to FGS Astrometric Calibration	Establish the locations of the NICMOS detectors within the FGS coordinate system.
11	NICMOS Plate Scale and Astrometric Calibration	Determine plate scales, relative field rotations, and field distortions for each camera.
12	NICMOS Coarse Optical Alignment	Initial focus and tip/tilt adjustment of the Pupil alignment mirror based on modeled images.
13	NICMOS Fine Optical Alignment	Optimal positioning of the PAM based on grid of small PAM motions.
14	NICMOS Point Spread Function Characterization	Characterization of the imaging performance of NICMOS and initial set of PSF observations.
15	NICMOS Persistence Test	Characterize the effect of severe overexposure of the NICMOS detectors.
16	NICMOS Inflat Transfer and Stability Test	Demonstration of flat fielding capability and stability monitoring. Bootstrap of SLTV flat fields.
17	NICMOS HST Thermal Background Test	Characterization of HST generated thermal background over a broad range of situations.
18	NICMOS Absolute Photometry Test	Standard star observations across NICMOS wavelength range. Updates SLTV throughput calibration.
19	NICMOS Differential Photometry Test	Inter-camera photometric precision and stability test obtained from observations of a star at 25 positions.
20	NICMOS Detector Noise and Dark Characterization	Characterization of detector noise and dark current. Verification of stability since SLTV.
21	Coronagraph Verification	Optical characterization of coronagraphic stray light rejection and PSF of the obscured star.
22	Limb Avoidance Determination	Determination of the appropriate bright and dark earth limb angle restrictions for normal and low-background NICMOS observations.

program with appropriate modification following the TAC decisions on the GO program in late 1996. Technical problems with NICMOS (discovered either during SLTV or SMOV) may lead to significant changes in this program.

## Photometry

Photometric observations of standard stars from both the white dwarf and solar analog samples (see below) will be obtained in all filters and grisms. Experiments to determine the reproducibility of photometric measurements as a function of both position on the detectors and time will be carried out.

## Detector Performance

All three detectors will be characterized to the same extent. Since dark current is a highly non-linear function of exposure time, we will obtain high quality dark frames for only a limited subset (~30) of the possible exposure times. Other exposure times will require interpolated dark current subtraction which *may* be less satisfactory. The selected exposure times will be published in the Phase 2 proposal instructions. Changes in detector performance (bad pixels, dark current, read noise, linearity) will be monitored.

## Flat Fields

All filters will have SLTV flat fields. We expect to bootstrap these to on-orbit flat fields during SMOV and to monitor their stability with the internal flat field lamps. As was done for WFPC2, this bootstrap calibration will be based on a small number of on-orbit flats. We expect to obtain sky and earth flats for all NICMOS filters during the course of Cycle 7 with some filters being designated for a greater calibration effort based on usage and their role in the photometric system.

## Background Characterizations

NICMOS will see significant thermal background from the HST optics. Continuing characterization and definition of optimal observing strategies (particularly for very deep observations) will be performed during SMOV and Cycle 7.

## Point Spread Function

We will obtain a detailed characterization of the PSF in a few filters during SMOV including the effects of intra-pixel sampling. As with WFPC2, standard star observations will result in nominally exposed PSFs at the default aperture positions. Observers who require PSFs in specific filters and/or locations within

the field of view are advised to include these in their own programs. The stability of the PSF will be monitored and the optical alignment and focus maintained.

## Coronagraph

The ability to position a star behind the coronagraphic mask will be enabled during SMOV. This necessitates a fairly high quality astrometric calibration of Camera 2 and should also result in high quality Camera 1 and 3 astrometry. The PSF within the coronagraph will also be characterized.

## Grisms

The dispersion and flux calibration of the grism multi-object spectrographs will be carried out during Cycle 7. The PSF as a function of wavelength will be determined.

## Polarizers

Throughput, position angle, and polarization calibrations will be obtained during Cycle 7.

## Time Variability

While the instrument is expected to be very stable these calibration observations will monitor any aspects of the NICMOS performance that might be time variable. Typically, observations will be made at 3 monthly intervals to verify that the performance has not changed significantly.

---

# Photometric Calibration

## Flux Standards for NICMOS Absolute Calibration

The absolute flux calibration of NICMOS will be calculated from observations of standard stars with known flux distributions  $F(\lambda)$ . The sensitivity as a function of wavelength for the dispersed spectra from the grisms is determined directly from the known  $F(\lambda)$  and the observed response, after any required corrections for flat field response. Sensitivities for the filters are calculated from observations of the standard stars according to the synthetic photometry procedure detailed in Koomeef *et al.* (1986). Since the pipeline calibration cannot utilize color information, the header of the reduced data will contain the calibration constant for the filter that specifies the equivalent flux for a constant spectral distribution as a function of wavelength. For convenience, this calibration constant appears

twice, once in Jansky units and once in  $\text{erg s}^{-1} \text{cm}^{-2} \text{\AA}^{-1}$  units. Color transformations could be defined for post-pipeline data analysis.

### White Dwarf Absolute Standards

The flux distributions of our primary standard stars are defined by models for the four pure hydrogen white dwarfs in Table 15.2 (Bohlin, Colina, & Finley 1995). Bohlin (1996) transfers these calibrations to FOS and IUE data in the UV and to the optical spectra of Oke (1990) to obtain a set of standards with fluxes that are accurate to a few percent from 1150–9200 Å. Observations of this set of standard stars produces consistent absolute flux calibrations on the WD scale for the current HST instrument complement. Unfortunately, only the four white dwarf flux distributions are currently available to the limit of NICMOS coverage at 2.5  $\mu\text{m}$ .

Table 15.2: WD Standard Stars

Star	K	Sp.T.	V	B-V
G191B2B	12.7	DA0	11.781	-0.33
GD71	13.8	DA1	13.032	-0.25
GD153	14.2	DA1	13.346	-0.27
HZ43	13.7	DA1	12.914	-0.31

### Solar Analog Absolute Standards

In order to expand the set of IR standard stars in the appropriate flux range for NICMOS, M. Rieke, R. Thompson, and collaborators at the University of Arizona are making photometric observations of solar-analog stars, which will be used to normalize the solar spectrum to the observed IR magnitudes. This method consists of several steps:

1. The solar colors in the photometric system are determined by assuming that the average colors of the solar analogs are equal to those of the Sun (classified as a G2V star).
2. The zero point of the absolute flux density in each near-infrared photometric bandpass is calculated from the photometric magnitudes for the Sun and the absolute flux spectrum of the Sun.
3. The absolute solar flux density in each photometric band is scaled in proportion to the magnitude of the solar analog star relative to that of the Sun.

The final absolute flux accuracy achieved by the solar-analog method relies on two basic assumptions:

1. That the absolutely calibrated reference spectrum of the Sun is known with an uncertainty of a few percent (Colina, Bohlin, & Castelli 1996).
2. That the spectra of the solar-analogs are identical to the solar spectrum, i.e., agree within the 2% uncertainty in the shape of the flux distribution at infrared wavelengths.

The solar-analog method was used in the past to determine the absolute calibration of near-infrared photometry (Campins, Rieke, and Lebofsky, 1985) at ground-based observatories. The accuracy in the absolute calibration was at least 5%, and for some bands, 2% to 3% (Campins et al., 1985).

As a check on the solar analog method, the ground-based program includes observations of the WD G191B2B. Furthermore, FOS observations of three prime solar analog candidates listed in Table 15.3 will be made during Cycle 6. The FOS red detector will be used with the high resolution G780H, G570H, G400H and G270H to obtain high signal to noise spectra of these three candidates over the 2200 to 8500 angstroms range to verify agreement with the solar flux distribution.

Table 15.3: Prime Solar Analog Candidates

Star	V	K	E(B-V)	B-V	V-I	RA(1950)	DEC(1950)	No. <sup>a</sup>
P041-C	11.99	10.56	0.01	0.62	0.69	14:51:42.9	+71:55:36	4
P177-D	13.50	12.09	0.01	0.63	0.71	15:57:43.2	+47:45:07	5
P330-E	13.03	11.62	0.01	0.63	0.74	16:29:35.8	+30:15:09	5

a. No. indicates the number of observations in hand by the U. of Arizona group as of 96Feb22. For the Sun, B-V=0.633 (Taylor 1994), and V-I=0.703 (Bessell and Norris 1984).

## Ground Based Calibrations

The existing near-infrared standard star lists used by ground-based telescopes are inadequate for NICMOS because they are too bright and there is a dearth of suitable observations to rule out low-level Near-IR variability for most stars. As we mentioned previously, to counter this problem, a large program of J, H, K photometry has been conducted by a team lead by Marcia Rieke of Steward Observatory. The star selection is based upon HST Guide Star Availability/Suitability Windows.

In the Northern Hemisphere observations have been performed with a NICMOS2 array on the Mt. Lemmon 60" & Kitt Peak 90" and in the Southern Hemisphere with a NICMOS3 array on the Las Campanas 40".

The primary goals of the program were:

- Relative flux references accurate to 1.5% for standard photometry.
- Color transformations between ground based and NICMOS systems.
- Relative absolute wavelength & spectrophotometric references for Grisms.
- Polarization standards.

### Sample Selection

Solar analogs from HST Guide Star Photometric Survey (Lasker and Sturch) form the main flux references to bridge the gaps in atmospheric transmission. Solar analogs were chosen because:

- Dispersion in Near IR colors is very small in G-stars.

- Minimum number of strong spectral features in Near-IR.
- Solar spectrum available throughout range of NUCMOS sensitivity.

A small number of non-variable M-dwarfs, with  $V-K \leq 8$ , and which do not show emission lines in their spectrum have also been used to enable color transformations, as have three White Dwarfs (HZ44, Feige 66, and G191B2B) taken from Table 15.2.

The data has been cross-calibrated using the list of Elias et al. (1982, *AJ*, **87**, 1029). The majority of the targets will have been observed on at least 5 nights to screen for variables at the 1.5% level.

---

## References

- Bessell, M., and Norris, 1984, *ApJ*, 285, 622.
- Bohlin, R. C., 1996, *AJ*, 111, April.
- Bohlin, R. C., Colina, L., and Finley, D. S., 1995, *AJ*, 110, 1316.
- Campins, H., Rieke, G. H., and Levofsky, M. J., 1985, *AJ*, 90, 896.
- Colina, L., Bohlin, R. C., and Castelli, F., 1996, *AJ*, in press.
- Koomneef, J., Bohlin, R. C., Buser, R., Horne, K. D., and Turnshek, D. A. 1986, *Synthetic Photometry and the Calibration of the HST, Highlights in Astronomy*, Vol. 7, ed. J.-P. Swings (Reidel), p. 833; also Appendix 1 of Turnshek, D. A., Baum, W. A., Bohlin, R. C., Dolan, J. F., Horne, K. D., Koomneef, J., Oke, J. B., and Williamson, R. L. 1989, Standard Astronomical Sources for HST: 2. Optical Calibration Targets, STScI.
- Oke, J. B. 1990, *AJ*, 99, 1621.
- Taylor, 1994, *PASP*, 106, 444.



# Appendix

## In This Appendix...

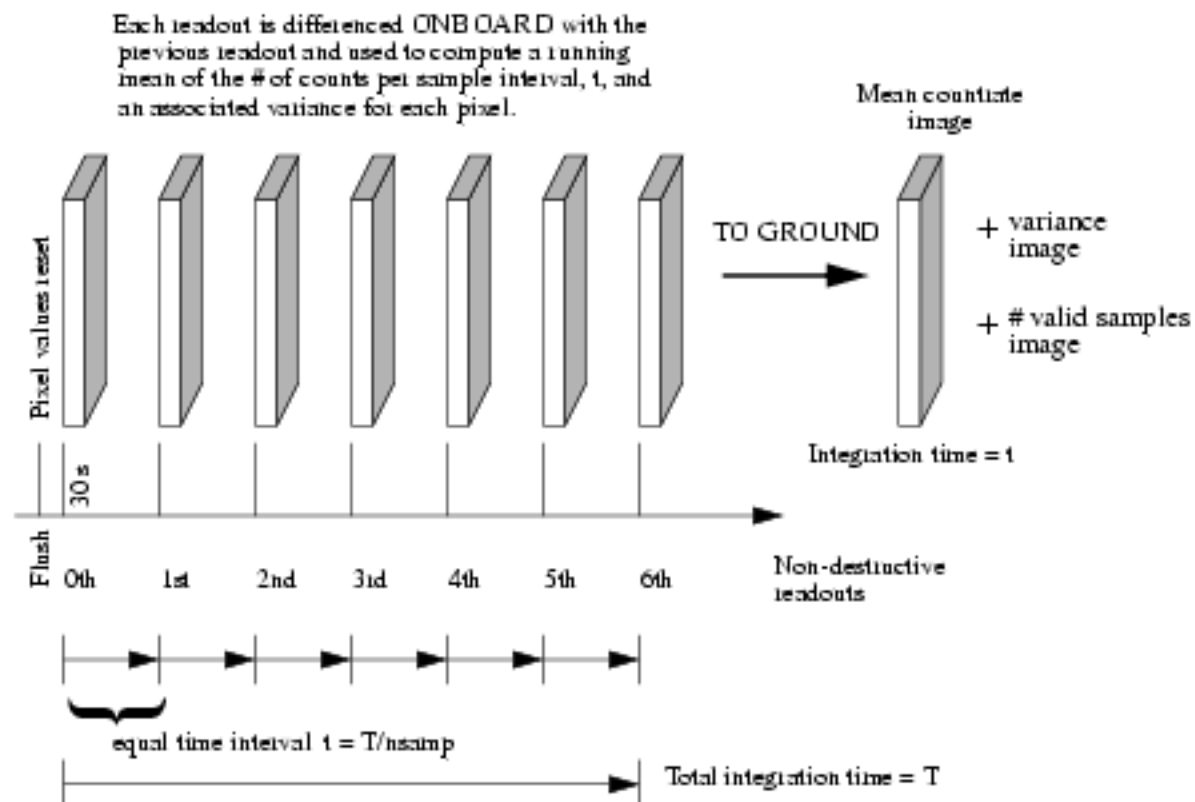
Ramp Mode / 301

---

## Ramp Mode

The RAMP mode is an intrinsically different way of obtaining an image which can be thought of as an on-board hybrid between ACCUM and MULTIACCUM, providing a limited version of the advantages we described for MULTIACCUM with the simplicity of ACCUM, producing a single output image at the end of the exposure. RAMP mode is appropriate when high dynamic range or cosmic ray cleaned observations are required but the data volume is constrained. The basic ideas behind the RAMP mode are illustrated in Figure 7.4.

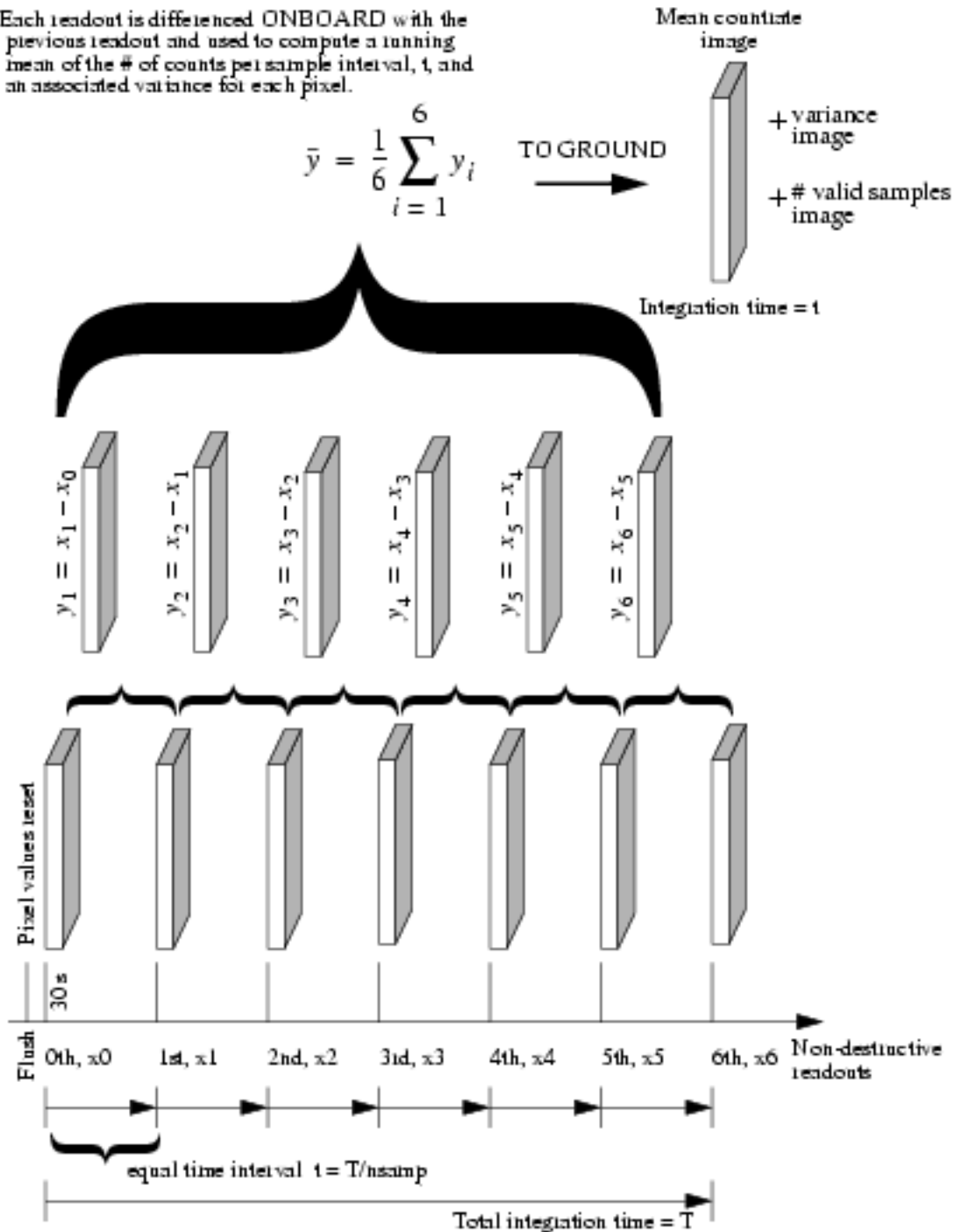
Figure A.1: Basic Ramp-Mode for NSAMP = 6



As in the case of the MULTIACCUM mode, in RAMP mode the initial detector readout, which obtains the initial pixel values, is followed by a number, NSAMP, of non-destructive readouts, up to a maximum of 254. Both the integration time  $T$  and the number of passes NSAMP are set by the observer in the proposal. Unlike the readouts of MULTIACCUM the intermediate readouts in RAMP mode must be at equal intervals during the exposure and are not individually downlinked to the ground. The integration time is the time between the initial non-destructive read of the first pixel and the last non-destructive read of the first pixel. If  $T$  is the total integration time the sub-reads occur at intervals of  $T/NSAMP$ . As illustrated in Figure 7.5, each of the ramp samples are formed by taking the difference between the cumulative signal recorded after the current read and that obtained at the previous read.

Figure A.2: The On-Board Ramp Mode Calculations

Each readout is differenced ONBOARD with the previous readout and used to compute a running mean of the # of counts per sample interval,  $t$ , and an associated variance for each pixel.



The time taken to perform the ramp calculation is ~7 seconds per camera and this sets the minimum time between successive ramp samples. Thus if 3 cameras are in use in ramp mode this restriction expands to > 21 seconds (there are other overheads involved). Ramp mode produces three data arrays; the image which contains the mean values of the slope or ramp of each pixel derived from the

difference images; the number of samples which were used to determine the slope, and the variance over all the samples used in the calculation of the image.<sup>1</sup>

The aware reader will have realized that if all the difference images are used to form this final mean the output of RAMP mode will be identical to that of an ACCUM for a time  $T/115AMP$ . However, the great power of RAMP mode is that during the calculation of the slope it is also possible to detect pixel saturation and optionally cosmic rays, but not without penalties as we will explain shortly. A variety of ways of using this saturation and cosmic ray hit information are available to the user. The samples array becomes meaningful when one of these options is chosen.

## Using Ramp Mode to Reject Cosmic Rays and Detect Saturation

Ramp mode provides processing mechanisms for the detection, and elimination of cosmic rays (CR) and for saturation detection. The optional parameter CR-ELIMINATION (see the proposal instructions) selects from four available processing modes for handling cosmic ray events. We have already described the first of these in which no action is taken, and the data returned is equivalent to a simple ACCUM exposure. Since the ramp mode computes a progressively updated variance at each sample cosmic ray events are detected by changes in slope which are more than  $3\sigma$  away from the slope determined by the previous reads. The basic principles behind cosmic ray rejection are illustrated in Figure A.3 and Figure A.4.

In the CONTINUE method, which is the default setting, when a cosmic ray is detected at a given pixel the value from that ramp sample for that pixel is eliminated from the image and variance arrays. Other pixels are unaffected by the detection. The ramp sampling then continues until the end of the exposure, removing any subsequent suspect samples in the same way on a pixel-by-pixel basis.

In the RETAIN method when a cosmic ray is detected at a given pixel, processing for that pixel is suspended and the mean pixel and variance values obtained up to the sample in which the CR hit occurred are recorded and the number of valid samples is set to that before the hit occurred. As before, other pixels are unaffected by the detection. The ramp sampling continues processing these until either they also receive a CR hit, and are themselves suspended, or the end of the exposure is reached.

In The MARK method any pixel which receives a detected CR hit is flagged as bad (set = 0) in the data quality array, but the sample in which this occurred, and all subsequent samples, are still used in the variance and pixel value calculations.

---

1. The term *ramp* came from the original concept of performing an updating linear least-squares fit to the data, which was not implemented due to the limited computer power of the NICMOS computer. Over 20 seconds would be required to compute the LSQ-fit at each ramp step.

The user then has the responsibility for deciding what to do with suspect pixels during analysis.

Figure A.3 shows the ramp mode operation for an uncontaminated signal. In the top panel we see the cumulative counts with time. Marked is the time interval between ramp samples,  $t$ , and the signal associated with each ramp sample. The middle panel shows a plot of the signals measured in each of the ramp samples. Since there is no cosmic ray contamination, this is essentially a constant except for statistical fluctuations. The bottom panel shows how the data quality flag would have been evaluated for each ramp sample by the flight software. In this case all samples are good.

Figure A.3: Ramp Mode Operation for Uncontaminated Signal

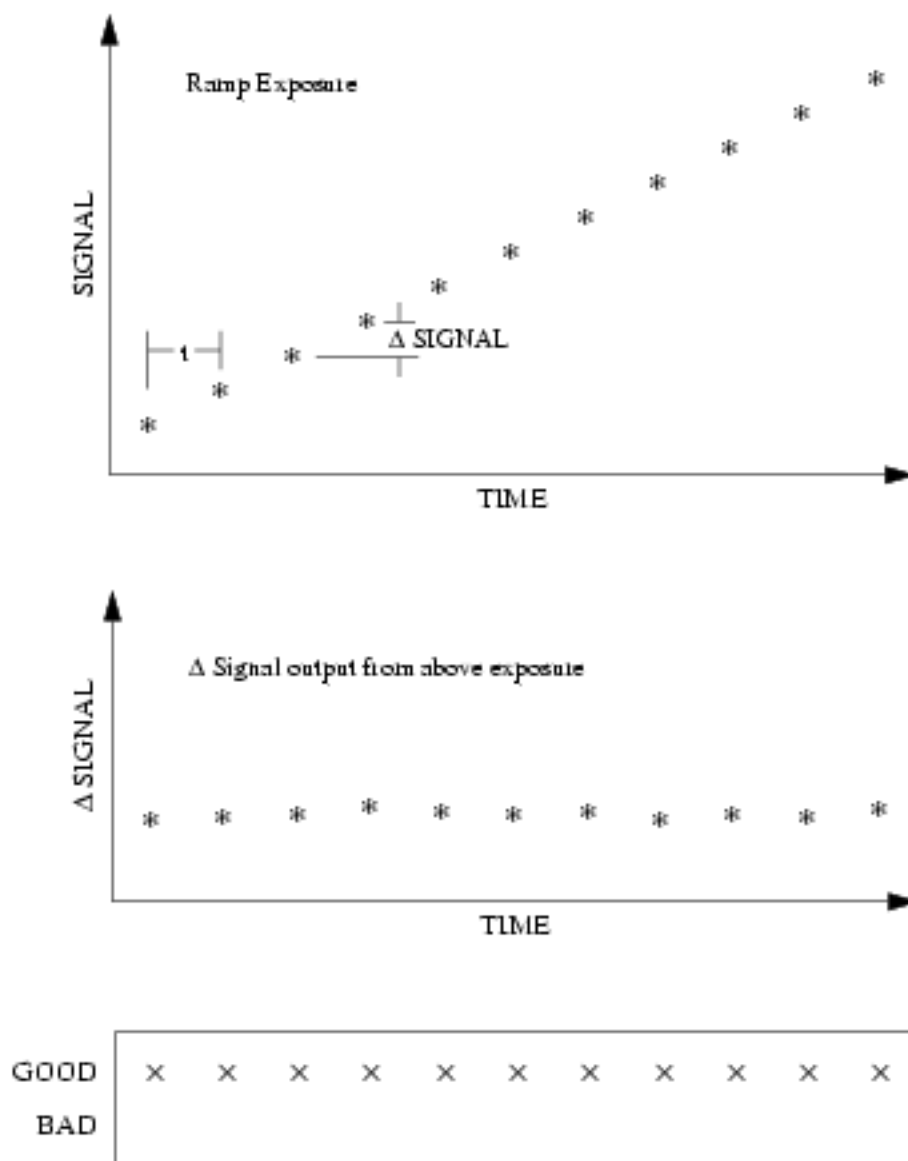
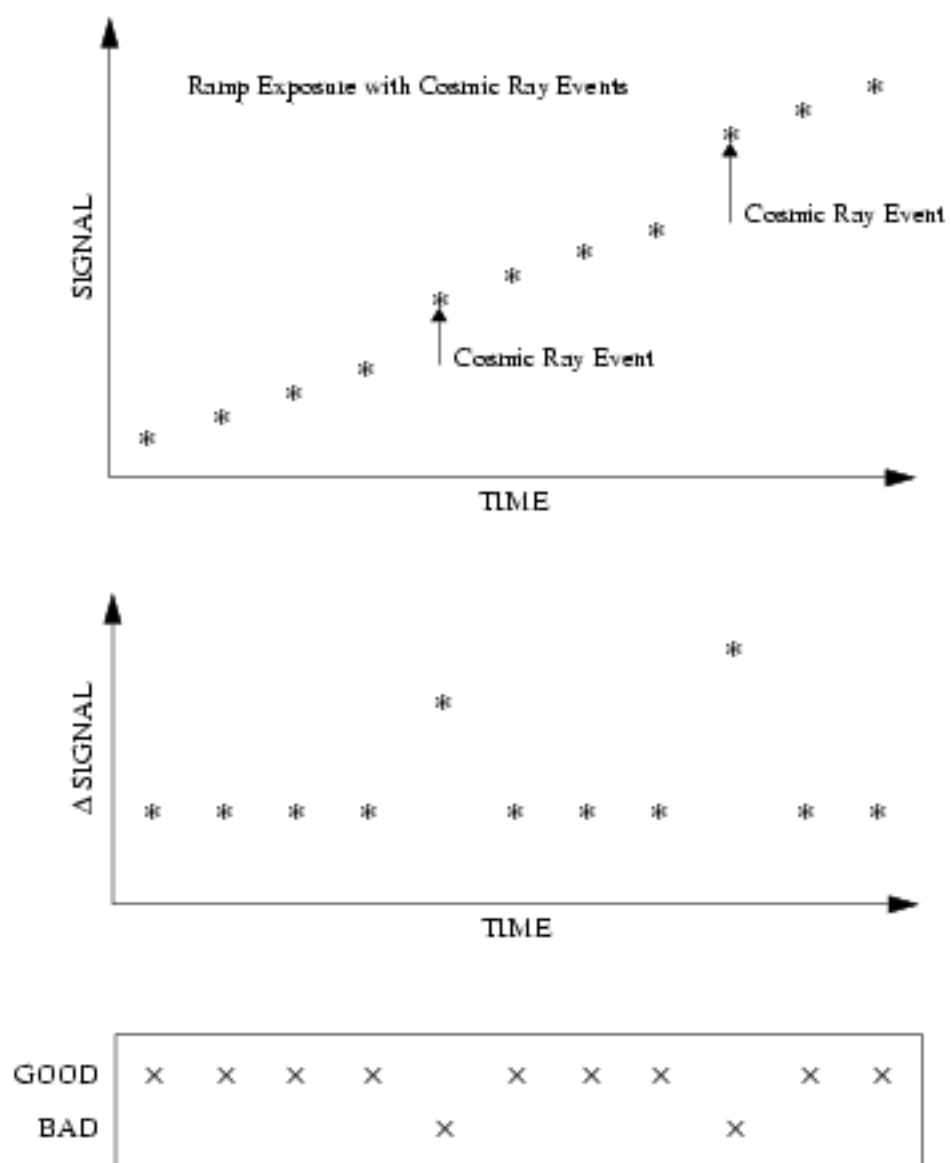


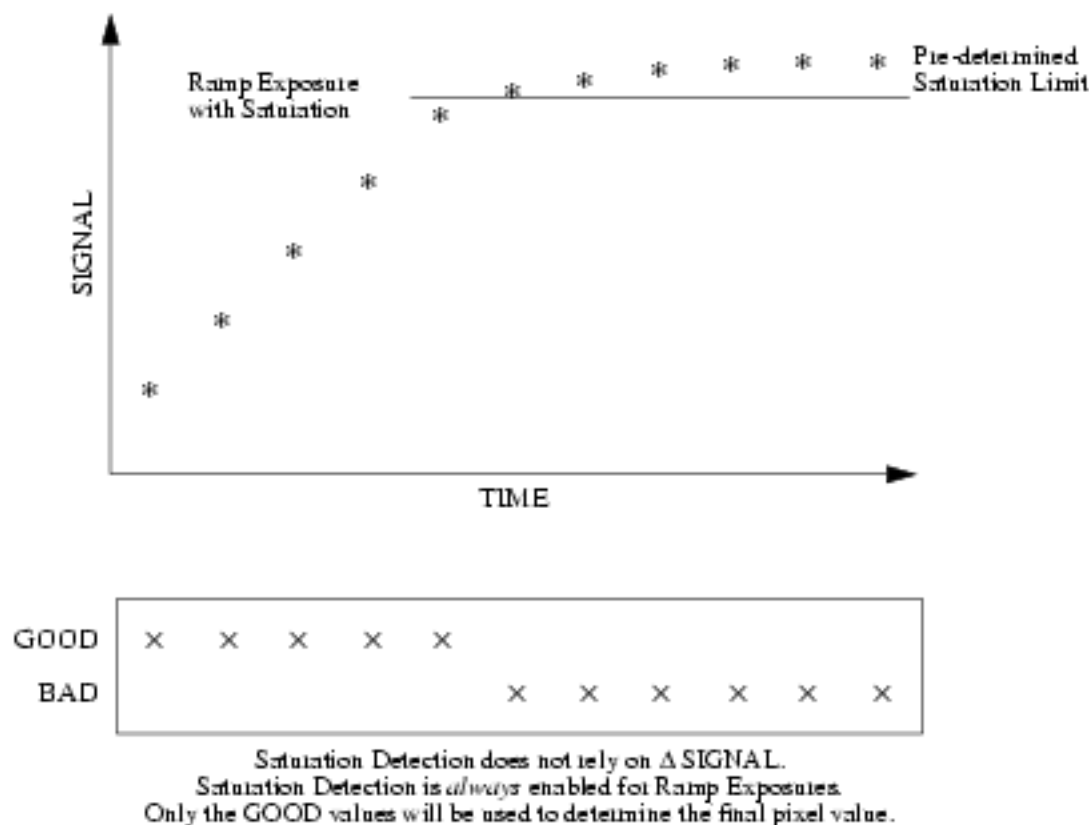
Figure A.4 shows ramp mode operation for a signal contaminated with cosmic rays. In the top panel we again see the cumulative counts with time. Two cosmic ray events are marked. The middle panel again shows a plot of the signals measured in each of the ramp samples. Notice that the samples effected by the cosmic rays are outliers from the trend we saw in Figure A.3. The bottom panel shows how the quality flag would have been evaluated for each ramp sample by the flight software. The two samples with cosmic ray hits have been identified as bad and are not used in the final calculation of the mean signal.

Figure A.4: Ramp Mode Operation for Signal Contaminated by Cosmic Rays



RAMP mode also discontinues the processing on a pixel once the signal in the pixel reaches a level in which the deviation from linearity is  $> 2\%$ . As shown in Figure A.5, the result up to that time, and the number of samples which had been collected are stored and downlinked. This can be very useful in images where the expected flux levels are not well known and in serendipitous or survey observations. Figure A.5 shows ramp mode operation for a signal which reaches the saturation or nonlinear limit prior to the end of the exposure. In the top panel we again see the cumulative counts with time. The horizontal line marks the saturation or nonlinear threshold. The bottom panel shows how the quality flag would have been evaluated for each ramp sample by the flight software. All the samples which occur after the saturation limit have been identified as bad and are not used in the final calculation of the mean signal.

Figure A.5: Ramp Mode Operation for Signal Reaching Saturation Before Exposure End



## Limitations of Ramp Mode

### Dark Current Removal

The real science data sits on a plateau of dark current which is a varying function of time since reset (the shading effect—see Chapter 7). As this dark current varies significantly, at least in the first minute, in order to update the mean and variance without bias its contribution has to be removed. Moreover, with either or both the *saturation* and *rejection* actions turned on, each pixel can essentially have a different integration time (number of valid samples). Since the ramp mode will return an output array without the dark current removed this has to be accounted for in the subsequent data reduction, either using an empirical correction or a model. How this model is implemented is therefore *crucial* to the functioning of the mode as a failure to treat it properly will invalidate ramp mode data for faint sources. At present it is not clear how well this can be done. One must ensure that sufficient ramp samples are obtained in order for the ramp calculations to be reliable. Ideally this should be a number  $> 30$ , but numbers as low as 16 or so might well suffice, if the frequency of cosmic ray hits on orbit is



not too high. Because the start of the ramp calculation has to be delayed for ~30 seconds to avoid the effects of shading ramp mode will not be useful for bright sources

### Cosmic Ray ADU Distribution Function

In an automatic sigma clipping procedure a crucial parameter is the *threshold* at which the rejection occurs. If this is set too high then there can be many low level cosmic rays which are not removed. With the ramp mode data it will not be possible to remove them without interpolating over them. Even detected CR hits will potentially have *halos* of distributed charge around them which might still contaminate the data if the CR hits turn out to not be confined to single pixels. This is a significant disadvantage compared to MULTI-ACCUM mode. More seriously if it is set too low then the underlying statistical distribution of the real events is censored invalidating the basic assumptions implicit in standard error analysis. This difficulty has led statisticians to develop robust iterative techniques for such problems. However these are computationally expensive, and require all the data to be kept in memory, so that a dynamic adjustment of the rejection criteria can take place. On board HST, the timing restriction created by the limited computing power of the flight computers eliminate this as a practical possibility.

### Cosmic Rays that Won't be Detected

Detection of cosmic rays (CR) in RAMP mode relies on discontinuities in the detected count rate for a pixel. However, three readouts are needed in order to make an estimate of the count rate. Cosmic ray hits before the fourth readout are therefore not detected. The first readout cannot occur earlier than 30 seconds into the integration, and the minimum time between readouts in RAMP mode is about 7 seconds. Therefore, the fourth readout cannot occur any sooner than 51 seconds into the integration. There is a significant probability that cosmic ray hits will occur during the first minute of an integration. These hits will not be detected or removed in RAMP mode (in MULTACCUM, on the other hand, since all the readouts are accessible to the pipeline calibration software, cosmic rays can be detected at any stage during the integration).



# Glossary

The following terms and acronyms are used in this handbook.

*A-D*: Analog to digital.

*CCD*: Charge-coupled device. Solid-state, light detecting device.

*CDBS*: Calibration Data Base. System for maintaining reference files and tables used to calibrate HST observational datasets.

*CIT*: California Institute of Technology.

*COSTAR*: Corrective Optics Space Telescope Axial Replacement.

*CP*: Call for Proposals.

*CR*: Cosmic ray.

*CVZ*: Continuous viewing zone.

*DQ*: Data quality.

*DQE*: Detector quantum efficiency.

*DN*: Data number.

*FAQ*: Frequently asked questions.

*FGS*: Fine Guidance Sensors.

*FITS*: Flexible Image Transport System. A generic IEEE- and NASA-defined standard used for storing image data.

*FOC*: Faint Object Camera.

*FOM*: Field Offset Mirror (or mechanism)

*FOS*: Faint Object Spectrograph.

*FOV*: Field of view.

*FPA*: Focal plane array.

*FSW*: Flight software.

*FTP*: File Transfer Protocol. Basic tool used to retrieve files from a remote system. Ask your system manager for information about using FTP.

*FUV*: Far ultraviolet.

*FWHM*: Full width at half maximum.

- GEIS*: Generic Edited Information Set. The multigroup format used by STSDAS for storing some HST image data.
- GHR*: Goddard High-Resolution Spectrograph.
- GO*: General Observer.
- GTO*: Guaranteed Time Observer.
- HSP*: High-Speed Photometer.
- HST*: Hubble Space Telescope.
- ICD*: Interface control document. Defines data structures used between software or systems to ensure compatibility.
- IDT*: Instrument Development Team.
- IR*: Infrared.
- IRAF*: Image Reduction and Analysis System. The system on which STSDAS is built.
- IUE*: International Ultraviolet Explorer.
- K*: Degree Kelvin.
- LSF*: Line spread function.
- MOS*: Multi-object spectroscopy.
- ND*: Neutral density.
- NICMOS*: Near-Infrared Camera and Multi-Object Spectrograph.
- NUV*: Near ultraviolet.
- OPUS*: OSS and PODPS Unified Systems.
- OSS*: Observation Support System.
- OTA*: Optical Telescope Assembly.
- PAM*: Pupil Alignment Mirror (or mechanism).
- PI*: Principal investigator.
- PODPS*: Post-Observation Data Processing System.
- PSF*: Point spread function.
- QE*: Quantum efficiency.
- RA*: Right ascension.
- rms*: Root mean square.
- SAM*: Small angle motion.
- SLTV*: System level thermal vacuum (testing phase).
- SMOV*: Servicing Mission Orbital Verification.
- S/N*: Signal-to-noise ratio.
- SSR*: Solid state recorder.
- ST-ECF*: Space Telescope European Coordinating Facility.

*STEIS*: Space Telescope Electronic Information System. The World Wide Web host from which information, software, documentation, and other resources pertaining to the HST can be obtained.

*STIS*: Space Telescope Imaging Spectrograph.

*STScI*: Space Telescope Science Institute.

*STSDAS*: Space Telescope Science Data Analysis System. The complete suite of data analysis and calibration routines used to process HST data.

*SV*: Science verification. Process of taking observations that can be used for HST instrument calibration.

*TAC*: Telescope Allocation Committee.

*URL*: Uniform resource locator. Address for WWW.

*UV*: Ultraviolet.

*WF/PC*: Wide Field/Planetary Camera.

*WFPC2*: Wide Field Planetary Camera-2. Replacement for WF/PC installed during first servicing mission of December 1993.

*WWW*: World Wide Web. Hypertext-oriented method for finding and retrieving information over the Internet.

*YSO*: Young stellar object.



# Index

## A

- abbreviations
  - in this manual 297
- ACCUM
  - dark current calibration 112
  - data format 282
  - example, grism overhead 130
  - example, map overhead 128
  - function of 106
  - minimum time 108
  - mode, described 25, 107
  - multiple reads 108
  - overheads 123
- accumulate mode, see "ACCUM"
- accuracy
  - expected for calibration 285
- ACQ
  - data format 282
  - function of 106
  - mode, described 116
- acronyms
  - used in this manual 297
- aperture
  - defining 48
  - NIC1 through NIC3-FLX 48
  - NIC2-ACQ 52
  - NIC2-CORON 52
- archive
  - calibrated data 275
  - file formats 13
  - reference files 276
- array
  - comparison to CCD 25
  - dataset 282
  - read 107
  - reset 107
- association

- datasets
- atomic lines 264
- attached parallel 27

## B

- background radiation
  - calibration exposures 292
  - ground-based 28
  - in exposure calculations 76
  - infrared 28
  - low sky 31
  - spectroscopy 68
  - stability 30, 287
  - subtraction 139
  - thermal 14, 30, 92, 125, 126, 129, 139, 142, 286
  - zodiacal light 30
- bad pixels
  - detector 92
- bandpass
  - see "filter"
- bright object mode, see "BRIGHT-OBJ"
- BRIGHTOBJ
  - data format 282
  - exposure times 115
  - function of 106
  - mode, described 114
  - overheads 123

## C

- calibration
  - background 292
  - calnica 278
  - calnicb 281
  - coronagraphy 287, 293
  - cycle 7 goals 287, 289

- described 275
  - detector performance 287, 292
  - expected accuracy 285
  - flat fields 97, 292
  - grism 293
  - photometric 287, 292, 293–296
  - point spread function 287, 292
  - polarimetry 293
  - reference files 276
  - software 278
  - sources 289
  - stats
    - P330E 295
    - stats, G191B2B 294
    - stats, GD153 294
    - stats, GD71 294
    - stats, H243 294
    - stats, P041-C 295
    - stats, P177D 295
    - unsupported modes 13
  - calnica task 278
  - calnicb task 281
  - camera
    - attached parallel 27
    - changing, overhead 123, 128
    - coronagraphy 51
    - field of view 22
    - filters 36, 155
    - orientation 22
    - overhead 123, 128
    - polarimetry 56
    - resolution 22
    - spectroscopy, camera 3 64
  - camera 1 through camera 3
    - see "camera" and "filter"
  - CCD
    - compared to NICMOS array 25
  - chop
    - described 141
    - examples 147
    - overhead 123
    - pattern 143, 145
    - size 153
    - SPIRAL-DITH-CHOP 131
    - TWO-CHOP 128
    - YSTRIP-DITH-CHOP 130
  - CO lines 264
  - color
    - effect on sensitivity 102
  - coordinate system
    - NICMOS 49
  - coronagraphy 18
    - aperture 48
    - calibration exposures 293
    - coronagraphic mask 52
    - coronagraphic spot 51
    - expected accuracy 287
    - image contrast, PSF
      - centering 54
    - target acquisition 52, 116
    - target acquisition overhead 122
  - cosmic rays
    - effect 96
    - RAMP 304, 309
    - uncertainty 286
  - Cycle 7
    - calibration goals 287
    - see also "proposal"
- ## D
- dark current
    - calibration in ACCUM or MULTIACCUM 112
    - detector 25, 92
    - exposure times 113
    - RAMP 308
  - data
    - associations
    - calibration process 275
    - dataset 117, 283
    - described 276, 282
    - error array 283
    - format 282
    - integration time array 283
    - quality 283
    - quality flags 283
    - readout, overhead 123
    - samples array 283
    - science dataset, structure 117
    - science image 283
  - definitions
    - terms used in this manual 297



## detector

- array reset 107
- arrays 91, 95
- bad pixels 92
- bias 93, 107
- dark current 25, 92, 112, 287
- dark frames 93
- described 25, 91
- DQE 92
- dynamic range 92, 95
- flat fields 97, 102, 287
- flat fields, for spectroscopy 104
- flat fields, photometric
  - accuracy 102, 104
- flat fields, wavelength
  - dependence 100, 104
- intra-pixel sensitivity 97
- large scale variation 97
- linearity 92, 95
- pixel response 97
- pixel-to-pixel variation 97, 99, 102
- quadrants 91
- quantum efficiency 92, 101
- readnoise 92, 95
- readout modes 25, 105
- response 92, 95, 101
- saturation 92, 95
- shading 26, 93, 112, 287

## dewar 20

## dither

- described 141, 145
- examples 147
- overhead 123
- pattern 143, 145
- size 153
- SPIRAL-DITH-PATTERN 134
- SQUARE-WAVE-DITH 127
- XSTRIP-DITH 128
- YSTRIP-DITH-CHOP 130

## documentation

- World Wide Web 9

## dynamic range

- detector 92

**E**

## EIGHT-CHOP 146

## emission lines

- exposure times 78

## epsilon diagrams 42, 68,

## error array

- described 283

## examples

- chop 147
- dither 147
- signal-to-noise calculation 84

## exclusion

- diagrams, described 44

- diagrams, use of 86

F090M, camera 1 157

F095M, camera 1 159

F097N, camera 1 161

F108N, camera 1 163

F108N, camera 3 221

F110M, camera 1 165

F110W, camera 1 167

F110W, camera 2 189

F110W, camera 3 223

F113N, camera 1 169

F113N, camera 3 225

F140W, camera 1 171

F145M, camera 1 173

F150W, camera 3 227

F160W, camera 1 175

F160W, camera 2 191

F160W, camera 3 229

F164N, camera 1 177

F164N, camera 3 230

F165M, camera 1 179

F165M, camera 2 193

F166N, camera 1 181

F166N, camera 3 232

F170M, camera 1 183

F171M, camera 2 195

F175W, camera 3 234

F180M, camera 2 197

F187N, camera 1 185

F187N, camera 2 199

F187N, camera 3 236

F187W, camera 2 201

- F190N, camera 1 187
  - F190N, camera 2 203
  - F190N, camera 3 238
  - F196N, camera 3 240
  - F200N, camera 3 242
  - F204M, camera 2 205
  - F205W, camera 2 207
  - F207M, camera 2 209
  - F212N, camera 2 211
  - F212N, camera 3 244
  - F215N, camera 2 213
  - F215N, camera 3 246
  - F216N, camera 2 215
  - F222M, camera 2 217
  - F222M, camera 3 248
  - F237M, camera 2 219
  - F240M, camera 3 250
  - grisms 68-74
  - polatizets 59-63
  - exclusion diagrams, use of 86
  - exposure (see "data" and "imaging")
  - exposure times
    - background radiation 76, 79
    - BRIGHTOBJ 115
    - calculating 75, 80
    - calculating by hand, emission line source 88
    - calculating by hand, line plus continuum 88
    - calibration star 87
    - dark current 113
    - emission line contribution 78
    - emission line source 88
    - exclusion diagrams, using 86
    - grism observations 90
    - high background 85
    - instrument parameters 80
    - instrumental factors 76
    - line plus continuum source 88
    - low background 84
    - overhead 122
    - signal-to-noise, calculating 78
    - software tools 82
    - World Wide Web 82
  - extended source
    - background subtraction 142
    - exclusion diagrams 44
    - sensitivity curves 42
- F**
- F090M through F237M
    - see "filter"
  - FAST
    - overheads 123
    - readout mode 113
    - readout mode, described 107
  - field of view
    - cameras 22
  - field offset mirror 13
    - optical path 20
    - PSF 47
  - file
    - data formats 13, 282
  - filter
    - available, list of 36
    - bandpasses 37, 39, 41
    - camera 1 36
    - camera 2 38
    - camera 3 40
    - described 22, 36
    - encircled energy 45
    - F090M, camera 1 156
    - F095N, camera 1 158
    - F097N, camera 1 160
    - F108N, camera 1 162
    - F108N, camera 3 220
    - F110M, camera 1 164
    - F110W, camera 1 166
    - F110W, camera 3 222
    - F113N, camera 1 168
    - F113N, camera 3 224
    - F11W, camera 2 188
    - F140W, camera 1 170
    - F145M, camera 1 172
    - F150W, camera 3 226
    - F160W, camera 1 174
    - F160W, camera 2 190
    - F160W, camera 3 228
    - F164N, camera 1 176
    - F164N, camera 3 230

F165M, camera 1 178  
 F165M, camera 2 192  
 F166N, camera 1 180  
 F166N, camera 3 232  
 F170M, camera 1 182  
 F171M, camera 2 194  
 F175W, camera 3 234  
 F180M, camera 2 196  
 F187N, camera 1 184  
 F187N, camera 2 198  
 F187N, camera 3 236  
 F187W, camera 2 200  
 F190N, camera 1 186  
 F190N, camera 2 202  
 F190N, camera 3 238  
 F196N, camera 3 240  
 F200N, camera 3 242  
 F204M, camera 2 204  
 F205W, camera 2 206  
 F207M, camera 2 208  
 F212N, camera 2 210  
 F212N, camera 3 244  
 F215N, camera 2 212  
 F215N, camera 3 246  
 F216N, camera 2 214  
 F222M, camera 2 216  
 F222M, camera 3 248  
 F237M, camera 2 218  
 F240M, camera 3 250  
 G096 69  
 G141 71  
 G206 73  
 leaks, out of band 44  
 nomenclature 36  
 overheads 122  
 POLOL 62  
 POLOS 60  
 POL120L 62  
 POL120S 60  
 POL240L 62  
 POL240S 60  
 polarimetry 59  
 PSF area 45  
 red leaks 44  
 sensitivity curves, polarizers 59  
 spectroscopy 36, 68

filter sensitivity parameters 80–82  
 FITS  
   data format, handling 284  
   NICMOS data format 282  
 flatfield  
   calibration exposures 292  
   characteristics 97  
   response 97  
 flux  
   Jansky 255  
   magnitude systems 254  
   magnitudes, zero point 32  
   unit conversion 32, 255  
   unit conversion, examples 264  
   units 4, 32, 253, 255  
 flux calibration  
   standard stars 293  
 FOM  
   see "field offset mirror"  
 FOUR-CHOP 146

## G

grism  
   available 40  
   B continuum, F150W, camera 3 226  
   calibration exposures 293  
   described 64  
   exposure times 90  
   flat fielding 104  
   overhead 130  
   spectroscopy 18, 64  
   spectroscopy, multi-object 104  
 guide star  
   acquisition overhead 122  
   reacquisition overhead 122

## H

helium lines 264  
 Help Desk  
   contacting 8  
 high background  
   signal-to-noise 85  
 hydrogen lines 264

**I**

- image
  - background 139
- imaging
  - described 17
  - filters 36, 155
  - polarimetry 18
  - sensitivity 24, 42
  - sensitivity limits 18
- instrument 48
  - see also "ACCUM," and "MULTLACCUM"
  - array, linearity 95
  - camera orientation 22
  - capabilities 23
  - compared to WFPC2 or STIS 23
  - coordinate system 49
  - design 18
  - field offset mirror 13, 20
  - filters 4
  - optics 20
  - overview 3, 18
  - polarization 56
  - polarizers 56
  - pupil alignment mechanism 20
  - RAMP mode 13
  - setup time, overhead 122
  - unsupported modes 13
- integration time
  - exclusion curves, using 86
- integration time array
  - described 283
- integration times 75

**L**

- linearity
  - detector 92, 95
- lines
  - atomic 264
  - molecular 264
- low background
  - signal-to-noise 84
- LOW-SKY
  - background option 31

**M**

- magnitude
  - CIT system 257
  - flux conversion 256
  - infrared system 254
  - UKIRT system 257
  - zero points 257
- modes
  - detector readout 25, 105
  - unsupported 13
- molecular lines 264
- mosaic
  - example overhead 127
  - overheads 131
- motion
  - telescope 141
- MULTLACCUM
  - dark current calibration 112
  - data format 284
  - dynamic range 111
  - example, overhead 125, 128
  - function of 106
  - mode, described 25, 110
  - overheads 123
  - SAMP-TIME 110
- multi-object spectroscopy 65
- multiple accumulate mode, see "MULTLACCUM"

**N**

- NIC1 through NIC3-FLX
  - see "aperture" 48
- NICMOS
  - see "instrument"
- NICMOS-ORIENT 49
- non-destructive readout 107, 111
- NREAD 108
- NSAMP 111, 302

**O**

- observation
  - attached parallel 27
  - coronographic, planning 54
  - grism, planning 66
  - polarimetry, planning 58

- observations
  - planning 32
- ONE-CHOP 146
- operating mode
  - overheads 122
- optical elements
  - filters 36, 155
  - grisms 40, 64
  - polarizers 36
- optics
  - dewar 20
- OPUS (see "calibration" and "pipeline")
- orbits
  - example calculation, map 127
  - example, change camera 128
  - required, calculating 124
- ORIENT 49
- orientation
  - described 49
- overhead 128
  - camera change 123
  - chopping 123
  - coronagraphy 124
  - data management 123
  - dithering 123
  - example, calibration star 134
  - example, camera change 128
  - example, grism 130
  - example, map 127, 131
  - example, polarimetry 126
  - example, spectroscopy 130
  - examples 124
  - exposure 122
  - generic 122
  - guide star acquisition 123
  - in observations 121
  - instrument setup 123
  - instrument-specific 122
  - observatory level 122
  - slews 123
- overheads
  - POSTARG 123

## P

- PAM
  - see "pupil alignment mechanism"
- parallels
  - attached 27
- pattern
  - chop 131, 141
  - chop size 153
  - dither 131, 141, 145
  - dither size 153
  - EIGHT-CHOP 146
  - FOUR-CHOP 146
  - number of steps 153
  - ONE-CHOP 146
  - orient 153
  - overhead 128
  - overheads 131
  - parameters 153
  - SPIRAL-DITH 145
  - SQUARE-WAVE-DITH 145
  - TWO-CHOP 146
  - XSTRIP-DITH 145
  - YSTRIP-DITH 145
- Phase II
  - see "proposal"
- photometry
  - calibration 293-296
  - calibration exposures 292
  - expected accuracy 287
- pipeline
  - calibration process 275
- point source
  - background subtraction 142
  - exclusion diagrams 44
  - sensitivity curves 42
- point spread function (see "PSF")
- polarimetry 18
  - example 126
  - expected accuracy 287
  - filters 36
  - instrumental polarization 56
  - polarization angle 57
  - polarization degree 57
  - polarized intensity 57

- sensitivity 42
- spectral coverage 36, 56
- Stokes parameters 56
- polarizers
  - calibration exposures 293
  - camera 1 60
  - camera 2 62
  - described 56
- POSTARG 123, 152
- proposal
  - instructions 7
  - overheads, exposure 122
  - performance updates 12
  - submission process 7
  - thermal background 14
  - unsupported modes 13
- PSF
  - area of 45
  - calibration 292
  - encircled energy 45
  - field offset mirror 47
- pupil alignment mechanism
- optical path 20

**Q**

- quality flags array
  - described 283

**R**

- RAMP
  - cosmic rays 304, 309
  - dark current 308
  - data format 282
  - function of 106
  - limitations 308
  - readout mode, described 13, 302
  - saturation 304
- readnoise
  - described 95
  - detector 92
- readout
  - ACCUM mode 106, 108
  - ACQ mode 106, 116
  - BRIGHTOBJ mode 106, 114
  - BRIGHTOBJ, exposure

- times 115
- FAST mode 107, 113
- modes, detector 105
- MULTIACCUM mode 106, 110
- non-destructive 107
- NSAMP 111
- overhead 123
- RAMP mode 106, 302
- SAMP-TIME 110
- SLOW mode 107, 113
- readout modes
  - detector 25
- reference files
  - calibration 276
- resolution
  - cameras 22
- re-use target acquisition
  - described 26

## S

- SAM
  - see "small angle motion" 48
- samples array
  - described 283
- SAMP-TIME 110
- saturation
  - detector 92
  - software 83
  - RAMP 304
- science image
  - described 283
  - see also "data"
- sensitivity
  - calculating 78
  - curves 42
  - F090M, camera 1 156
  - F095N, camera 1 158
  - F097N, camera 1 160
  - F108N, camera 1 162
  - F108N, camera 3 220
  - F110M, camera 1 164
  - F110W, camera 1 166
  - F110W, camera 2 188
  - F110W, camera 3 222
  - F113N, camera 1 168
  - F113N, camera 3 224

- F140W, camera 1 170
- F150W, camera 3 226
- F160W, camera 1 174
- F160W, camera 2 190
- F160W, camera 3 228
- F164N, camera 1 176
- F164N, camera 3 230
- F165M, camera 1 178
- F165M, camera 2 192
- F166N, camera 1 180
- F166N, camera 3 232
- F170M, camera 1 182
- F171M, camera 2 194
- F175W, camera 3 234
- F180M, camera 2 197
- F187N, camera 1 184
- F187N, camera 2 198
- F187N, camera 3 236
- F187W, camera 2 200
- F190N, camera 1 186
- F190N, camera 2 202
- F190N, camera 3 238
- F196N, camera 3 240
- F200N, camera 3 242
- F204M, camera 2 204
- F205W, camera 2 206
- F207M, camera 2 208
- F212N, camera 2 210
- F212N, camera 3 244
- F215N, camera 2 212
- F215N, camera 3 246
- F216N, camera 2 214
- F222M, camera 2 216
- F222M, camera 3 248
- F237M, camera 2 218
- F240M, camera 3 250
- grisms 68
- imaging 24
- limits 18
- polarizers 59
- variation, intra-pixel 97
- variation, wavelength 99
- servicing mission observatory verification (see "SMOV") 289
- shading
  - dark current removal 112
  - described 26,93
- shutter
  - detector reset 107
- signal-to-noise
  - calculating 78
  - example calculations 84
  - software 83
- sky brightness
  - zodiacal background 30
- SLOW
  - overheads 123
  - readout mode 113
  - readout mode, described 107
- SLTV 289,290
- small angle motion 48,153
- SMOV 290
  - activities 291
  - testing 289
- software
  - exposure times 82
  - spectroscopy reduction 66
- solar analog
  - absolute standards 294
- spectroscopy 18
  - central wavelength 64
  - complex fields 66
  - data reduction software 66
  - dispersion 65
  - G096 69
  - G141 71
  - G206 73
  - grism, described 64
  - grism, general 18
  - grism, multi-object 65,104
  - multi-object 65
  - sensitivity 42,68
  - spectral coverage 64
- SPIRAL-DITH 145
- SPIRAL-DITH-CHOP 145
- SQUARE-WAVE-DITH 145
- standard stars
  - calibration 294
  - G191B2B 294
  - GD153 294

- GD71 294
- ground-based calibration 295
- H243 294
- P041-C 295
- P177-D 295
- P330-E 295
- STIS
  - compared to NICMOS 23
- Stokes parameters
  - polarimetry 56
- STSDAS
  - calibration 276
- system level thermal vacuum test
  - (see "SLTV")

## T

- target acquisition
  - ACQ mode, described 26
  - aperture 48
  - coronagraphy 52
  - interactive 26
  - onboard 26, 116
  - onboard acquisition 52
  - overheads 122
  - re-use target offset 26
- telescope
  - motion 48, 141
  - motion, overhead 122
  - small angle motion 48, 153
- thermal background 14, 30, 286
- thermal vacuum test
  - (see "SLTV")
- time
  - overheads 121
- time variability
  - calibration exposures 293
- TWO-CHOP 146

## U

- units
  - in Handbook 4
  - see also "flux" and "wavelength"
- unsupported modes
  - calibration 13
- user support

- Help Desk 8

## W

- wavelength
  - sensitivity variation 99
  - units 4
- WFPC2
  - compared to NICMOS 23
- white dwarf
  - calibration standards 294
- World Wide Web
  - documents 9
  - exposure time calculations 82
  - grism exposure times 90
  - NICMOS web page 9

## X

- XSTRIP-DITH 145
- XSTRIP-DITH-CHOP 145

## Y

- YSTRIP-DITH 145
- YSTRIP-DITH-CHOP 145

## Z

- zodiacal light
  - background 30